



**Francisca Maria
Morais de Matos**

**Interlaced viscoelastic damping treatments with
tridimensional distribution**

Tratamentos viscoelásticos entrelaçados com distribuição
tridimensional



**Francisca Maria
Morais de Matos**

**Interlaced viscoelastic damping treatments with
tridimensional distribution**

Tratamentos viscoelásticos entrelaçados com distribuição
tridimensional

Dissertação apresentada à Universidade de Aveiro para cumprimento dos requisitos necessários à obtenção do grau de Mestre em Engenharia Mecânica, realizada sob a orientação científica de Rui António da Silva Moreira, Professor Auxiliar do Departamento de Engenharia Mecânica da Universidade de Aveiro.

o júri / the jury

presidente / president

Prof. Doutor Alfredo Manuel Balacó de Moraes

Professor Associado da Universidade de Aveiro

Prof. Doutor José Fernando Dias Rodrigues

Professor Associado da Faculdade de Engenharia da Universidade do Porto

Prof. Doutor Rui António da Silva Moreira

Professor Auxiliar da Universidade de Aveiro (orientador)

agradecimentos / acknowledgements

Em primeiro lugar, gostaria de agradecer ao Professor Rui Moreira pelo seu profissionalismo que me motivou desde o primeiro ano, por me incentivar a aceitar novos desafios e acreditar que seria capaz, pelo rigor científico sempre demonstrado e por aceitar orientar-me nesta última etapa disponibilizando o tempo e conhecimento necessários para o desenvolvimento desta dissertação.

Gostaria também de agradecer aos projetos do TEMA - Centro de Tecnologia Mecânica e Automação da Universidade de Aveiro.

Um agradecimento especial à minha mãe por ser um exemplo de determinação, motivação e constante aprendizagem, ao meu pai por ser um exemplo de conhecimento, paciência e altruísmo, e ao meu irmão por ser um verdadeiro “role model”. Aos três quero agradecer por todo o apoio e motivação não só nesta, mas em todas as fases da minha vida.

Un ringraziamento speciale a Edo per tutto il supporto durante quest'anno, per tutte le lunghe conversazioni motivazionali, per essere sempre al mio fianco, soprattutto quando ne ho più la necessità, e per essere una parte chiave nella realizzazione di questa tesi. Per te amore mio, un grande grazie.

Gostaria de agradecer também à Patrícia por ser a minha parceira incondicional nestes cinco anos, ao Ruben pela amizade, sessões de estudo e chamadas de três horas, ao Limas por ser o meu “bro” no curso e na vida, à Mariana e ao Rui por toda a amizade.

Um forte agradecimento ao Lameira por todos os ensinamentos, pela dedicação e pela amizade. Ao Miguel, ao Tomás, ao Gonçalo e ao João Tomás quero agradecer o voto de confiança e salientar o facto de me deixarem tão orgulhosa.

À Leonor, à Mafalda e à Mariana quero agradecer por serem quem são, por estarem sempre lá e por serem as melhores companheiras de viagem que existe.

Um agradecimento especial à Raquel e restante “Dream Team” por fazerem parte de todo o meu percurso, por terem travado comigo tantas batalhas e por terem contribuído para a pessoa que me tornei.

Por fim, mas não menos importante, um grande agradecimento à Camila, à Natália, à Luísa e à Gabrielle: as minhas “León Girls” por seis meses de aventuras, cumplicidade e de amizade que pretendo levar comigo para sempre.

keywords

Viscoelastic damping treatments, Passive damping control, Viscoelastic treatments modelling, Combined Models, Modal strain energy, Interlaced viscoelastic treatments.

abstract

Viscoelastic damping treatments, as passive damping control mechanism, have a wide application due to their high efficiency and reduced structural modification. The strong frequency and temperature dependency of these material's properties, and the representation of the deformation pattern developed in the dissipative layer are key elements to the numerical simulation of such damping treatments.

Free layer damping configurations provide a simple solution, but despite being characterized by an expeditious and simple application procedure, its efficiency is comparatively reduced and therefore are usually disregarded as valid solutions for critical structures. To increase the efficiency of these damping treatments, while maintaining the advantages of an application procedure based on a simple deposition of a single layer of material on the structure surface, a new configuration – Interlaced damping layer – is herein proposed and assessed.

This new configuration takes advantage of the shear effect and border effect provided by a three-dimensional interlaced layering scheme combining one or several materials. The numerical and experimental results demonstrate the feasibility of this proposed and promising configuration, that can provide a valid replacement for constrained damping layers, which often require a time consume and laborious placement procedures, and in some cases, such those where the target component has a complex geometry, is even impracticable or severely damaged during the application.

palavras-chave

Tratamentos viscoelásticos, Controlo passivo de vibrações, Modelação de tratamentos viscoelásticos, Modelos Combinados, Energia de deformação modal, Tratamentos viscoelásticos entrelaçados.

resumo

Os tratamentos de amortecimento viscoelástico, como controlo passivo de vibrações, têm uma ampla aplicação devido à sua elevada eficiência e reduzida modificação estrutural. A forte dependência das propriedades destes materiais em relação à frequência e temperatura, e a representação do campo de deformações correspondente a essa camada dissipativa são aspetos fulcrais na modelação espacial de estruturas que apresentam estes tratamentos.

Os tratamentos superficiais sem restrição proporcionam uma solução simples, porém mesmo caracterizados por simples e rápida aplicação, a sua eficiência é reduzida e por essa razão, são normalmente desconsiderados como solução de estruturas críticas. Com o intuito de aumentar a eficiência, mantendo as vantagens de um procedimento baseado na simples deposição de uma camada material sobre a superfície da estrutura, uma nova configuração - Tratamentos entrelaçados - é aqui proposta e analisada.

Esta nova configuração beneficia do efeito de corte e fronteira proporcionado pela camada tridimensional entrelaçada, que combina um ou vários materiais. Os resultados numéricos e experimentais demonstram a viabilidade desta inovadora configuração, que pode proporcionar uma válida alternativa para os tratamentos superficiais com restrição. Estes são caracterizados por longos e laboriosos procedimentos de aplicação e, para geometrias complexas, podem ser impraticáveis ou sofrerem danos durante a sua aplicação.

Contents

1	Introduction	3
1.1	Motivation	3
1.2	Objective of the dissertation	4
1.3	Outline of the dissertation	5
2	State-of-art review	7
2.1	Viscoelastic damping treatments	7
2.2	Configuration of viscoelastic treatments	8
2.2.1	Unconstrained layer or free layer damping treatments	9
2.2.2	Constrained layer damping treatments	9
2.2.3	Integrated layer damping treatments	10
2.3	Optimization of viscoelastic treatments	10
2.3.1	Partial damping treatments	11
2.3.2	Optimized multilayer and multi material damping treatments	12
2.3.3	Special spatial configurations	13
2.3.4	Hybrid damping treatments	13
2.3.5	Broad spectrum materials	14
2.4	Design of viscoelastic damping treatments: fundamental rules	14
2.5	Applicability of viscoelastic treatments	15
2.6	Characterization and modelling of viscoelastic treatments	16
2.7	Analysis of viscoelastic damping treatments	17
3	Viscoelastic Damping Treatments	21
3.1	Viscoelastic Materials	21
3.1.1	Experimental characterization of VEMs	22
3.1.2	Experimental data analysis and constitutive model	24
3.2	Numerical Simulation of Viscoelastic damping treatments	24
3.2.1	Spatial model of VEM damping treatments	25
3.2.2	Viscoelastic constitutive models	27
3.2.3	Analysis Methods	29
4	Methodology	33
4.1	Numerical study	33
4.1.1	Pre-processing	33
4.1.2	1D waves configuration	35

4.1.3	2D waves configuration	36
4.1.4	Interlaced configuration	37
4.1.5	Postprocessing	42
4.2	Experimental study	43
4.2.1	Experimental Specimens	44
4.2.2	Experimental Setup	48
4.2.3	Experimental modal analysis	51
5	Numerical Results	53
5.1	Preliminary Numerical Results	53
5.1.1	Combined model approach	53
5.1.2	VEM thickness	54
5.2	Beam-kind models	54
5.3	Plate-kind models	56
5.3.1	Square plate models	57
5.3.2	Rectangular plate models	66
6	Experimental Results	73
6.1	MDOF system modal identification (PolyMAX)	73
6.1.1	Beam specimens	73
6.1.2	Plate specimens	74
6.2	SDOF system modal identification (Circle Fit)	75
6.2.1	Beam specimens	75
6.2.2	Plate specimens	76
7	Results Analysis	77
7.1	Preliminary Numerical Results Analysis	77
7.1.1	Combined model approach	77
7.1.2	VEM thickness	78
7.2	Beam-kind models	78
7.2.1	Numerical results analysis	78
7.2.2	Experimental results analysis	79
7.2.3	Numerical/Experimental comparison	80
7.3	Plate-kind models	81
7.3.1	Numerical results analysis	81
7.3.2	Experimental results analysis	85
7.3.3	Numerical/Experimental comparison	86
8	Conclusions and future work	89
8.1	Conclusions	89
8.2	Future Work	90
A	Pre-processing: Model	91
B	Representation of the interlaced configurations developed	93

C	MSE method based code	97
D	Circle Fit method	99
	D.1 SDOF Assumption	99
	D.2 Properties of the Modal Circle	99
E	Numerical Results for the other natural modes	103
	E.1 Beam-kind models	103
	E.2 Plate-kind models	106
	E.2.1 Square plate models	106
	E.2.2 Rectangular plate models	133
	References	141

Intentionally blank page.

List of Tables

4.1	Characteristics of the sandwich beam to evaluate the combined model strategy.	34
4.2	Plates developed for comparison.	35
4.3	Characteristics of the developed 1D wave beams.	36
4.4	Characteristics of the developed 2D wave plates.	37
4.5	Nomenclature of square interlaced models.	39
4.6	Nomenclature of rectangular interlaced models.	42
4.7	Characteristics of the FLD experimental specimens.	45
4.8	Characteristics of the CLD experimental specimens.	46
4.9	Characteristics of the ILD1 experimental specimen.	47
4.10	Characteristics of the beam experimental specimens.	48
5.1	Natural frequencies and modal loss factor for the developed combined model approaches.	53
5.2	Natural frequencies and normalized loss factor for the Brick+Brick approach with two different VEM thicknesses.	54
5.3	Natural frequency values for the Plate with offset+Brick approach with two different VEM thicknesses.	54
5.4	Distribution of the modal strain energy (1 st mode) for the beam models developed with free boundary conditions.	55
5.5	Natural frequencies and normalized loss factor for the developed beam-kind models.	56
5.6	Distribution of the modal strain energy (1 st mode) for the 2D wave models developed with free boundary conditions.	57
5.7	Natural frequencies and loss factor for the 2D wave models with amplitude A_1	58
5.8	Natural frequencies and loss factor for the ILD2_2D_0.5 model with two different amplitudes.	59
5.9	Distribution of the modal strain energy (1 st mode) for the ILD square models developed with free boundary conditions.	59
5.10	Natural frequencies and normalized loss factor for the developed ILD square models.	60
5.11	Distribution of the modal strain energy (1 st mode) for the CLD square models developed with free boundary conditions.	61
5.12	Natural frequencies and normalized loss factor for the developed CLD square models.	61

5.13	Distribution of the modal strain energy (1 st mode) for the FLD square models without constraining stripes developed with free boundary conditions.	62
5.14	Natural frequencies and normalized loss factor for the FLD square models without constraining stripes.	63
5.15	Distribution of the modal strain energy (1 st mode) for the FLD square models with single layered constraining stripes developed with free boundary conditions.	63
5.16	Natural frequency and normalized loss factor (1 st mode) for the FLD square models with single layered constraining stripes.	64
5.17	Distribution of the modal strain energy (1 st mode) for the FLD square models with single and double layered constraining stripes developed with free boundary conditions - top view.	65
5.18	Distribution of the modal strain energy (1 st mode) for the FLD square models with single and double layered constraining stripes developed with free boundary conditions - bottom view.	65
5.19	Natural frequency and normalized loss factor (1 st mode) for the FLD square models with single and double layered constraining stripes.	66
5.20	Distribution of the modal strain energy (1 st mode) for the CLD rectangular models developed with free boundary conditions.	67
5.21	Natural frequency values for the developed CLD rectangular models.	67
5.22	Loss factor values for the developed CLD rectangular models.	68
5.23	Distribution of the modal strain energy (1 st mode) for the FLD rectangular models developed with free boundary conditions.	68
5.24	Natural frequency values for the developed FLD rectangular models.	69
5.25	Loss factor values for the developed FLD rectangular models.	69
5.26	Distribution of the modal strain energy (1 st mode) for the ILD rectangular model developed with free boundary conditions.	70
5.27	Natural frequency values for the developed ILD rectangular model.	70
5.28	Loss factor values for the developed ILD rectangular model.	70
5.29	Distribution of the modal strain energy (1 st mode) for the plain plate with free boundary conditions.	71
5.30	Natural frequency values for the plain plate.	71
6.1	Natural Frequency values for the beam specimens obtained by the PolyMAX method.	74
6.2	Damping ratio values for the beam specimens obtained by the PolyMAX method.	74
6.3	Natural frequency values for the plate specimens obtained by the PolyMAX method.	75
6.4	Damping ratio values for the plate specimens obtained by the PolyMAX method.	75
6.5	Natural frequency values for the beam specimens obtained by the Circle Fit method.	75
6.6	Loss factor values for the beam specimens obtained by the Circle Fit method.	76

6.7	Natural frequency values for the plate specimens obtained by the Circle Fit method.	76
6.8	Loss factor values for the plate specimens obtained by the Circle Fit method.	76
B.1	Characteristics of the developed interlaced square plates.	96
E.1	Distribution of the modal strain energy (2^{nd} mode) for the beam models developed with free boundary conditions.	103
E.2	Distribution of the modal strain energy (3^{rd} mode) for the beam models developed with free boundary conditions.	104
E.3	Distribution of the modal strain energy (4^{th} mode) for the beam models developed with free boundary conditions.	105
E.4	Distribution of the modal strain energy (2^{nd} mode) for the 2D wave models developed with free boundary conditions.	106
E.5	Distribution of the modal strain energy (3^{rd} mode) for the 2D wave models developed with free boundary conditions.	107
E.6	Distribution of the modal strain energy (4^{th} mode) for the 2D wave models developed with free boundary conditions.	108
E.7	Distribution of the modal strain energy (5^{th} mode) for the 2D wave models developed with free boundary conditions.	109
E.8	Distribution of the modal strain energy (2^{nd} mode) for the ILD square models developed with free boundary conditions.	110
E.9	Distribution of the modal strain energy (3^{rd} mode) for the ILD square models developed with free boundary conditions.	111
E.10	Distribution of the modal strain energy (4^{th} mode) for the ILD square models developed with free boundary conditions.	112
E.11	Distribution of the modal strain energy (5^{th} mode) for the ILD square models developed with free boundary conditions.	113
E.12	Distribution of the modal strain energy (2^{nd} mode) for the CLD square models developed with free boundary conditions.	114
E.13	Distribution of the modal strain energy (3^{rd} mode) for the CLD square models developed with free boundary conditions.	114
E.14	Distribution of the modal strain energy (4^{th} mode) for the CLD square models developed with free boundary conditions.	115
E.15	Distribution of the modal strain energy (5^{th} mode) for the CLD square models developed with free boundary conditions.	116
E.16	Distribution of the modal strain energy (2^{nd} mode) for the FLD square models without constraining stripes developed with free boundary conditions.	116
E.17	Distribution of the modal strain energy (3^{rd} mode) for the FLD square models without constraining stripes developed with free boundary conditions.	117
E.18	Distribution of the modal strain energy (4^{th} mode) for the FLD square models without constraining stripes developed with free boundary conditions.	118

E.19	Distribution of the modal strain energy (5^{th} mode) for the FLD square models without constraining stripes developed with free boundary conditions.	119
E.20	Distribution of the modal strain energy (2^{nd} mode) for the FLD square models with single layered constraining stripes developed with free boundary conditions.	120
E.21	Natural frequency values (2^{nd} mode) for the FLD square models with single layered constraining stripes.	121
E.22	Normalized loss factor values (2^{nd} mode) for the FLD square models with single layered constraining stripes.	121
E.23	Distribution of the modal strain energy (3^{rd} mode) for the FLD square models with single layered constraining stripes developed with free boundary conditions.	121
E.24	Natural frequency values (3^{rd} mode) for the FLD square models with single layered constraining stripes.	122
E.25	Normalized loss factor values (3^{rd} mode) for the FLD square models with single layered constraining stripes.	122
E.26	Distribution of the modal strain energy (4^{th} mode) for the FLD square models with single layered constraining stripes developed with free boundary conditions.	123
E.27	Natural frequency values (4^{th} mode) for the FLD square models with single layered constraining stripes.	124
E.28	Normalized loss factor values (4^{th} mode) for the FLD square models with single layered constraining stripes.	124
E.29	Distribution of the modal strain energy (5^{th} mode) for the FLD square models with single layered constraining stripes developed with free boundary conditions.	124
E.30	Natural frequency values (5^{th} mode) for the FLD square models with single layered constraining stripes.	125
E.31	Normalized loss factor values (5^{th} mode) for the FLD square models with single layered constraining stripes.	125
E.32	Distribution of the modal strain energy (2^{nd} mode) for the FLD square models with single and double layered constraining stripes developed with free boundary conditions - top view.	126
E.33	Distribution of the modal strain energy (2^{nd} mode) for the FLD square models with single and double layered constraining stripes developed with free boundary conditions - bottom view.	126
E.34	Natural frequency values (2^{nd} mode) for the FLD square models with single and double layered constraining stripes.	127
E.35	Normalized loss factor values (2^{nd} mode) for the FLD square models with single and double layered constraining stripes.	127
E.36	Distribution of the modal strain energy (3^{rd} mode) for the FLD square models with single and double layered constraining stripes developed with free boundary conditions - top view.	127
E.37	Distribution of the modal strain energy (3^{rd} mode) for the FLD square models with single and double layered constraining stripes developed with free boundary conditions - bottom view.	128

E.38	Natural frequency values (3^{rd} mode) for the FLD square models with single and double layered constraining stripes.	129
E.39	Normalized loss factor values (3^{rd} mode) for the FLD square models with single and double layered constraining stripes.	129
E.40	Distribution of the modal strain energy (4^{th} mode) for the FLD square models with single and double layered constraining stripes developed with free boundary conditions - top view.	129
E.41	Distribution of the modal strain energy (4^{th} mode) for the FLD square models with single and double layered constraining stripes developed with free boundary conditions - bottom view.	130
E.42	Natural frequency values (4^{th} mode) for the FLD square models with single and double layered constraining stripes.	131
E.43	Normalized loss factor values (4^{th} mode) for the FLD square models with single and double layered constraining stripes.	131
E.44	Distribution of the modal strain energy (5^{th} mode) for the FLD square models with single and double layered constraining stripes developed with free boundary conditions - top view.	131
E.45	Distribution of the modal strain energy (5^{th} mode) for the FLD square models with single and double layered constraining stripes developed with free boundary conditions - bottom view.	132
E.46	Natural frequency values (5^{th} mode) for the FLD square models with single and double layered constraining stripes.	132
E.47	Normalized loss factor values (5^{th} mode) for the FLD square models with single and double layered constraining stripes.	132
E.48	Distribution of the modal strain energy (2^{nd} mode) for the CLD rectangular models developed with free boundary conditions.	133
E.49	Distribution of the modal strain energy (3^{rd} mode) for the CLD rectangular models developed with free boundary conditions.	133
E.50	Distribution of the modal strain energy (4^{th} mode) for the CLD rectangular models developed with free boundary conditions.	134
E.51	Distribution of the modal strain energy (5^{th} mode) for the CLD rectangular models developed with free boundary conditions.	134
E.52	Distribution of the modal strain energy (2^{nd} mode) for the FLD rectangular models developed with free boundary conditions.	135
E.53	Distribution of the modal strain energy (3^{rd} mode) for the FLD rectangular models developed with free boundary conditions.	136
E.54	Distribution of the modal strain energy (4^{th} mode) for the FLD rectangular models developed with free boundary conditions.	136
E.55	Distribution of the modal strain energy (5^{th} mode) for the FLD rectangular models developed with free boundary conditions.	137
E.56	Distribution of the modal strain energy (2^{nd} mode) for the ILD rectangular model developed with free boundary conditions.	138
E.57	Distribution of the modal strain energy (3^{rd} mode) for the ILD rectangular model developed with free boundary conditions.	138
E.58	Distribution of the modal strain energy (4^{th} mode) for the ILD rectangular model developed with free boundary conditions.	138

E.59	Distribution of the modal strain energy (5^{th} mode) for the ILD rectangular model developed with free boundary conditions.	139
E.60	Distribution of the modal strain energy (2^{nd} mode) for the plate without treatment with free boundary conditions.	139
E.61	Distribution of the modal strain energy (3^{rd} mode) for the plate without treatment with free boundary conditions.	140
E.62	Distribution of the modal strain energy (4^{th} mode) for the plate without treatment with free boundary conditions.	140
E.63	Distribution of the modal strain energy (5^{th} mode) for the plate without treatment with free boundary conditions.	140

List of Figures

2.1	Viscoelastic damping treatment configurations, FLD configuration (on the left) and CLD configuration (on the right) [1].	9
2.2	ILD configuration [2].	10
2.3	Strain energy distribution inside the VEM layer for FLD, CLD and ILD (free-free beam – first mode) [1].	15
3.1	3D representation of the complex modulus of VEM [3].	22
3.2	Beam configurations [3].	23
3.3	Combined models: a) plate+beam, b) plate with rigid link + brick, c) plate with offset + brick, d) brick + brick [3].	26
3.4	Layerwise model [3].	26
4.1	1D waves configuration module representation.	36
4.2	2D waves configuration module representation.	37
4.3	Interlaced configuration concept.	38
4.4	Representation of the interlaced configuration using 2 different materials.	39
4.5	Representation of the interlaced rectangular plates: a) CLD0.5_IL2; b) FLD2_IL2_C70 and c) FLD2_IL2_C70_2b.	43
4.6	Representation of the FLD rectangular plates: a) FLD2; b) FLD2_IL2_C70 and c) FLD2_IL2_C70_2b.	44
4.7	Experimental FLD specimens: a) FLD2; b) FLD2_IL2_C70 and c) FLD2_IL2_C70_2b.	45
4.8	Representation of the CLD rectangular plates: a) CLD0.5 and b) CLD0.5_IL2.	45
4.9	Experimental CLD specimens: a) CLD0.5 and b) CLD0.5_IL2.	46
4.10	Representation of the ILD1 rectangular plate.	47
4.11	Experimental ILD1 specimen.	47
4.12	Representation of the 20 x 20 mm modules for 140 x 20 mm beams: a) ILD2 and b) ILD2_1D.	48
4.13	Experimental beam specimens: a) ILD2 and b) ILD2_1D_4.	49
4.14	Experimental ILD2_1D_4 beam specimen during the phase of assembly.	49
4.15	Experimental Setup.	49
4.16	Experimental Setup for the plate specimens.	50
4.17	Experimental Setup for the beam specimens.	50
4.18	Measuring mesh.	51
5.1	Mode shapes of the first four natural modes of the sandwich beam.	55
5.2	Mode shapes of the first five natural modes of the aluminium square plate.	57

5.3	Mode shapes of the first five natural modes of the aluminium rectangular plate.	67
6.1	Mode shapes of the first two natural modes of the sandwich beam.	73
6.2	Mode shapes of the first five natural modes of the aluminium rectangular plate.	74
7.1	Comparison between the analysed combined model approaches.	77
7.2	Normalized loss factor comparison between the two VEM thicknesses.	78
7.3	Normalized loss factor comparison between the beam-kind models.	79
7.4	Modal loss factor comparison between the beam specimens.	80
7.5	Natural frequencies comparison between numeric and experimental study.	80
7.6	Loss factor comparison between numeric and experimental study.	81
7.7	Modal loss factor comparison between the 2D wave models with A_1 amplitude.	82
7.8	Modal loss factor comparison between the ILD2_2D_0.5 with two different amplitudes.	82
7.9	Normalized loss factor comparison between the ILD square models.	83
7.10	Normalized loss factor comparison between the CLD square models.	83
7.11	Normalized loss factor comparison between the FLD square models.	84
7.12	Normalized loss factor comparison between the FLD square models.	85
7.13	Normalized loss factor comparison between the rectangular plate models.	85
7.14	Modal loss factor comparison between the plate specimens - PolyMax.	86
7.15	Modal loss factor comparison between the plate specimens - Circle Fit.	86
7.16	Comparison between numeric and experimental study - CLD0.5.	87
7.17	Comparison between numeric and experimental study - CLD0.5_IL2.	87
7.18	Comparison between numeric and experimental study - FLD2.	87
7.19	Comparison between numeric and experimental study - FLD2_IL2_C70.	88
7.20	Comparison between numeric and experimental study - FLD2_IL2_C70_2b.	88
7.21	Comparison between numeric and experimental study - ILD1.	88
B.1	Representation of the ILD interlaced square plates: a) ILD2_IL2; b) ILD2_IL4; c) ILD2_IL8.	93
B.2	Representation of the CLD interlaced square plate: CLD0.25_IL2.	94
B.3	Representation of the FLD interlaced square plates: a) FLD2_IL2; b) FLD2_IL4; c) FLD2_IL2_C Δ ; d) FLD2_IL4_C Δ ; e) FLD2_IL8_C Δ ; f) FLD2_IL2_C70_2a; g) FLD2_IL4_C70_2a; h) FLD2_IL8_C70_2a; i) FLD2_IL2_C70_2b; j) FLD2_IL4_C70_2b and k) FLD2_IL8_C70_2b.	95
D.1	Properties of modal circle [4].	101

Nomenclature

Acronyms

<i>ADF</i>	Anelastic Displacement Fields
<i>ATF</i>	Augmenting Thermodynamics Fields
<i>CLD</i>	Constrained Layer Damping
<i>CMA</i>	Complex Modulus Approach
<i>DFA</i>	Direct Frequency Analysis
<i>FD</i>	Fractional Derivative model
<i>FEM</i>	Finite Element Method
<i>FLD</i>	Unconstrained or Free Layer Damping
<i>FRF</i>	Frequency Response Function
<i>GA</i>	Genetic Algorithms
<i>GHM</i>	Golla-Hughes-McTavish model
<i>ILD</i>	Integrated Layer Damping
<i>ILLD</i>	Interlaced Layer Damping
<i>MAC</i>	Modal Assurance Criterion
<i>MDOF</i>	Multiple degree of freedom
<i>MSE</i>	Modal Strain Energy method
<i>PCLD</i>	Partial Constrained Layer Damping
<i>RKU</i>	Ross-Kerwin-Unger model
<i>SDOF</i>	Single degree of freedom
<i>TDA</i>	Time Domain Analysis
<i>VEM</i>	Viscoelastic Material

Model Treatments

CLD_{\square} Constrained layer damping, \square mm of constrained layer

$CLD_{\square}IL_{\circ}$ Constrained layer damping, \square mm of constrained layer and \circ interlaced VEM stripes in each direction

FLD_{\square} Free layer damping, \square mm of host structure

$FLD_{\square}IL_{\circ}$ Free layer damping, \square mm of host structure and \circ interlaced VEM stripes in each direction

$FLD_{\square}IL_{\circ}.C_{\triangle}$ Free layer damping, \square mm of host structure and \circ interlaced stripes of VEM and an aluminium with $E=\triangle$ GPa

$FLD_{\square}IL_{\circ}.C_{\triangle}2a$ Free layer damping, \square mm of host structure and double layer of \circ interlaced stripes of VEM and an aluminium with $E=\triangle$ GPa

$FLD_{\square}IL_{\circ}.C_{\triangle}2b$ Free layer damping, \square mm of host structure and double layer interleaved of \circ interlaced stripes of VEM and an aluminium with $E=\triangle$ GPa

ILD_{\square} Integrated layer damping, \square mm of host structure and constrained layer

$ILD_{\square}IL_{\circ}.C_{\triangle}$ Integrated layer damping, \square mm of host structure and constrained layer, and \circ interlaced stripes of VEM and an aluminium with $E=\triangle$ GPa

$ILD_{\square}IL_{\circ}$ Integrated layer damping, \square mm of host structure and constrained layer, and \circ interlaced VEM stripes in each direction

$ILD_{\square}1D_{\circ}$ Integrated layer damping beam, \square mm of host structure and constrained layer, and \circ 1D waves per modulus

$ILD_{\square}2D_{\circ}$ Integrated layer damping, \square mm of host structure and constrained layer, and \circ 2D waves per modulus

Coordinate Systems

X, Y, Z Global cartesian coordinate system

x, y, z Local cartesian coordinate system

Indexes

i general index counter

j general index counter

k finite element index

r modal index

Matrices []

$[\bar{K}]$ Complex stiffness matrix $\in \mathbb{C}$

$[C]$ Viscous damping matrix $\in \mathbb{R}$

$[K]$	Stiffness matrix	$\in \mathbb{R}$
$[K_e]$	Extensional stiffness matrix	$\in \mathbb{R}$
$[K_I]$	Stiffness matrix imaginary part	$\in \mathbb{R}$
$[K_R]$	Stiffness matrix real part	$\in \mathbb{R}$
$[K_s]$	Transverse shear stiffness matrix	$\in \mathbb{R}$
$[K_v]$	Viscoelastic component of the stiffness matrix	$\in \mathbb{R}$
$[M]$	Mass matrix	$\in \mathbb{R}$
$[P]$	Projection matrix	$\in \mathbb{R}$

Operators

$[\]^H$	Complex conjugate transpose matrix operator
$[\]^T$	Transpose matrix operator
$\ddot{(\bullet)}$	Second order in time derivative
$\dot{(\bullet)}$	First order in time derivative
$\mathfrak{D}^\alpha(\bullet)$	Fractional derivative of α order ($0 < \alpha < 1$)

Scalars (\bullet)

$\alpha(\omega)$	Receptance function [m/N]	$\in \mathbb{C}$
$\bar{\lambda}$	Complex eigenvalue	$\in \mathbb{C}$
\bar{E}	Complex modulus [Pa]	$\in \mathbb{C}$
\bar{G}	Complex shear modulus [Pa]	$\in \mathbb{C}$
\bar{R}	Flexural stiffness ratio	$\in \mathbb{C}$
Δ_i, Ω_i	ADF model parameters	$\in \mathbb{R}$
η	Loss factor	$\in \mathbb{R}$
η_r	Modal loss factor	$\in \mathbb{R}$
$\hat{\alpha}, \hat{\beta}$	Fractional derivative model parameters	$\in \mathbb{R}$
$\hat{\alpha}_i, \hat{\zeta}_i, \hat{\omega}_i$	GHM model parameters	$\in \mathbb{R}$
λ	Eigenvalue	$\in \mathbb{R}$
ν	Poisson's ratio	$\in \mathbb{R}$
ω	Circular frequency [rad/s]	$\in \mathbb{R}$
ω_{0r}	Natural frequency for the undamped structure of mode shape r [rad/s]	$\in \mathbb{R}$

ω_r	Natural frequency for the damped structure of mode shape r [rad/s]	$\in \mathbb{R}$
Π	Strain energy [J]	$\in \mathbb{R}$
ρ	Material density [kg/m^3]	$\in \mathbb{R}$
A	Wave amplitude [m]	$\in \mathbb{R}$
a, a_j	Fractional derivatives model parameter	$\in \mathbb{R}$
b, b_j	Fractional derivatives model parameter	$\in \mathbb{R}$
E	Young's modulus [Pa]	$\in \mathbb{R}$
E_0	Real Extensional modulus [Pa]	$\in \mathbb{R}$
e_i	Modulus ratio: $e_i = E_i/E_1$	$\in \mathbb{R}$
F	Force [N]	$\in \mathbb{R}$
G	Shear modulus [Pa]	$\in \mathbb{R}$
G^0	Relaxed or low frequency modulus $G^0 = G(t \rightarrow \infty)$ [Pa]	$\in \mathbb{R}$
G_0	Real shear modulus [Pa]	$\in \mathbb{R}$
I	Inertia moment [$kg \cdot m^2$]	$\in \mathbb{R}$
j	Complex operator $j = \sqrt{-1}$	$\in \mathbb{C}$
m	Length [m]	$\in \mathbb{R}$
n	Width [m]	$\in \mathbb{R}$
s	<i>Laplace</i> variable	$\in \mathbb{C}$
T	Temperature [$^{\circ}C$]	$\in \mathbb{R}$
t	Time variable	$\in \mathbb{R}$
Tg	Glass transition temperature [$^{\circ}C$]	$\in \mathbb{R}$
E'	Storage modulus [Pa]	$\in \mathbb{R}$
E''	Loss modulus [Pa]	$\in \mathbb{R}$
G'	Storage shear modulus [Pa]	$\in \mathbb{R}$
G''	Loss shear modulus [Pa]	$\in \mathbb{R}$
Vectors { }		
$\{\bar{\phi}\}$	Complex eigenvector $\{\bar{\phi}\} = \{\phi_R\} + j \{\phi_I\}$	$\in \mathbb{C}$
$\{\phi\}$	Eigenvector	$\in \mathbb{R}$
$\{F(\omega)\} / \{F(s)\}$	Fourier/ Laplace transform load vectors	$\in \mathbb{C}$

$\{X(\omega)\} / \{X(s)\}$ Fourier/ Laplace transform response vectors	$\in \mathbb{C}$
$\{x(t)\}$ Displacement vector (in time domain)	$\in \mathbb{R}$
$\{f(t)\}$ Force vector (in time domain)	$\in \mathbb{R}$
$\sigma / \{\sigma\}$ Stress field/ vector	$\in \mathbb{C}$
$\varepsilon / \{\varepsilon\}$ Strain field/ vector	$\in \mathbb{C}$

Intentionally blank page.

Chapter 1

Introduction

1.1 Motivation

The evolution of structural engineering in the last decades has contributed to the development of more efficient structures. This has been achieved not only with improvements on production and assembly processes, and the conception of new materials that allow the construction of lighter, efficient and optimized structures, but also with innovative structure configurations and the use of simulation tools that support the implementation of new and ingenious ideas with optimized results [1, 3].

Structures made of light and stiff materials are commonly the first choice for structural engineering, but these are not an efficient energy dissipation mechanism. More recently, starts to be more frequent the use of more efficient materials like aluminium and titanium alloys, carbon and aramid composites, polymeric and metal foams. These materials combine structural strength and lightness, but the problem of low energy dissipation remains. Due to this, improvements have been made to combine these materials with a way to recover the lost damping capacity. The damping treatments were conceived to for this purpose [1].

Vibration is a mechanical phenomenon that is characterized as a cyclic or oscillate movement from the rest position of the structure. Vibration is an inevitable natural consequence and usually unwanted, due to the fact that high vibration levels can cause expensive or life-threatening consequences. The effect of vibration caused by, for example, earthquakes, wind or environmental noise in mechanical and structural components of structures can carry major consequences, like fatigue or, in extreme cases, failure of the structures. This effect can happen in every structure with low damping capacity, but it has notorious impact in structures with large dimensions that cause uncontrolled vibrational effects because of their low natural frequencies. It is important to note that these consequences can be avoided if the vibration energy is efficiently dissipated [2].

The damping capacity of a structure has to be capable of dissipating the energy that is continuously converted and accumulated during vibration, preventing thus the occurrence of accidents due to structural collapse. These accidents, generated in structures such as vehicles, bridges and buildings, are related to fatigue induced by cyclic loads, impact or even noise, that create irreversible damage, reducing the lifetime and security level [2].

To prevent these situations, it is possible to add a material or device that introduces additional damping capacity to structures. These dissipation mechanisms, that

are added, can be introduced in several ways into a structure, successfully increasing the damping of the system. These are called passive damping treatments when there are not active or induced by external means. One of the most effective passive damping mechanism is titled as Viscoelastic damping treatment [1–3]. These and other types of damping mechanisms are presented later.

The research carried out in this dissertation is directed towards finding some innovative results that hopefully can serve by instrument for furthering the knowledge of viscoelastic damping treatments. This is the principal motivation behind this work. In order to achieve this, the objective of the dissertation is defined in the following section.

1.2 Objective of the dissertation

As aforementioned, viscoelastic damping treatments are effective passive control mechanisms able to mitigate vibration in light structures. This ability depends on two main aspects: the energy that is stored inside the viscoelastic material (VEM) when the structure deforms during vibration, and the material capability to dissipate that stored energy as heat. In fact, despite the high loss factor that a material may have at a specific temperature and frequency range, if the deformation imposed on the material is reduced then the stored energy may not represent a significant part of the global energy of the structure and the damping effect is thus negligible. This level of deformation depends significantly on the damping treatment configuration. Therefore, an interesting way to understand how to maximize the stored energy in the VEM layer is by research on new configurations for these treatments, that represents the main topic of this thesis.

New and effective solutions can be achieved taking advantage from the already known configurations, multi-layer, multi-material, partial configurations and other interesting configurations that are going to be mentioned later in the document. The design of a new configuration for VEM damping treatments can involve several design parameters, such as layer thickness, material properties, natural modes, boundary conditions and the location of the VEM patches for partial treatments. The process to obtain the highest level of damping for a natural mode, or modes, entails finding a reasonable combination having in consideration these parameters.

The main objective of this work is to propose a new configuration for VEM damping treatments that can provide a valid replacement for other efficient configurations, which often require a time-consuming and laborious placement procedures or may require special care when handling complex geometries. This new configuration is hereby named as the Interlaced Layer Damping (ILLD) configuration. The numerical and experimental study have the objective of demonstrating the feasibility of this promising configuration. To understand the mechanisms behind the interlaced layer configuration, it is initially developed a set of other spatial configurations. This process includes the analysis of beam-kind structures with 1D waves, plates with 2D waves and, finally, the assessment of the proposed interlaced configuration, that is characterized by a three-dimensional interlaced layering scheme combining one or several materials. It is made a numerical study to compare these different spatial configurations with some of the usual configurations that can be found in the literature. Additionally, an experimental validation was conducted on some of the configurations, those that were considered more promising within the scope of this work.

Other objectives are focused on: present an analysis of the state-of-the-art relevant for this work, allowing to gather important knowledge; establish a comparison between the models developed; and propose efficient damping treatment solutions.

1.3 Outline of the dissertation

This dissertation is organised into eight chapters, that includes the present one, which is dedicated to the motivation description for the work and main research goals followed by the structure of the dissertation.

In the second chapter a brief introduction to some considerations is presented including a review on the state-of-the-art, relevant for this work, divided in sections to simplify the comprehension of the contents.

Chapter 3 presents a detailed analysis on viscoelastic damping treatments, focusing on the characterisation of the properties of viscoelastic materials, including the methods that are usually applied to determine the complex modulus of viscoelastic materials applied on passive damping, and the modelling and analysis of these damping treatments.

Chapter 4 describes the methodology for both numerical and experimental study developed within the context of this work. This fourth chapter includes the presentation of the models proposed and analysed, and the procedure used to develop each analysis.

In the fifth and sixth chapters are presented the results of the numerical and experimental study, respectively. Subsequently, chapter 7 is devoted to the analysis of the results gathered and presented in the previous chapters and presents a comparison of the obtained results.

Chapter 8 concludes this dissertation with the main conclusions and suggestions for future research work.

Intentionally blank page.

Chapter 2

State-of-art review

In the fifties started to emerge the application of damping treatments to improve the characteristics of structures. However, some scientific work on the subject started to be published in the thirties. There have been many contributions since that time about viscoelastic damping treatments. In this work it is merely mentioned the most important ones due to the impossibility of describing all of the contributions in a concise and brief revision.

When a natural consequence as damping results from adding a specific material, fluid or electrical system that is able to dissipate a significant amount of the deformation energy into a structure exposed to the vibration field, the damping treatment that results from that is designated passive damping treatment. Effective examples of these treatments are the aforementioned Viscoelastic damping treatments, viscous dampers, and piezo-shunt devices [3].

Another form of damping treatment is called active damping treatment. Active devices have the ability to react against the vibratory movement of a structure or in other cases modify the damping properties of the structure in an active way [2,3]. Piezo-electric materials, electro- and magneto-rheological fluids, and shape memory alloys and polymers are effective materials used for this purpose. These mechanisms, with a variation of a strain, electrical, magnetic, or thermal field, can change some physical or material properties. The adverse side of active control relies on the requirement of complex control systems and external power supply [1,3].

Hybrid damping treatments are the combination of both active and passive damping treatments, retaining all their advantages, while removing or minimising the disadvantages. An example of these treatments can be the use of viscoelastic patches with piezo-electric constraining layers, allowing structures to obtain really good damping properties with a controllable response [3].

Despite the benefits of the hybrid VEM treatments, the passive configurations using these materials are massively used, provide an important damping effect and are still a target of continuous and intensive research. This work is focused on viscoelastic damping treatments as passive mechanisms.

2.1 Viscoelastic damping treatments

According to Denoyer and Johnson [5], among the existing passive damping treatments, the distributed treatments and the localised dampers based on viscoelastic materials

represent an efficient solution that is simple to apply, inexpensive, and provides a reduced structural modification.

Viscoelastic damping treatments consist on adding, to the host structure, layers of VEMs. These layers can be placed onto or inserted in the structure and can have various placement strategies [3].

VEMs present low structural efficiency, due to its low mass and reduced mechanical strength [2]. However, they are formed by long reticulated molecular chains that cause an important energy dissipation effect when deformed cyclically and continuously [1,2]. These materials have the ability to convert strain energy into heat, this is possible by the cyclic deformation caused by the adjacent vibrating structure, that is dissipated to the surroundings [6]. Consequently, since this energy portion is dissipated as heat to the surrounding environment, it contributes to a reduction of the kinetic energy of the structure. This effect provides an effective vibration attenuation process with demonstrated and assessed feasibility in several structural applications, including aeronautical, aerospace, and automotive structures. This ability depends on the amount of energy stored inside the VEM layer during the vibration of the structure. Therefore, it is possible to take advantage of this damping effect by integrating VEMs in structures made of highly resistant and light materials, providing thus the required dissipative effect to passively control unwanted levels of vibration [2].

The treatments using viscoelastic materials started to have a broad application in the fifties, at the time that the aerospace development called for efficient passive treatments with reduced added mass [2]. It was the high efficiency of these treatments, the simple application and the reduced cost that provide its expansion to other industries, like aeronautic and automotive, where it allowed the reduction of vibration levels in structural panels and mitigation of acoustic transmission [7–9].

The VEM treatment effectiveness is closely related to the amount of deformation energy transferred to the dissipative mechanism, for that reason the treatment should be designed in order to maximize the deformation imposed to the VEM layer [10]. Therefore, it is necessary to consider the material modulus and the configuration of the VEM patches into the structure, and the percentage of energy loss dissipated by this material, that is affected only by the characteristics of the material [3]. Additionally, it is required to consider the deformation of the viscoelastic layer, due to the pure bending motion of the structure, and also the torsional deformation of the plate and the effect caused by border of the treatment [6]. The placement of the VEM patches dictates if it is deformed mainly in shear or mainly in extension [1].

Nakra [11] presents a general analysis of viscoelastic treatments, its configurations and an analysis of the effects introduced in the treated structure. Jones [12] makes a chronological presentation of the VEM treatment evolution up to the end of the twentieth century, including its origins and perspectives for the future. It is worth noting that the publications of Nashif *et al.* [13] and Jones [14] represent iconic literature related to the concept of viscoelastic damping treatments.

2.2 Configuration of viscoelastic treatments

The different positioning strategies to place the VEM layer in a structure are: the Unconstrained or Free Layer Damping (ULD or FLD, accordingly), the Constrained

Layer Damping (CLD) and the Integrated Layer Damping (ILD) configurations. While the first two are damping treatments that are applied onto the final structure, as depicted in Figure 2.1, the last one is inserted during manufacture of the raw material [3].

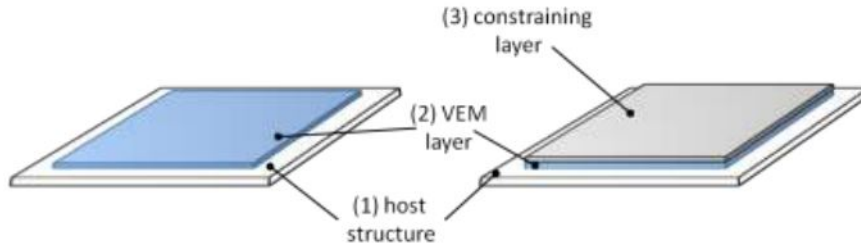


Figure 2.1: Viscoelastic damping treatment configurations, FLD configuration (on the left) and CLD configuration (on the right) [1].

2.2.1 Unconstrained layer or free layer damping treatments

In this configuration (left image of Figure 2.1) a homogeneous layer of VEM layer is placed onto the surface of the structure. The application cost is reduced for these treatments configuration and its numeric simulation is relatively simple. When the structure vibrates, usually undergoing bending and torsion vibration modes, the layer of VEM is cyclically deformed in extension and compression.

FLD treatments require thick layers to have a reasonable efficiency. According to [14], the efficiency of these treatments increases significantly when the thickness of the VEM layer is increased until one or two times that of the host structure; above this value, the efficiency maintains constant. Therefore, the added mass makes these treatments not so cost effective and limited in application [3].

The efficiency of these treatments also varies directly with the ratio between the storage modulus of the VEM layer and Young's modulus of the host structure, that is why VEMs with high storage modulus are commonly used, like plasticised PVCs [13].

Additionally, due to the considerable VEMs thickness for this configuration, this treatment is usually restricted to applications where the added mass is not an important factor or when an efficient form of thermal insulation and acoustic isolation [2] is needed. These treatments are usually applied in household appliances and automotive panels [3].

2.2.2 Constrained layer damping treatments

In this configuration (right side of Figure 2.1) the VEM layer is placed between the host structure and a stiff thin layer known as constraining layer (usually a metal-based or high modulus composite skin) [1]. According to Moreira and Rodrigues [6], the dissipation of vibration energy to the structure surroundings as heat is larger when the viscoelastic layer is covered by a stiff constraining layer which induces a considerable shear deformation. Moreira [2], mentions that normally a VEM layer with a thickness under 0.5 mm is applied to this configuration. The deformation obtained in CLD treatments, contrary to what happens with the previous treatment, is mainly shear strain due to the presence of the constraining layer [1,3].

One of the advantages of this treatment is the possibility to use thin layers of VEM that provide a reasonable damping efficiency. Therefore, it is a cost efficient damping treatment, presenting minimal modification of the final structure, eliminating the impact of the added VEM mass [3]; another advantage is an additional function of protection caused by the constraining layer [2]. A disadvantage of CLD is the complexity of its design, since it requires special care when representing the high shear strain levels in the VEM layer due to the effect caused by the constraining layer [2,3,6]. Its use is limited to structures with planar surfaces or surfaces with reduced curvature. In fact, when applied to surfaces with complex geometry and curvilinear edges, the stiff constraining layer may severely remove the VEM layer integrity, promoting the appearance of wrinkles, gaps and defective bounding areas. For such structures, the placement of FLD treatments is simpler and effective; but the damping achieved with this configuration may not justify its use, especially if weight is a concern.

The CLD configuration treatment has been applied successfully in aeronautic and aerospace industry, and more recently in other industries like the automotive industry, where it is important to increase the structural performance, reducing premature failure and improving occupant safety [6].

2.2.3 Integrated layer damping treatments

In this configuration the VEM layer is placed symmetrically between the host structure and a constrained layer, where the host structure and the constraining layer have the same thickness and material properties [3]. This treatment takes advantage of its position to obtain the maximum level of shear strain distribution and producing one of the most effective damping solutions. However, this configuration cannot be considered as a post-production or healing treatment since it must be considered at the initial stages of product design [2]. ILD treatments are commercially available and are conceived using stamping, riveting, and adhesive assembly manufacturing processes. Some of the limitations present in this treatment are associated with the manufacturing processes, like limited tolerance to heat during welding, the spring-back effect during stamping and bending, and the core collapse during cutting and bending [3].

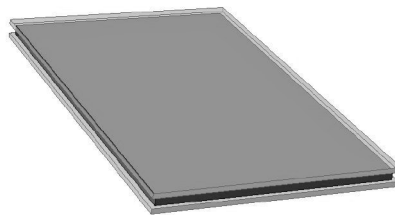


Figure 2.2: ILD configuration [2].

2.3 Optimization of viscoelastic treatments

Optimization of viscoelastic damping treatments can be an interesting approach to reduce their cost and weight, while maintaining their efficiency [1,3].

In FLD configuration treatments, the optimization is based on redesigning the coverage area and the location of the damping treatment. Due to the underlying characteristics of these configurations (that include the use of thick VEM layers), the reduction of the coverage area and the correct location of the treatment allows for a significant reduction of the damping treatment cost and added mass [1].

This optimization strategy can also be applied to CLD treatments. Numerical and experimental studies [15] show that the ILD configuration, that can be seen as a symmetric configuration of a CLD treatment, represents the most effective solution when the structure total thickness is maintained constant [1].

Moreira and Rodrigues [16] presented a possible division of optimization strategies in groups. The three main groups are named as: localized optimal placement, multi-layered distribution and shear strain amplification (includes special spatial configurations and hybrid treatments based on the addition of active devices). Moreira [2] considered an additional group called broad spectrum materials.

2.3.1 Partial damping treatments

An interesting way to reduce the cost and quantity of the VEM in damping treatments is by reducing the treatment area without notoriously reducing its efficiency [6]. Several results [17–19] show that this configuration can provide an efficient passive solution, reducing the material cost and structural modification. The partial damping treatments can be used in FLD treatments where, as was mentioned, the thick thickness of the VEM layer represents the typical configuration used in this methodology. This methodology in FLD treatments can be obtained by placing VEM layers with the same thickness [17] or with different thicknesses [18].

Akanda *et al.* [19] proposed a solution where the FLD treatments are perforated. With this solution a reduction of coverage between 40 and 50% is obtainable. The efficiency of the treatment maintains while the mass added is undoubtedly reduced.

The application of this methodology is more common on FLD treatments, but it can be also performed in CLD treatments [2]. However, most publications about application in CLD treatments are related to treatments applied on beams [20, 21]. It is unknown the existence of solutions for the application of this methodology in ILD configuration treatments [2].

Some authors [10, 22] focusing on the direct relation between the shear strains and the displacement first derivative of the mode shapes in the Mindlin's plate theory, defend that the ideal location for the partial treatments is over areas close to the nodes of each mode. However, Jones *et al.* [13] defend that the treatment should be applied over areas close to the anti-nodes of the natural mode, due to the deformations occurring mainly in the form of extension. Moreira and Rodrigues [6] clarify that both opinions seem to be correct since its efficiency depends on the relative position of the VEM layer inside the composite structure.

The contribution on the total strain energy, caused by the different parts of the host structure into the VEM layer, define the placing strategy. The areas that have less contribution can be disregarded for the treatment. This means that, if a specific portion of the viscoelastic layer is not deformed significantly, the amount of energy that can be dissipated by this portion of viscoelastic material is also neglectful and therefore it does not represent a valuable contribution to the to the overall damping treatment effect [3].

These areas can be simply found using numerical methods, to analyse the shear strain energy distribution into the VEM layer [6], or using numerical optimization methods, like Genetic Algorithms (GA) and Topology optimization [23].

GA method is an evolutionary scheme where the individuals of a population are evaluated and combined according to its fitness values. Combining these individuals with a probability proportional to their relative fitness is possible to obtain a new and improved population [24]. This iterative procedure ends when the population with the best performance within the evaluated ones is found [1].

Topology optimization is a mathematical method that relies in the predefinition of a treatment configuration evaluated in terms of its damping efficiency. The influence of each subdomain, which corresponds to the domain of each finite element if the Finite Element Method is used, is determined. This influence in the damping efficiency of the entire structure defines if the VEM should be redistributed, removed or introduced according to the topologic strategy [1].

2.3.2 Optimized multilayer and multi material damping treatments

A possible approach to Viscoelastic damping treatments is the insertion of one or more thin layers on top of a CLD configuration structure. This configuration is called multilayer configuration. A possible advantage of the multilayer configuration is the extension of the temperature range of the damping treatment, achieved by using thin layers of viscoelastic materials with different transition temperatures [16, 25, 26]. Therefore, the treatment efficiency for this approach is obtained by the combination of the relative efficiencies of each applied material [2].

The multi material configuration consists in combining materials with different transition temperatures that maintain the efficiency of the treatment within a temperature range and larger than the one provided by a single material. This configuration results in materials like VEM that present a peak in loss factor distribution around its transition temperature, so its damping efficiency outside this region is greatly reduced. By combining with another materials, a larger temperature range is covered [3].

Multi material configuration can be really interesting in applications where a large temperature range is necessary, such as aeronautic and aerospace structures. This configuration is performed by adding a set of thin layers of VEM, that can have internal constraining layers [3]. The order of this addition and the existence of internal constraining layers requires a complete numerical analysis due to the difficulty associated with the planning. Moreira and Rodrigues [16] conclude that, even when using a VEM with the same properties, but split into a set of thinner layers, can increase the stiffness of the structure and efficiency levels. The use of multiple VEM layers intercalated with constraining layers causes a maximization of the shear deformation in each VEM layer [3].

According to Sher and Moreira [23], using thin viscoelastic layers can provide an efficient solution. Multiple thin VEM layers can be more efficient than a single VEM layer with the same total thickness. To attain this goal, the VEM layers should be properly restrained.

2.3.3 Special spatial configurations

Special spatial configurations can be an interesting way to optimise a VEM damping treatment. These configurations can be divided in two strategies, in-plane and out-of-plane arrangement [16].

In-plane arrangements can be performed by modifying the VEM layer to increase shear strain on it or also by creating segmentation of the treatment to amplify shear strain that is established into the VEM layer. The objective of this strategy is to promote the shear strain that can be provided to the VEM layer. Despite of the isotropic behaviour that VEMs can present, if the loss factor and storage modulus have a directional behaviour, it is possible to benefit from it. For example, by a form of selective treatment where, depending on the natural mode, different efficiencies are obtainable [1].

Alberts and Xia [27] proposed an application into FLD configuration, that added fibers into the VEM layer. This strategy provided a way to improve the damping efficiency, since the fibers promote the localized shear deformation of the VEM, which makes this configuration comparable, by efficiency levels, to CLD configurations. With the added advantage introduced by the simplicity of FLD treatments.

Biggerstaff and Kosmatka [28] used this procedure to obtain an orthotropic viscoelastic material, integrated in a composite material, with the objective of making it selective to control by the natural modes.

Lepoittevin and Kress [29] explored other in-plane strategy introducing cuts into the damping layer, called segmentation procedure, obtaining efficient results for a two-dimensional beam model.

The other strategy, the out-of-plane arrangement, uses some kind of amplifying mechanism inserted between the host structure and the VEM layer, promoting this way, the shear strain imposed to the VEM layer [30,31]. This amplification device, usually a light structure with high shear modulus [19, 31], is designed with the intention of amplifying the deformation that is imposed to the interior face of the VEM layer [1]. Usually, for this purpose, honeycomb sandwich plates or polymeric foam plates are applied [2].

SPADD [®] [32] developed by ARTEC Aerospace (France), has the form of discrete elements that are applied locally onto the structure. These elements can amplify deformation by its metallic arms bonded in the structure, and creates shear deformation leading to an efficient dissipation method by the VEM layer that interconnects the metallic arms.

2.3.4 Hybrid damping treatments

Viscoelastic damping treatments are considered a highly dissipative mechanism. VEMs characteristics make it safe, reliable, and autonomous. But the strong dependency on temperature and frequency of vibration in these materials, make it a vulnerable solution for low excitation frequencies ($f < 10 - 20\text{Hz}$) and is highly dependent on application conditions (specially the temperature range). To overcome this limitation, hybrid damping treatments combine viscoelastic damping treatments with active control mechanisms. The addition of active control mechanisms to the treatment covers the limitation presented by VEM damping mechanisms, due to the fact that active control systems are effective for low excitation frequencies ($f < 10 - 20\text{Hz}$). They are, however, limited for high frequencies and that is why the combination of both mechanisms represents an effective solution for a wide frequency range [3].

A single hybrid dynamic control system can combine the efficiency provided by viscoelastic materials with the ability of control, by the high efficiency at low frequencies provided by active or smart materials, such as, piezoelectric crystals [33, 34] and magnetic tape [35]. The high efficiency of viscoelastic materials as a dissipative mechanism, especially for medium or high frequencies, can lead to an attenuation of the spillover effect (effect of instability control) adding piezoelectric devices [36].

Among all the literature related to this topic, the work from Liao and Wang [37] stands out. In this work the effects of VEM properties and the VEM layer thickness, in its passive and active form, are analysed. They concluded that the performance of the active control mechanism strongly depends on the VEM storage modulus, that should be high enough to transfer the actuation effect to the structure. It is important to note that a very high storage modulus could compromise the passive damping mechanism due to the attenuation of the shear effect [3].

2.3.5 Broad spectrum materials

It is important to note that the limitation of the efficient range of the viscoelastic material is imposed by the VEM itself. Therefore, one way of increasing the efficiency range of the treatment is by using VEMs with a high loss factor and a low storage modulus, approximately constant, within a broad frequency range. Pritz [38] verified that it is possible to develop materials with a high loss factor within a broad temperature or frequency range. Allen *et al.* [39] developed a set of viscoelastic materials that fulfill this requirement. The efficiency of these materials is directly related with their high thermal conductivity.

2.4 Design of viscoelastic damping treatments: fundamental rules

The design of viscoelastic damping treatments requires full understanding of the mechanism behind this dynamic control technology. It is important to note that the main advantage of viscoelastic materials for damping treatments is the ability to dissipate part of the strain energy as heat [3]. For that reason, the design of VEM damping treatments has to be focused mainly on how to maximize the strain energy produced and dissipated in the VEM layer [3].

There are several parameters that affect the strain energy developed inside the VEM layer, but the most important parameters to have in consideration when choosing the VEM are the temperature range of the application and the frequency range of interest [1]. These two important parameters are not easy to fulfil, because it is necessary that the glass transition temperature of the VEM is within the temperature range of interest. For that, some strategies can be considered such as, the multilayer configuration discussed previously, and the introduction of new viscoelastic materials with broader ranges of temperature and/or frequency for applications with high temperature gradients, like aerospace, aeronautic and automotive structures [3].

Another critical parameter for the design of these damping treatments is the thickness of the VEM layer related to the host structure and the constraining layer thicknesses. For FLD configurations, it is known that thicker viscoelastic layers increase damping levels. However, for CLD configurations the approach is not so simple [1], since it

usually requires numerical simulation tools to find a reasonable solution. For CLD configurations, a thicker VEM layer adds volume of VEM, leading to an increase in the potential of energy dissipation, but also a decrease of shear strain imposed on the VEM layer [1, 3]. The relation between VEM thickness and the damping efficiency of the total structure is not proportional, it is asymptotic for treatments with thicker VEM layer and, for cases where the VEM layer is significantly thin and the host structure thick, a peak in its curve efficiency is observed that depends on geometry and material parameters [23].

The damping treatments with in-plane localization can be divided in two solutions, total or partial placements. The total placement treatments are effective for every mode shape configuration. The partial placement treatments are a reasonable choice when the objective is to reduce cost of the treatment, weight, and structural modification. It is the responsibility of the designer to be aware of the importance of the placement of each patch, that can be designed using experimental or numerical studies. For CLD treatments the main focus of the correct placement is to increase shear strain and for FLD is to increase the extensional strain [3].

In Figure 2.3, it is possible to observe the strain energy distribution inside the VEM layer for FLD, CLD and ILD configurations for a free-free beam (first mode). In the FLD configuration, the maximum of strain deformation energy occurs near the antinodes of the first flexural model. For CLD and ILD treatments it is observed that this maximum of strain energy occurs along the nodal lines. Figure 2.3 supports this observation. However, one must be aware that is this specific structure and mode shape, the edge effect is more pronounced. This second observation is in fact the foundation of the Interlaced configuration proposed in this work.

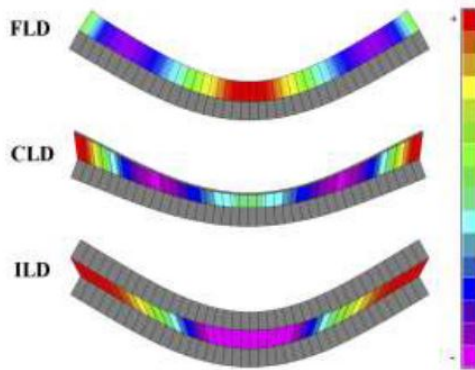


Figure 2.3: Strain energy distribution inside the VEM layer for FLD, CLD and ILD (free-free beam – first mode) [1].

In [3] a comparison between several partial (localized) constrained layer damping configurations (PCLD) is made, analyzing the modal damping ratio of each configuration and the ratio between it and the mass of the applied patch.

2.5 Applicability of viscoelastic treatments

The viscoelastic surface treatments can be applied on any structure material, from a variety of metallic materials to polymer matrix composites. However, it is necessary

to ensure the adherence between the VEM layer and the substrate surface, and the conditions imposed by the material, like the temperature range, the chemical products that VEM does not tolerate and the humidity and steam limited conditions.

For the integrated layer damping (ILD) configuration, it is necessary to have extra precautions. As aforementioned, for this configuration the VEM is added into the raw material in an early production phase. Therefore, taking in consideration that these materials cannot support extreme high temperatures, the production processes should be selected according to this. There has been no, or almost no, publication about possible solutions for this limitation. For this reason, Moreira [2] suggests that the assembly using thermal processes should be replaced by mechanical coupling or adhesive joints.

The application of ILD treatments in composites requires also some care during the manufacturing process, even if apparently does not show any type of restriction. Besides the limitations concerning pressure and temperature, it is also important having in consideration the increase in the storage modulus and the decrease in the loss factor verified in the embedded VEMs, originated from the penetration of the resin into the molecular structure of the material during the productive process. Biggerstaff and Kosmatka [40,41] experimentally verified this effect and proposed a solution that consists on adding a barrier layer between the viscoelastic material layer and the composite layer.

2.6 Characterization and modelling of viscoelastic treatments

One of the most important aspects when working on the optimization of passive treatments is the accurate development of models representing the VEMs behaviour and its properties.

The experimental characterization of the mechanical properties, noting the strong dependency on temperature and frequency of excitation, represents one of the most difficult and complex tasks to accomplish during the development of such treatments. Another difficulty is the representation of the material properties through an accurate model.

The development of the dynamic behaviour of polymeric materials started to generate interest among several authors in the decade of 1950. The important work published by Ferry [42, 43], specially with the book “Viscoelastic Properties of Polymers” [44], but also by Maxwell [45] and Oberst [46], among many others, is a reference for the characterization of the polymeric materials behaviour and its dissipative mechanism.

Over the years, it was possible to use these same referenced methodologies for experimental characterization with more evolved treatment and verification methods using powerful numerical tools.

It is also during this decade that is presented, for the first time, the complex modulus concept [47] in the representation of VEMs behaviour. In that period, it was common to use simple rheological models to represent VEMs dynamic behaviour by the combination of elastic and viscous elements. *Maxwell* and *Voigt* elements are usually combined with multiple models to obtain a better approximation for the real material behaviour. These elements represent a simpler and more popular solution. However, the accurate representation of the complex modulus for a broad frequency range, requires a high number of adjustments.

Bagley and Torvik [48] brought, in the eighties, the concept of fractional derivatives (FD) for the representation of VEM behaviour. This model is commonly used for the analysis of passive treatments and describes the behaviour over a broad frequency range with only one derivative term. Other models using FD constitutive model appears since then, defined by a different number of parameters [49–52]. This model can be introduced into a numerical integration scheme in the time domain [53,54] by the Grünwald concept [55].

During the decade of 1990 alternative models that can represent the variation of the material properties within the frequency range were proposed. Lesieutre *et al.* [56,57], proposed the *Anelastic Displacement Field* (ADF) model. This model establishes the variation effect by a set of inelastic variables. To represent the same effect, *Golla-Hughes-McTavish* (GHM) model [58] uses a set of oscillators. Both of these models can be easily implemented. The disadvantage is that it requires the use of more than a set of relaxation parameters, normally 3 to 5 oscillators [59,60] or inelastic terms to accurately represent the VEM properties for passive treatments. The GHM model is commonly used to represent VEM properties of hybrid damping treatments [59–62]. Wagner and Adhikari [63] made a comparison between the aforementioned models and the ones proposed by them, and extend the traditional state-space approach for its application.

The spatial model is an important step for a passive damping treatment project. It is important to note that this step has special importance when CLD and ILD configurations take place due to the high shear strain caused by the high damping capacity of VEMs.

The combined models are based on conventional finite elements applied in layers. Each layer is represented separately and solid elements are used to obtain the three-dimensional representation of the VEM layer [64,65]. Beams, plates and hexahedral solids are the common finite elements used for this spatial model [3]. These models provide a good representation of the deformation pattern for the VEM damping treatments. However, the modelling can be complex and expensive, computationally speaking, for multi-layer configurations.

Other possible spatial model is named layerwise model. This model ensures the continuity of the layers when the definition of the finite element displacements takes place [66,67]. It has the advantage of reducing the problem complexity. It is normally restricted to particular treatment geometries like single layer beams based on approximations for the displacements field [67]. However, Moreira *et al.* [68] based their work on this theory applied on multi-layer damping treatments. The *Euler-Bernoulli* and *Kirchhoff-Love* are the main assumptions applied in the external layers for beams and plates, respectively. *Timoshenko-Ehrenfest* and *Reissner-Mindlin* theories can also be used for this purpose.

2.7 Analysis of viscoelastic damping treatments

Oberst [69] and his team were one of the pioneers on analysing and applying the FLD configuration for viscoelastic damping treatments. The equations of *Oberst* [69], based on the assumption that the beam flat sections remain flat, are still an important tool to establish the FLD treatment effect and characterize VEMs.

In 1959, Kerwin Jr. [70] proposed an analytical model to determine the efficiency of CLD treatments on beam-kind structures. The model, based on the propagation of bending waves, can only be applied on treatments with a constrained layer thickness, much thinner than the thickness of the host structure. The efficiency of the treatment depends on the wavelength of vibration in the damped plate and on the thickness and Young's modulus of each layer of the treatment.

Ross, Ungar and Kerwin [71] proposed a fourth-order equation of differential motion for the behaviour of CLD configuration treatments applied in beam-kind structures. The proposed equations, named *Ross-Kerwin-Ungar* (RKU), were developed in 1959 and are still considered in the study of CLD and ILD configuration treatments with viscoelastic materials. These equations were developed carrying a set of assumptions, such as, imposing that the modal forms are sinusoidal and not considering the shear strain present in the VEM layer. Even with this restrictive assumptions, the equations mentioned are broadly used for plate and beam-kind structures with CLD configuration, being considered the methodology that supports most of the experimental procedures of the complex modulus of VEMs.

In 1994, the RKU equations were extended to be applied in CLD damping treated structural cables by Yamaguchi and Adhikari [72]. Bhimaraddi [73] proposed a numerical comparison between the RKU equations and an analytical model that intends to overcome some restrictions imposed by the RKU equations. The work of Bhimaraddi allowed him to understand that the RKU model underestimates the loss factor of simply supported beams for VEMs with a high storage modulus. Teng and Hu [74] evaluate the effects on CLD treatment parameters using RKU equations applied on beam-kind structures.

DiTaranto [75] proposed a sixth-order equation of motion for a sandwich beam with VEM core based on Ross, Kerwin and Ungar's work, where was eliminated the assumption of simply supported end and adapted for any end conditions. The DiTaranto work allowed the simplification of the general forced vibration problem by his discussion of natural frequencies and modes that constitute a special class of resonance frequencies and forced modes of vibration for sandwich beam structures. Mead and Markus [76, 77] took DiTaranto's theory and applied it to fixed ended beams. Rao [78] proposed a reformulation of the mentioned theory to obtain the exact solution for beams under various boundary conditions.

It is more common to find publications about analytical models related to beam-kind structures. However, there is also work on analytical models applied to FLD and CLD treatments on plates. Yan and Dowell [79] adapted the fourth-order differential equation of motion for the behaviour of isotropic and homogeneous layers on sandwich beams and plates. Rao and Nakra [80] proposed the analysis of unsymmetrical sandwich beams and plates. In addition to the transverse inertia effects, the longitudinal translatory and rotary inertial effects were included in the equation of motion.

The intention of reducing the treatments cost and the structural modification by partial treatments, led to the development of approximated analytical models based, the majority, on the analysis of the modal strain energy of undamped plates or beams. Ungar and Kerwin [81] proposed the definition of the loss factor by the strain energy of host structure modal forms. Stevens and Hsu [82] used the model mentioned previously to analyse the regular partial treatment efficiency with CLD configuration. Stevens *et al.* [83] also uses this methodology to determine the efficiency of partial treatments with

FLD configuration applied on fixed shafts with circular section, and Pei and Li [10] use it to optimize CLD treatments placement on plate-kind structures. Dechang and Zuguang [21] analysed the effect of CLD partial treatments applied on simply supported beams, using the *Galerkin* method.

Chen and Levy [20] analysed symmetric CLD partial treatments applied on cantilever beams. Based on the *Hamilton's* principle, they developed a set of differential equations of motion. This set of equations are compared with the ones proposed by Rao [78] in 1978.

The analytical models, exact or an approximation, allow the structural analysis of simple structures with well-defined boundary conditions. However, the structures where normally VEM damping treatments are applied, are three-dimensional structures with a highly complex geometry. For that reason, over the years, techniques based on numerical methods have been developed. Numerical methods of analysis create the possibility of establishing the dynamic effects and estimating the efficiency of VEM damping treatments, and also allow the development of improved methodologies for passive treatments optimization.

The Finite Element Method (FEM) has a widespread application in the structural engineering field. Therefore, the development of numerical models based on this method led to efficient solutions for the behaviour analysis of VEM damping treatments. Nevertheless, Lee and Kim [84] proposed the application of the finite difference method on ILD configuration square plates with clamped boundary conditions.

FEM allows the representation of the spatial model by calculating the mass and stiffness matrices of the structure. Therefore, to obtain the dynamic behaviour of the treated structure, it is necessary to develop a specific analysis process.

Lumsdaine and Scott [18] proposed the optimization of partial damping treatments with FLD configuration applied on plates with various boundary conditions. For this optimization it was used the finite element method through the direct frequency analysis (DFA) and the complex modulus method. These methods can be applied assuming harmonic stationary vibration. It takes advantage of the material complex modulus representation to develop a DFA where the VEM properties are updated for each frequency value. This approach presents some downsides due to the high computational cost since the equation system is solved for each frequency step value.

The aforementioned analytical methods involve complex calculation and consequently their computational costs are high. Therefore, it was developed an analysis method with only real components that allows a significant reduction of computational costs. The modal strain energy (MSE) model, firstly introduced by Johnson and Kienholz [64], is based on the energy ratio proposed by Ungar and Kerwin [81]. The MSE method takes advantage from the natural frequencies and modal forms of the undamped structure to obtain the modal loss factor of the treated structure. The method assumes that the real natural modes of the undamped structure can represent the complex modes of the damped structure under analysis. The loss factor is simply obtained by the ratio between the strain energy of the VEM layer and the total strain energy.

Shin and Maurer [85] made a comparison between the results obtained by the MSE method with the ones obtained by the DFA method for CLD configuration treatment applied on plate-kind structures. The experimental results obtained by this work verify that the MSE represents a satisfactory approximation with a significantly lower computational cost.

Several authors relied on other approximated analytical methods. Balmès [86, 87] and Plouin *et al.* [88, 89] based their strategies on the Modal projection onto a modified modal subspace method. Kelly and Stevens [22], and Lin and Lim [90] relied on the perturbation method to find the treatment effects and efficiency.

Chapter 3

Viscoelastic Damping Treatments

3.1 Viscoelastic Materials

Viscoelastic materials have the particularity of behaving as both elastic and viscous materials. VEMs are known for being highly dependent on room temperature and on the applied cyclic load frequency [1, 3]. VEM applied, as it was told before, in passive damping treatments are mostly polymer-based with a considerable loss factor for the concerned frequency and temperature range. The morphology of these materials, formed by long and tangled molecular chains, makes the dynamic response dependent on the motion of this molecular structure, that is dependent of the frequency of the excitation and temperature of the material. For these reasons, VEM for damping treatments have a limited range of admissible frequency and temperature, that should include the peak of the loss factor. The peak of the loss factor is coincident with the glass transition, which corresponds to the temperature range over which the amorphous regions change from a fragile glassy state to a flexible rubbery state as the temperature is increased. Under the temperature that the glass transition occurs, the structure of the polymer is glassy and rigid with narrow molecular mobility. At higher temperatures, the structure of the polymer as a considerable molecular mobility [3, 91].

These materials are characterized by a phase delay between a cyclic harmonic load and the resulting strain response. The complex modulus approach, shown in Equation 3.1 [1], relates the extensional modulus with the stress and strain fields on a uniaxial harmonic deformation of a VEM specimen [1].

$$E^*(\omega, T) = E'(\omega, T) + jE''(\omega, T) \quad (3.1)$$

In Equation 3.1, $E'(\omega, T)$ and $E''(\omega, T)$ represent, respectively, the storage modulus (corresponding to the real component) and loss modulus (corresponding to the imaginary part). The loss factor (η), that represents the damping capacity of the VEM, is given by the ratio between the imaginary and the real parts [1]. As mentioned before and as it is possible to see by the Equation 3.1, both real and imaginary parts of the complex modulus are frequency and temperature dependent.

In Figure 3.1, it is possible to see a three-dimensional graph of storage modulus (top graph) and of loss factor (bottom graph), both for an acrylic-based viscoelastic material at room temperature. By the temperature-time superposition principle [13, 44], increasing the temperature results in an effect onto the material that can be equally

produced by a reduction of the excitation frequency. This is one of the conclusions that is possible to take from the isolines in the storage modulus and loss factor graphs. The other conclusion stands for the superior effect of temperature when compared with frequency [3].

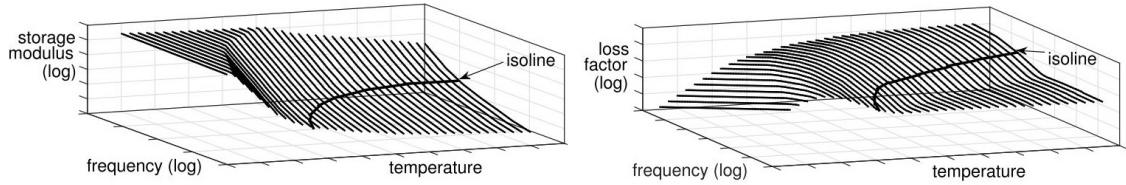


Figure 3.1: 3D representation of the complex modulus of VEM [3].

VEM damping treatments are available commercially with various material formulations and treatment configurations within different temperature ranges. The temperature range associated to each product includes the glass transition temperature, T_g . Like this it is possible to obtain the highest values for the loss factor, that represents the highest values for efficiency of the treatment in that temperature range [3].

3.1.1 Experimental characterization of VEMs

The characterization of these materials depends on a perfect control and measure of temperature and frequency, due to the strong effect that these variables produce onto the dynamic properties of VEMs. One of the characterization techniques relies on the dynamic modulus characterization using a dynamic system that can be represented by a single degree of freedom (SDOF) system, where the specimen of the selected viscoelastic material represent the unknown stiffness. It is constrained in a way that reduces the system to a SDOF system within the frequency range of interest and makes possible the representation by a single equation of motion. The material specimen can be deformed in shear or extension, depending on the configuration of the setup, providing the corresponding complex modulus data. This technique is simple but relies on the necessity of designing correctly the system to obtain an unique degree of freedom. It is usual to introduce corrections according to the temperature and frequency range, material, and the testing configuration [3]. Another possible configuration takes advantage of the perturbation effect caused by the introduction of the VEM layer to the dynamic response of a continuous system. After measuring the excitation force and the response, this information is correlated to obtain the complex modulus data. This characterization can be evaluated on FLD or CLD beams [1].

ASTM E756-98 standard [92] describes a configuration of the resonating fixed beam tested in 4 ways: a beam with an unconstrained VEM layer also called Oberst beam, a symmetric unconstrained layer also denominated as Van Oort beam, a single symmetric constrained configuration and finally a double configuration of the previous one [14, 69], respectively a), b), c) and d) from Figure 3.2 [3].

The Ross-Kerwin-Unger (RKU) model [70, 71] is used to determinate the storage modulus and the loss factor of the VEM. This model is an analytic representation of a conventional sandwich beam with three layers where the middle layer is a viscoelastic material. RKU model requires care and correction procedures to achieve valid results,

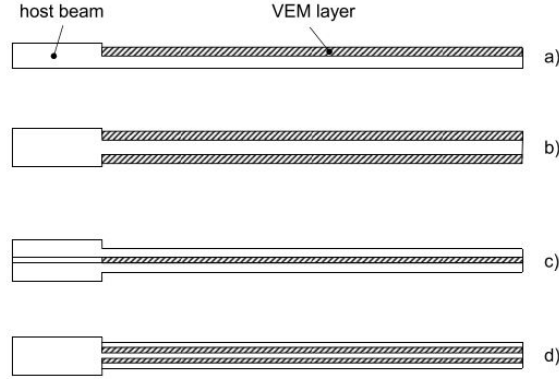


Figure 3.2: Beam configurations [3].

due to some limitations like the sinusoidal form of mode shapes. Another critical aspect is the use of an elastic material for the host beam with insignificant material damping considering that RKU equations rely on that assumption [3].

For the Oberst beam, showed in Figure 3.2 a), the flexural stiffness ratio based on RKU model [70, 71] is given by [3],

$$\bar{R} = \frac{\bar{E}I}{E_1 I_1} = \left(1 + \frac{\rho_2}{\rho_1} h_2\right) \left(\frac{\omega_r}{\omega_{0r}}\right)^2 (1 + j\eta_r) \quad (3.2)$$

where \bar{E} represents the complex modulus of the structure, E_1 the Young's modulus of host beam material, I and I_1 are the second order inertia moment of the cross-section of the structure and the host beam, respectively. Parameters ρ_1 and ρ_2 are the density for host beam and VEM material, respectively. The non-dimensional parameter h_2 is obtained from the ratio between thicknesses of VEM layer and host beam. Frequency parameters ω_r and ω_{0r} are the natural frequencies, for the damped and the undamped beams, respectively, corresponding to the mode shape under analysis. Finally, η_r represents the modal loss factor [3].

With the flexural stiffness ratio it is possible to obtain a relation that gives the complex modulus of the VEM layer, as follows [3],

$$\bar{E}_2 = E_1 \frac{-\hat{h} + \sqrt{\hat{h}^2 + 4h_2^2 (\bar{R} - 1)}}{2h_2^2} \quad (3.3)$$

where the thickness parameter \hat{h} is given by [3],

$$\hat{h} = (4 - \bar{R} + 4h_2^2 + 6h_2) \quad (3.4)$$

For each temperature stage, it is usual to analyse three mode shapes and measure the complex modulus for the natural frequencies associated to them. Gathering complex modulus data for different temperatures and different natural frequencies provides enough data to obtain a master curve, benefiting from the frequency-temperature superposition effect. To surpass the limitations associated with the assumptions that RKU model is based on, numerical models are introduced [93]. Numerical models, normally

implemented using the Finite Element Method, are used in this case where the material properties are obtained from an updating procedure [3].

3.1.2 Experimental data analysis and constitutive model

VEMs for passive damping treatments are considered thermorheologically simple, that is why it is possible to apply the time-temperature or frequency-temperature superposition principle. Also, during the host structure vibration, these materials are treated as linear viscoelastic in a reduced range of the imposed strain [3].

The complex modulus approach is a relatively easy procedure to characterise the VEM properties in the frequency domain. The function that describes the viscoelastic material properties by the complex modulus has a real part that represents the storage modulus function in frequency domain with a previous defined temperature, and has an imaginary part describes the loss modulus function. From the ratio between imaginary and real part one can obtain the loss factor of the material [3].

When applying these type of methods that have the objective of characterize the VEM properties, it is necessary to remove errors, systematic and random, that are caused, for example, by test conditions, fixture, or by limitations of the testing configuration. The Wicket plot is a tool that can eliminate these errors to obtain a single curve for loss factor or loss modulus against the storage modulus [3].

Then, with the frequency-temperature superposition principle, it is possible to obtain, by an horizontal translation of both data, storage modulus and loss factor data, making a master curve. This translation procedure is a function of temperature and provides the translation factor function that can be represented by the Williams-Landel-Ferry relation or the Arrhenius relation [3, 14].

3.2 Numerical Simulation of Viscoelastic damping treatments

For treatments that are added during the host structure design, it is necessary to define properly the material properties and geometric characteristics. In the case of simple geometries of the host structure, the designer assigned for the project can use analytical solutions. For geometries that have a higher level of complexity, boundary conditions, or loading cases, the designer opts to use numerical methods. For structures that present a dynamic problem and for that reason it's necessary to add a VEM treatment, the designer already has knowledge about the dynamic response of the host structure, so it's possible to use it for the creation of the viscoelastic damping treatment [3].

The design and simulation of viscoelastic damping treatments presents some difficulties, such as, the correct representation of the strain field imposed to the VEM layer, the proper modelling of the VEM properties and a logic solution method that manages the viscoelastic constitutive model in the desired domain [1].

The Finite Element Method has been implemented over the years to solve a big variety of problems, particularly of structural analysis. This method allows a spatial domain to be discretized into several parts with regular domain, called finite elements. According to FEM, the characteristics of the continuum can be predicted by assembling the field distribution inside each finite element, the constitutive relations, and a set of equations that describe the physics of the problem, of the discretized elements per

node [3, 94]. The resulting set of equations is solved obtaining the unknown field or vector of variables for the all set of nodes.

In the part of the project where it is performed numerical analysis, it is essential to be aware of the spatial discretization methodology selected, on the constitutive model representing the properties of the VEM, and on the chosen analysis method [3].

3.2.1 Spatial model of VEM damping treatments

The spatial model of the damping treatments with the use of viscoelastic material has to be chosen with extra care to represent the strain field correctly, which is developed inside the VEM layer. The FLD treatment configuration can be easily represented by the Equivalent Single Layer (ESL) approach or by a model based on the Classic Laminate Plate Theory (CLPT) [1]. For the CLD and ILD treatment configurations, it is necessary to be aware that the main deformation component inside the VEM layer is the shear strain, and for that reason the shear strain pattern induced inside has to be correctly reproduced, even though the thickness of the VEM layer is considerably small. For this reason, it is possible to conclude that, to estimate a correct damping efficiency for the treatment, a correct representation of the model is essential [3]. Combined models and layerwise models are the two different strategies to model adequately the structure of a VEM damping treatment [1, 3].

Combined Models

The spatial model strategy, called combined model or also known as layered model, consists in a group of layers formed by piled up conventional finite element solids. This approach uses standard finite elements, such as beams, plates and hexahedral elements [1]. Some examples of this strategy are shown in Figure 3.3, which are used by many authors [1, 3, 15].

The beam-plate model (Figure 3.3a) was initially proposed by Killian and Lu [65] and uses four beams to represent the shear and compression in the VEM layer, and two plates (QUAD4) with the nodal positions of the beams representing the host and constraining layer. The brick-plate with rigid link (Figure 3.3b) and the brick-plate with offset (Figure 3.3c) also use two plates (QUAD4) to represent the host and constraining layer, but use hexahedral (commonly called brick) finite element (HEXA8) to represent the core of VEM. The difference between these two models is the connection mechanism between the VEM core and the outer plates. The brick-plate with rigid link uses rigid link connections (RBE) while the other introduces an offset constrain into the plate formulation. The layered brick model (Figure 3.3d) uses three bricks, that share nodal locations, to represent the physical layers. This approach can be used in any finite element package. However, it is important to be aware of numerical locking due to the aspect ratio of the stiff outer bricks [1, 15].

This representation allows the proper representation of the transverse shear strain pattern in the VEM core using available commercial finite element codes. The disadvantage of combined models strategy is the time that consumes on its creation and the difficult modelling assignment. This limitation widely restricts optimization studies where a continuous update of layering scheme and thicknesses of each layer is necessary [3].

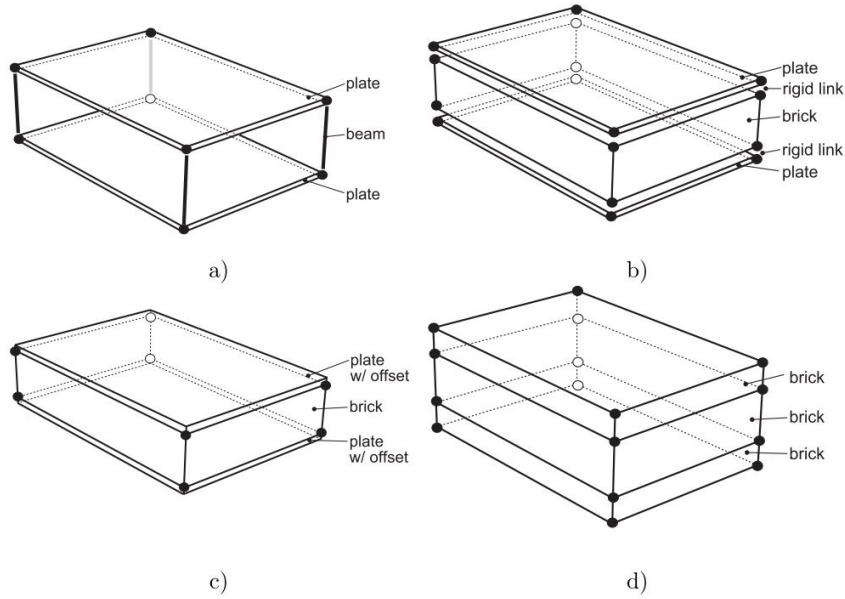


Figure 3.3: Combined models: a) plate+beam, b) plate with rigid link + brick, c) plate with offset + brick, d) brick + brick [3].

Layerwise Models

The layerwise model can consist in beams, plates, or facet-shell geometries, defined by its midplane. This scheme can be seen in Figure 3.4 [3].

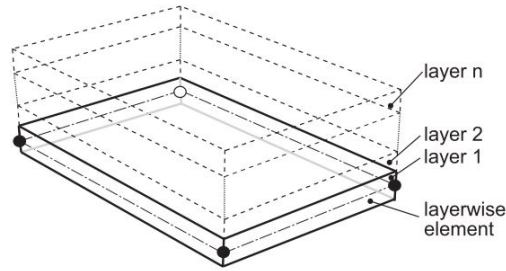


Figure 3.4: Layerwise model [3].

These discrete layer models rely on a partial [68] or full layerwise theory [66].

The layerwise model does not define, inside the software, the properties associated with the model. These properties are in an external database, that contains the number of layers, the layering scheme, the thicknesses, and the material properties of individual layers. Then, the external data based is added when it is time to calculate the stiffness, damping and mass matrices for the finite element. This strategy suppresses the limit told previously about combined models, since it avoids updating the finite element mesh when a redefinition is proposed [3].

The displacement field is characterized by making sure that a continuity between the layers exists. Additionally, mixed formulation can be applied to impose continuity of stresses at the layers interfaces [66, 67].

3.2.2 Viscoelastic constitutive models

The properties of the viscoelastic materials present a significant dependency upon time/frequency and temperature [1]. For dynamic or transient analyses, the time/frequency dependency has to be taken in consideration, even when isothermal conditions are applied [3]. This assumption is not recommended, for example, for aerospace and marine applications where simulations require high temperature gradients [3]. This temperature dependency is commonly introduced in frequency dependent models that rely on frequency-temperature superposition principle [57, 95, 96].

According to Moreira [1], the search for effective constitutive models that represent the real behaviour of VEMs is going to continue, being an open topic of researchers interest. The focus of these models is the correct representation of VEMs properties while providing a numerical implementation that should also be cost-effective.

Complex modulus model

The Complex modulus approach (CMA) in direct frequency analysis (DFA) is one of the efficient linear viscoelastic models available commercially in finite element packages [3]. The CMA, despite of its simplicity and accuracy, is a model that uses a long tabular data file which includes the storage modulus and loss modulus values for various frequency-temperature pairs [1].

The equation of motion in time domain for a damped system, can be written as [1],

$$[M] \{\ddot{x}(t)\} + [C] \{\dot{x}(t)\} + [\bar{K}] \{x(t)\} = \{f(t)\} \quad (3.5)$$

where matrices $[M]$, $[C]$ and $[\bar{K}]$ represent, respectively the mass, viscous damping and complex stiffness matrices of the dynamic system [1]. The complex stiffness matrix $[\bar{K}]$ is divided in a real matrix and a complex matrix. The real matrix represents the stiffness of the elastic layers, therefore represents the host structure and the constraining layer. The complex matrix $[\bar{K}_v(\omega)]$ represents the stiffness of the viscoelastic layer and, as it is possible to see in Equation 3.6 [1], it combines extensional stiffness terms with transverse shear component terms.

$$[\bar{K}_v(\omega)] = \bar{E}_v(\omega) \frac{K_e(E_0)}{E_0} + \bar{G}_v(\omega) \frac{K_s(G_0)}{G_0} \quad (3.6)$$

In Equation 3.6, $K_e(E_0)$ represents the extensional stiffness matrix calculated for a predefined real extensional modulus E_0 and $K_s(G_0)$ represents the transverse shear stiffness matrix calculated for a predefined real shear modulus G_0 [1]. The equation of motion for a stationary harmonic motion assumption, where the excitation and response function are both harmonic, can be represented as [1],

$$(-\omega^2 [M] + j\omega[C] + \bar{K}(\omega)) \{\bar{X}(\omega)\} = \{F(\omega)\} \quad (3.7)$$

Other examples available commercially are, Prony series in time domain analysis (TDA), and classic linear viscoelastic models, such as Maxwell, Kelvin–Voigt, and standard linear solid (SLS) models. It is important to note that these models present some limitations, therefore alternative constitutive models that have been proposed in literature [3].

Anelastic displacement fields model - ADF

Developed by Lesieutre and co-workers [56, 57], the ADF model represents the complex modulus in the frequency domain as

$$G(\omega) = G^0 \left[1 + \sum_{i=1}^n \Delta_i \frac{\omega^2 + j\omega\Omega_i}{\omega^2 + \Omega_i^2} \right] \quad (3.8)$$

where G^0 represents the relaxed or low frequency modulus, Ω_i and Δ_i are model parameters that characterize the relaxation process of the material and introduce the frequency dependency. This model is based on *augmenting thermodynamic fields* (ATF) Model [97, 98] and represents the displacement field, that is imposed on the VEM layer, with an elastic part and an anelastic component that can be subdivided in individual anelastic fields that describe different relaxation processes [1, 3].

Golla-Hughes-McTavish model - GHM

The model proposed by Golla, Hughes and McTavish [58] introduces the frequency dependency through a set of mini-oscillators [1, 3]. It represents the complex VEM modulus in Laplace domain as,

$$\bar{G}(s) = G^0 \left(1 + \sum_i^n \hat{\alpha}_i \frac{s^2 + 2\hat{\zeta}_i \hat{\omega}_i s}{s^2 + 2\hat{\zeta}_i \hat{\omega}_i s + \hat{\omega}_i^2} \right) \quad (3.9)$$

where G^0 represents, as before, the relaxed modulus and parameters $\hat{\alpha}$, $\hat{\zeta}$ and $\hat{\omega}$ are real positive constants, obtained by curve fitting the experimental data of complex modulus [59] for each mini-oscillator i [1]. Both the previous and this model are easily implemented. The disadvantage is that it requires the use of more than a set of relaxation parameters. Some authors [59, 60] defend that 3 or more GHM oscillators are necessary to get a valid representation of commonly used VEMs. In GHM model, final matrices lose the original rank of initial mass and stiffness matrices of the linear elastic system [3, 58, 59].

The equations of motion in the Laplace domain introduced by this model are [1],

$$(s^2[M] + s[C] + \bar{K}(s)) \{ \bar{X}(s) \} = \{ F(s) \} \quad (3.10)$$

where $\bar{X}(s)$ and $F(s)$ represent the Laplace transform of response and load vectors, respectively. Complex stiffness matrix $\bar{K}(s)$ can be divided into the elastic stiffness matrix of both host structure and constraining layer. The viscoelastic stiffness matrix $[K_v(s)]$ can be divided as described in Equation 3.6, where $E_v(s)$ and $G_v(s)$ are replaced by the GHM model given by the Equation 3.9 [1].

Fractional Derivative model - FD

The Fractional Derivative (FD) model proposed by Bagley and Torvik [48] combines the stress and strain fields as shown in the relation that follows,

$$\sigma(t) + \sum b_i \mathcal{D}^{\beta_i} \sigma(t) = E^0 \varepsilon(t) + \sum a_j \mathcal{D}^{\alpha_j} \varepsilon(t) \quad (3.11)$$

where a_j , b_j , α_j and β_j are the fractional derivative model parameters. Bagley and Torvik [48] defines VEM modulus by a series of fractional derivatives,

$$\bar{G}(s) = \frac{G_0 + a(j\omega)^\alpha}{1 + b(j\omega)^\beta} \quad (3.12)$$

Based on to the FD model, other models using fractional derivatives appear in literature, such as, Rossikhim and Shitikova [49] that made a comparison between FD model with 5 parameters [48] and the Schmidt and Gaul models [50–52] with 4 and 7 parameters. These models have been highly used due to the fact that they can represent the complex VEMs modulus data with just one set of derivatives. The disadvantage of using fractional derivative models is a constitutive law associated with VEMs inside a finite element analysis that requires algebraic conditioning of the finite element matrices. This increases the dimension of the problem [48]. Alternatively, the Grünwald concept [55] can be applied to introduce this model into a numerical integration scheme in the time domain [53,54].

3.2.3 Analysis Methods

The choice of the analysis method is normally done according to the constitutive model chosen to represent the viscoelastic material properties, due to the fact that both model and analysis method have to work in the same domain. The following methods are the ones available and most commonly used [1,3].

Direct Frequency analysis-DFA

DFA method is often used when the characterization of VEM is done by raw data of complex modulus, nevertheless it can be used with any VEM model as long as the complex modulus is described in the frequency domain. Representing the equation of motion as [3],

$$[M] \{\ddot{x}(t)\} + [\bar{K}(\omega, T)] \{x(t)\} = \{f(t)\} \quad (3.13)$$

where $[M]$ is the mass matrix and $[\bar{K}]$ represents the complete stiffness matrix, containing the stiffness terms of both elastic layers and VEM core. In the case of an application of a harmonic force, obtaining in this way, an harmonic response, it is possible to obtain the frequency response function solving the previous equation in the frequency domain with isothermal conditions [3],

$$[[\bar{K}(\omega, T)] - \omega^2[M]] \{\bar{X}(\omega)\} = \{F(\omega)\} \quad (3.14)$$

This analysis method allows the correction of the stiffness matrix using the updated value of storage and loss modulus of the viscoelastic material [3].

Numerical integration in time domain

Constitutive models, like GHM, ADF and fractional derivatives, when described in the time domain lead to the choice of using numerical quadrature. This method relies on the assumption that the equation of motion can be verified for set of time steps and that is predetermined a variation law for acceleration, velocity or displacement [3].

Newmark and Wilson- Θ algorithms are commonly used in this solution method [99]. GHM, ADF and fractional derivatives have a simple introduction when the equation of motion is already described in the time domain, moreover it is possible to apply an usual numerical integration procedure [99].

It is possible to introduce the FD model in a time domain analysis applied directly by a numerical integration procedure when the Grünwald definition [55] is used, as Schmidt and Gaul [50–52] and Enelund [53] suggested.

Complex modes solution

In this method it is assumed that the VEM has constant properties within a predefined range of frequencies, therefore the response of the system is described by the complex modes calculated using this assumption. The mean values for the storage modulus and loss factor contemplated within the range of frequency around the desired natural mode frequency.

From the Equation 3.14, it is possible to write the complex eigenvalue problem as [3],

$$[\bar{K}(\omega)] \{\bar{\phi}_r\} = \bar{\lambda}^2 [M] \{\bar{\phi}\}_r \quad (3.15)$$

where $[\bar{K}(\omega)]$ is the complex stiffness matrix calculated using the assumed constant mean values for storage modulus and loss factor, $\bar{\lambda}$ is the complex eigenvalue and $\{\bar{\phi}\}$ is the complex eigenvector. The system modal loss factor η_r , assuming symmetry of the stiffness matrix, can be written in the form [3],

$$\eta_r = \frac{\{\bar{\varphi}\}_r^H [K_I] \{\bar{\varphi}\}_r}{\{\bar{\varphi}\}_r^H [K_R] \{\bar{\varphi}\}_r} \quad (3.16)$$

where subscripts R and I represent, respectively, the real and imaginary parts of the matrices, and superscript H identifies the complex conjugate transpose operator. Finally, the subscript r represents the mode. Physically, this relation represents the ratio between the dissipated energy, proportional to the imaginary part of the stiffness matrix, and the storage energy, proportional to the real part of the stiffness matrix.

In the literature, the complex modes solution is used by Mitsuma *et al.* [100], to calculate the complex modes and its modal loss factors for structural panels. The results obtained by them are in agreement with the experimental results, even with the assumption proposed by the complex modes solution.

When the assumption of constant value for the complex modulus within the frequency range of interest is not considered, and the VEM properties vary significantly within the frequency range containing the entire set of analysed complex modes, it is possible to use narrow frequency bands around one or small sets of complex modes and the constant modulus is determined as the mean value of the complex modulus values within this narrow band [101]. The procedure presented can be substituted by an iteratively procedure. In this procedure, the VEM properties are updated using the complex mode frequency being calculated [90, 102].

Modal Strain Energy method - MSE

The MSE method, proposed in 1982 by Johnson and Kienholz [64], establishes the loss factor of a damped structure on the analysis of the strain energy contribution.

This method relies on the assumption that the real modes of the undamped system can represent the damped structure [1,3]. This assumption must be considered only for structures with low damping, due to the difference that can occur between the modes of the damped structure and the modes calculated for the undamped [1].

For this analysis, it is necessary that the spatial model of the final structure represents accurately the high shear deformation pattern of the viscoelastic layer and defines a set of trial configurations before its performance [6,15].

This method evaluates the damping effect of the treatments relating the energy that is effectively stored inside the VEM layer with the total energy of the structure. In fact, the damping effect provided by the VEM treatment depends on two main factors: its ability to remove energy from the structure, converting its deformation energy into heat that is dissipated to the surrounding medium, but specially the ability to store deformation energy during the motion of the vibrating host structure. The MSE method measures the ratio between the energy that is stored inside the VEM material and the total deformation energy of the structure, and multiplies this ratio by the VEM loss factor, representing thus the lost energy.

The MSE method benefits from the relation presented before, Equation 3.15, to obtain the structure loss factor. The main difference between this method and the one presented before is the use of real modes of the undamped system instead of complex modes [3].

Numerically, this analysis method is straightforwardly used in commercial finite element packages by applying a post processing analysis using the strain energy results for each natural mode within the frequency range of interest [1], as:

$$\eta_r = \frac{\sum_k \eta_{kr} \prod_{kr}}{\sum_k \prod_{kr}} \quad (3.17)$$

where \sum_k represents the sum that is performed over the entire set of finite elements k , and \prod_{kr} is the strain energy calculated at a finite element k for a specific natural mode r . Since the loss factor is negligible, and considered null, for all the structure components except the VEM parts, the numerator evaluates the energy that is stored inside the VEM layer when a unitary value is used to represent the loss factor of the finite elements of the VEM and a null value is used to represent those finite elements describing the elastic components (host structure and constraining layers).

The MSE method can be performed in a commercial finite element package. However, it is limited to low damping structures. Another limitation present in the method is referring to the approach of calculation of the representative mode shapes [1].

For damping treatments with CLD configuration, the real eigenvalue problem is often solved taking into consideration simply the host structure. For CLD treatments where the damping treatment does not introduce a considerable modification in the mass and stiffness of the complete structure, the MSE method can provide satisfactory approximations [1,3]. However, when the CLD configuration presents the thickness of both host and constraining layer in the same order of magnitude, where the presence of the damping treatment causes changes in the natural frequencies and mode shapes of the host structure, the original MSE method is not enough to obtain satisfactory results, therefore it is necessary to apply correction strategies [1,3].

Some modifications for MSE method were proposed in literature. Hu *et al.* [103] proposed that the imaginary part of the damped structure was taken into consideration

when the original modes were determined. Vasques *et al.* [102] proposed an approach where the changes in stiffness and complex modulus update the modes iteratively, caused by the introduction of the damping treatment and changes in natural frequencies that happen in consequence.

Modal projection onto a modified modal subspace

As the name suggests, with this method the system of equations of motion is projected onto a modified modal subspace $[P]$ as follows [3],

$$[[P]^T[M][P]\omega^2 + [P]^T[K][P]] \{X(\omega)\} = [P]^T\{F(\omega)\} \quad (3.18)$$

The main difficulty with this method is the proper selection of the subspace described by the selected matrix of mode shapes $[P]$. This modal subspace matrix has to properly represent the variation in the properties of the material with frequency. It can be composed of a group of mode shapes with natural frequencies around the frequency range of interest.

Different strategies were presented in literature to overcome possible corrections. Balmès [86, 87] proposed the multi-model approach. The multi-model approach consists in constructing the projection modal matrix by real natural modes calculating it with distinct natural frequencies within the frequency range of interest. This approach can have a static correction term that represents the effect of the omitted mode shapes and a subset of modes representing the effect of the introduced damping. Plouin *et al.* [88, 89] proposed an approach that consists in using modal matrix based on “pseudo-normal” modes. This “pseudo-normal” modes are obtained by the real eigenproblem using the updated real part of the stiffness matrix.

Perturbation method

The perturbation method relies on the assumption that the natural modes of the undamped system and the modifications in stiffness and mass matrix produced by adding damping treatment can describe the structural modification produced onto the modal parameters. The approximate solution that is obtained with this method provides the complex eigenproblem with an iterative perturbation or modification scheme applied onto the real eigensolution obtained for the undamped system. It is recommendable the use of this method in FLD treatments due to the relatively small modifications caused by the addition of the damping treatment in terms of mass, stiffness, and introduced damping [22]. A different approach for the perturbation method was proposed by Lin and Lim [90], where the modifications were only done on the stiffness matrix.

Chapter 4

Methodology

The present chapter provides the methodology applied to accomplish the main objective of this work. Several studies were performed to assist a reasonable path to the pioneer configurations developed. The numerical study for this work and the experimental validation were developed according to the following procedures.

4.1 Numerical study

This section presents the process adopted for the numerical study for this dissertation. The methodology includes the pre-processing in the FEM software environment that allowed the design of each model analysed further, the presentation of each configuration and strategy adopted to achieve the interlaced configuration, and the post-processing where it is explained how the results were extracted and analysed.

4.1.1 Pre-processing

The pre-processing for this work was based on the finite element method applied on *Siemens FEMAP* [104,105] software.

The model for each structure was directly developed by a proper mesh using a direct mesh generation strategy following the methodology detailed in Appendix A.

In order to demonstrate the similarity between the examples provided by the Combined Models in the Section 3.2.1, a parallel study was developed. It was taken into consideration the *Brick+Brick* (Hexa8 elements) and the *Plate with offset+Brick* (Quad4 + offset elements) strategy for spatial model (mentioned in the Figure 3.3 c) and d)). These two strategies were implemented in a sandwich beam with VEM core according to the characteristics presented in the Table 4.1. Noting that the host structure corresponds to the layer 1, the VEM core to layer 2 and the constraining layer to layer 3.

The *Brick+Brick* (Figure 3.3 d)) strategy was implemented following the steps presented in the beginning of this section. For the *Plate with offset + Brick* (Figure 3.3 c)) it was used plate (Quad4) elements to design the layers 1 and 3 and brick (Hexa8) elements to develop the VEM core. The offset was created using the *Update Elements* in the *Modify* menu followed by *Adjust Plate Thickness/offset* tool that was applied into each *quad4* element. The constant value adopted for the offset was half of the thicknesses of layer 1 and 3.

Table 4.1: Characteristics of the sandwich beam to evaluate the combined model strategy.

Dimension	Length	280 mm
	Width	20 mm
	Thickness of layer 1	2 mm
	Thickness of layer 2	0.254 mm
	Thickness of layer 3	2 mm
Aluminium Properties: Layers 1 and 3	Young's Modulus E	70E9 Pa
	Poisson's ratio ν	0.3
	Density ρ	2670 kg/m^3
VEM Properties: Layer 2	3M ISD112 [106]	
Boundary Conditions	free body	

As is going to be further presented in detail, the results show, as expected, that both strategies present similar natural frequencies and loss factor values for each natural mode analysed. This short-version conclusion is being made in this section due to the fact that this preliminary study, combined with the analysed bibliography, helped to decide which spatial model was reasonable to use. Due to the complex geometries that were intended to be further develop, for the analyzed models, the combined model strategy with *Brick+Brick* approach was implemented.

Another developed preliminary study involved the comparison between two different thicknesses for the VEM core. These values were chosen according to literature and what is available commercially. Using the combined models strategy, it was developed a sandwich beam with the characteristics presented in the Table 4.1, and another with the same characteristics, with the exception that the VEM thickness is the double of the one considered before (0.508 mm). The results of this study are presented later in detail. However, to justify the thickness used for each model design, the conclusions taken by this study are here resumed. After evaluating both sandwich beams for the two aforementioned strategies (*Brick+Brick* and *Plate with offset+Brick*, it was realised that increasing the VEM layer thickness to the double decreased the treatments damping effect. Considering this information and considering also the results from the literature on this particular subject, the constant value of 0.254 mm for the VEM thickness was used.

Several models were developed to be used as comparison for the innovative configurations presented in the following sections. To simplify the understanding of each model configuration, it was created a proper terminology presented in the *Nomenclature* section in the beginning of this document. This nomenclature was based on the acronyms used by many authors that were presented on Section 2.2.

The models created for the purpose of comparison include the sandwich beam model aforementioned but with a length of 140 mm (further presented as ILD2 beam). Following the characteristics presented in Table 4.1, several developed plates are presented in the Table 4.2. It is important to note that only the distinctive characteristics and the nomenclature are presented, since all the other characteristics are already mentioned in

the Table 4.1.

Table 4.2: Plates developed for comparison.

Nomenclature	Description	Length x Width
<i>CLD0.25</i>	Constrained layer damping, 2 mm of host structure, 0.25 mm of constrained layer	140 x 140 mm
<i>FLD2</i>	Free layer damping, 2 mm of host structure (layer 3 not applicable)	140 x 140 mm
<i>ILD2</i>	Integrated layer damping, 2 mm of host structure and 2 mm constrained layer	140 x 140 mm
<i>CLD0.5</i>	Constrained layer damping, 0.5 mm of constrained layer	210 x 140 mm
<i>FLD2</i>	Free layer damping, 2 mm of host structure (layer 3 not applicable)	210 x 140 mm
<i>ILD1</i>	Integrated layer damping, 1 mm of host structure and 1 mm constrained layer	210 x 140 mm
<i>Untreated</i>	Plain plate, 2 mm of plate thickness	210 x 140 mm

The first three models presented in Table 4.2 are the plates developed having just in consideration the numerical study. For the experimental study, to avoid double natural modes (two natural modes with the same natural frequency), rectangular specimens were considered and therefore these were also analysed numerically.

4.1.2 1D waves configuration

The first configuration explored was the 1D waves configuration applied on beam-kind structures. The model was designed by a module of 20 x 20 mm that was reproduced along the direction of the wave until the 140 mm of length is achieved, obtaining the final beam with dimensions of 140 x 20 mm. A representation of this module can be observed in Figure 4.1, where it is possible to observe that both host structure and constraining layer have the internal faces waved like the VEM core.

In Figure 4.1, m and n represent the length and width of the module structure, respectively. The parameter h_1 symbolizes the highest thickness of the host structure, h_2 the thickness of the VEM core and h_3 the highest thickness of the constraining layer. Table 4.3 shows the main characteristics of the 1D wave beams developed during this work.

The aforementioned table shows the characteristics of the eight beam-kind structures developed with the 1D wave configuration. The first 1D wave beam developed was the one represented on Figure 4.1, 1 wave per module. As it is possible to deduce, it means that there are 7 waves in the total beam. Then, the frequency of the wave was increased by one wave per module until the last model of 8 waves per module (56 waves in the total beam) was obtained. For the eight analyzed models the wave amplitude was maintained constant, with the value of h_2 .

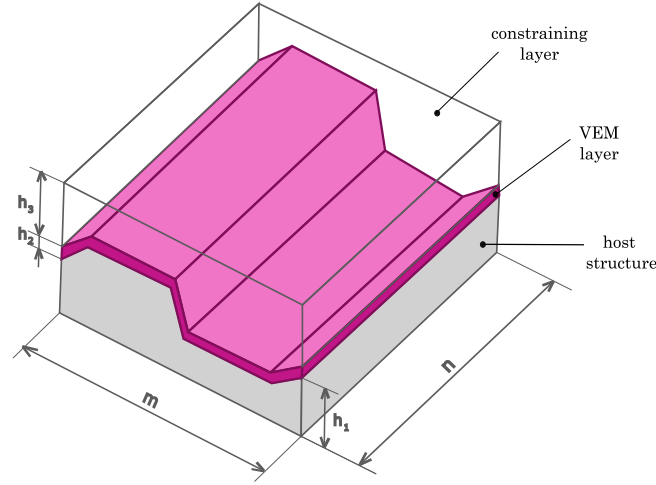


Figure 4.1: 1D waves configuration module representation.

Table 4.3: Characteristics of the developed 1D wave beams.

Dimension	Length	140 mm
	Width	20 mm
	h_1	2 mm
	h_2	0.254 mm
	h_3	2 mm
Aluminium Properties: Layers 1 and 3	Young's Modulus E	70E9 Pa
	Poisson's ratio ν	0.3
	Density ρ	2670 kg/m^3
VEM Properties: Layer 2	3M ISD112 [106]	
Boundary Conditions	free body	

The effect of increasing the waves per module and their comparison with the uniform sandwich beam are shown and discussed later.

4.1.3 2D waves configuration

The 2D waves configuration was applied on plate-kind structures. Similar to the previous configuration, this model was designed primarily by a module of 20 x 20 mm. This module was reproduced along the two directions of the wave until the final plate dimensions of 140 x 140 mm were achieved. A representation of this module can be observed in Figure 4.2. The pink lines represent the waves in both directions, being easier to understand when the model is observed from its sides. Also in this configuration, the host structure and the constraining layer follow the VEM layer, having their internal faces waved.

In the Figure 4.2, m and n represent the length and width of the module structure, respectively. The parameter h_1 symbolizes the mean thickness of the host structure, h_2 the thickness of the VEM core and h_3 the mean thickness of the constraining layer. In

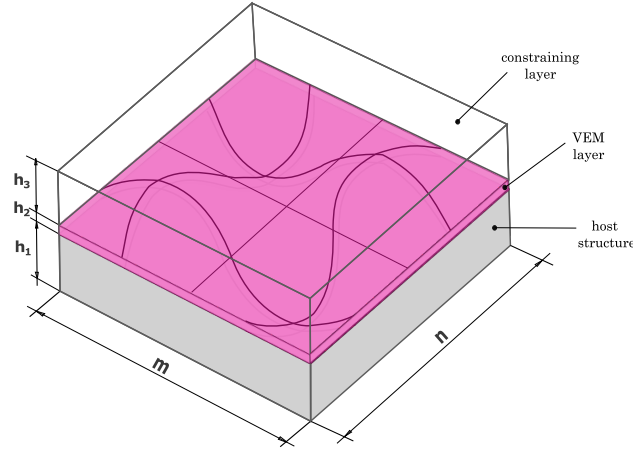


Figure 4.2: 2D waves configuration module representation.

the Table 4.4, it is possible to observe the characteristics of the 2D wave plates developed during this work.

Table 4.4: Characteristics of the developed 2D wave plates.

Dimension	Length	140 mm
	Width	140 mm
	h_1	2 mm
	h_2	0.254 mm
	h_3	2 mm
Aluminium Properties: Layers 1 and 3	Young's Modulus E	70E9 Pa
	Poisson's ratio ν	0.3
	Density ρ	2670 kg/m^3
VEM Properties: Layer 2	3M ISD112 [106]	
Boundary Conditions	free body	

Based on the characteristics provided by the Table 4.4, a study to comprehend the effect of the number of waves on the treatment efficiency and another study to evaluate the effect of the wave amplitude were developed. The number of waves effect on the treatment was tested by two plates with the same amplitude, $A_1=2xh_2$, but with different frequencies. One plate was designed with 0.5 waves per module and the other with 1 wave per module. Regarding the other study, one of these plates (0.5 waves per module and amplitude A_1) was used, along with another with the same frequency but with a wave amplitude of $A_2=h_2$. The results obtained by these studies and its conclusions are shown further in the document.

4.1.4 Interlaced configuration

In this work a new configuration, the Interlaced Layer Damping (ILLD), is proposed and assessed. This configuration is materialized by a three-dimensional layout of stripes of

VEM, possibly combined with stripes of other materials, including stiff materials providing a form of internal constraining effect. This treatment configuration aims to join the benefits of the FLD configuration, namely the simplicity of application, and the damping efficiency usually achieved with the CLD configuration. In the ILLD configuration the VEM layer is highly deformed, increasing the stored energy in it due to the interaction between the VEM stripes (and with the constraining stripes if these are also included in the treatment).

For the purpose of this study, the ILLD configuration was applied on plate-kind structures. Contrarily to the configurations presented above, the interlaced was directly designed with the total 140 x 140 mm plate.

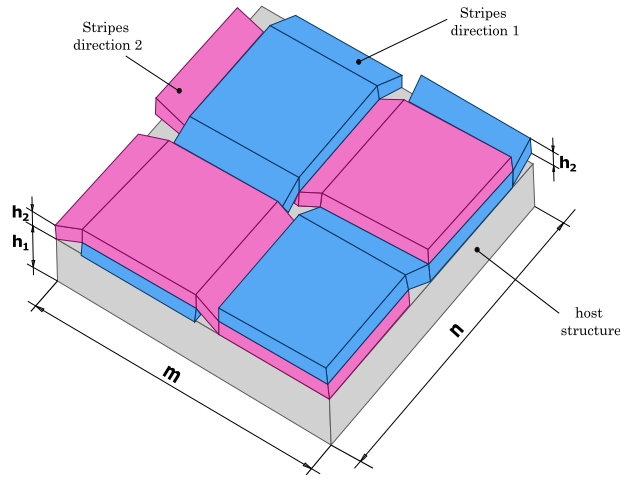


Figure 4.3: Interlaced configuration concept.

A representation of this plate-kind structure is shown in Figure 4.3, which shows two stripes in direction 1 (in blue in the figure) and other two stripes in the other direction (pink in the figure). In contrast with the configurations in the sections 4.1.2 and 4.1.3, the host structure and constraining layer (if applied) are uniform plates with the flat faces. Variables m and n represent the length and width of the plate, respectively. Following the same nomenclature, h_1 symbolizes the thickness of the host structure, h_2 the thickness of the stripes and h_3 the thickness of the constraining layer, if applied.

Several models were designed and analysed by exploring this configuration. The first approach consisted on designing the stripes using the same VEM material in both directions. This strategy was applied on plate structures with and without constraining layer. This approach was studied while using 2 (example shown on Figure 4.3), 4 and 8 stripes per plate in both directions.

In order to take advantage of the simple development and production provided by FLD configuration treatments, the interlaced configuration approaches explored further were based on it. Models using stripes of two different materials, interleaved in both directions, were developed. It is important to note that one of these is always a viscoelastic material (defined as Material 1). The representation of this configuration can be observed in Figure 4.4, where in dark pink are represented the stripes of Material 1 (VEM) and in light pink the stripes of Material 2 (constraining material).

Initially, the combination of VEM stripes (Material 1) with aluminium (Material 2) ones was explored, using the same aluminium as the host structure ($E=70\text{GPa}$). This

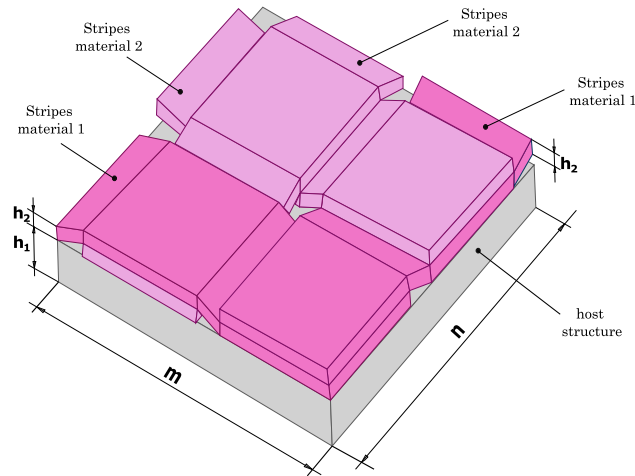


Figure 4.4: Representation of the interlaced configuration using 2 different materials.

approach was developed with 2, 4 and 8 stripes per plate in both directions, which means that there are 1, 2 and 4 stripes of each material in each direction, respectively.

A study was developed to evaluate the effect of the material stiffness of the constraining stripes (Material 2) on the treatment efficiency. Besides the aforementioned model using an aluminium with $E=70\text{GPa}$, models using constraining stripes of materials with Young's modulus of 50, 10 and 1GPa were developed. These approaches were developed with 2 and 4 stripes in both directions.

The last strategy considered was the application of a second layer of interlaced stripes using two materials, VEM and aluminium with a Young's modulus of 70GPa. This strategy was developed following two approaches: one where the second layer has the same disposition as the first layer and another where the second layer presents the stripes, interleaved comparing with the first layer. The representation of this and all the other developed interlaced models, their dimensions and material properties are presented in the Appendix B, in order to clarify the configuration of the developed models.

Table 4.5 presents a summary of all the developed interlaced configurations of plates with 140 x 140 mm, based on the explained strategies. Appendix B contains a visual representation of these configurations.

Table 4.5: Nomenclature of square interlaced models.

Nomenclature	Description	Length x Width
<i>ILD2_IL2</i>	Integrated layer damping, 2 mm of host and constrained layer and 2 interlaced VEM stripes in each direction	140 x 140 mm

Continuation of Table 4.5		
<i>ILD2_IL4</i>	Integrated layer damping, 2 mm of host and constrained layer and 4 interlaced VEM stripes in each direction	140 x 140 mm
<i>ILD2_IL8</i>	Integrated layer damping, 2 mm of host and constrained layer and 8 interlaced VEM stripes in each direction	140 x 140 mm
<i>CLD0.25_IL2</i>	Constrained layer damping, 0.25 mm of constraining layer and 2 interlaced VEM stripes in each direction	140 x 140 mm
<i>FLD2_IL2</i>	Free layer damping, 2 mm of host structure and 2 interlaced VEM stripes in each direction	140 x 140 mm
<i>FLD2_IL4</i>	Free layer damping, 2 mm of host structure and 4 interlaced VEM stripes in each direction	140 x 140 mm
<i>FLD2_IL2_C70</i>	Free layer damping, 2 mm of host structure and 2 interlaced stripes of VEM and an E=70GPa material	140 x 140 mm
<i>FLD2_IL4_C70</i>	Free layer damping, 2 mm of host structure and 4 interlaced stripes of VEM and an E=70GPa material	140 x 140 mm
<i>FLD2_IL8_C70</i>	Free layer damping, 2 mm of host structure and 8 interlaced stripes of VEM and an E=70GPa material	140 x 140 mm
<i>FLD2_IL2_C50</i>	Free layer damping, 2 mm of host structure and 2 interlaced stripes of VEM and an E=50GPa material	140 x 140 mm
<i>FLD2_IL4_C50</i>	Free layer damping, 2 mm of host structure and 4 interlaced stripes of VEM and an E=50GPa material	140 x 140 mm
<i>FLD2_IL2_C10</i>	Free layer damping, 2 mm of host structure and 2 interlaced stripes of VEM and an E=10GPa material	140 x 140 mm

Continuation of Table 4.5		
<i>FLD2_IL4_C10</i>	Free layer damping, 2 mm of host structure and 4 interlaced stripes of VEM and an E=10GPa material	140 x 140 mm
<i>FLD2_IL2_C1</i>	Free layer damping, 2 mm of host structure and 2 interlaced stripes of VEM and an E=1GPa material	140 x 140 mm
<i>FLD2_IL4_C1</i>	Free layer damping, 2 mm of host structure and 4 interlaced stripes of VEM and an E=1GPa material	140 x 140 mm
<i>FLD2_IL2_C70_2a</i>	Free layer damping, 2 mm of host structure and double layer of 2 interlaced stripes of VEM and an E=70GPa material	140 x 140 mm
<i>FLD2_IL4_C70_2a</i>	Free layer damping, 2 mm of host structure and double layer of 4 interlaced stripes of VEM and an E=70GPa material	140 x 140 mm
<i>FLD2_IL8_C70_2a</i>	Free layer damping, 2 mm of host structure and double layer of 8 interlaced stripes of VEM and an E=70GPa material	140 x 140 mm
<i>FLD2_IL2_C70_2b</i>	Free layer damping, 2 mm of host structure and double layer interleaved of 2 interlaced stripes of VEM and an E=70GPa material	140 x 140 mm
<i>FLD2_IL4_C70_2b</i>	Free layer damping, 2 mm of host structure and double layer interleaved of 4 interlaced stripes of VEM and an E=70GPa material	140 x 140 mm
<i>FLD2_IL8_C70_2b</i>	Free layer damping, 2 mm of host structure and double layer interleaved of 8 interlaced stripes of VEM and an E=70GPa material	140 x 140 mm

As previously explained, to prepare the experimental study, rectangular plate models were developed. These models are presented in the Table 4.6. As it is possible to observe, the nomenclature *IL2* represents 2 interlaced stripes in each direction in a 140 x 140

mm plate, which means that in the 210 x 140 mm plate there are 3 stripes lengthwise and 2 stripes widthwise. To clarify the perception of these four models, a diagram is presented in Figure 4.5. As before, the dark pink stripes represent the Material 1, VEM, and the light pink stripes represent the Material 2, Aluminium with a Young's modulus of 70GPa, for these plates. The properties of both materials are the same as for the models mentioned in previous sections (Table 4.4).

Table 4.6: Nomenclature of rectangular interlaced models.

Nomenclature	Description	Length x Width
<i>CLD0.5_IL2</i>	Constrained layer damping, 0.5 mm of constraining layer and 2 interlaced VEM stripes in each direction	210 x 140 mm
<i>FLD2_IL2_C70</i>	Free layer damping, 2 mm of host structure and 2 interlaced stripes of VEM and an E=70GPa material	210 x 140 mm
<i>FLD2_IL2_C70_2b</i>	Free layer damping, 2 mm of host structure and double layer interleaved of 2 interlaced stripes of VEM and an E=70GPa material	210 x 140 mm

4.1.5 Postprocessing

For all the models presented during the previous sections, a methodology to obtain the modal loss factor for each treatment was proposed, based on the MSE method, in order to provide a logical comparison between different passive damping treatment strategies. An analysis in the frequency domain was applied, where it is possible to include a modal analysis. For the set of treatments proposed, the MSE method was applied as a ratio between energies: the energy that is lost and the total strain energy. The loss factor of the structure depends directly on the lost energy and because of this an adopted strategy is to quantify the energy stored having in consideration that the lost energy is part of it. It is possible to consider that the lost energy is the one lost by the VEM layer/stripes. This assumption is reasonable because the lost energy of the other materials is considerably low, due to the fact that these materials loss factor is approximately zero.

To summarize, the treatment loss factor based on the MSE method can be obtained by the ratio between the strain energy of VEM times the loss factor of VEM, and the total strain energy of the structure. For this work, the loss factor of VEM is considered to be 1, which means that all the energy that is stored by the VEM layer/stripes is lost.

For the purpose of this study, where the idea is to compare spatial models solutions, the main focus is to maximize the strain energy of the viscoelastic layer since the lost energy is part of it.

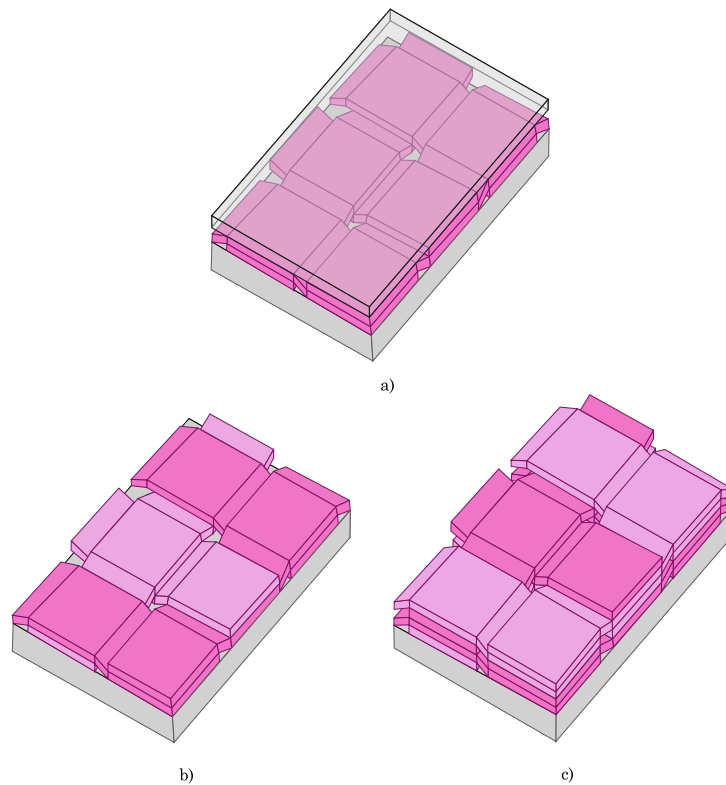


Figure 4.5: Representation of the interlaced rectangular plates: a) CLD0.5_IL2; b) FLD2_IL2_C70 and c) FLD2_IL2_C70_2b.

After running the analyses on *NX Nastran* [104, 107], a file containing the modal strain energy for each element was exported. The first five natural modes were evaluated for each developed treatment. The five files for each treatment were imported into *Matlab*, where a simple code was developed to allow the calculation of the modal loss factor of the structure. The codes created for treatments with only one core material (VEM) and treatments where a second material was applied (interlaced configuration treatments using 2 different materials) can be found in Appendix C.

The results provided by the developed *Matlab* codes and the natural frequencies for each treatment provided by the software *NX Nastran* were listed and compared using *Microsoft Excel*. These results are presented in Chapter 5, Numerical Results, along with the contour modal strain energy for each treatment.

4.2 Experimental study

This experimental study section describes the methodology that allowed obtaining the experimental results for a set of specimens. Initially, the configurations experimentally analysed are presented. Then, the experimental setup used for the analyses for each specimen can be observed, and finally the methods used to evaluate the results in the experimental modal analysis are described.

4.2.1 Experimental Specimens

Based on the numerical results and the resources provided a set of configurations to validate experimentally by an experimental modal analysis was defined. The set of specimens are divided by groups to allow an easier perception of the analysed configurations and a logical comparison between them. The FLD group of specimens is presented on Figure 4.6, where the VEM material plate/stripes is represented in dark pink and the aluminium stripes in light pink. The host structure is shown in grey.

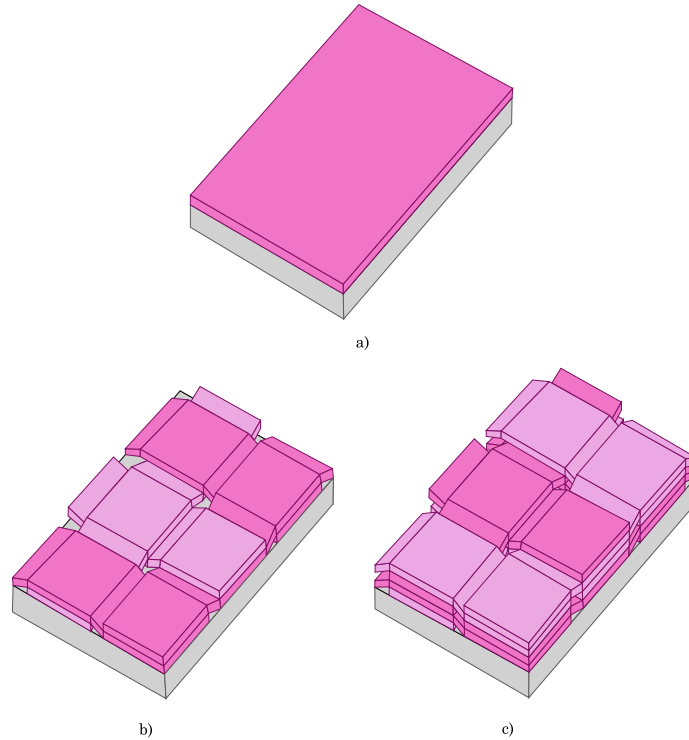


Figure 4.6: Representation of the FLD rectangular plates: a) FLD2; b) FLD2_IL2_C70 and c) FLD2_IL2_C70_2b.

The characteristics for this set of specimens can be observed in Table 4.7. Similarly to before, h_1 represents the host structure thickness and h_2 the thickness of both layer 2 (VEM layer in FLD2), VEM and aluminium stripes. $M1$ means Material 1 (dark pink stripes), that for this study is VEM, and $M2$ Material 2 (light pink stripes) and is the aluminium presented in the table.

The stripes were cut with the dimensions above listed and assembled with the configuration of the Figure 4.6. The Figure 4.7 shows the specimens without constraining layer performed in the laboratory for the experimental study.

The Figure 4.8 presents the CLD group of experimental specimens, where in pink is represented the VEM layer/stripes, in grey the host structure and on top, in grey with reduced opacity, is represented the constraining layer.

The two CLD specimens follow the characteristics showed on Table 4.8. As before, h_2 represents the thickness of the layer 2/stripes. However, this set of specimens has different values, that are presented in the Table 4.8. Layer 1 and 3 are the host structure and constraining layer, respectively. Layer 2 represents the core in the CLD0.5 specimen.

Table 4.7: Characteristics of the FLD experimental specimens.

Dimension	Total Length	210 mm
	Total Width	140 mm
	Stripes Width	67.5 mm
	h_1	2 mm
	h_2	0.5 mm
Aluminium Properties: Layer 1 and Stripes M2	AW5754-H111	
VEM Properties: Layer 2/ Stripes M1	3M ISD112 [106]	
Boundary Conditions	free body	

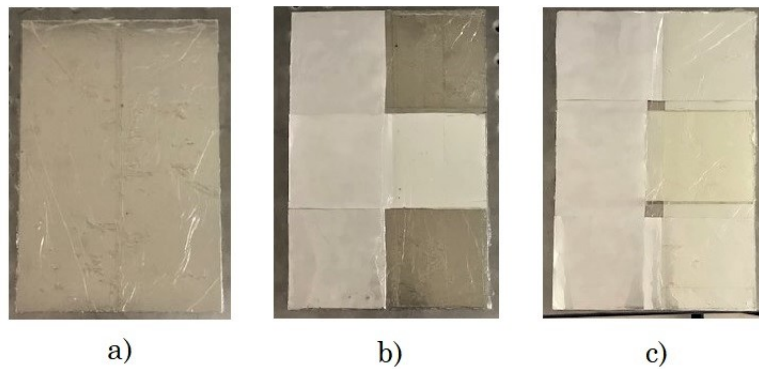


Figure 4.7: Experimental FLD specimens: a) FLD2; b) FLD2_IL2.C70 and c) FLD2_IL2_C70_2b.

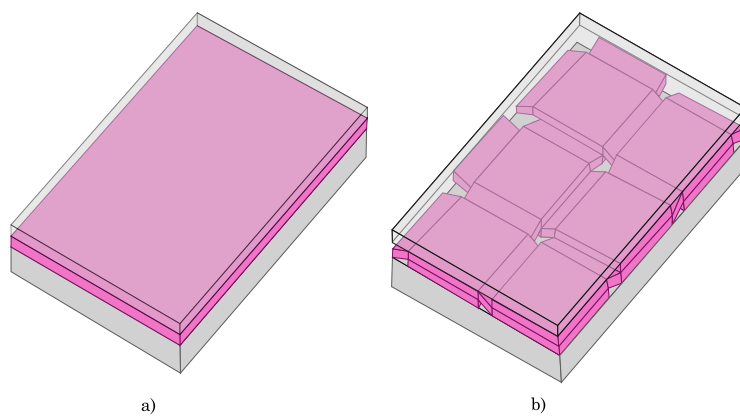


Figure 4.8: Representation of the CLD rectangular plates: a) CLD0.5 and b) CLD0.5_IL2.

Figure 4.9 shows the specimens with constraining layer prepared in the laboratory for the experimental study. These specimens were developed by a similar process to the

Table 4.8: Characteristics of the CLD experimental specimens.

Dimension	Total Length	210 mm
	Total Width	140 mm
	Stripes Width	67.5 mm
	h_1	2 mm
	h_2	a)0.254 mm ; b) 0.5 mm
	h_3	0.5 mm
Aluminium Properties: Layer 1 and Layer 3	AW5754-H111	
VEM Properties: Layer 2/ Stripes	3M ISD112 [106]	
Boundary Conditions	free body	

aforementioned one.

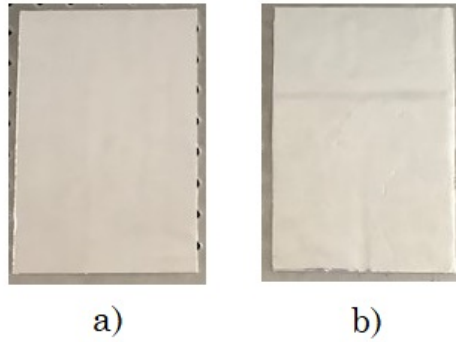


Figure 4.9: Experimental CLD specimens: a) CLD0.5 and b) CLD0.5_IL2.

Figure 4.10 presents the ILD1 specimen that serves as reference treatment for future comparison. As for the CLD specimens, pink represents the VEM layer, grey the host structure and on top, in grey with reduced opacity, is represented the constraining layer.

The ILD1 specimen follows the characteristics showed on Table 4.9, where layer 1 represents the host structure, layer 2 the core and layer 3 the constraining layer.

Figure 4.11 shows the specimen with integrated layer prepared in the laboratory for the experimental study.

The last group of experimental specimens can be observed in Figure 4.12, where a module of 20 x 20 mm is representative of the beam that is obtained by reproducing this module along the length direction (or in the wave direction for the ILD2.1D). The used 1D configuration beam was in fact the one with 4 waves per module, ILD2.1D.4. However, with the Figure 4.12 b), that represents 1 wave per module, it is possible to understand how is the model analysed, picturing it with 4 waves instead of 1 per module. In the figure, the host structure is shown in opaque grey, the VEM core in pink and the constraining layer on top in transparency with grey outlines.

The beam set of specimens follows the characteristics shown on Table 4.10, where

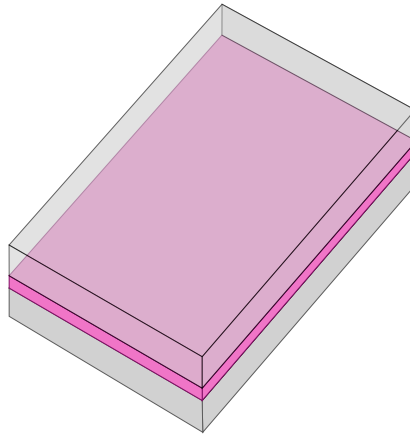


Figure 4.10: Representation of the ILD1 rectangular plate.

Table 4.9: Characteristics of the ILD1 experimental specimen.

Dimension	Total Length	210 mm
	Total Width	140 mm
	h_1	1 mm
	h_2	0.254 mm
	h_3	1 mm
Aluminium Properties: Layer 1 and Layer 3	AW5754-H111	
VEM Properties: Layer 2	3M ISD112 [106]	
Boundary Conditions	free body	

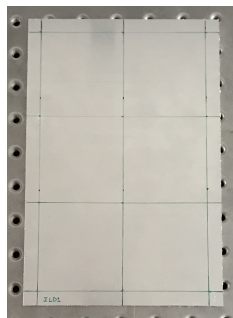


Figure 4.11: Experimental ILD1 specimen.

layer 1 represents the host structure, layer 2 the core and layer 3 the constraining layer.

Figure 4.13 shows the specimens with constraining layer prepared in the laboratory for the experimental study.

The experimental ILD2_1D_4 beam specimen was prepared using copper wires with 0.5 mm of diameter, spaced 5 mm between each other. This set of wires were placed on top of the host structure with the help of tape, to straight the wires as much as

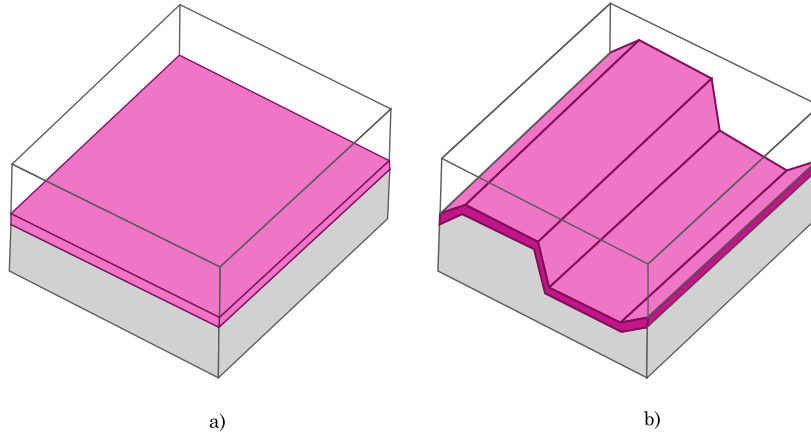


Figure 4.12: Representation of the 20 x 20 mm modules for 140 x 20 mm beams: a) ILD2 and b) ILD2_1D.

Table 4.10: Characteristics of the beam experimental specimens.

Dimension	Total Length	140 mm
	Total Width	20 mm
	h_1	2 mm
	h_2	0.254 mm
	h_3	2 mm
Aluminium Properties: Layer 1 and Layer 3	AW5754-H111	
VEM Properties: Layer 2	3M ISD112 [106]	
Boundary Conditions	free body	

possible. After this step, a layer of VEM was placed on top, due to the configuration of this material it was possible to fix the next layer of copper wires interleaved with the ones under to create the wave effect into the VEM layer. Figure 4.14 shows the setup of this specimen during the second wire layer phase. Then, the constraining layer was placed on top to finalize the sandwich beam. Finally, the excess of wires in the sides was cut to obtain the final result previously shown on Figure 4.13.

4.2.2 Experimental Setup

An experimental modal analysis was performed to experimentally validate the optimization procedure based on the modal strain energy for the FLD2_IL_C70, FLD2_IL_C70_2b, CLD0.5_IL2, ILD2_1D_4 and for the reference models, the Plain plate, FLD2, CLD0.5, ILD1 and ILD2 beam. With these analysis the natural frequencies, mode shapes and the modal loss factor for each specimen was obtained.

The size and geometry of the specimens are decisive factors for choosing how to excite it. The two most common technologies are the impact hammer testing and the

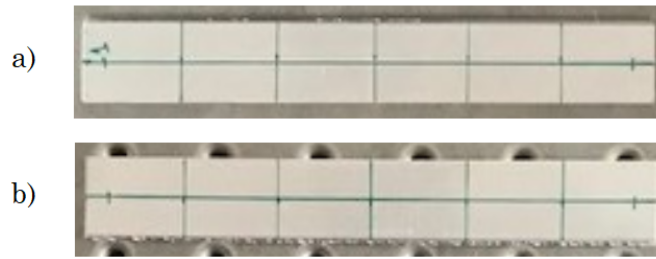


Figure 4.13: Experimental beam specimens: a) ILD2 and b) ILD2_1D_4.

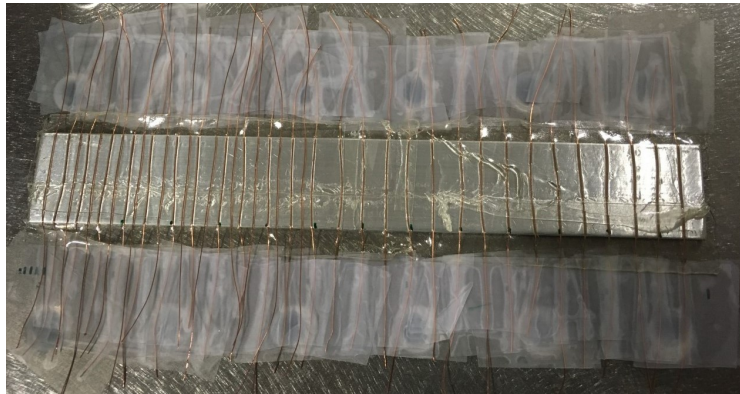


Figure 4.14: Experimental ILD2_1D_4 beam specimen during the phase of assembly.

shaker testing. For the experimental modal analysis of this work the impact hammer testing was used.

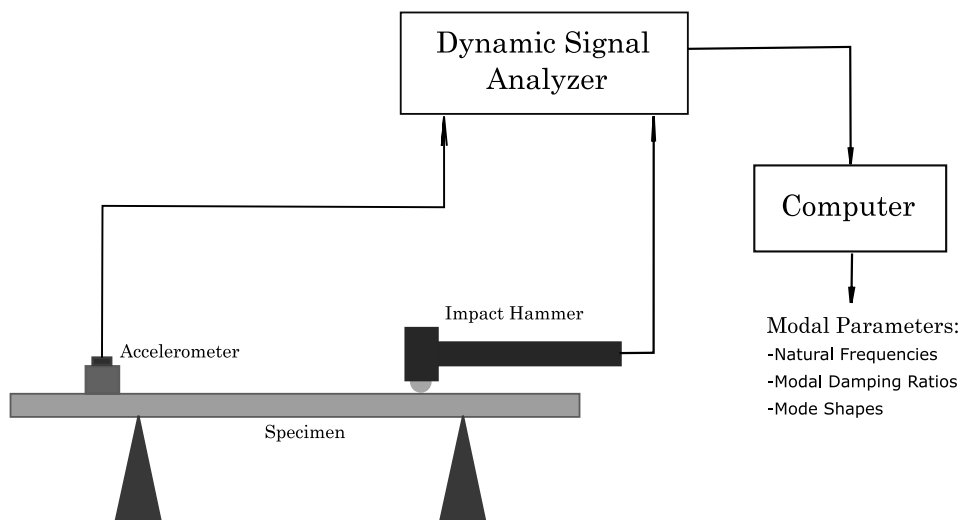


Figure 4.15: Experimental Setup.

In Figure 4.15 is shown the scheme of the setup used for these set of analysis. The plate specimens were supported by three prismatic blocks of soft foam (Figure 4.16) and the beam specimens were suspended using the extremity point (Figure 4.17), in order to

make the experimental boundary conditions close to the theoretical free body conditions considered in the Finite Element simulation.

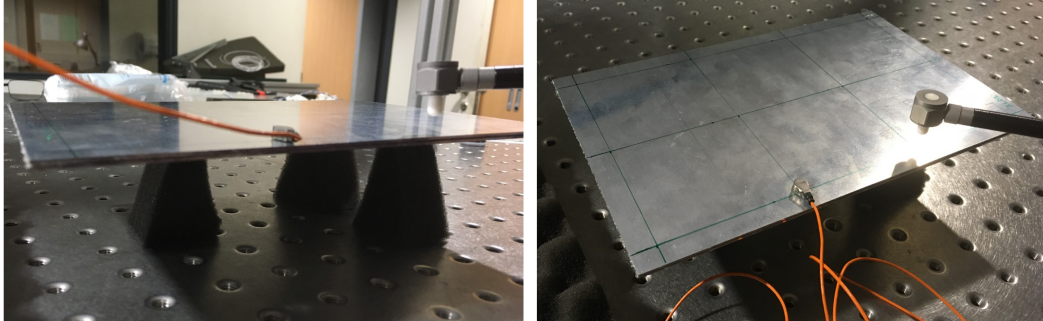


Figure 4.16: Experimental Setup for the plate specimens.

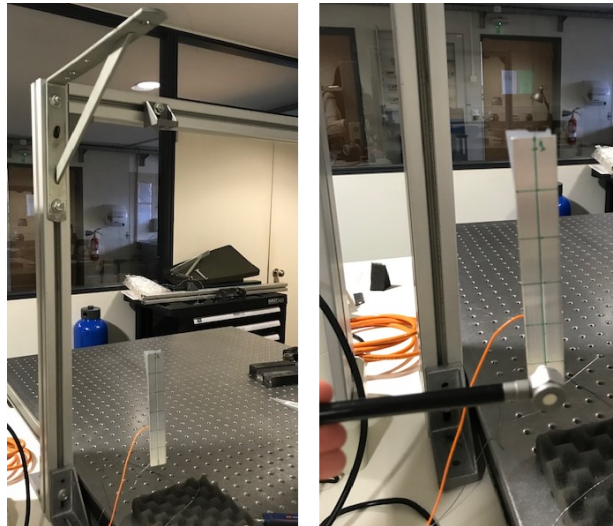


Figure 4.17: Experimental Setup for the beam specimens.

A measuring mesh of 12 points was devised for each plate specimen, as shown in Figure 4.18a. The point number 4 represents the reference measurement point. For the beam specimens a linear mesh with 7 points was defined, as shown in Figure 4.18b. The point number 5 represents the reference measurement point for the beam specimens.

In the Figure 4.15, it is possible to observe that the excitation equipment adopted for these analysis was the *impact hammer*, which is normally applied manually. It is a reasonable solution to excite small and light structures, easy to use and transport, and its cost is low compared to other equipment [108].

A DJB IH/01-50 miniature impact hammer was utilized to provide the excitation to each of the 12 measuring mesh points for the plate specimens, and 7 points for the beam specimens, applying a hammer roving technique. The specimen acceleration response to this excitation was measured at point number 4 for the plate specimens, and number 5 for the beam specimens, using a DYTRAN 3225F miniature IEPE (Integrated Electronics

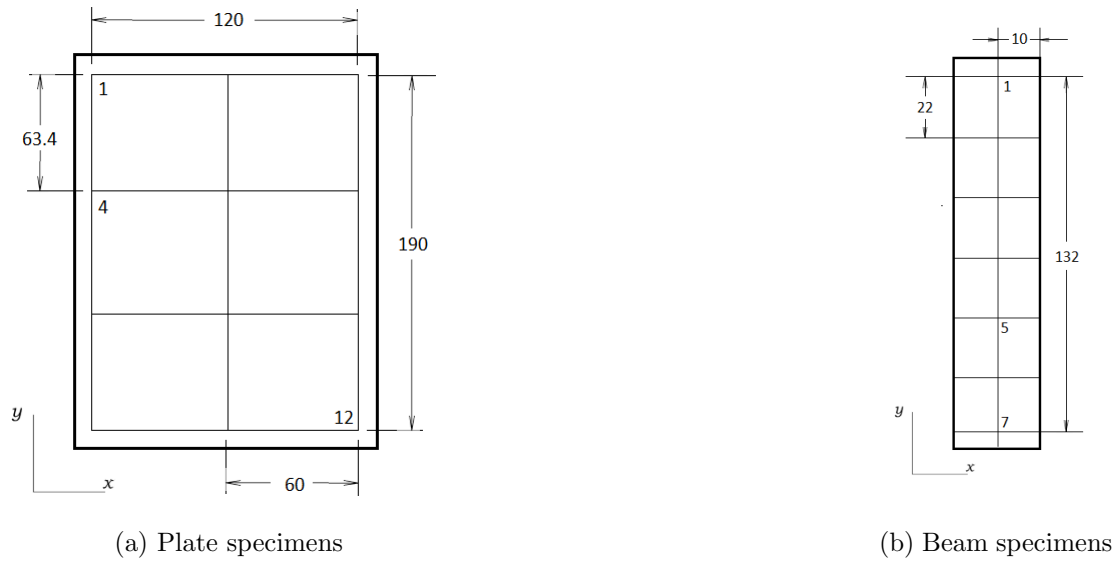


Figure 4.18: Measuring mesh.

Piezo-Electric) accelerometer attached using bee wax. Being IEPE transducers, the accelerometer and the impact hammer were connected directly to the analyzer without extra signal conditioning. The excitation and the response signals provided by the impact hammer and accelerometer, respectively, were conditioned and analysed using a spectral analyser (DSPT Siglab 2042), that has an internal DSP processor capable to perform all the required signal analysis towards the calculation of the set of Frequency Response Functions for both specimen configurations. Therefore, the *Frequency Response Function* (FRF) is obtained, one for each excited point, meaning there are 12 for each plate specimen and 7 for each beam specimen. The parameters estimation by FRF curve fitting is performed in the *Computer* step shown on Figure 4.15. This last phase of the process is shown in the next section, where the methods used to obtain the modal parameters are presented and explained.

4.2.3 Experimental modal analysis

The performance of an experimental modal analysis allows obtaining the modal parameters for each specimen. The modal parameters, as shown on Figure 4.15, correspond to the natural frequencies, modal damping ratios and respective mode shapes within the frequency range [0–1000Hz] considered in the measuring process. Therefore, modal identification procedures were used to accomplish this goal. The identification process was assisted by two different methods, the X-Modal 3 package, from SDRL, using the Polyreference Least-Squares Complex Frequency-Domain identification algorithm (hereby identified as PolyMAX), and the *Circle Fit* method, developed on *Matlab*.

The *X-Modal 3* method, uses a multiple degree of freedom (MDOF) model to identify the modal parameters.

The first step consisted on selecting the measured FRFs to be analyzed and setting the frequency range of analysis. Then, the software created a visual guide, called a stabilization diagram. The stabilization diagram allowed the identification of potential

modes. After selecting the best set of potential modes, the mode shapes that are listed by the software were calculated. After obtaining the results, the validation step was performed. Two commonly used validation methods are: *Modal Synthesis* and *Modal Assurance Criterion* (MAC) [109].

The *Modal Synthesis* method allows the identification of the modes that might have been missed. In this method the FRFs can be synthesized and compared against the originally measured FRFs. A correlation and error percentage are calculated, allowing the identification of the missing modes.

The Modal Assurance Criterion (MAC) method is based on the analysis of mode shapes similarity, i.e. the criterion shall provide a value of 100% when a mode shape is compared to itself and zero when compared to the remaining ones. Experimentally this tool can provide valid information on if the used measurement mesh is detailed enough to represent the mode shape being identified [110].

The other method, *Circle Fit*, is one of the existing single degree of freedom (SDOF) methods [4]. The basis behind the performance of this method is presented along the Appendix D. The procedure to obtain the modal parameters using the Circle Fit method developed on *Matlab* is presented in this section.

The Circle Fit analysis procedure developed on *Matlab*, starts by running the file that contains the FRF (previously converted to a Receptance) related to one of the excited points. A window related to this file opens allowing the user to select a frequency range around each resonance. Since this set of points contain the resonance peak, it shall describe a circular distribution, providing the data required to fit the parameters defining a circle equation. In the end of this part the circle radius and center is determined, as well as the quality factor, which is the mean square deviation of the chosen points from the circle [4]. If the choice was satisfactory, the natural frequency is located and the loss factor for that natural mode is obtained. The process is repeated for the remaining peaks found in the FRF due to the fact that this method is performed for each mode individually. Analysing this file the natural frequencies and loss factors for the natural modes found in the FRF for one of the measured points are obtainable. This process has now to be performed for all the other measured frequency response functions, which means 12 times in total for each plate specimen and 7 times in total for each beam specimen. Finally, it is necessary to calculate a mean value from the identified values to get an approximate value for the natural frequency and corresponding modal loss factor for each natural mode.

For this work it was decided to use two different experimental modal analysis methods, in order to have a better reference for comparison with the numerical study. The experimental results are going to be presented and discussed in chapters 6 and 7, respectively.

Chapter 5

Numerical Results

In this chapter, the numerical results for the developed models are presented. For the beam-kind models, the numerical results are presented for the first four natural modes. For the plate-kind models, they are presented for the first five natural modes. It is important to note that the modal strain energy distributions shown in this document are limited to the VEM layer or stripes, i.e. the modal strain energy of the host structure and constraining layer and stripes is omitted in these representations.

5.1 Preliminary Numerical Results

5.1.1 Combined model approach

In Table 5.1 it is possible to observe the natural frequencies and modal loss factors for the two analysed combined model approaches, respectively.

Table 5.1: Natural frequencies and modal loss factor for the developed combined model approaches.

combined model approach	Natural frequencies [Hz]			
	mode 1	mode 2	mode 3	mode 4
<i>Brick+Brick</i>	161.154	387.783	738.843	1059.496
<i>Plate with offset +Brick</i>	161.134	387.679	738.179	1079.894

combined model approach	Loss Factor [%]			
	mode 1	mode 2	mode 3	mode 4
<i>Brick+Brick</i>	28.33	11.44	6.32	00.76
<i>Plate with offset +Brick</i>	28.31	11.43	6.33	00.41

5.1.2 VEM thickness

In this section, it is presented the natural frequencies and the mass normalized loss factors for the *Brick+Brick* (Table 5.2) and for the *Plate with offset +Brick* approach (Table 5.3), analysing two different VEM (layer 2) thicknesses.

The VEM layer mass varies when its thickness changes. Therefore, for these models, the loss factor obtained by the MSE method was divided by the VEM mass in order to obtain a mass normalized loss factor indicator for each specimen, providing information on the treatment efficiency based on the amount of VEM used. This indicator also allows a proper analysis of the models having into consideration the added mass.

Table 5.2: Natural frequencies and normalized loss factor for the Brick+Brick approach with two different VEM thicknesses.

Brick+Brick	Natural frequencies [Hz]			
h_2	mode 1	mode 2	mode 3	mode 4
<i>0.254mm</i>	161.154	387.783	738.843	1059.496
<i>0.508mm</i>	150.296	374.858	721.493	1039.703

	Normalized Loss Factor [1/kg]			
h_2	mode 1	mode 2	mode 3	mode 4
<i>0.254mm</i>	19.92	8.04	4.44	0.53
<i>0.508mm</i>	7.99	2.70	1.43	0.42

Table 5.3: Natural frequency values for the Plate with offset+Brick approach with two different VEM thicknesses.

Plate with offset +Brick	Natural Frequencies [Hz]			
h_2	mode 1	mode 2	mode 3	mode 4
<i>0.254mm</i>	161.134	387.679	738.179	1079.894
<i>0.508mm</i>	150.338	374.851	720.965	1060.243

	Normalized Loss Factor [1/kg]			
h_2	mode 1	mode 2	mode 3	mode 4
<i>0.254mm</i>	19.90	8.04	4.45	0.29
<i>0.508mm</i>	8.00	2.70	1.44	0.07

5.2 Beam-kind models

In this section, the results obtained for the analysed beam-kind models are presented. The finite element method was used to determine the mode shapes (Figure 5.1) and the VEM modal strain energy distribution (Table 5.4) for the developed beam-kind models. The four mode shapes correspond to the first order bending mode, the second order bending mode, the first order torsion mode and the third order bending mode, respectively.

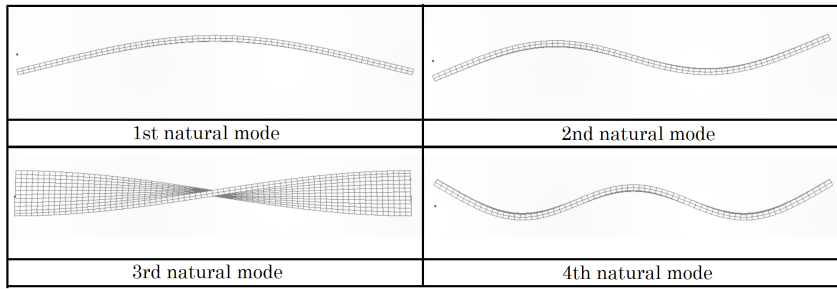


Figure 5.1: Mode shapes of the first four natural modes of the sandwich beam.

Table 5.4: Distribution of the modal strain energy (1^{st} mode) for the beam models developed with free boundary conditions.

1^{st} natural mode		
Nomenc.	Top View 	Bottom View
<i>ILD2</i>		
<i>ILD2_1D_1</i>		
<i>ILD2_1D_2</i>		
<i>ILD2_1D_3</i>		
<i>ILD2_1D_4</i>		
<i>ILD2_1D_5</i>		
<i>ILD2_1D_6</i>		

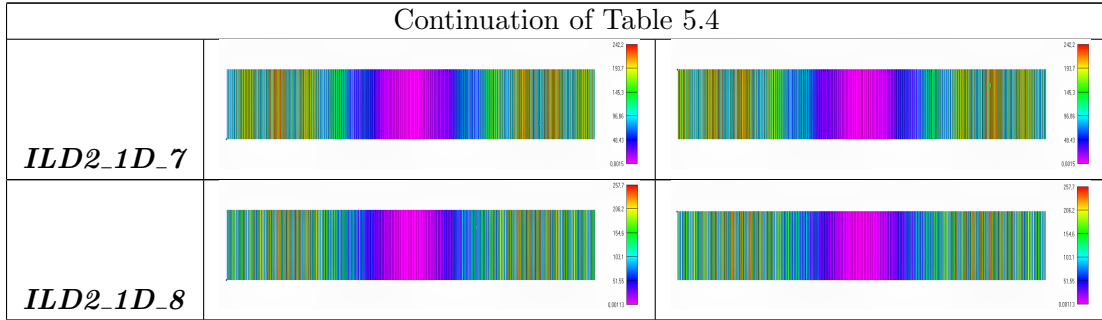


Table 5.4 only presents the modal strain energy distribution for the first natural mode, whereas the one for the remaining natural modes can be observed on the section *Beam-kind models* of Appendix E. Table 5.5 presents the natural frequencies and normalized loss factor for all the developed beam-kind models.

Table 5.5: Natural frequencies and normalized loss factor for the developed beam-kind models.

Nomenclature	Natural Frequencies [Hz]			
	mode 1	mode 2	mode 3	mode 4
<i>ILD2</i>	562.829	1480.620	2110.582	2884.231
<i>ILD2_1D_1</i>	496.122	1232.028	1864.142	2370.549
<i>ILD2_1D_2</i>	513.364	1230.060	1835.901	2344.45
<i>ILD2_1D_3</i>	520.066	1215.066	1782.224	2299.064
<i>ILD2_1D_4</i>	553.980	1239.743	1758.618	2309.859
<i>ILD2_1D_5</i>	584.324	1269.955	1741.149	2334.641
<i>ILD2_1D_6</i>	623.866	1319.684	1739.053	2385.803
<i>ILD2_1D_7</i>	630.421	1365.118	1817.758	2499.275
<i>ILD2_1D_8</i>	686.628	1445.367	1838.996	2587.732

Nomenclature	Normalized loss Factor [%]			
	mode 1	mode 2	mode 3	mode 4
<i>ILD2</i>	163.10	47.24	47.95	24.89
<i>ILD2_1D_1</i>	302.23	104.71	31.11	57.22
<i>ILD2_1D_2</i>	349.39	136.04	34.54	75.54
<i>ILD2_1D_3</i>	355.04	150.02	36.56	84.70
<i>ILD2_1D_4</i>	405.42	203.28	48.38	118.87
<i>ILD2_1D_5</i>	420.50	241.53	59.93	145.98
<i>ILD2_1D_6</i>	433.11	292.07	78.29	184.42
<i>ILD2_1D_7</i>	428.05	262.11	69.86	160.51
<i>ILD2_1D_8</i>	450.59	343.56	101.23	224.36

5.3 Plate-kind models

In this section, the results obtained for the developed plate-kind models are presented. In order to organize the section, it was divided in two subsections, one that presents the

results for the square plates (140 x 140 mm) and another for the rectangular plates (210 x 140 mm).

5.3.1 Square plate models

The mode shapes for the square plate models (Figure 5.2) were determined by the Finite Element Method implemented in the *SIEMENS NX.Nastran* software

The first modal strain energy distribution for each treatment is presented throughout this section, while the other modes are presented in the Appendix E.

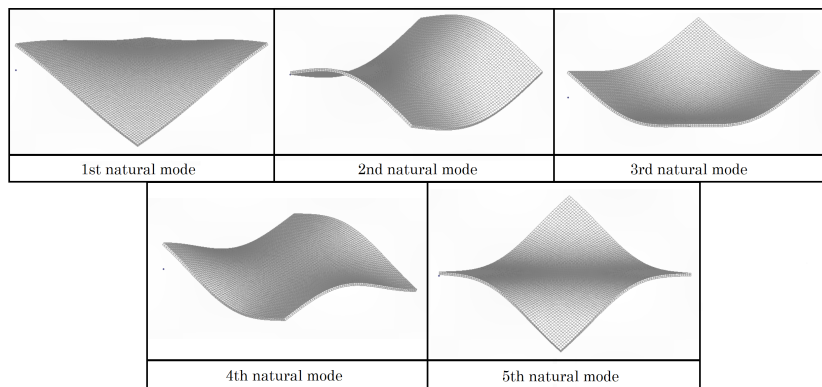


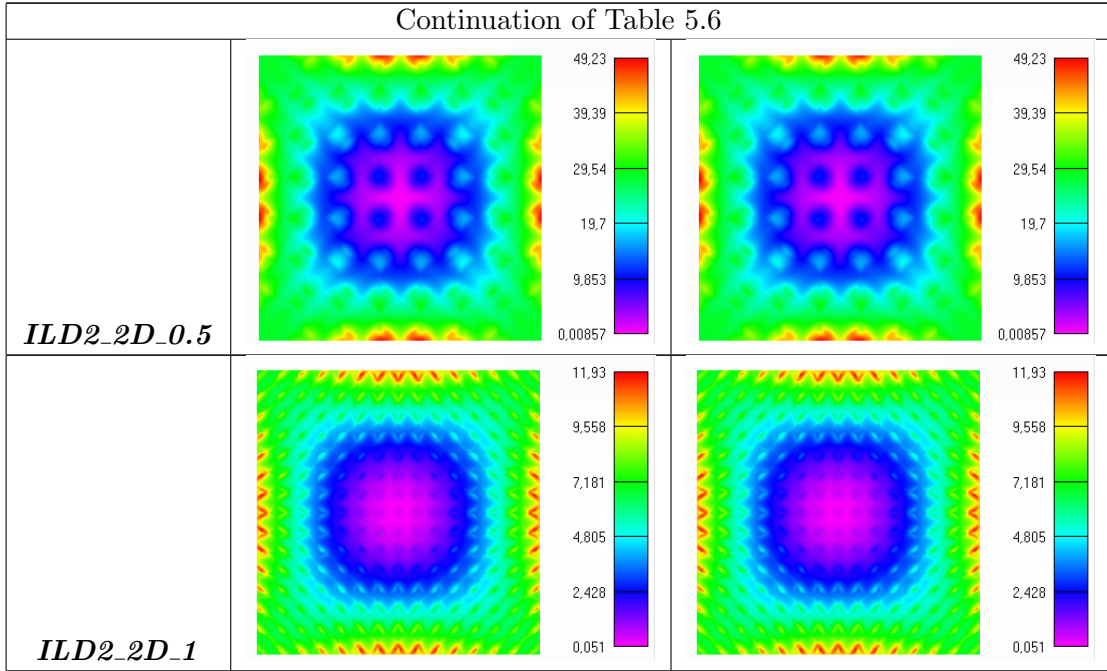
Figure 5.2: Mode shapes of the first five natural modes of the aluminium square plate.

2D wave models

The numerical results for the 2D wave models are herein presented and listed with the ILD2 model as reference. In the Table 5.6 can be observed the strain energy distribution for the first natural mode of the 2D wave treatments and the reference treatment for this set, ILD2.

Table 5.6: Distribution of the modal strain energy (1st mode) for the 2D wave models developed with free boundary conditions.

1 st natural mode		
Nomenc.	Top View 	Bottom View
<i>ILD2</i>		



Following the same organization applied in the presentation of the results for the beam results, the modal strain energy distribution for the other natural modes can be found in Appendix E.

Table 5.7 shows the natural frequencies and the modal loss factor for the 2D waves treatments developed with an amplitude of $2 \times h_2$, denominated as A_1 , and for the reference ILD treatment. The parameter h_2 represents the VEM layer thickness.

Table 5.7: Natural frequencies and loss factor for the 2D wave models with amplitude A_1 .

$A_1 = 2 \times h_2$		Natural Frequencies [Hz]				
Nomenclature	mode 1	mode 2	mode 3	mode 4	mode 5	
<i>ILD2</i>	356.161	523.016	629.668	882.621	882.621	
<i>ILD2_2D_0.5</i>	281.406	414.398	485.736	686.042	686.073	
<i>ILD2_2D_1</i>	279.828	413.663	478.704	678.075	678.099	

Loss Factor [%]					
Nomenclature	mode 1	mode 2	mode 3	mode 4	mode 5
<i>ILD2</i>	12.50	13.68	9.10	5.75	5.75
<i>ILD2_2D_0.5</i>	17.14	17.82	14.99	9.60	9.60
<i>ILD2_2D_1</i>	17.06	18.50	14.51	8.78	8.78

The treatment natural frequency and loss factor effect of decreasing the 2D waves amplitude to half is presented in Table 5.8. The number of waves was maintained constant for both treatments with the value of 0.5 waves per module.

Table 5.8: Natural frequencies and loss factor for the ILD2_2D_0.5 model with two different amplitudes.

<i>ILD2_2D_0.5</i>		Natural Frequencies [Hz]				
Amplitude	mode 1	mode 2	mode 3	mode 4	mode 5	
A_1	281.406	414.398	485.736	686.042	686.073	
A_2	316.225	465.359	555.384	778.603	778.609	

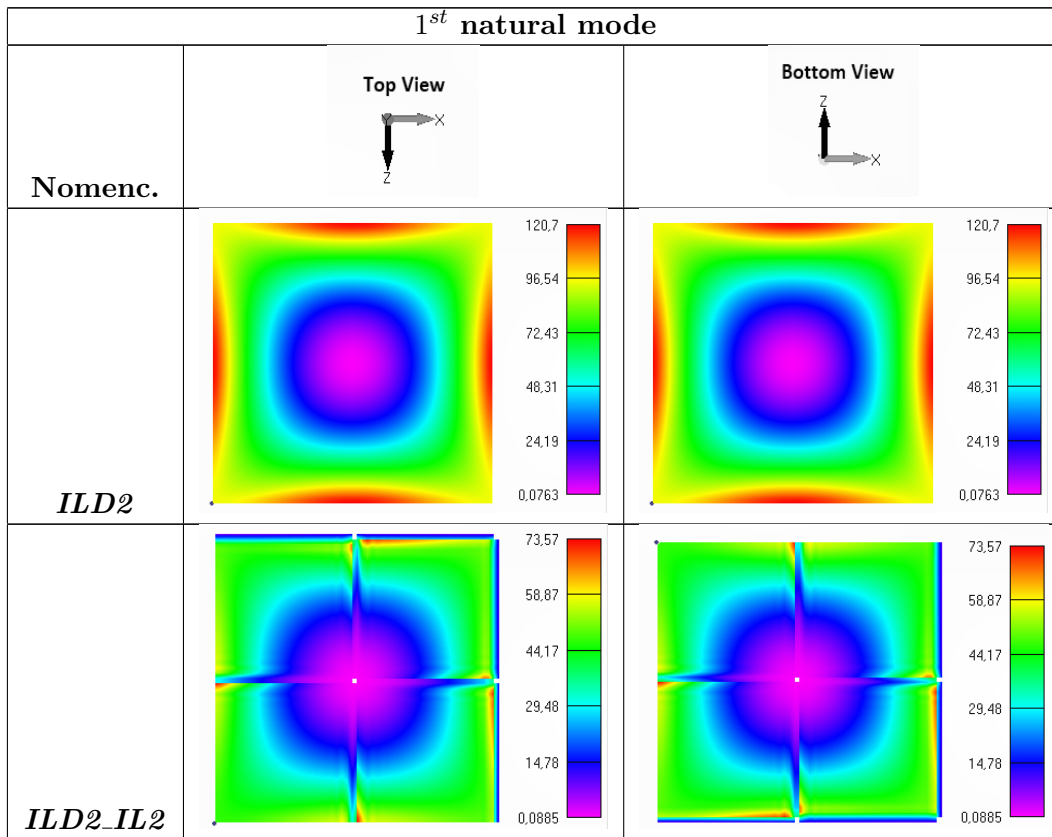
		Loss factor [%]				
Amplitude	mode 1	mode 2	mode 3	mode 4	mode 5	
A_1	17.14	17.82	14.99	9.60	9.60	
A_2	14.39	15.57	11.03	7.01	7.01	

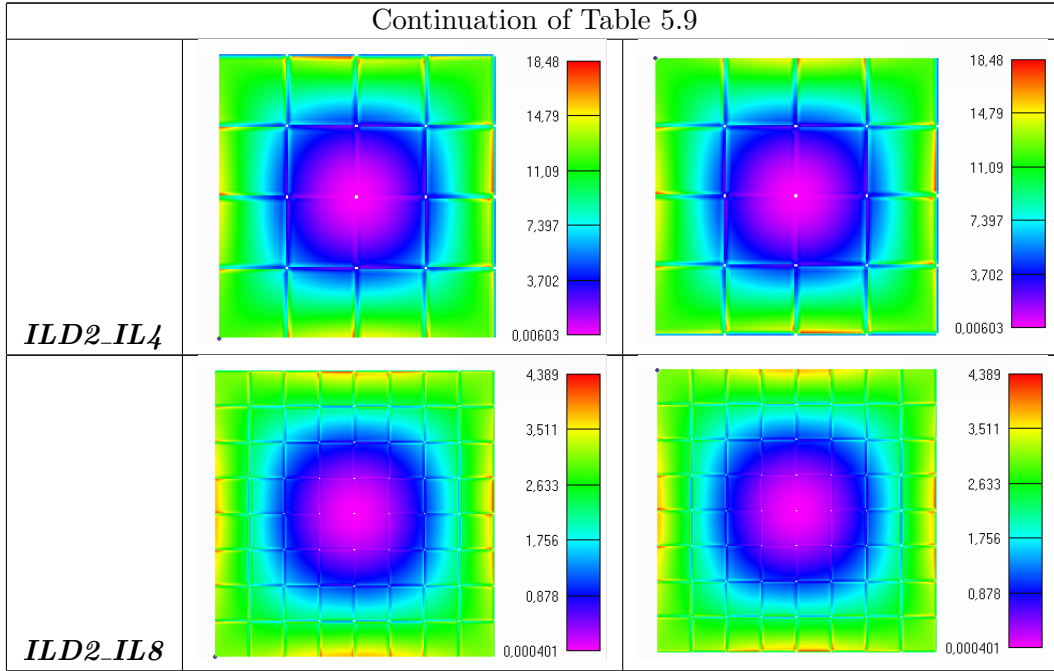
Interlaced models

The results obtained for the interlaced models are divided by configurations to help the organization of the document and further results analysis.

In the Table 5.9 the strain energy distribution for first natural mode of each ILD square model is presented. This table contains the ILD uniform treatment (reference treatment) and the 2, 4 and 8 interlaced stripes ILD treatments.

Table 5.9: Distribution of the modal strain energy (1^{st} mode) for the ILD square models developed with free boundary conditions.





The modal strain energy distribution for the other four natural modes are presented in the *Interlaced models* section in the Appendix E. In Table 5.10 the natural frequencies and the normalized loss factor for each ILD square plate treatment are presented. The modal loss factor, obtained by the application of the MSE method, was divided by the mass of viscoelastic material on each treatment. This approach was performed on this set of treatments due to the different VEM mass added to each one, in order to obtain an adequate comparison between models.

Table 5.10: Natural frequencies and normalized loss factor for the developed ILD square models.

Nomenclature	Natural Frequencies [Hz]				
	mode 1	mode 2	mode 3	mode 4	mode 5
<i>ILD2</i>	356.161	523.016	629.668	882.621	882.621
<i>ILD2_IL2</i>	342.952	502.429	611.344	863.128	863.136
<i>ILD2_IL4</i>	342.892	502.768	611.388	862.738	862.740
<i>ILD2_IL8</i>	342.871	502.982	611.518	862.557	862.558

Nomenclature	Normalized Loss Factor [1/kg]				
	mode 1	mode 2	mode 3	mode 4	mode 5
<i>ILD2</i>	25.11	27.48	18.28	11.55	11.55
<i>ILD2_IL2</i>	8.42	9.25	5.95	3.62	3.62
<i>ILD2_IL4</i>	8.57	9.34	5.98	3.69	3.69
<i>ILD2_IL8</i>	8.66	9.41	6.01	3.74	3.74

The following information is related to the comparison between the uniform CLD treatment and the interlaced configuration. Table 5.11 presents the strain energy distribution for the first natural mode of these two treatments. The corresponding tables for

the other natural modes are presented in the *Interlaced models* section on Appendix E.

Table 5.11: Distribution of the modal strain energy (1st mode) for the CLD square models developed with free boundary conditions.

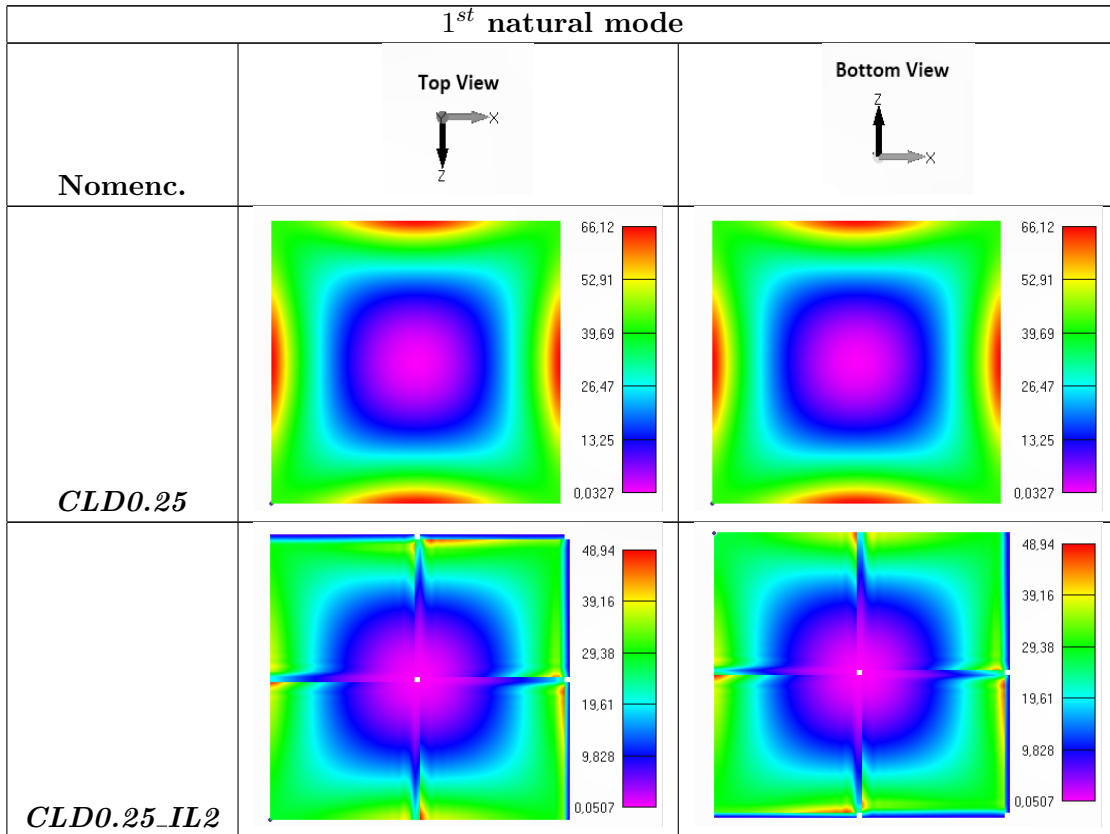


Table 5.12 presents the natural frequencies and normalized loss factor corresponding to the CLD square plate models.

Table 5.12: Natural frequencies and normalized loss factor for the developed CLD square models.

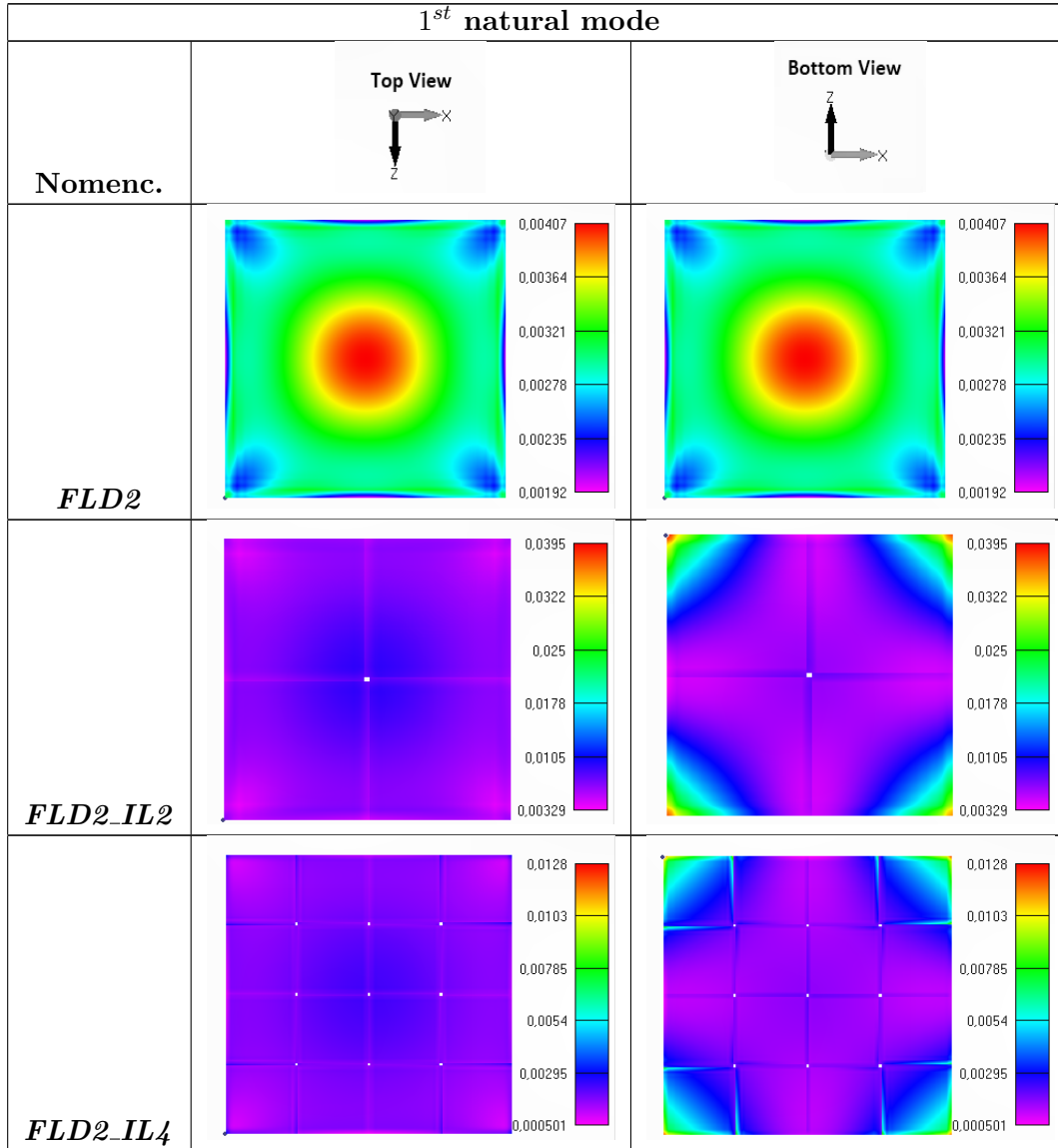
Nomenclature	Natural Frequencies [Hz]				
	mode 1	mode 2	mode 3	mode 4	mode 5
<i>CLD0.25</i>	324.606	476.355	579.767	817.496	817.496
<i>CLD0.25_IL2</i>	315.152	461.726	564.135	798.216	798.223

Nomenclature	Normalized Loss Factor [1/kg]				
	mode 1	mode 2	mode 3	mode 4	mode 5
<i>CLD0.25</i>	14.00	16.27	11.77	7.59	7.59
<i>CLD0.25_IL2</i>	6.08	6.94	4.70	2.93	2.93

Regarding the single material interlaced treatments based on a FLD configuration, to which set the FLD2 treatment was used as reference, Table 5.13 shows the distribution of the modal strain energy for the first natural mode. Similarly to before, the other

natural modes for all the analysed modes are available in Appendix E

Table 5.13: Distribution of the modal strain energy (1^{st} mode) for the FLD square models without constraining stripes developed with free boundary conditions.



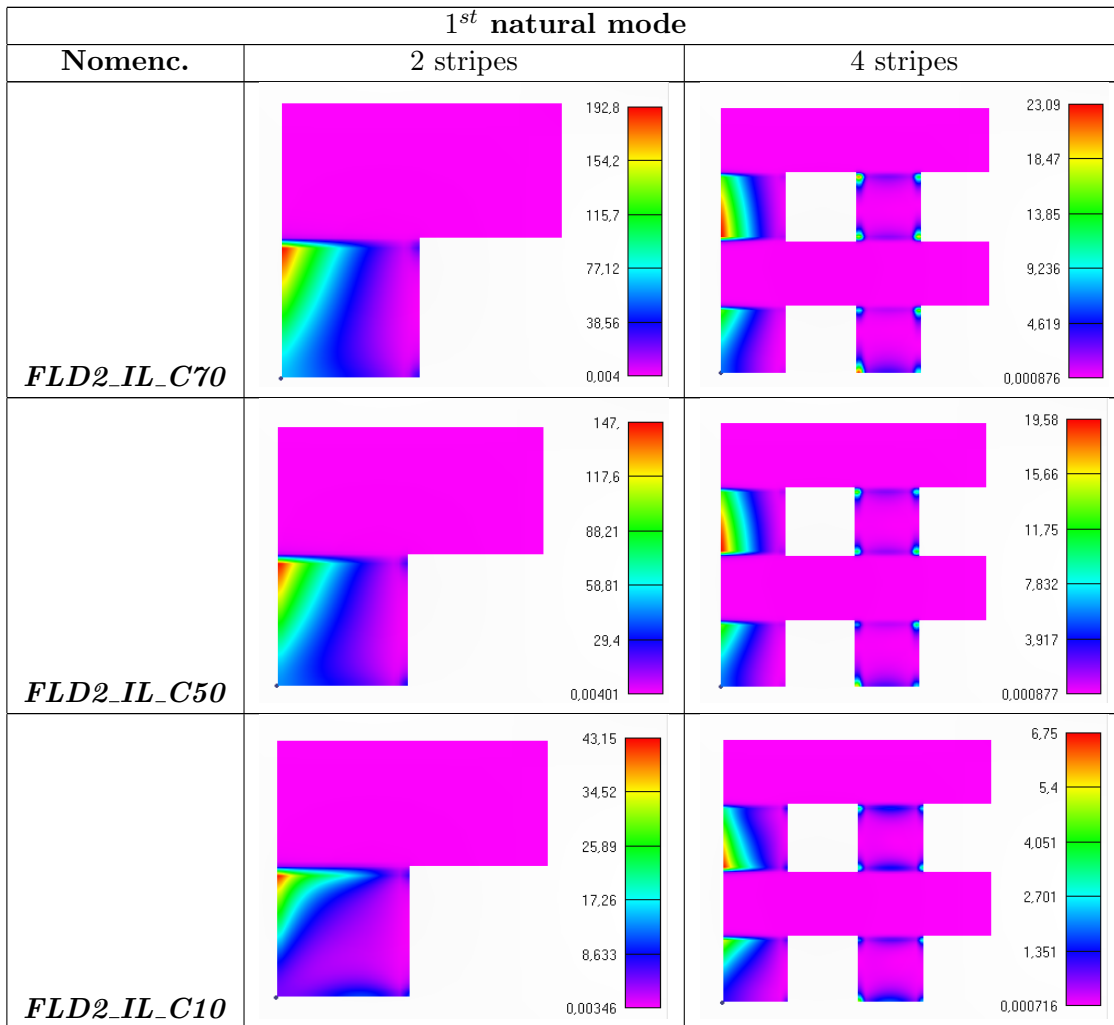
Tables 5.14 shows the natural frequencies and the determined normalized loss factor for each treatment and each mode. The loss factor based on the MSE method was divided by the VEM mass of each treatment in order to obtain the available results.

The results of the study regarding the influence of the stiffness in the double material interlaced treatments are shown as follows. Table 5.15 presents the strain energy distribution for the first natural mode. For these treatments, only the top view is presented due to the fact that the bottom view corresponds to the symmetric (in relation to the x axis) of the former. Therefore, one column of the table is used to show the treatments with two interlaced stripes and the other for four interlaced stripes. The distribution of the remaining modes can be found in Appendix E.

Table 5.14: Natural frequencies and normalized loss factor for the FLD square models without constraining stripes.

Nomenclature	Natural Frequencies [Hz]				
	mode 1	mode 2	mode 3	mode 4	mode 5
<i>FLD2</i>	327.94	478.46	592.62	846.49	846.49
<i>FLD2_IL2</i>	322.18	470.05	582.17	832.18	832.33
<i>FLD2_IL4</i>	321.48	469.51	581.39	830.26	830.30

Nomenclature	Normalized Loss Factor [1/kg]				
	mode 1	mode 2	mode 3	mode 4	mode 5
<i>FLD2</i>	0.00144	0.00169	0.00225	0.00254	0.00254
<i>FLD2_IL2</i>	0.00237	0.00339	0.00477	0.00712	0.00711
<i>FLD2_IL4</i>	0.00239	0.00344	0.00483	0.00731	0.00730

Table 5.15: Distribution of the modal strain energy (1st mode) for the FLD square models with single layered constraining stripes developed with free boundary conditions.

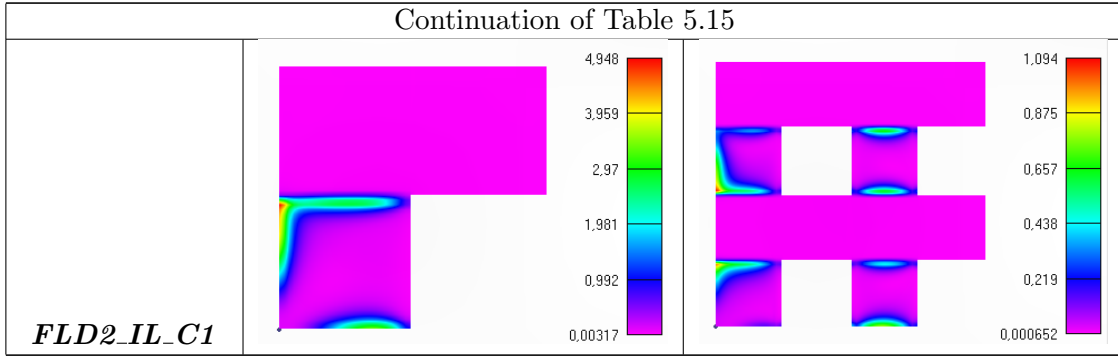


Table 5.16 presents the natural frequencies and the loss factor for the first natural mode. Even though the VEM mass is the same for this set of specimens, the normalized loss factor is presented to compare with the other treatments. For the other modes, the normalized loss factor values are presented in Appendix E.

Table 5.16: Natural frequency and normalized loss factor (1st mode) for the FLD square models with single layered constraining stripes.

<i>mode 1</i>	Natural Frequencies [Hz]	
Nomenclature	2 stripes	4 stripes
<i>FLD2_IL_C70</i>	358.476	363.823
<i>FLD2_IL_C50</i>	346.336	348.575
<i>FLD2_IL_C10</i>	321.328	320.230
<i>FLD2_IL_C1</i>	313.212	311.988

<i>mode 1</i>	Normalized loss Factor [1/kg]	
Nomenclature	2 stripes	4 stripes
<i>FLD2_IL_C70</i>	2.97	0.84
<i>FLD2_IL_C50</i>	2.31	0.74
<i>FLD2_IL_C10</i>	0.57	0.29
<i>FLD2_IL_C1</i>	0.05	0.05

The next set of analysed models corresponds to the double material interlaced with single and double layer. For these treatments, the VEM and aluminium (same material characteristics of the host structure) stripes were used. Tables 5.17 and 5.18 present the top and bottom view, respectively, of the first modal strain energy distribution analysed with 2, 4 and 8 stripes in both directions.

Table 5.17: Distribution of the modal strain energy (1^{st} mode) for the FLD square models with single and double layered constraining stripes developed with free boundary conditions - top view.

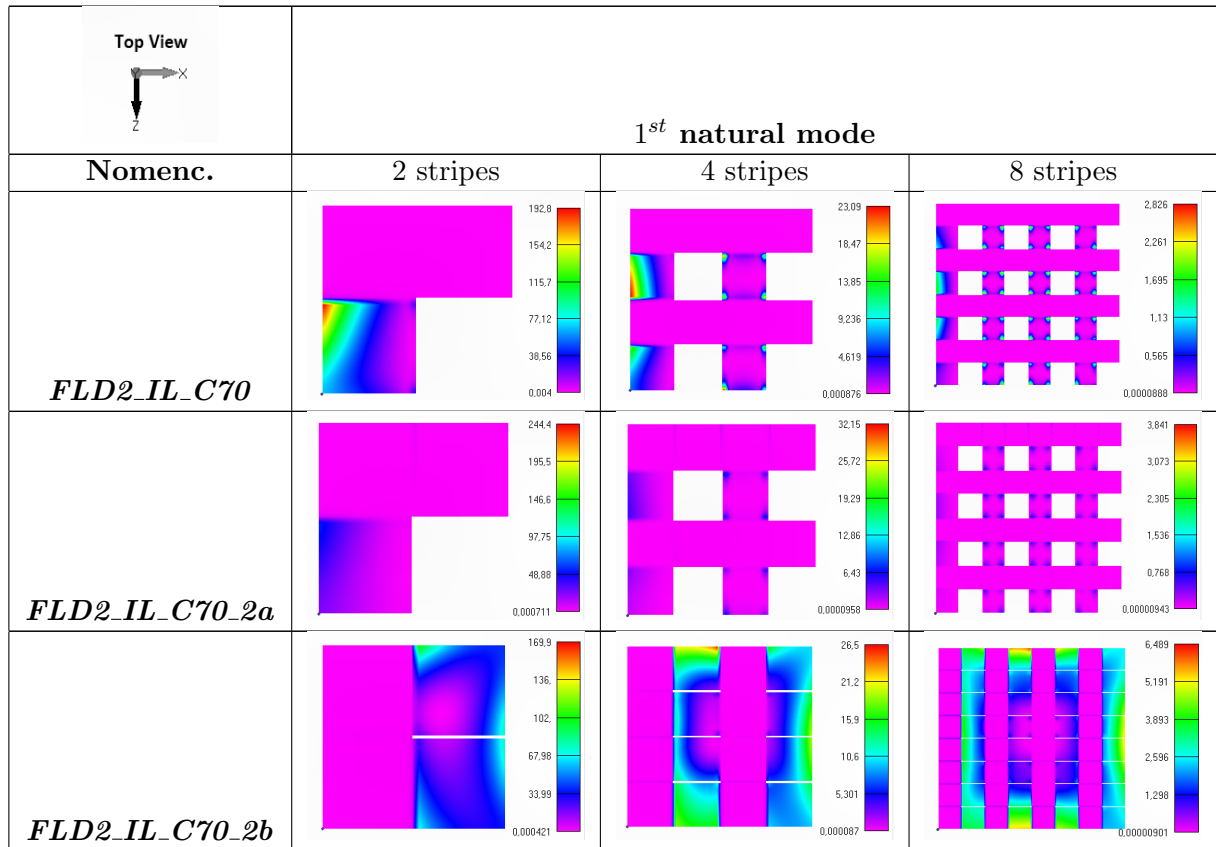
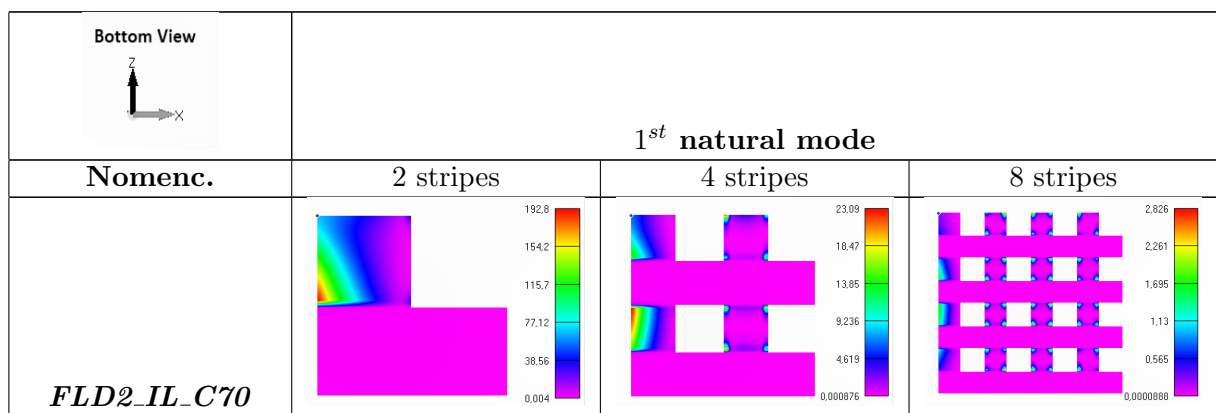
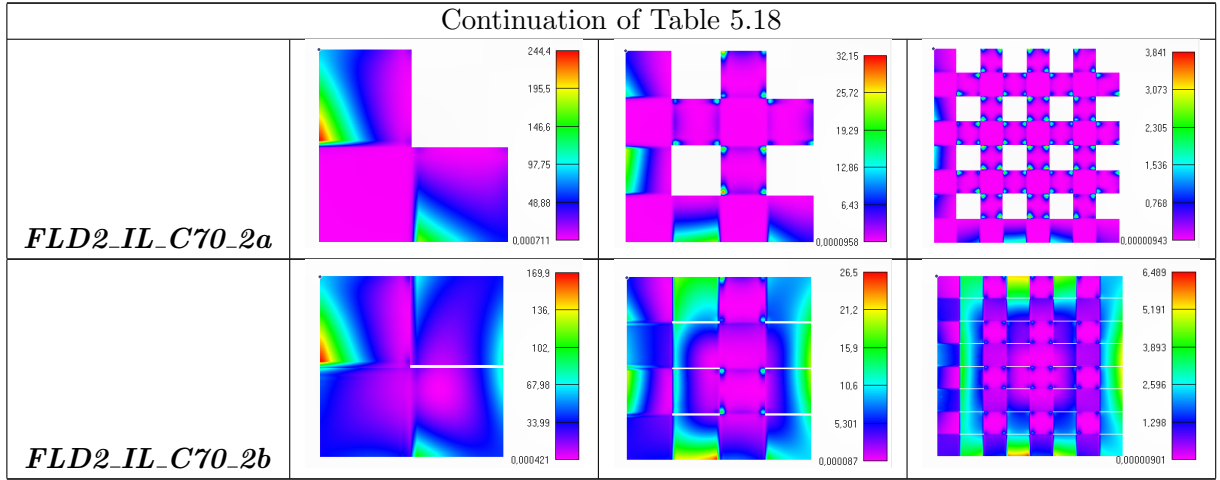


Table 5.18: Distribution of the modal strain energy (1^{st} mode) for the FLD square models with single and double layered constraining stripes developed with free boundary conditions - bottom view.





The distribution for the second to fifth natural modes are presented in Appendix E. In the Table 5.19 it is possible to find the natural frequencies and the normalized loss factor for the first natural mode. The natural frequencies and the normalized loss factor for the other natural modes are available in the aforementioned appendix.

Table 5.19: Natural frequency and normalized loss factor (1st mode) for the FLD square models with single and double layered constraining stripes.

<i>mode 1</i>	Natural Frequencies [Hz]		
Nomenclature	2 stripes	4 stripes	8 stripes
<i>FLD2_IL_C70</i>	358.476	363.823	365.855
<i>FLD2_IL_C70_2a</i>	363.634	386.035	394.518
<i>FLD2_IL_C70_2b</i>	344.871	349.201	350.852

<i>mode 1</i>	Normalized Loss Factor [1/kg]		
Nomenclature	2 stripes	4 stripes	8 stripes
<i>FLD2_IL_C70</i>	2.97	0.84	0.27
<i>FLD2_IL_C70_2a</i>	3.44	0.88	0.32
<i>FLD2_IL_C70_2b</i>	5.01	3.52	3.13

5.3.2 Rectangular plate models

The mode shapes for the rectangular plates (Figure 5.3) were also calculated by the Finite Element Method. The first natural mode corresponds to the first order torsion mode, the second one to the first order bending mode (longitudinal direction), the third to the second order torsion mode, the fourth to the first order bending mode (transversal direction) and finally the fifth natural mode corresponds to the second order bending mode (longitudinal direction).

The first set of treatments presented in this section is the uniform and the interlaced CLD rectangular models. Table 5.20 presents the modal strain energy distribution for the first natural mode for this set of treatments, for both top and bottom view. The other modes are presented in section *Rectangular plate models* in Appendix E.

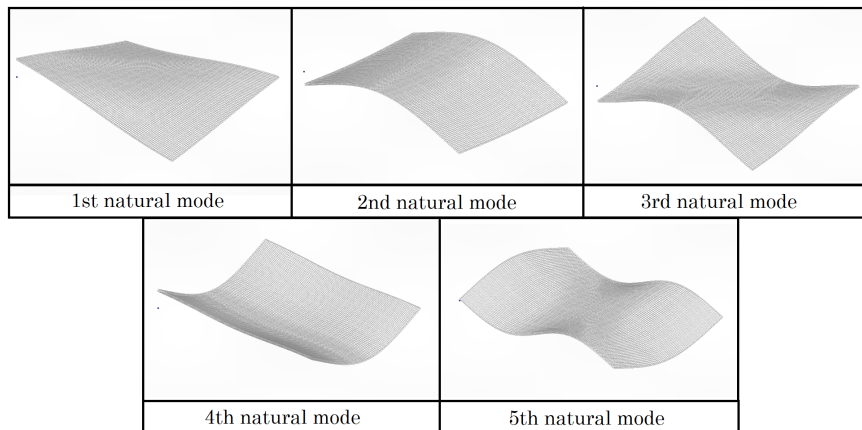
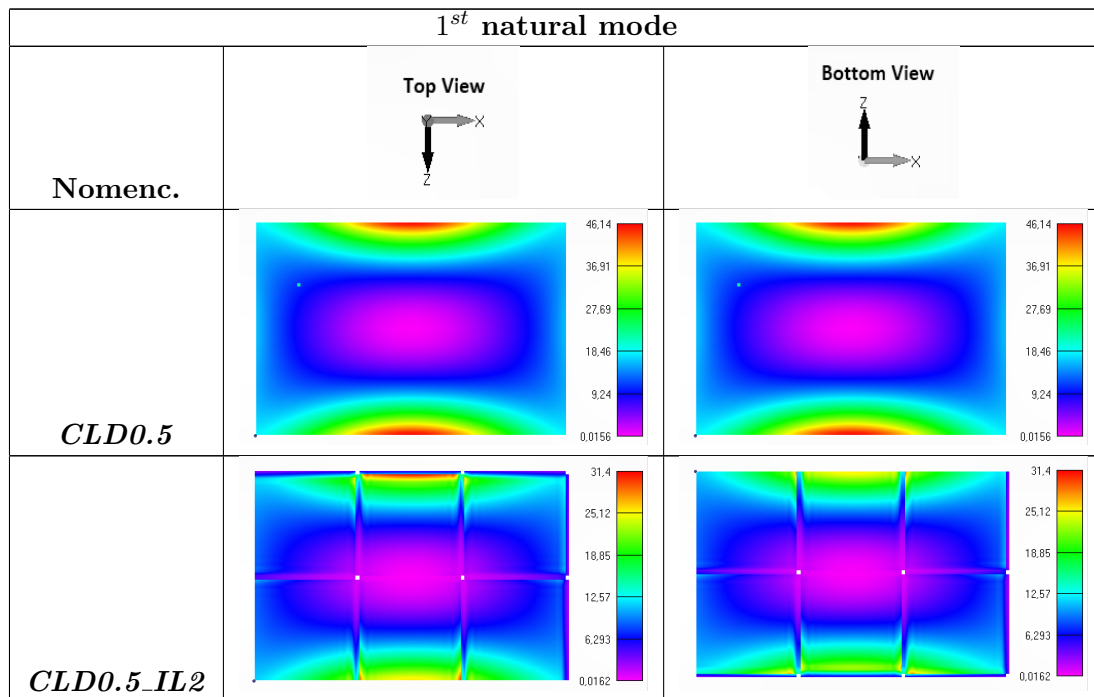


Figure 5.3: Mode shapes of the first five natural modes of the aluminium rectangular plate.

Table 5.20: Distribution of the modal strain energy (1^{st} mode) for the CLD rectangular models developed with free boundary conditions.



The rectangular models section contains the natural frequencies table in the document for further comparison with the results obtained experimentally. Therefore, Table 5.21 shows the natural frequencies for the CLD rectangular models.

Table 5.21: Natural frequency values for the developed CLD rectangular models.

Nomenclature	Natural Frequencies [Hz]				
	mode 1	mode 2	mode 3	mode 4	mode 5
<i>CLD0.5</i>	212.555	233.999	471.768	515.667	587.727
<i>CLD0.5_IL2</i>	204.699	223.840	458.529	499.564	571.554

Table 5.22 presents the loss factor values for comparison with the results obtained experimentally and the normalized loss factor for further comparison between these two models, since the treatments added mass differs between them.

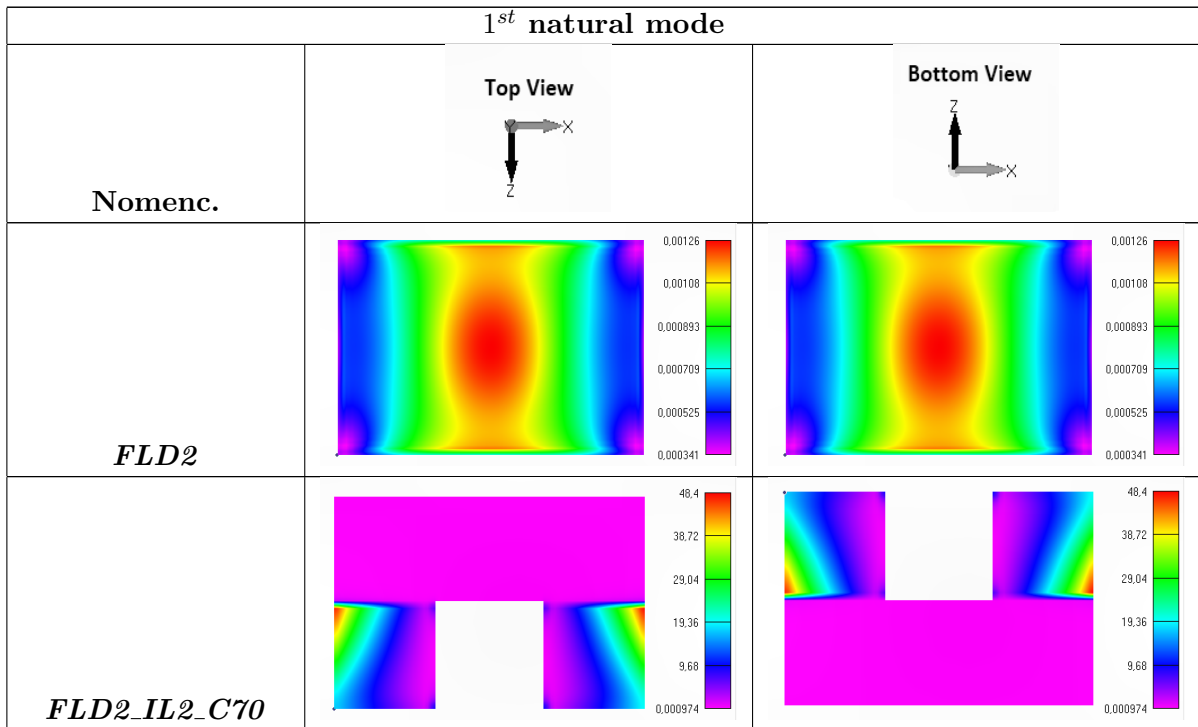
Table 5.22: Loss factor values for the developed CLD rectangular models.

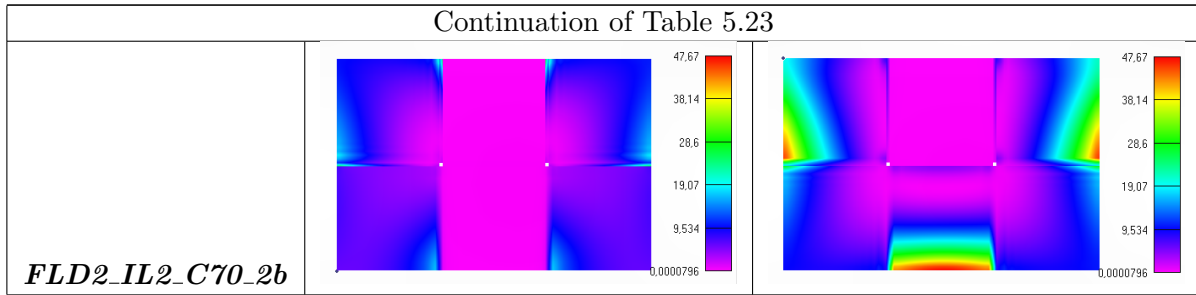
Nomenclature	Loss Factor [%]				
	mode 1	mode 2	mode 3	mode 4	mode 5
<i>CLD0.5</i>	11.65	15.44	6.70	8.73	6.59
<i>CLD0.5_IL2</i>	9.32	12.90	4.78	6.40	4.72

Nomenclature	Normalized Loss Factor [1/kg]				
	mode 1	mode 2	mode 3	mode 4	mode 5
<i>CLD0.5</i>	15.60	20.68	8.97	11.69	8.82
<i>CLD0.5_IL2</i>	6.47	8.96	3.32	4.44	3.28

The following set of models contains the developed FLD rectangular treatments, including uniform and interlaced layers, single and double material, and single and double layers. The corresponding strain energy distribution for the first natural mode is presented in Figure 5.23. The corresponding table for the remaining modes, can be found in section *Rectangular plate models* in Appendix E.

Table 5.23: Distribution of the modal strain energy (1st mode) for the FLD rectangular models developed with free boundary conditions.





As before, the natural frequencies for the FLD rectangular treatments are shown in Table 5.24.

Table 5.24: Natural frequency values for the developed FLD rectangular models.

Nomenclature	Natural Frequencies [Hz]				
	mode 1	mode 2	mode 3	mode 4	mode 5
<i>FLD2</i>	217.624	232.565	501.632	541.636	625.613
<i>FLD2_IL2_C70</i>	240.454	263.255	519.231	572.205	651.078
<i>FLD2_IL2_C70_2b</i>	228.911	253.696	495.289	549.072	615.803

Table 5.25 presents the loss factor values for comparison with the results obtained experimentally and the normalized loss factor for further comparison between the FLD rectangular models, since the treatments added mass differs between them.

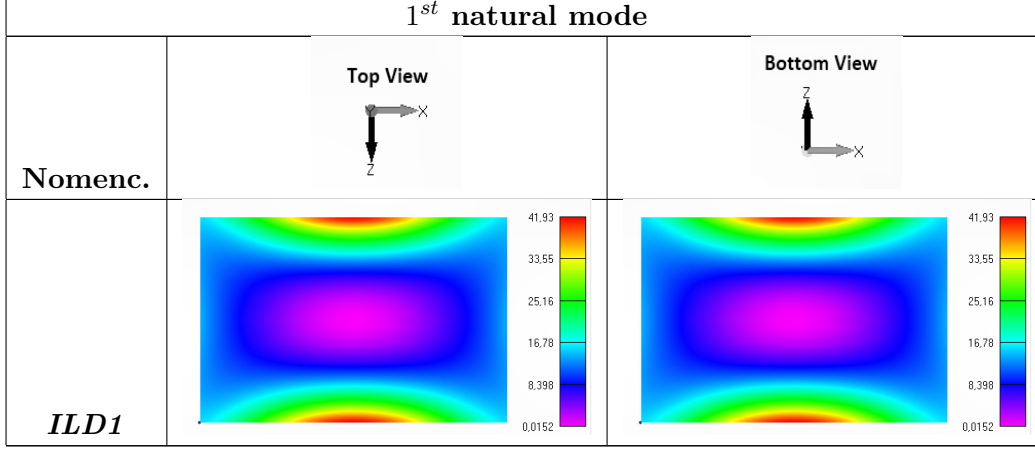
Table 5.25: Loss factor values for the developed FLD rectangular models.

Nomenclature	Loss Factor [%]				
	mode 1	mode 2	mode 3	mode 4	mode 5
<i>FLD2</i>	0.000668	0.000761	0.000862	0.00101	0.000999
<i>FLD2_IL2_C70</i>	1.64	1.46	1.57	0.41	2.47
<i>FLD2_IL2_C70_2b</i>	5.55	6.14	4.55	4.98	5.52

Nomenclature	Normalized Loss Factor [1/kg]				
	mode 1	mode 2	mode 3	mode 4	mode 5
<i>FLD2</i>	0.000894	0.00102	0.00115	0.00136	0.00134
<i>FLD2_IL2_C70</i>	1.98	1.77	1.90	0.50	2.99
<i>FLD2_IL2_C70_2b</i>	3.91	4.33	3.21	3.51	3.89

The ILD1 rectangular treatment was added to this study as a reference for the other developed treatments. The distribution of the first modal strain energy for this treatment can be found in Table 5.26, while for the other modes is located in Appendix E.

Table 5.26: Distribution of the modal strain energy (1st mode) for the ILD rectangular model developed with free boundary conditions.



In Table 5.27, the natural frequencies for the five first natural modes of the ILD1 treatment are shown.

Table 5.27: Natural frequency values for the developed ILD rectangular model.

Nomenclature	Natural Frequencies [Hz]				
	mode 1	mode 2	mode 3	mode 4	mode 5
ILD1	132.404	150.776	278.183	309.176	345.416

Table 5.28 presents the loss factor values for comparison with the results obtained experimentally and the normalized loss factor for further comparison with the other rectangular models.

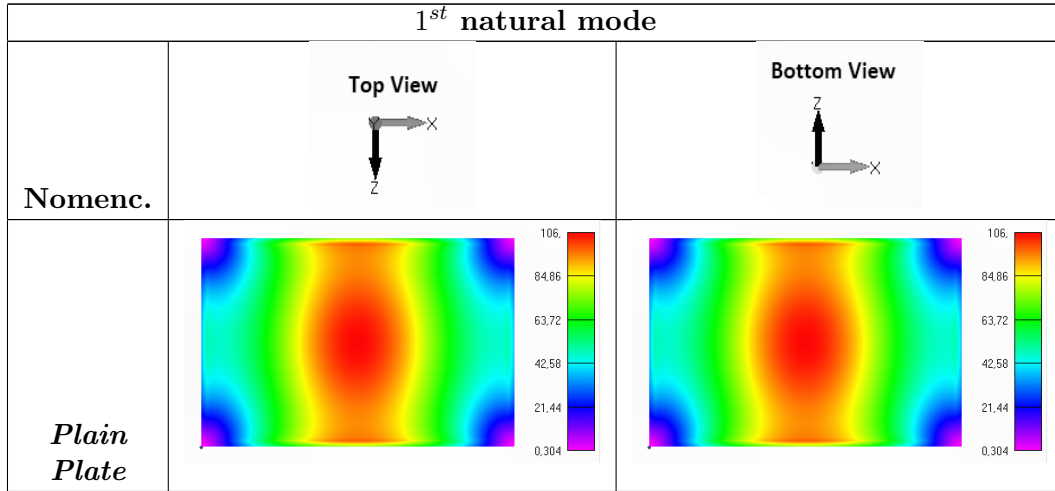
Table 5.28: Loss factor values for the developed ILD rectangular model.

Nomenclature	Loss Factor [%]				
	mode 1	mode 2	mode 3	mode 4	mode 5
ILD1	27.50	33.83	17.00	21.48	16.54

Nomenclature	Normalized Loss Factor [1/kg]				
	mode 1	mode 2	mode 3	mode 4	mode 5
ILD1	36.83	45.30	22.77	28.76	22.15

Finally, the results for the reference plain plate are presented. Table 5.29 shows the first modal strain distribution for the plain rectangular plate, while the second to fifth natural modes are presented at the end of section *Rectangular plate models* in Appendix E.

Table 5.29: Distribution of the modal strain energy (1st mode) for the plain plate with free boundary conditions.



And in Table 5.30, can be observed the natural frequencies of each plain plate mode.

Table 5.30: Natural frequency values for the plain plate.

Nomenclature	Natural Frequencies [Hz]				
	mode 1	mode 2	mode 3	mode 4	mode 5
<i>Plain Plate</i>	222.686	237.975	513.305	554.248	640.182

Intentionally blank page.

Chapter 6

Experimental Results

In this chapter, the experimental results of the developed models are presented. The results of the beam specimens followed by the ones of plate specimens are presented, for the MDOF (PolyMAX on X-Modal 3) and SDOF (Circle-fit) modal identification methods, respectively. For the beam-kind models, the experimental results are presented for the first two natural modes. For the plate-kind models, they are presented for the first five natural modes. The natural modes presented correspond to the ones found within the frequency range of analysis [0-1000Hz].

6.1 MDOF system modal identification (PolyMAX)

This section provides the experimental results, for both beam and plate specimens, obtained by the PolyMAX method implemented in the software X-Modal 3 from SDRL-Structural Dynamics Research Lab. from the University of Cincinnati. The PolyMAX method allowed the identification of the mode shapes, the natural frequencies and the modal damping ratios for each specimen.

6.1.1 Beam specimens

In the frequency range of analysis, two natural modes were identified for the beam-kind specimens. Figure 6.1 presents the mode shapes for the two first identified natural modes, which corresponds to the first order bending mode and the second order bending mode, respectively.

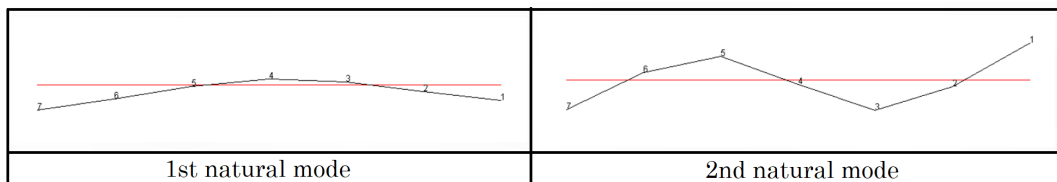


Figure 6.1: Mode shapes of the first two natural modes of the sandwich beam.

The natural frequencies for each identified natural mode are presented in Table 6.1. Table 6.2 presents the Damping ratio values calculated by the Polymax identification procedure. Additionally, considering the relation $\eta_r = 2 \times \zeta$ [14], the calculated modal loss factor values are added to the table.

Table 6.1: Natural Frequency values for the beam specimens obtained by the PolyMAX method.

<i>PolyMAX</i>	Natural Frequencies [Hz]	
Specimen	mode 1	mode 2
<i>ILD2</i>	678.85	1442.07
<i>ILD2_1D</i>	659.08	1490.60

Table 6.2: Damping ratio values for the beam specimens obtained by the PolyMAX method.

<i>PolyMAX</i>	Damping ratio [%] / (Loss factor [%])	
Specimen	mode 1	mode 2
<i>ILD2</i>	18.93 / (37.86)	11.89 / (23.77)
<i>ILD2_1D</i>	13.35 / (26.70)	9.29 / (18.58)

6.1.2 Plate specimens

In the frequency range of analysis, five natural modes were identified for the plate-kind specimens. Figure 6.2 presents the mode shapes for the first five identified natural modes, corresponding to the first order torsion mode, first order bending mode (longitudinal direction), second order torsion mode, first order bending mode (transversal direction) and the second order bending mode (longitudinal direction), respectively.

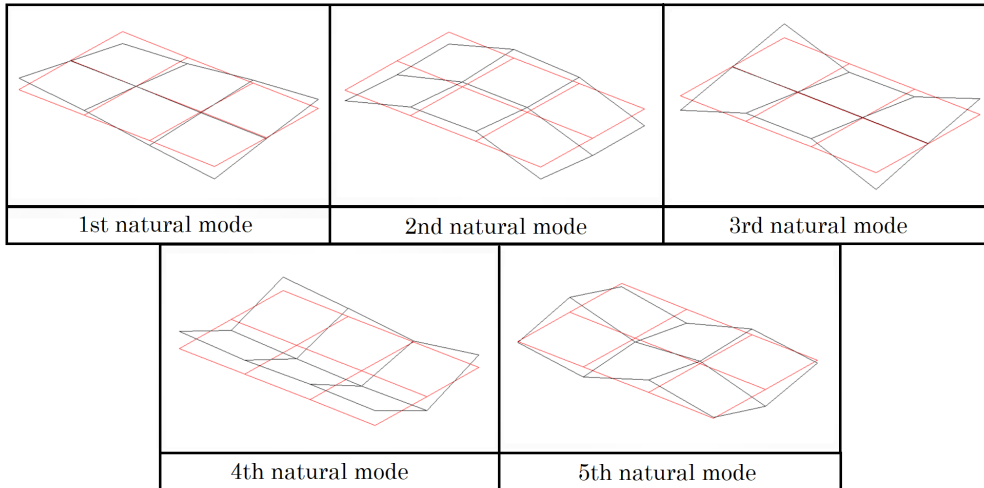


Figure 6.2: Mode shapes of the first five natural modes of the aluminium rectangular plate.

The natural frequencies and the damping ratio are presented, for each identified natural mode, in tables 6.3 and 6.4, respectively. Considering the relation aforementioned, the calculated modal loss factor values are added to Table 6.4.

Table 6.3: Natural frequency values for the plate specimens obtained by the PolyMAX method.

<i>PolyMAX</i>	Natural Frequencies [Hz]				
Specimen	mode 1	mode 2	mode 3	mode 4	mode 5
<i>CLD0.5</i>	216.641	237.574	497.006	552.691	629.975
<i>CLD0.5_IL2</i>	202.4681	228.663	478.430	530.849	604.644
<i>FLD2</i>	209.456	226.845	483.250	525.379	603.852
<i>FLD2_IL2_C70</i>	202.189	223.167	474.429	514.969	588.510
<i>FLD2_IL2_C70_2b</i>	200.491	226.081	471.348	513.361	586.009
<i>ILD1</i>	119.256	130.564	266.764	293.751	327.467

Table 6.4: Damping ratio values for the plate specimens obtained by the PolyMAX method.

<i>PolyMAX</i>	Damping ratio [%] / (Loss factor [%])				
Specimen	mode 1	mode 2	mode 3	mode 4	mode 5
<i>CLD0.5</i>	1.09/(2.17)	0.76/(1.53)	0.88/(1.76)	0.99/(1.98)	0.77/(1.54)
<i>CLD0.5_IL2</i>	1.74/(3.48)	2.79/(5.59)	2.97/(5.94)	3.34/(6.68)	3.23/(6.46)
<i>FLD2</i>	0.28/(0.56)	0.29/(0.59)	0.17/(0.34)	0.19/(0.38)	0.16/(0.33)
<i>FLD2_IL2_C70</i>	0.95/(1.90)	1.24/(2.48)	0.99/(1.99)	0.83/(1.65)	0.87/(1.75)
<i>FLD2_IL2_C70_2b</i>	2.51/(5.03)	2.66/(5.33)	3.61/(7.21)	3.12/(6.25)	2.95/(5.90)
<i>ILD1</i>	12.16/(24.32)	13.51/(27.02)	8.95/(17.89)	7.22/(14.44)	7.89/(15.79)

6.2 SDOF system modal identification (Circle Fit)

This section provides the experimental results, for both beam and plate specimens, obtained by the Circle Fit method. The Circle fit method allowed the identification of the natural frequencies and the modal loss factor for each specimen.

6.2.1 Beam specimens

In the frequency range of analysis, two natural modes were identified for the beam-kind specimens. The natural frequencies and the modal loss factor are presented, for each identified natural mode, in tables 6.5 and 6.6, respectively.

Table 6.5: Natural frequency values for the beam specimens obtained by the Circle Fit method.

<i>Circle Fit</i>	Natural Frequencies [Hz]	
Specimen	mode 1	mode 2
<i>ILD2</i>	671.08	1550.86
<i>ILD2_1D</i>	653.27	1519.98

Table 6.6: Loss factor values for the beam specimens obtained by the Circle Fit method.

<i>Circle Fit</i>	Loss Factor [%]	
Specimen	mode 1	mode 2
<i>ILD2</i>	35.06	19.45
<i>ILD2_1D</i>	31.49	18.95

6.2.2 Plate specimens

In the frequency range of analysis, five natural modes were identified for the plate-kind specimens. The natural frequencies and the modal loss factor are presented, for each identified natural mode, in tables 6.7 and 6.8, respectively.

Table 6.7: Natural frequency values for the plate specimens obtained by the Circle Fit method.

<i>Circle Fit</i>	Natural Frequencies [Hz]				
Specimen	mode 1	mode 2	mode 3	mode 4	mode 5
<i>CLD0.5</i>	216.654	237.451	499.589	553.554	629.471
<i>CLD0.5_IL2</i>	209.069	232.365	478.297	532.125	604.121
<i>FLD2</i>	209.404	226.870	483.220	525.470	604.013
<i>FLD2_IL2_C70</i>	202.719	223.317	474.512	515.481	588.723
<i>FLD2_IL2_C70_2b</i>	202.108	226.023	470.676	515.059	588.089
<i>ILD1</i>	120.708	132.723	264.917	298.975	327.877

Table 6.8: Loss factor values for the plate specimens obtained by the Circle Fit method.

<i>Circle Fit</i>	Loss Factor [%]				
Specimen	mode 1	mode 2	mode 3	mode 4	mode 5
<i>CLD0.5</i>	1.92	1.66	2.19	1.87	1.84
<i>CLD0.5_IL2</i>	5.84	6.56	6.01	6.49	6.54
<i>FLD2</i>	0.41	0.59	0.28	0.37	0.27
<i>FLD2_IL2_C70</i>	1.75	2.51	2.02	1.59	1.77
<i>FLD2_IL2_C70_2b</i>	5.33	6.79	7.59	6.56	6.20
<i>ILD1</i>	26.06	30.95	18.42	22.71	18.12

Chapter 7

Results Analysis

The results analysis chapter aims to provide a comparison between the developed models. The results comparing the numerical models between them and the rectangular numerical models with the corresponding experimental specimen are here analysed. The chapter is divided in several sections to support the organization of the document.

7.1 Preliminary Numerical Results Analysis

7.1.1 Combined model approach

In this section, the results for the two combined model approaches are analysed. The results in Table 5.1 provided in Chapter 5 are hereby graphically represented through bar charts allowing a straightforward and clear comparison and analysis.

Figure 7.1a presents the natural frequencies identified for each combined model. As expected, for each mode the natural frequencies of both combined models are similar. The main differences occur for the fourth natural mode that corresponds, for this beam dimensions, to the first order torsion mode (for the *Plate with offset + Brick* model, the relative differences to the *Brick+Brick* model results are presented).

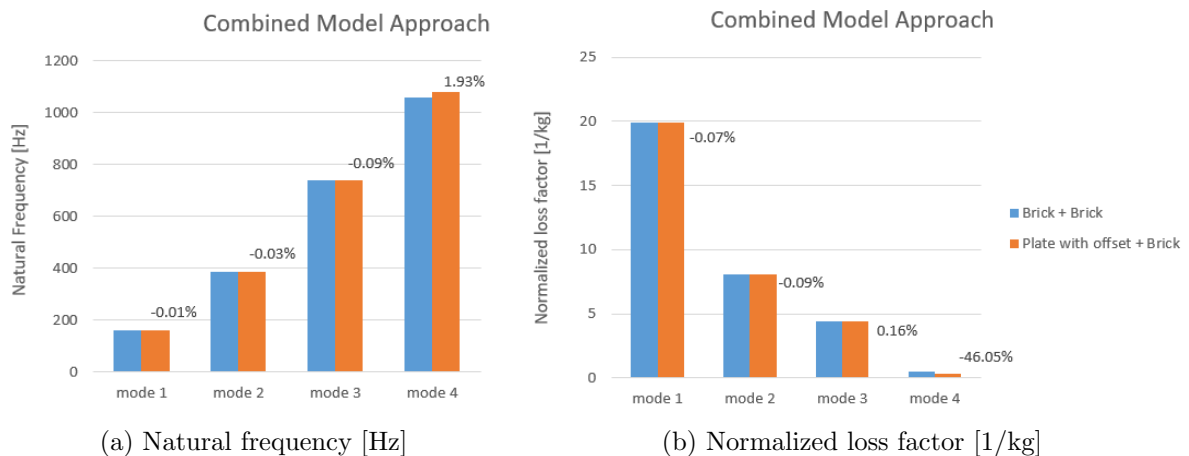


Figure 7.1: Comparison between the analysed combined model approaches.

Similarly to the natural frequencies, the modal loss factor based on the MSE method

presents similar values for both combined models for the first three bending modes (mode 1 to 3) and a slight difference for the first order torsion mode (mode 4). This comparison can be observed in Figure 7.1a.

As expected, the two analysed combined models present similar values. Therefore, and having in consideration the geometry complexity of the further developed models, the Brick + Brick (linear hexahedral finite elements) was chosen for the design of further models developed during this work. This spatial model selection was also supported by the reduced dimension of the problem.

7.1.2 VEM thickness

This section aims to provide the comparison between one thickness and its double for the two different combined model approaches developed for a sandwich beam.

Tables 5.2 and 5.3 presented in Chapter 5 show a decrease, from one thickness to its double, in natural frequencies for each mode, for both combined model approaches. These results are as expected, due to the fact that an increase of the mass in movement, leads to a decrease of natural frequencies (whereas the effect on the stiffness matrix is not significant due to this thickness increase).

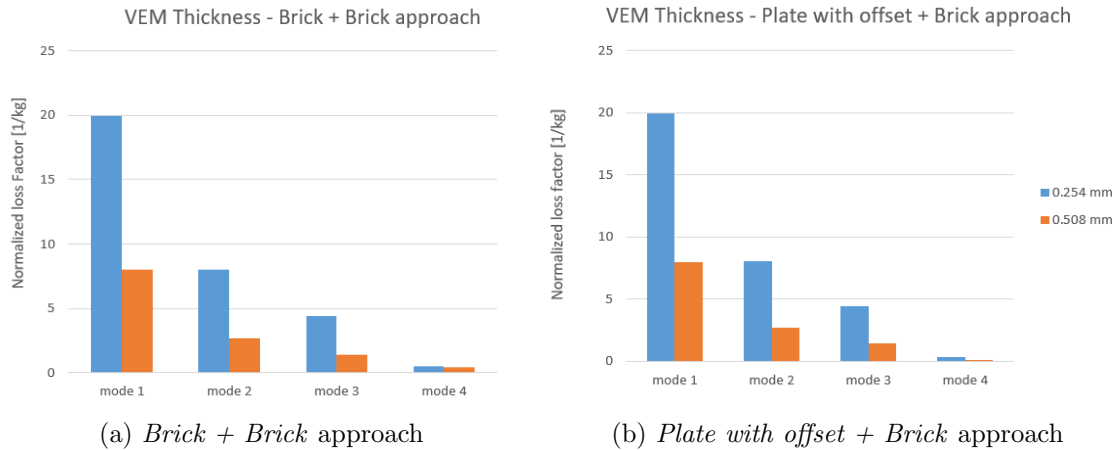


Figure 7.2: Normalized loss factor comparison between the two VEM thicknesses.

Figure 7.2 presents the normalized loss factor results for both combined model approaches. In this comparison, it is important to show the modal loss factor normalized to the model mass, due to the fact that one model presents double the mass of the other, in order to obtain results independent of the mass. Both approaches show a decrease of the normalized loss factor when the VEM thickness is increased.

7.2 Beam-kind models

7.2.1 Numerical results analysis

The results obtained and presented in the section *Beam-kind models*, from Chapter 5 are discussed in this section. The modal strain energy distribution for the beam models shows a clear increase of the strain energy on the border of the VEM core when the

number of waves is increased. The border effect is more notorious due to the beam dimensions. The red/orange vertical lines in the 1D waves model images demonstrate the effect caused by the model waves that creates high deformation lines compared to the deformation levels of its vicinity. As expected, the intensity of these vertical lines increases when the number of waves is increased.

Table 5.5 presented in Appendix E demonstrates, for the 1D waves developed models, an increase of the natural frequencies for each natural mode when the number of waves of each model is increased.

In Figure 7.3 the modal loss factor for each beam-kind model is presented in a form of bar chart. As it is possible to see in the figure, the increase of the number of waves (until 6 waves per module) results in an increase on the damping treatment efficiency for all the analysed natural modes. For the first order bending mode (mode 1), the damping treatment seems to loose its effect for the configuration with 7 and 8 waves per module. It is important to note that for all the analysed bending modes (mode 1, 2 and 4), the 1D waves models present a superior modal loss factor when compared to the uniform sandwich beam. For the first order torsion mode (mode 3), this conclusion is only verified for the configuration with 4 waves per module.

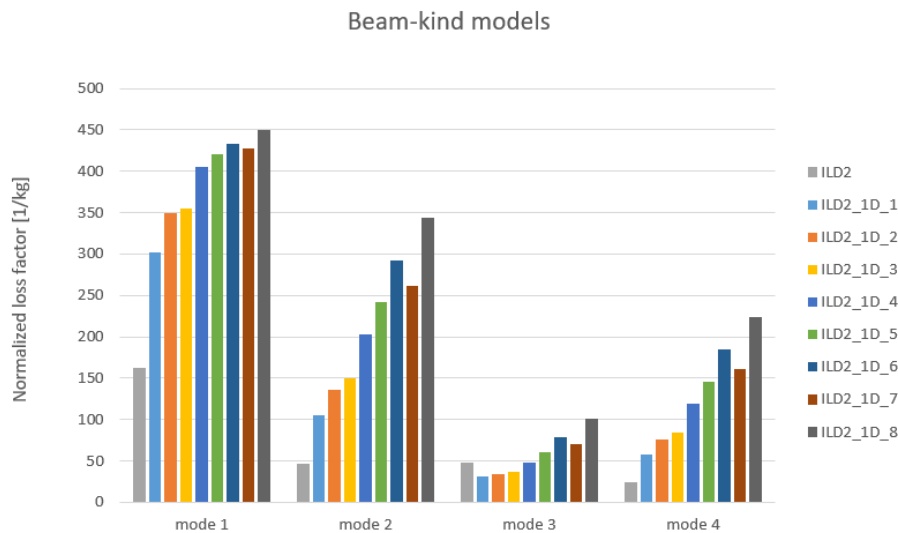


Figure 7.3: Normalized loss factor comparison between the beam-kind models.

This promising concept was experimentally analysed using the ILD2 and ILD2_1D_4 beam treatments. The ILD2_1D_4 beam treatment was chosen having in consideration the obtained numerical results, since this is the treatment that presents a higher normalized loss factor, when compared to the ILD2 beam treatment, with a lower number of waves for every analysed natural mode.

7.2.2 Experimental results analysis

The experimental results obtained for the beam specimens are presented in a form of a bar chart in Figure 7.4 for the two analysed methods.

Contrary to what was observed in the numerical analysis, the experimental results indicates the inferiority of the 1D waves beam loss factor when compared to the uniform

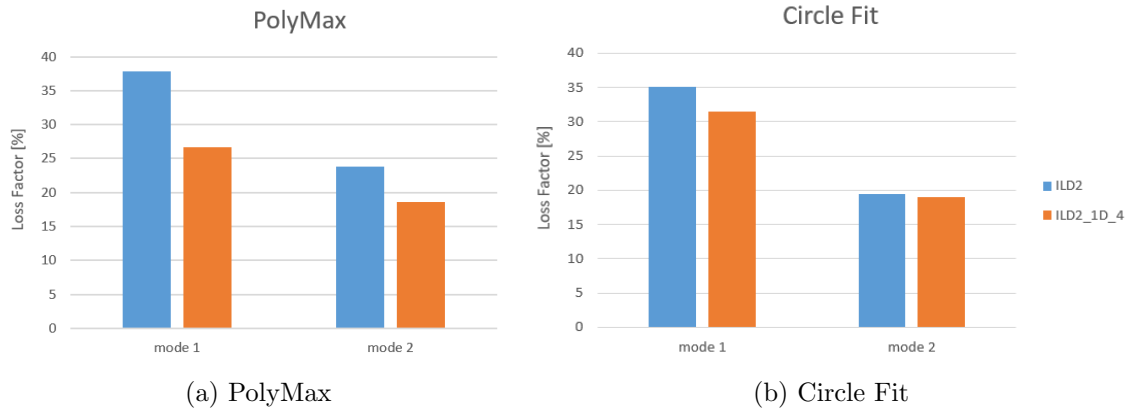


Figure 7.4: Modal loss factor comparison between the beam specimens.

sandwich beam. It is important to note that the experimental 1D wave specimen was not an accurate representation of the numeric model. While in the numeric one both host and constraining layer have the surfaces waved following the VEM core, in the experimental specimen copper wires were added to create the VEM layer waves. This difference in the configuration is a reasonable explanation for the 1D wave inferiority in the experimental results, due to the fact that the copper wires have a relative freedom to the adjacent aluminum beams that can severely reduce the shear effect on the VEM layer.

7.2.3 Numerical/Experimental comparison

This subsection provides a comparison between the numeric results and the experimental ones. The experimental study is important to validate the numerical work, for that, the mode shapes and the natural frequencies should be similar for each treatment.

As can be observed in figures 5.1 and 6.1, the identified mode shapes are a representation of the same natural mode for both studies.

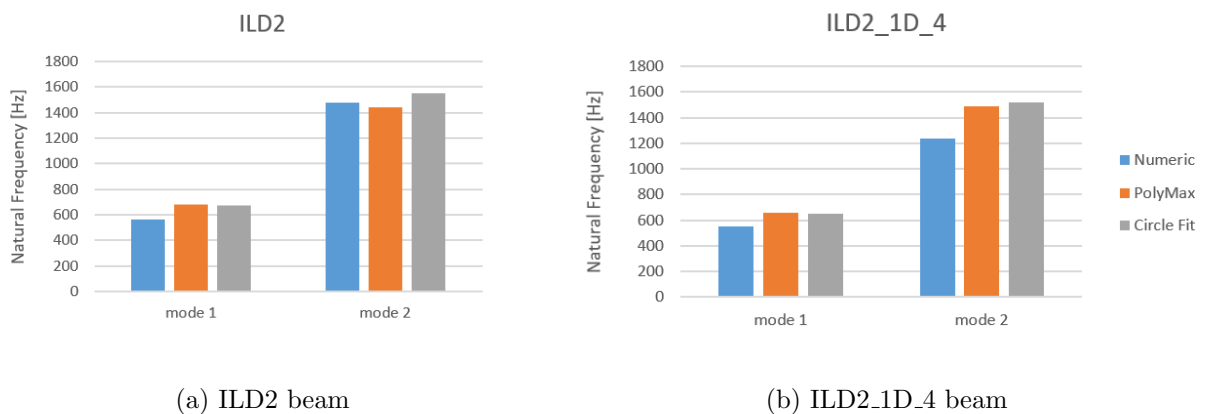


Figure 7.5: Natural frequencies comparison between numeric and experimental study.

Figure 7.5 shows the comparison between the natural frequencies for both numeric

and experimental study for the developed beam specimens. These figures evidence similar results when comparing the ones obtained numerically and experimentally (by both methods).

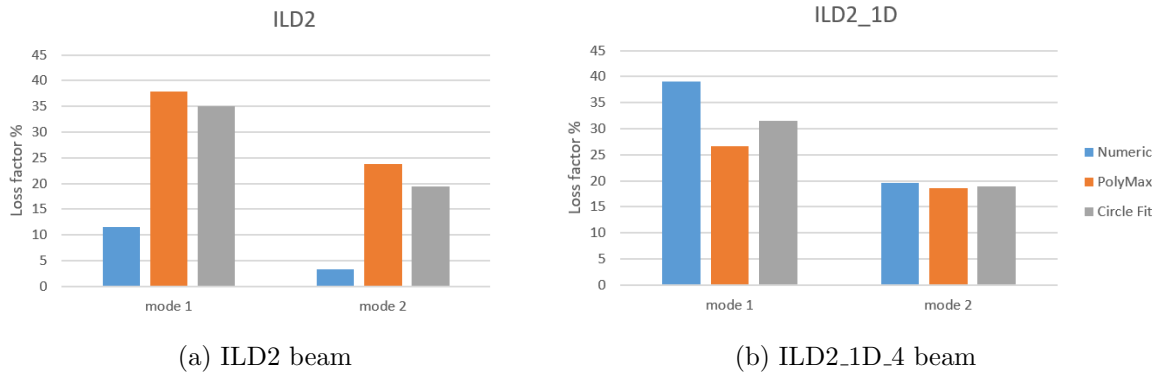


Figure 7.6: Loss factor comparison between numeric and experimental study.

Figure 7.6 shows the comparison between the loss factor for both numeric and experimental study for the developed beam specimens.

7.3 Plate-kind models

7.3.1 Numerical results analysis

The results obtained and presented in the section *Plate-kind models*, from Chapter 5 are discussed in this section.

Square plate models

The discussion of the results related to the developed square models (140 x 140 mm) is presented along this subsection. Initially, the 2D wave models are compared with the uniform ILD plate, followed by the discussion of the results obtained for the developed ILLD models

The 2D wave configuration treatments are compared with the uniform ILD square plate. Starting by the analysis of the strain energy distribution for the first natural mode presented in Table 5.6 of Chapter 5, even if the maximum strain energy obtained for each of the mentioned treatments is higher for the ILD2, the strain energy areas caused by the 2D waves, where the modal strain energy increase, can be easily noted in Figure 5.6. The same occurs for the remaining modes presented in figures E.4 to E.7 in Appendix E. This increase in various zones allows for a larger contribution of the total modal strain energy when compared to the uniform ILD treatment.

In Figure 7.7 the modal loss factors for the aforementioned models with an amplitude of $A_1 = 2 \times h_2$ (parameter h_2 represents the VEM layer thickness) are presented in the form of a bar chart. The graph shows that both 2D wave models constitute a better solution than the uniform integrated layer square plate, already known as the most effective treatment configuration. Another conclusion taken from the graph is that, with the exception of the second natural mode, when the number of waves is doubled, the

loss factor value decreases. It is important to note that the number of waves for the 0.5 waves per module is already high, due to the fact that it represents seven waves for both directions in the 140 x 140 mm square plate.

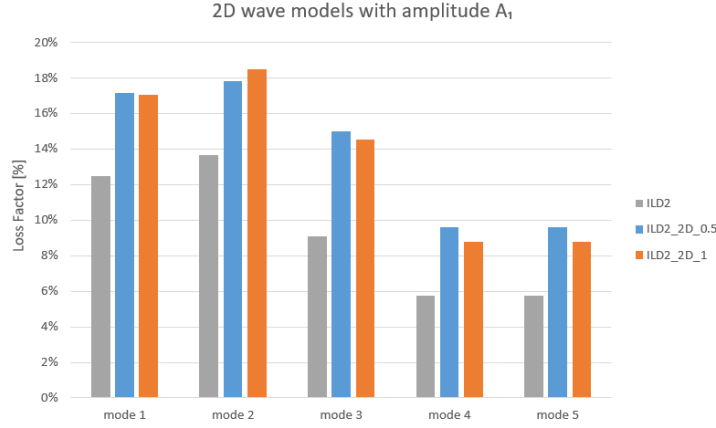


Figure 7.7: Modal loss factor comparison between the 2D wave models with A_1 amplitude.

Figure 7.8 represents the bar graph that compares the modal loss factor results for two different wave amplitudes of the ILD2_2D_0.5 model. It is possible to conclude that decreasing the wave amplitude to its half decreases the efficiency of the treatment.

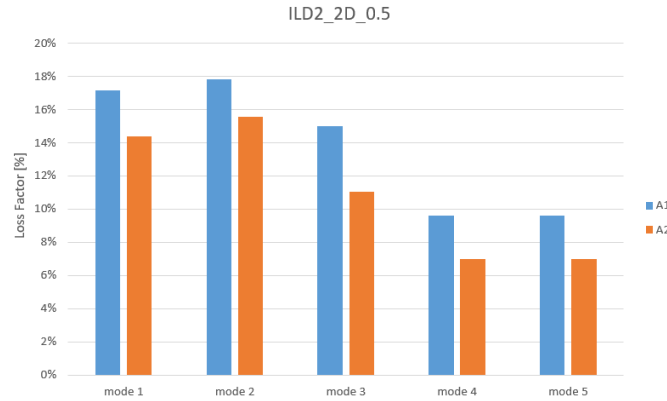


Figure 7.8: Modal loss factor comparison between the ILD2_2D_0.5 with two different amplitudes.

The ILLD configuration treatments with integrated layer are compared with the uniform ILD square model. It is important to note that the numerical models for these configurations neglects any relative motion between layers since all the nodes in the interface between layers are coincident. This condition can affect the numerical results, therefore, the experimental study was used to validate the ILLD treatments.

The modal strain energy distribution for the first natural mode of the VEM layer of the ILD square models was presented in Table 5.9 in Chapter 5. The table clearly demonstrates the stripes configuration of the ILLD models and the strain energy superiority of the uniform ILD treatment when compared to the other ones. For the other

analysed modes, presented in Appendix E, it is possible to draw the same observations.

In Figure 7.9 the normalized loss factors for the aforementioned models are presented in the form of a bar chart. The graph shows the superior efficiency of the ILD2 treatment when compared to the ILLD ones. A possible explanation could be related to how the models were developed, which was explained in the beginning of this section. The ILLD models present a slight loss factor increase when the number of stripes for both directions is increased.

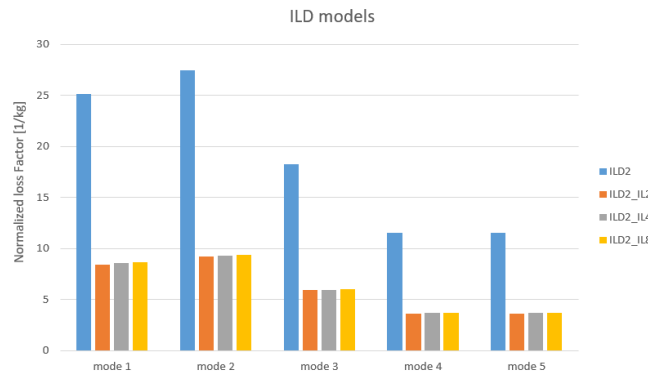


Figure 7.9: Normalized loss factor comparison between the ILD square models.

The developed CLD square models present, in Table 5.11 from Chapter 5 for the first natural mode and in Appendix E for the other natural modes, the VEM layer modal strain energy distribution. The analysis of these tables allows for the same conclusions as the ones obtained for the ILD square models to be taken.

Figure 7.10 presents, in the form of a bar graph, the normalized loss factor for the CLD square models. In this figure, the difference between both models is clear. The uniform CLD square plate presents better results when compared to the ILLD models with the same constraining layer. As aforementioned, the treatments were developed with connected nodes between layers, which implicates disregarding the motion between them. This implication can be a possible explanation for the inferior efficiency of the ILLD concept with constraining layer. Therefore, an experimental study evaluating both configurations was performed and the results are analysed later in this chapter.

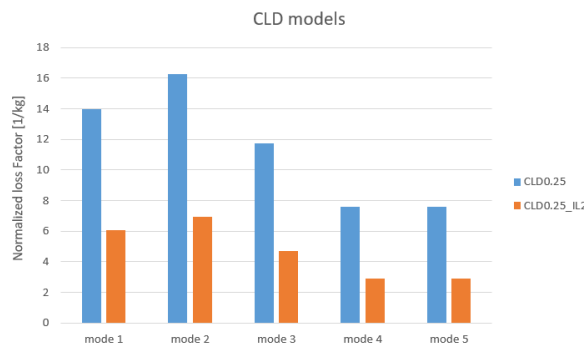


Figure 7.10: Normalized loss factor comparison between the CLD square models.

The ILLD free single material models were compared to the FLD uniform treatment.

The modal strain energy distribution for the first natural mode (Table 5.13 of Chapter 5) and for the other modes (Appendix E) presents the bottom view (VEM surface in contact with the host structure) and top view (VEM free surface). These tables clearly demonstrate the stripes configuration of the ILLD models and the influence of the host structure (bottom view) when compared to the free top view.

In Figure 7.11 the normalized loss factor for the aforementioned models are presented in the form of a bar chart. The results demonstrate the effect obtained when an uniform VEM layer is changed for the interlaced concept using VEM stripes. The increase of the VEM stripes in both directions represents a slight increase in the normalized loss factor.

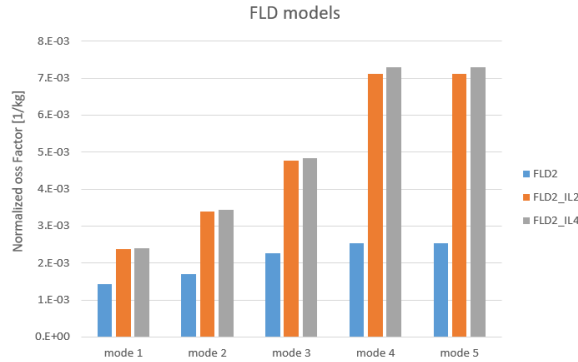


Figure 7.11: Normalized loss factor comparison between the FLD square models.

The FLD single layered constraining stripes models present, in Table 5.15 of Chapter 5 for the first natural mode and in Appendix E for the other natural modes, the VEM stripes modal strain energy distribution. These models allow the study of the material stiffness effect on the treatments efficiency. The aforementioned tables demonstrate a clear increase of the modal strain energy when the constraining material stiffness increases.

The natural frequencies for each mode (in Appendix E) demonstrate that, as expected, the natural frequencies increase when the constraining material stiffness increases. Figure 7.12a shows the effect of increasing the constraining material stiffness in the treatments efficiency for the first natural mode, however, the same conclusion can be taken for the other modes. This study allowed to conclude that, when mixing constraining stripes among the VEM stripes, a material with a higher Young's modulus is a more efficient solution to combine with the VEM stripes in the ILLD concept.

For the FLD configuration, with a single or double layer and with interlaced constraining layers, the numerical results are presented in tables 5.17 and 5.18 (Chapter 5) for the first natural mode (remaining results are gathered in Appendix E). The distribution evidences the effect caused by adding one layer and an interleaved one. The interleaved double layer causes an evident increase in the modal strain energy. In Appendix B (Figure B.3), it is possible to find a representation of the hereby analysed models.

In Figure 7.12b the normalized loss factor for the first natural mode can be observed. The figure shows the effect of adding another layer on the treatment efficiency. This effect is greater when the double layer is interleaved. These promising results are also verified for the other analysed natural modes.

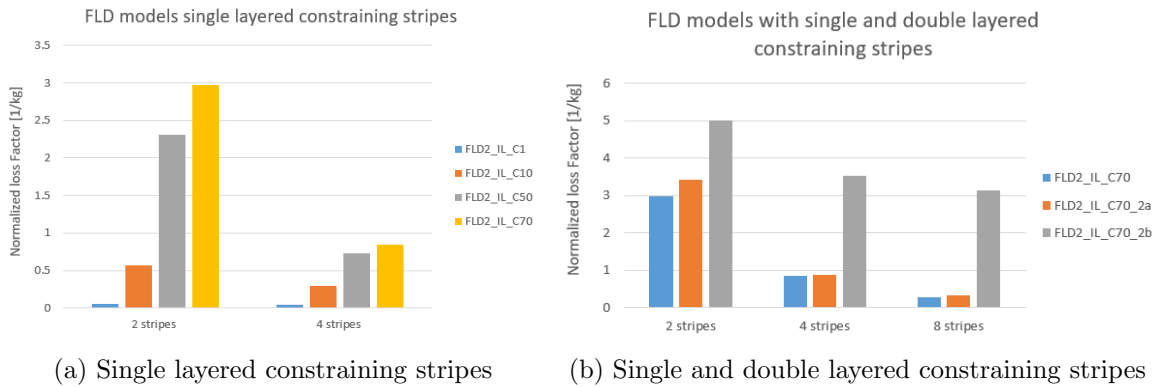


Figure 7.12: Normalized loss factor comparison between the FLD square models.

Rectangular plate models

According to the results obtained for the square models, a similar group of rectangular plates were also studied to be compared to the experimental ones were developed. The CLD uniform treatment and the CLD interlaced configuration were developed using a constraining layer with a thickness of 0.5 mm, since it was the one available at the laboratory. In Figure 7.13, the normalized loss factor values for this group are presented. From the results obtained for the numerical study of the CLD rectangular models is concluded the same as the mentioned for the CLD square ones.

The most promising ILLD models were developed in rectangular models to compare with the corresponding experimental specimens. These models, shown in Table 5.23 for the first natural mode and in Appendix E for the other natural modes, present equivalent results to those of the square models.

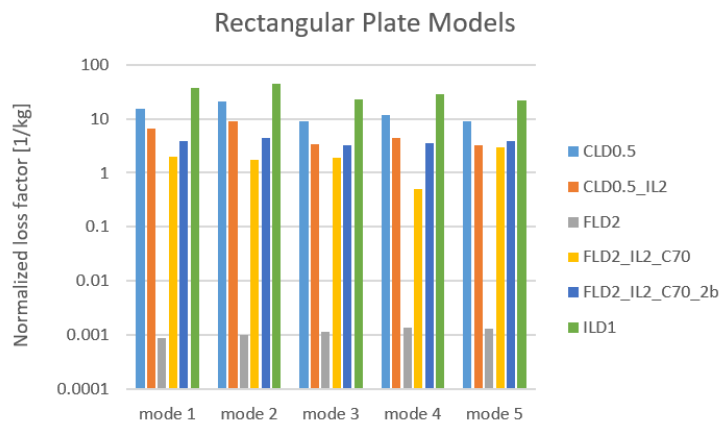


Figure 7.13: Normalized loss factor comparison between the rectangular plate models.

7.3.2 Experimental results analysis

The experimental results obtained for the plate specimens are presented in a form of a bar chart in Figure 7.14 (PolyMax method) and Figure 7.15 (Circle Fit method).

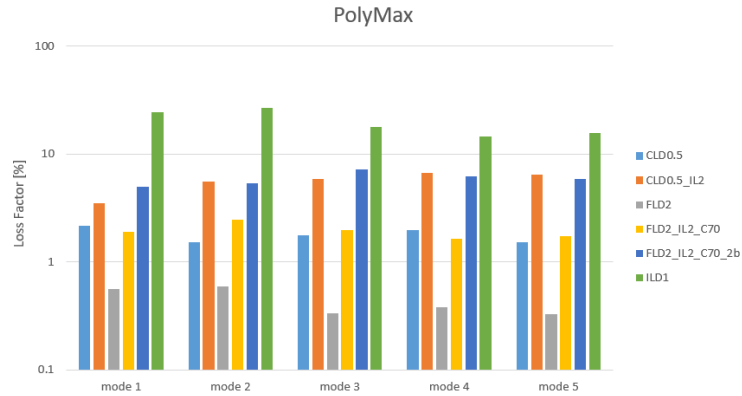


Figure 7.14: Modal loss factor comparison between the plate specimens - PolyMax.

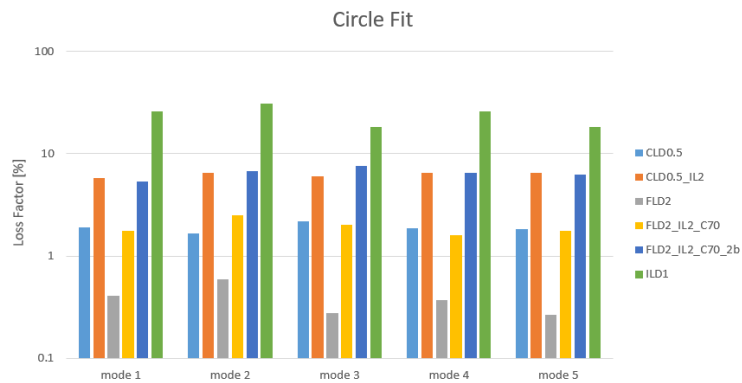


Figure 7.15: Modal loss factor comparison between the plate specimens - Circle Fit.

Several interesting conclusions can be taken from these graphs. Contrary to what was observed in the numerical analysis, the experimental results evidence a superiority of the CLD0.5_IL2 treatment loss factor when compared to the CLD0.5 configuration. This great conclusion can be explained by the aforementioned possible explanation, since for the numeric models the layers are attached (coincident nodes) and do not allow the representation of potential relative motion between adjacent layers, while in the experimental study such restraint is not imposed. Another information provided by the experimental results is that, not just the free ILLD concept provides a better solution than the uniform FLD treatment, but also provides a valid replacement for constrained uniform damping treatments, with the advantages of a free layer configuration.

7.3.3 Numerical/Experimental comparison

Figures 7.16 to 7.21 show the comparison between the natural frequencies and modal loss factor for both numeric and experimental study for the developed plate specimens. These figures demonstrate similar natural frequency results when comparing the ones obtained numerically and experimentally (by both methods) and similar modal loss factor values for both experimental analysis methods.

Based on the comparison analysis of the loss factor results, one cannot take valid and

sustained conclusions when analysing each treatment configuration. Nevertheless, general observations can be drawn by comparing the overall level of loss factor observed for all the configurations. Therefore, it is possible to observe that the proposed configuration, the interlaced layer damping treatment provided interesting results when compared to the FLD and CLD configurations.

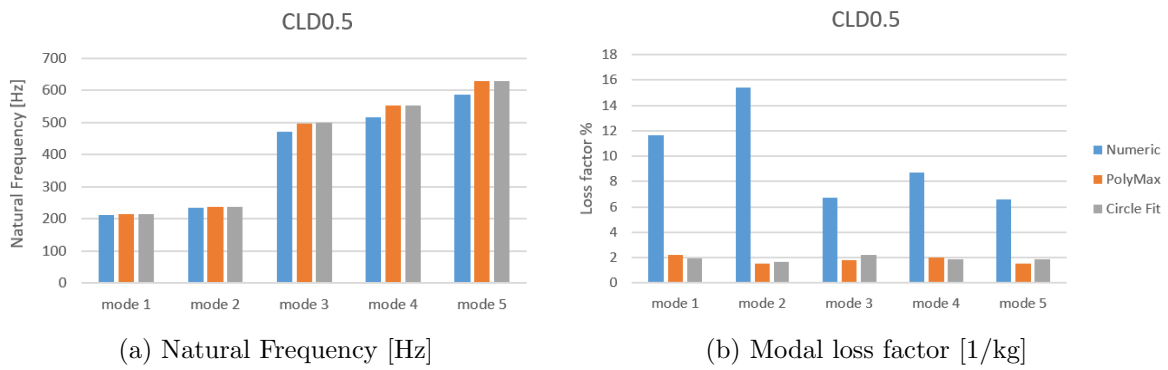


Figure 7.16: Comparison between numeric and experimental study - CLD0.5.

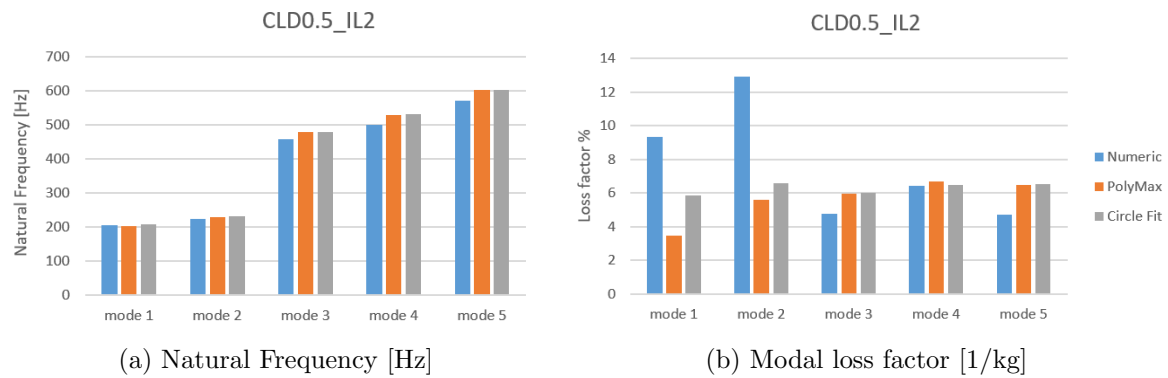


Figure 7.17: Comparison between numeric and experimental study - CLD0.5_IL2.

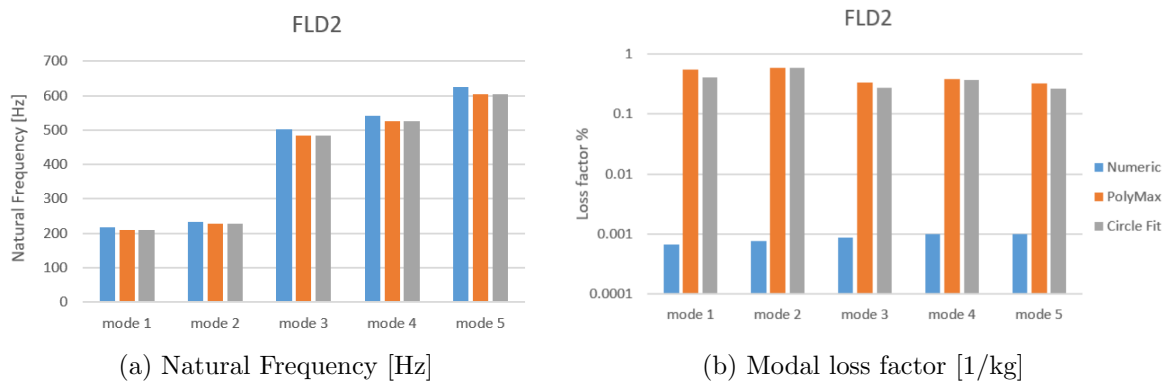


Figure 7.18: Comparison between numeric and experimental study - FLD2.

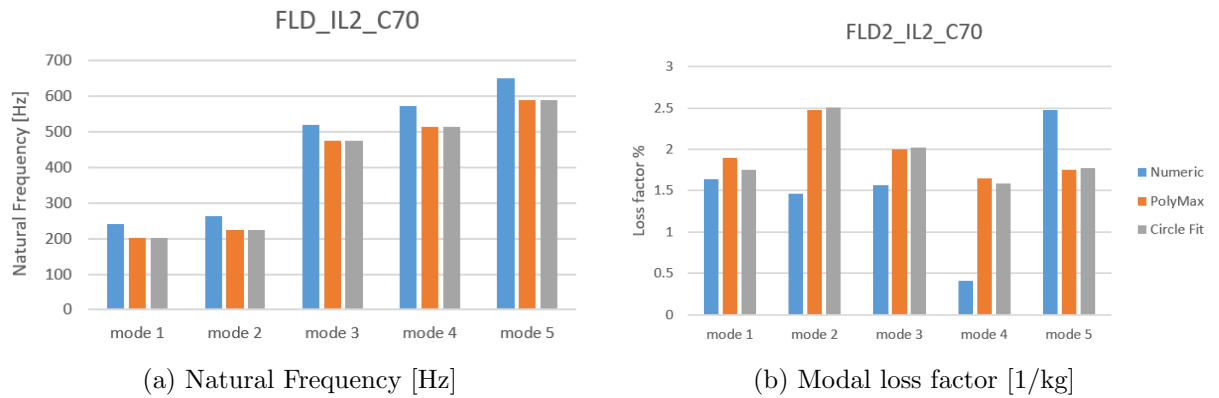


Figure 7.19: Comparison between numeric and experimental study - FLD2_IL2_C70.

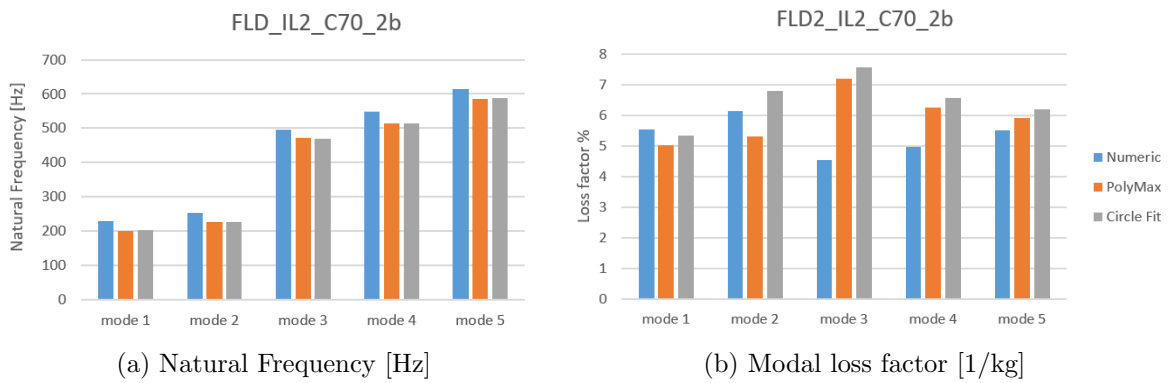


Figure 7.20: Comparison between numeric and experimental study - FLD2_IL2_C70_2b.

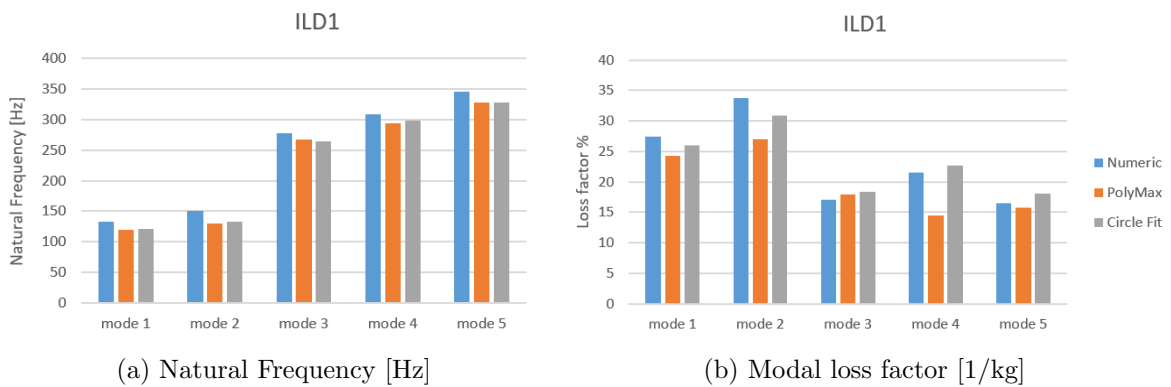


Figure 7.21: Comparison between numeric and experimental study - IL1.

Chapter 8

Conclusions and future work

In this chapter, the concluding remarks are presented along with some suggestions of related topics that may be developed in the future.

8.1 Conclusions

According to the main objectives of this thesis, the dissertation addresses the exploratory work of promising concepts for passive damping treatments.

The problem associated with vibration affects structures and machines, that shall be taken in consideration during the designing stage. Sometimes this specification is neglected or simply provided by later stage problems, even if the design was appropriate. For that, damping mechanisms are considered as a good alternative method for vibration control. Viscoelastic treatments are considered to be one of the most efficient methods to limit vibration levels.

The principal focus of the developed study was to explore alternative and effective new configurations for passive damping treatments using viscoelastic materials. For this purpose, the spatial model, based on the Finite Element Method, and the numerical and experimental analysis of the new configurations dynamic behaviour were developed.

The first promising configuration: the 1D waves configuration represents a valid solution for beam-kind treatments. The numerical study developed demonstrated that this concept can represent a more efficient solution when compared to the uniform sandwich beam treatment, while approximately maintaining the added VEM mass.

The 2D waves configuration represents an effective solution for ILD damping plate treatments. The numerical study developed for this configuration provided promising results by demonstrating an efficient solution that can be a reasonable replacement for uniform ILD plate treatments using the same amount of VEM.

The ILLD concept increases the efficiency of the viscoelastic damping treatments, while maintaining the advantages of an application procedure based on a simple deposition of a single layer of material on the structure surface. The numerical and experimental results demonstrated the feasibility of this proposed and promising configuration, that provides a valid replacement for constrained damping layers, which often require a time consuming and laborious placement procedures, and in some cases, such as those where the target component has a complex geometry, are even impracticable or severely damaged during the application. This concept aims to overcome the limitations of the

constrained damping treatments, while providing similar levels of damping.

The work developed in this dissertation provides important contributions to both science and industry. The developed study presents new concepts that enable saving computing and production time, laborious placement procedures and severe damages, and, therefore, leads to costs reduction.

8.2 Future Work

The work developed during this dissertation combined several concepts that can be further explored.

For the 1D wave concept, it is recommended to run an experimental validation procedure, using specimens that really mimic the assumed kinematic model considered in the numerical study. This would require more time, that was not available for this exploratory study carried on this work. In fact, it would be necessary to produce special host structures, possibly using CNC machining, press or controlled chemical reactions to obtain the required waved surface on the host beam and constraining layer.

Another suggestion relies on the experimental validation of the 2D waves concept applied in the numerical study developed within the scope of this work. This promising concept could be adapted to an experimental specimen benefiting from the new technologies, such as, 3D printing and CNC machining.

The ILLD concept is materialized by a three-dimensional layup of VEM stripes, possibly combined with stripes of other materials. An interesting approach would be including VEM with different transition temperatures, following the multi-material concept [16], benefiting from its advantages. This concept provides a set of other possible features that can be investigated to optimize or tailor the damping treatment. By changing the stripes arrangement, including a single layer or multiple layers of entangled stripes or the application of different materials depending on the stripe direction, and even by changing the angle of the stripes, one can explore the modification on the damping effect according to the mode shape, frequency band or temperature range. Other design parameters should also be analyzed, such as the gap size between stripes, the insert of localized slide areas, using small release films, and other possible solutions to take advantage of the internal border effects and relative motion between stripes.

Within the scope of hybrid treatments, the proposed configuration (ILLD) also opens new possibilities, where active fibers or stripes can be introduced inside the interlaced VEM layer to enhance its deformation during vibration. The use of shape-memory polymers in the form of stripes, or wires made from shape memory alloys or piezoelectric materials, can be used as active constraining stripes/fibers to increase or tailor the level of deformation imposed to the dissipative layers.

Appendix A

Pre-processing: Model

The model for each structure was directly developed by a proper mesh using the *Generate Between Corners* tool and the *Extrude* tool to create the solid elements in the *mesh* menu. For the majority of the models developed, a module that could be copied (*Copy* tool), rotated (*Rotate* tool), scaled (*Scale* tool), or reflected (*Reflect* tool) was initially performed, in order to obtain the intended configuration, as explained later for each case.

In order to prepare the analysis for each model in the software, the *Coincident Nodes* tool in the *Tools* menu was used. This tool removes a set of nodes that are coincident within a predefined tolerance. A group was created that includes the VEM elements. The elements of each material were renumbered using the *Renumber* tool in the *Modify* menu to aid the post-processing strategy.

The boundary condition was set as free in the *Model* menu with the *Constraint* tool. Therefore, everything was set for the creation of the analysis. By the *Analysis* on the *Model* menu it is possible to define the proper analysis for the models designed. For this work the NX Nastran analysis program and the *Normal Modes/Eigenvalue* type analysis were used. The desired number of eigenvalues for the modal analysis was defined, the free constraint was selected, and the elemental strain energy was chosen as output for all the model. It is important to note that it was unchecked the *Element Corner Results* option to interpolate the results and it was changed an option in the preview input in order to allow that all the values are taken in consideration even the ones that were approximately zero.

Intentionally blank page.

Appendix B

Representation of the interlaced configurations developed

In this appendix, it is presented every model mentioned in the Table 4.5, through a representation of each interlaced square plate developed in the software *Femap*, its dimensions and materials properties.

In the Figure B.1, it is possible to observe the ILD interlaced 140 x 140 mm models developed for the numerical study. The host structure is represented in opaque grey, the constraining layer on top in grey with reduced opacity and the stripes are all represented in dark pink to indicate that every stripe is VEM based.

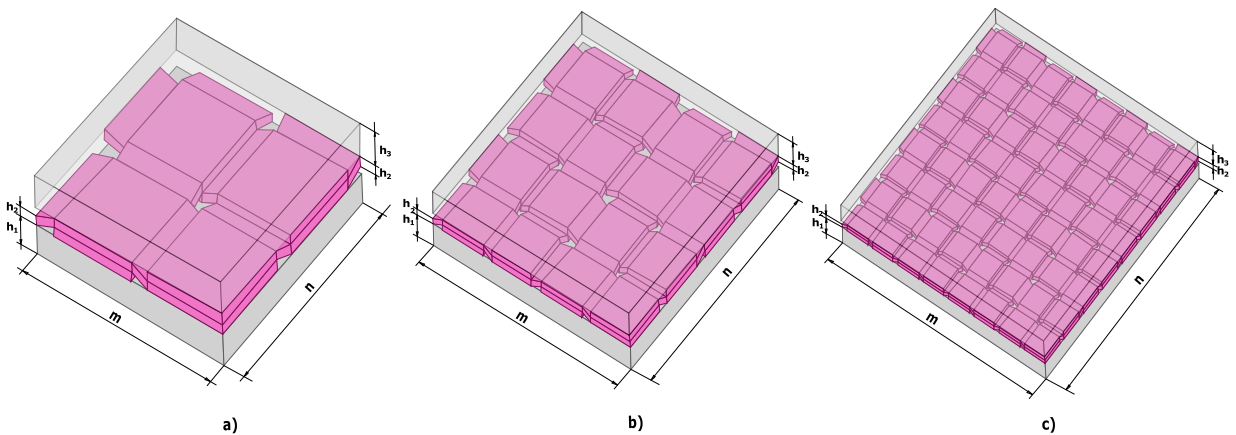


Figure B.1: Representation of the ILD interlaced square plates: a) ILD2_IL2; b) ILD2_IL4; c) ILD2_IL8.

m and n represent the length and width of the structure, respectively, h_1 the thickness of the host structure, h_2 the thicknesses of the stripes and h_3 the thickness of the constraining layer.

The Figure B.2 presents the CLD interlaced 140 x 140 mm model developed for the numerical study. As before, the host structure is represented in opaque grey, on top the constraining layer in grey with reduced opacity and the stripes are all represented in dark pink to indicate that every stripe is VEM based. The CLD interlaced configuration for these dimensions was only created with 2 stripes in both directions, due to the fact that was developed having in consideration the numerical results of the other models

and it is a reference model for future comparison.

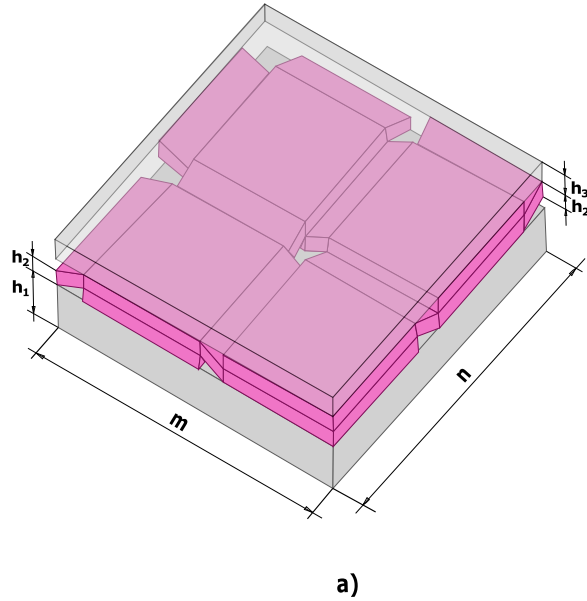


Figure B.2: Representation of the CLD interlaced square plate: CLD0.25_IL2.

m and n represent the length and width of the structure, respectively, h_1 the thickness of the host structure, h_2 the thicknesses of the stripes and h_3 the thickness of the constraining layer.

Figure B.3 presents the FLD interlaced 140x140mm models developed for the numerical study. The first line presents the FLD models developed with VEM stripes, the second line presents the ones using stripes with two different materials, and the third and fourth line present the double layer of stripes with two different materials as well as interleaved, respectively. The host structure is represented in opaque grey, the dark pink stripes represent the VEM ones and the light pink stripes represent the ones based on the second material. The models using a single layer of stripes with two different materials were analysed using a second material with an Young's modulus of 70, 50, 10 and 1GPa, represented by the Δ in Figure B.3 caption. After obtaining the results for these models, the double layer models (_2a and _2b) were developed using an aluminium with 70GPa Young's modulus as second material stripes. The justification for that choice is presented on the Chapter 5.

As before, m and n represent the length and width of the structure, respectively, h_1 the thickness of the host structure and h_2 the thicknesses of the stripes.

In the Table B.1, it is possible to observe the characteristics for the models presented in this appendix. The stripes width is shown for each number of stripes. The constraining layer thickness assumes a different value for ILD and CLD, as presented in the table. The layer 1 corresponds to the host structure, the layer 2 to the stripes layer and the layer 3 to the constraining layer, when applicable.

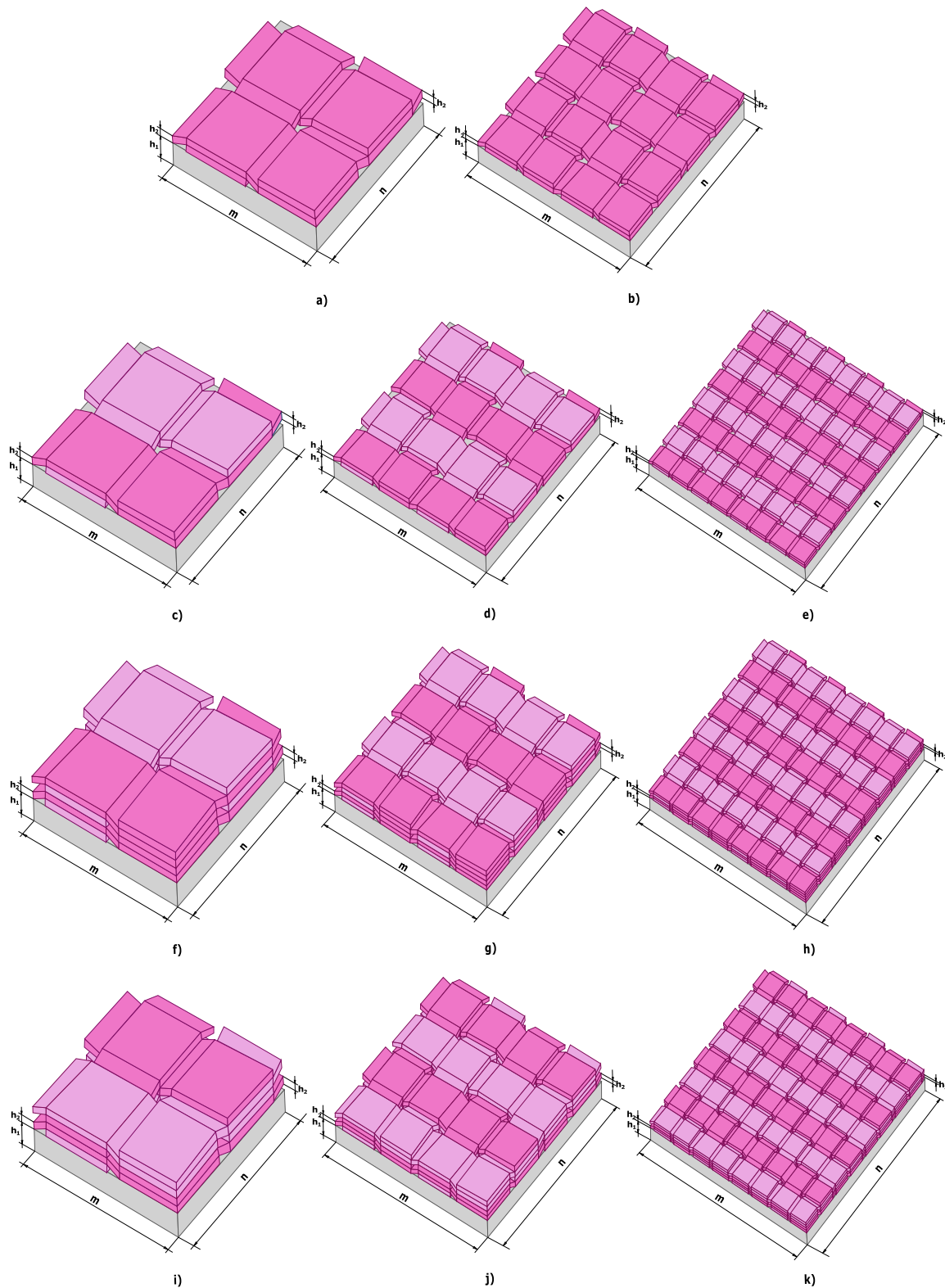


Figure B.3: Representation of the FLD interlaced square plates: a) FLD2_IL2; b) FLD2_IL4; c) FLD2_IL2_C Δ ; d) FLD2_IL4_C Δ ; e) FLD2_IL8_C Δ ; f) FLD2_IL2_C70_2a; g) FLD2_IL4_C70_2a; h) FLD2_IL8_C70_2a; i) FLD2_IL2_C70_2b; j) FLD2_IL4_C70_2b and k) FLD2_IL8_C70_2b.

Table B.1: Characteristics of the developed interlaced square plates.

Dimension	m	140 mm		
	n	140 mm		
	Stripes Width	2 stripes	67.5 mm	
		4 stripes	33.75 mm	
		8 stripes	16.875 mm	
	h_1	2 mm		
	h_2	0.254 mm		
	h_3	ILD	2 mm	
CLD		0.25 mm		
Aluminium Properties: Layer 1 and Layer 3	AW5754-H111			
VEM Properties: Layer 2 (stripes)	3M ISD112 [106]			
Boundary Conditions	free body			

Appendix C

MSE method based code

The following *Matlab* codes, listing C.1 and C.2, present the developed codes to provide the modal loss factor, based on the MSE method, for models using stripes with the same material and two different materials, respectively, since one of these is always a viscoelastic material.

Listing C.1: Matlab code to obtain Modal Loss Factor by MSE method.

```
1 %Table excluding the non numerical lines
2 %Reference:https://www.mathworks.com/matlabcentral/answers/323274-how-to
3 %-delete-rows-that-contain-nan-in-a-table
4 %Change file_name for the name of the file that contains the treatments
5 %modal strain energy for each element
6 T_total=file_name(~any(ismissing(file_name),2),:);
7
8
9 %Change number_VEM for the 1st VEM element number defined on FEMAP
10 index_first_VEM= find(T_total{:,1}==number_VEM);
11 %Table with VEM layer elements
12 T_vem=T_total(index_first_VEM:end,:);
13
14 %Sum of total modal Strain energy
15 Sum_Etotal=sum(T_total{:,2});
16
17 %Loss factor of VEM
18 eta_VEM=1;
19 %Sum of VEM modal Strain Energy
20 Sum_Evem=sum(T_vem{:,2}.*eta_VEM);
21
22 %Loss factor of the structure by MSE method
23 eta_structure=(Sum_Evem*eta_VEM)/Sum_Etotal
```

Listing C.2: Matlab code to obtain Modal Loss Factor for 2 different material's stripes by MSE method.

```

1  %Table excluding the non numerical lines
2  %Reference:https://www.mathworks.com/matlabcentral/answers/323274-how-to
3  %-delete-rows-that-contain-nan-in-a-table
4  %Change file_name for the name of the file that contains the treatments
5  %modal strain energy for each element
6  T_total=file_name(~any(ismissing(file_name),2),:);
7
8  %Change 1stnumber_VEM for the 1st VEM element number and Lastnumber_VEM
9  %for the last defined on FEMAP
10 %Change 1stnumber_2mat for the 1st Material 2 (Constraining Material)
11 %element number defined on FEMAP
12 index_first_VEM= find(T_total{: ,1}==1stnumber_VEM);
13 index_first_EndVEM= find(T_total{: ,1}==Lastnumber_VEM);
14 index_first_2mat= find(T_total{: ,1}==1stnumber_2mat);
15 %Table with VEM and Material 2(Constraining Material) layer elements
16 T_vem=T_total(index_first_VEM:index_first_EndVEM, :);
17 T_2mat=T_total(index_first_2mat:end, :);
18
19 %Sum of total modal Strain energy
20 Sum_Etotal=sum(T_total{: ,2});
21
22 %Loss factor of VEM
23 eta_VEM=1;
24 %Sum of VEM modal Strain Energy
25 Sum_Evem=sum(T_vem{: ,2}.*eta_VEM);
26
27 %Loss factor of the structure by MSE method
28 eta_structure=(Sum_Evem)/Sum_Etotal

```

Appendix D

Circle Fit method

The Circle Fit method is a SDOF method based on circle fitting the FRF plots in the surroundings of resonance. The *Nyquist* plot is a parametric plot of a frequency response, whose properties produce circle-kind curves. An exact circle can be obtained if the damping model parameter is chosen properly [4].

D.1 SDOF Assumption

In this section it is provided the assumptions and basis which this method is founded. The method takes advantage of the fact that in the surrounding of a resonance, the majority of the systems' behaviour is dominated by a single mode [4]. Therefore, the magnitude of the FRF is controlled by one of the terms in the series related to the mode whose resonance is being observed. The assumption mentioned can be expressed by a partial fractions series to represent the FRF receptance as follows [4],

$$\alpha_{jk}(\omega) = \sum_{s=1}^N \frac{sA_{jk}}{\omega_s^2 - \omega^2 + i\eta_s\omega_s^2} \quad (\text{D.1})$$

The expression above can be rewritten without simplification as [4],

$$\alpha_{jk}(\omega) = \frac{rA_{jk}}{\omega_r^2 - \omega^2 + i\eta_r\omega_r^2} + \sum_{s=1, s \neq r}^N \frac{sA_{jk}}{\omega_s^2 - \omega^2 + i\eta_s\omega_s^2} \quad (\text{D.2})$$

For a small range of frequency in the surroundings of the natural frequency of mode r , it's possible to assume that the second term on Equation D.2 is approximately independent of the frequency ω . Therefore, the receptance can be written as [4],

$$\alpha_{jk}(\omega) = \frac{rA_{jk}}{\omega_r^2 - \omega^2 + i\eta_r\omega_r^2} +_r B_{jk} \quad (\text{D.3})$$

D.2 Properties of the Modal Circle

Knowing that an individual modal circle can be obtained from a FRF plot, it's explored in this section the properties of the modal circle that can provide the required modal

parameters. Since the effect of modal constant ${}_r A_{jk}$ is to scale the size and rotate the circle, it's considered that [4],

$$\alpha = \frac{1}{\omega_r^2(1 - (\omega/\omega_r)^2 + i\eta_r)} \quad (D.4)$$

Figure D.1 represent the plot of the quantity α . For any frequency ω , it is possible to write the following relations [4],

$$\tan\gamma = \frac{\eta_r}{1 - (\omega/\omega_r)^2} \quad (D.5)$$

$$\tan(90^\circ - \gamma) = \tan\left(\frac{\theta}{2}\right) = \frac{1 - (\omega/\omega_r)^2}{\eta_r} \quad (D.6)$$

From which is obtained,

$$\omega^2 = \omega_r^2 \left(1 - \eta_r \tan\left(\frac{\theta}{2}\right)\right) \quad (D.7)$$

Equation D.8 is obtained by differentiation of Equation D.7 with respect to θ [4].

$$\frac{d\omega^2}{d\theta} = -\frac{\eta_r \omega_r^2}{2} \left(1 + \left(\frac{1 - (\omega/\omega_r)^2}{\eta_r}\right)^2\right) \quad (D.8)$$

The reciprocal of the above quantity reaches its maximum value (maximum sweep rate) when $\omega = \omega_r$, which corresponds to the natural frequency of the oscillator. The following differentiation is now performed with respect to frequency as [4],

$$\frac{d}{d\omega} \left(\frac{d\omega^2}{d\theta}\right) = 0 \quad \text{when} \quad (\omega_r^2 - \omega^2) = 0 \quad (D.9)$$

An estimation of the damping is provided by the sweep rate parameter as follows [4],

$$\left(\frac{d\theta}{d\omega^2}\right)_{\omega=\omega_r} = -\frac{2}{\omega_r^2 \eta_r} \quad (D.10)$$

Equation D.10 is useful for MDOF systems due to the fact that for these systems it is not known where the natural frequency is. However, for the Circle Fit method it is possible to obtain its value.

Considering two specific points on the circle, one at frequency ω_b below the natural frequency and other at frequency ω_a above the natural one. Having in consideration the image D.1, it is possible to write [4],

$$\tan\left(\frac{\theta_b}{2}\right) = \frac{1 - \left(\frac{\omega_b}{\omega_r}\right)^2}{\eta_r} \quad (D.11)$$

$$\tan\left(\frac{\theta_a}{2}\right) = \frac{\left(\frac{\omega_a}{\omega_r}\right)^2 - 1}{\eta_r} \quad (D.12)$$

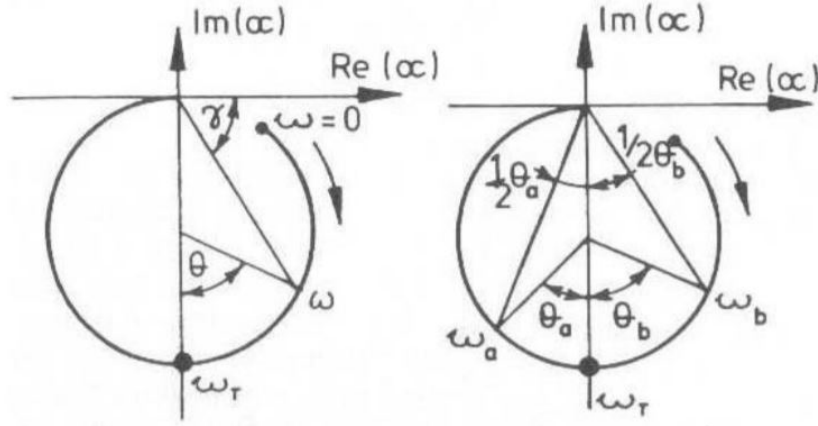


Figure D.1: Properties of modal circle [4].

According to the equations mentioned, it is obtainable the modal damping as [4],

$$\eta_r = \frac{\omega_a^2 - \omega_b^2}{\omega_r^2 \left(\tan\left(\frac{\theta_a}{2}\right) + \tan\left(\frac{\theta_b}{2}\right) \right)} \quad (\text{D.13})$$

For levels of damping lower than 2-3%, Equation D.13 can be simplified to [4],

$$\eta_r \equiv \frac{2(\omega_a - \omega_b)}{\omega_r \left(\tan\left(\frac{\theta_a}{2}\right) + \tan\left(\frac{\theta_b}{2}\right) \right)} \quad (\text{D.14})$$

In the case that $\theta_a = \theta_b = 90^\circ$, called the half-power points, the damping formula is reduced to the familiar one [4],

$$\eta_r = \frac{\omega_a - \omega_b}{\omega_r} \quad (\text{D.15})$$

If the damping considered is not light [4],

$$\eta_r = \frac{\omega_a^2 - \omega_b^2}{2\omega_r^2} \quad (\text{D.16})$$

Finally, the diameter of the circle, for the quantity specified in Equation D.4, is given by $1/\omega_r^2 \eta_r$. When scaled by a modal constant, the diameter is given by [4].

$${}_r D_{jk} = \frac{|{}_r A_{jk}|}{\omega_r^2 \eta_r} \quad (\text{D.17})$$

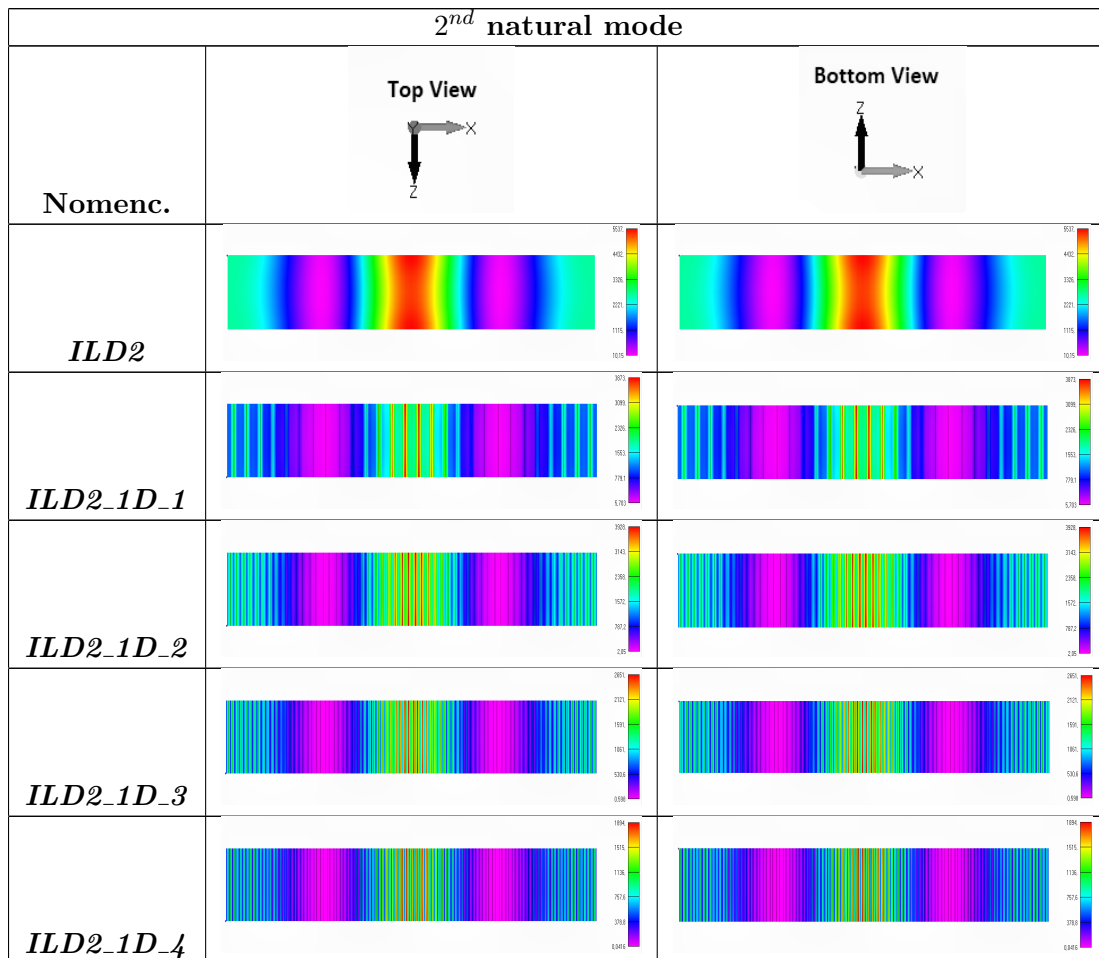
Intentionally blank page.

Appendix E

Numerical Results for the other natural modes

E.1 Beam-kind models

Table E.1: Distribution of the modal strain energy (2^{nd} mode) for the beam models developed with free boundary conditions.



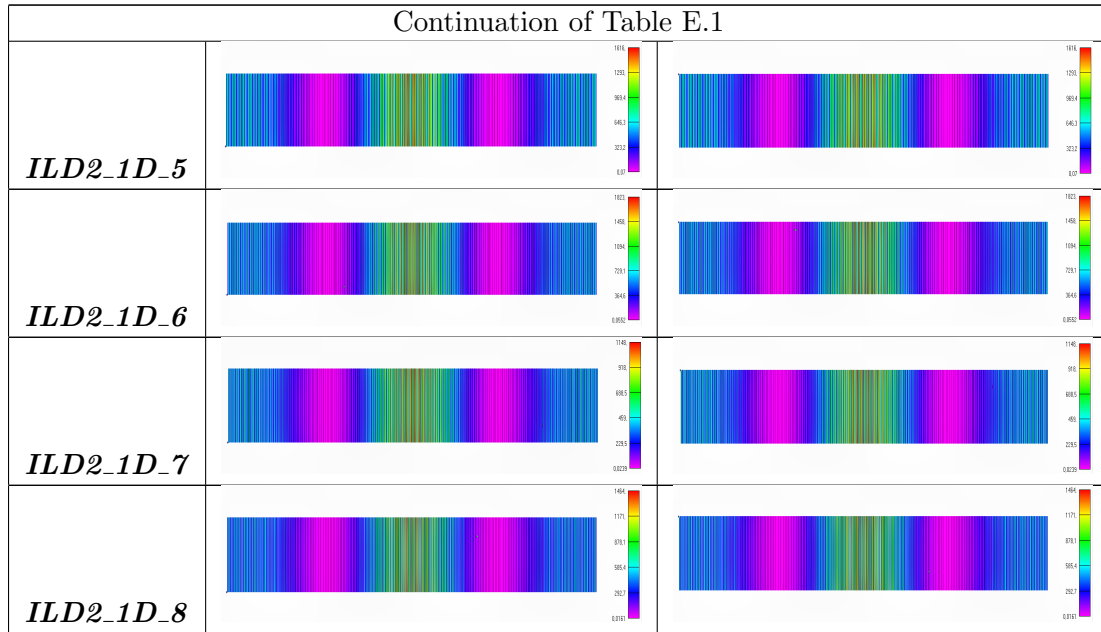
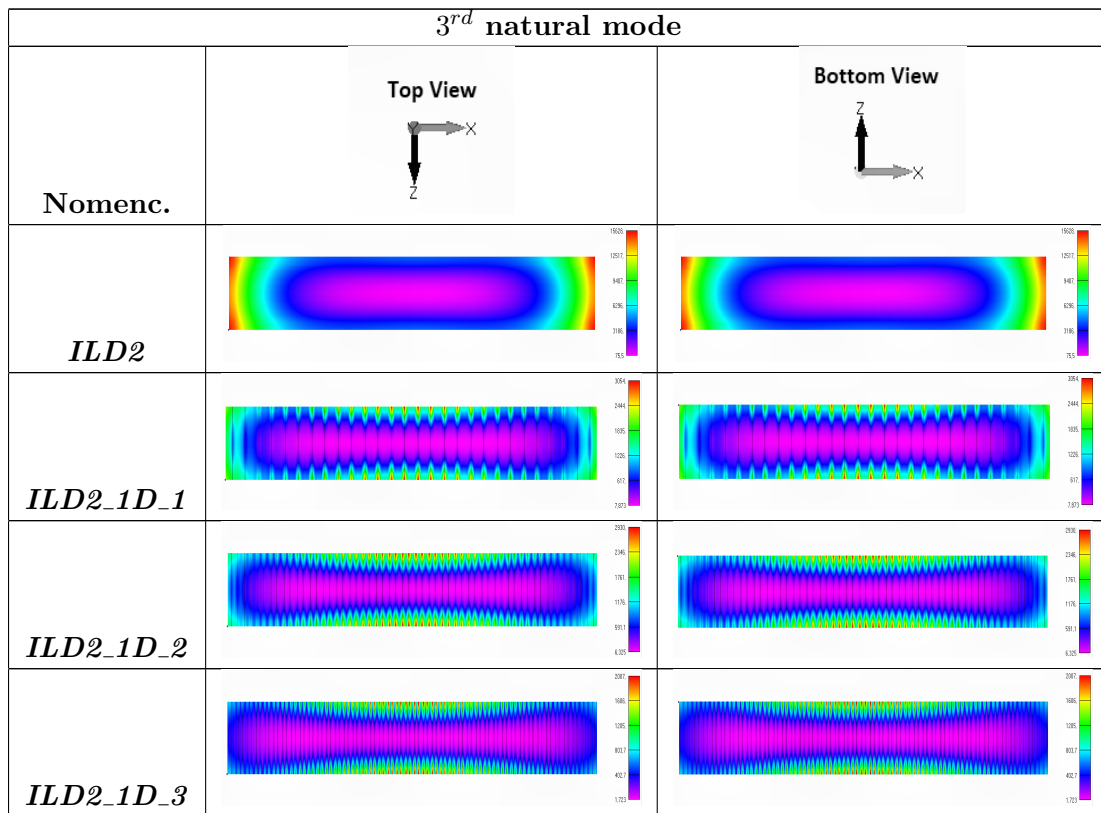


Table E.2: Distribution of the modal strain energy (3^{rd} mode) for the beam models developed with free boundary conditions.



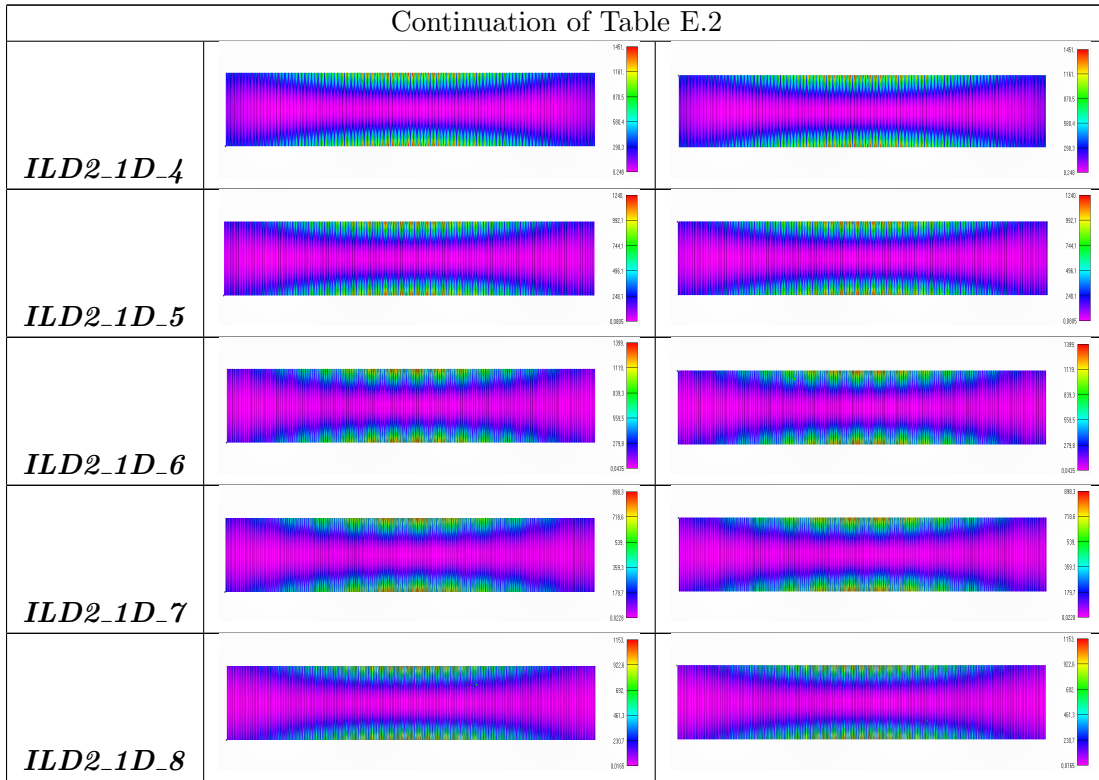
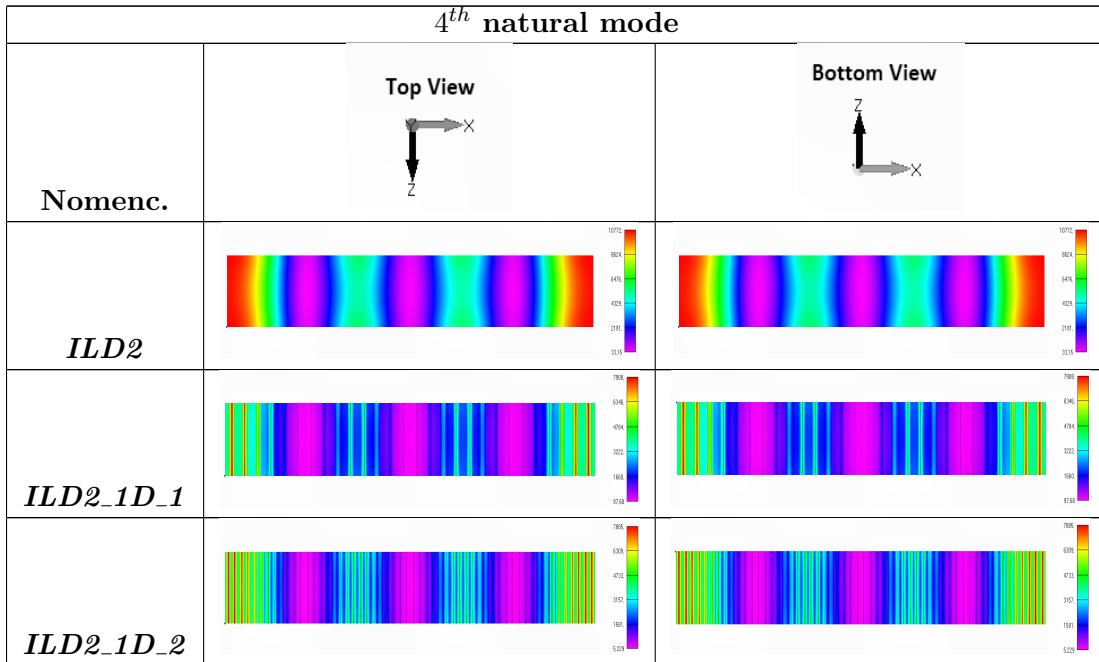
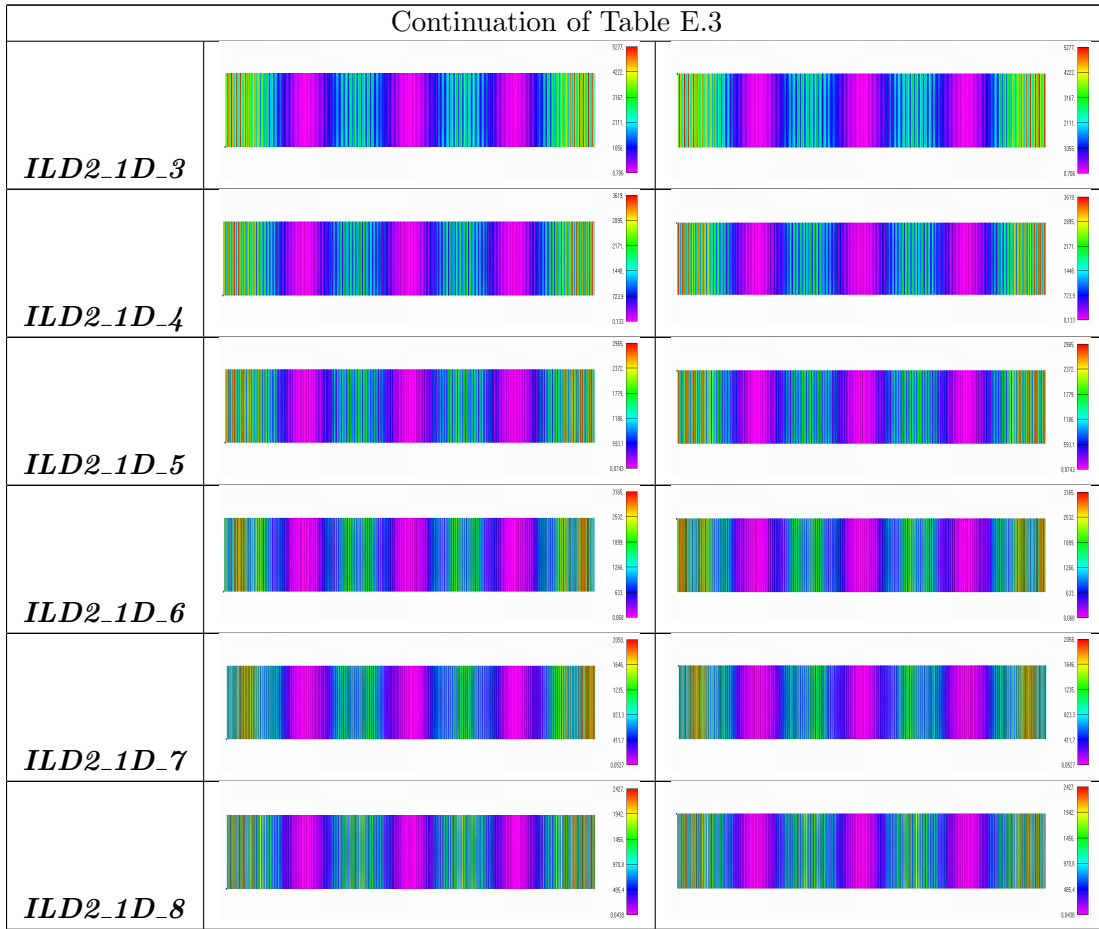


Table E.3: Distribution of the modal strain energy (4^{th} mode) for the beam models developed with free boundary conditions.





E.2 Plate-kind models

E.2.1 Square plate models

2D wave models

Table E.4: Distribution of the modal strain energy (2^{nd} mode) for the 2D wave models developed with free boundary conditions.

2^{nd} natural mode		
Nomenc.	<p>Top View</p>	<p>Bottom View</p>

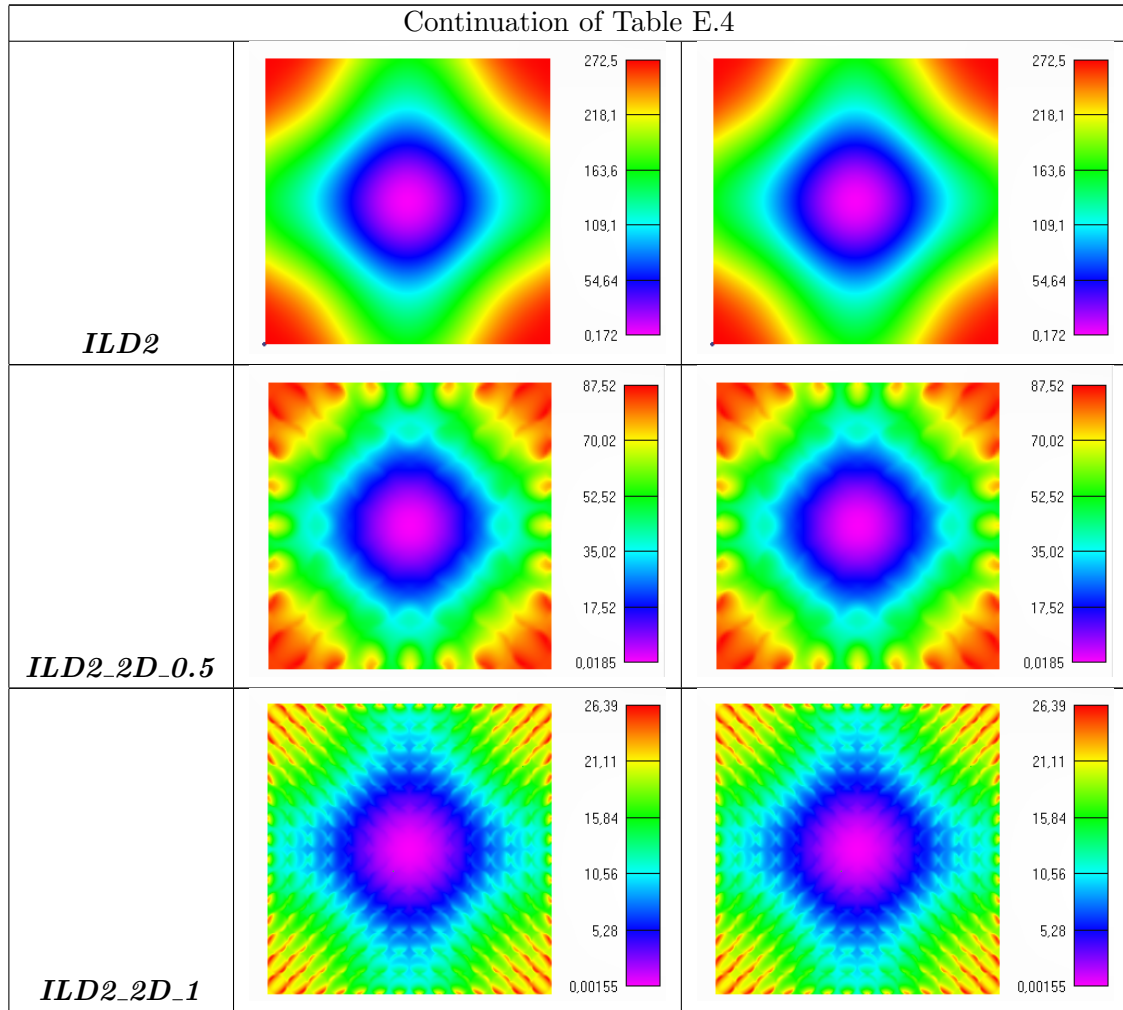
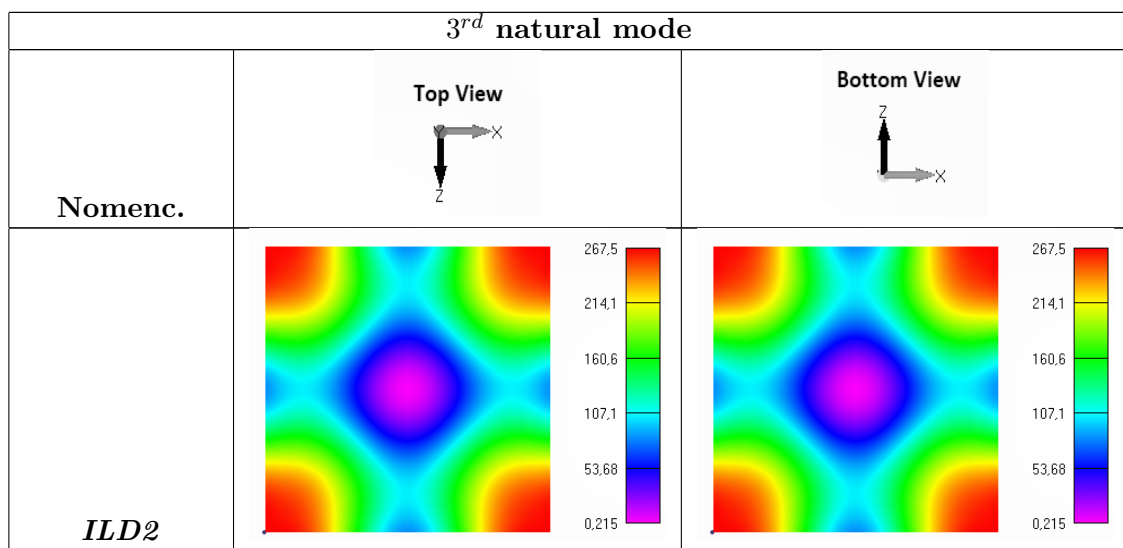


Table E.5: Distribution of the modal strain energy (3^{rd} mode) for the 2D wave models developed with free boundary conditions.



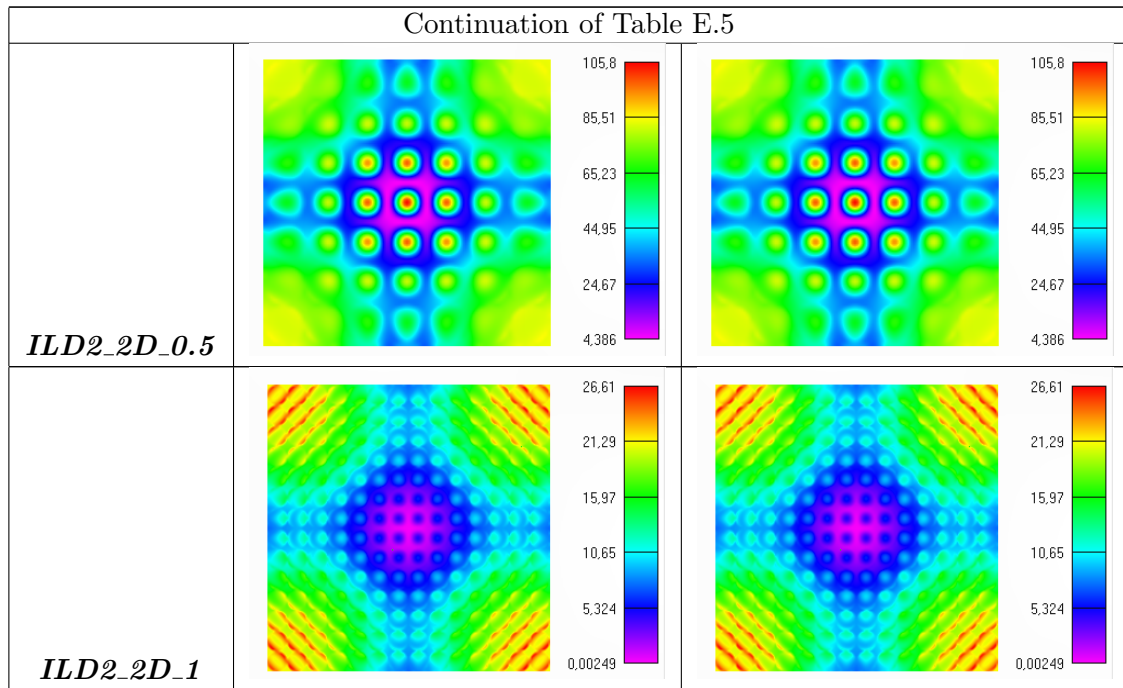
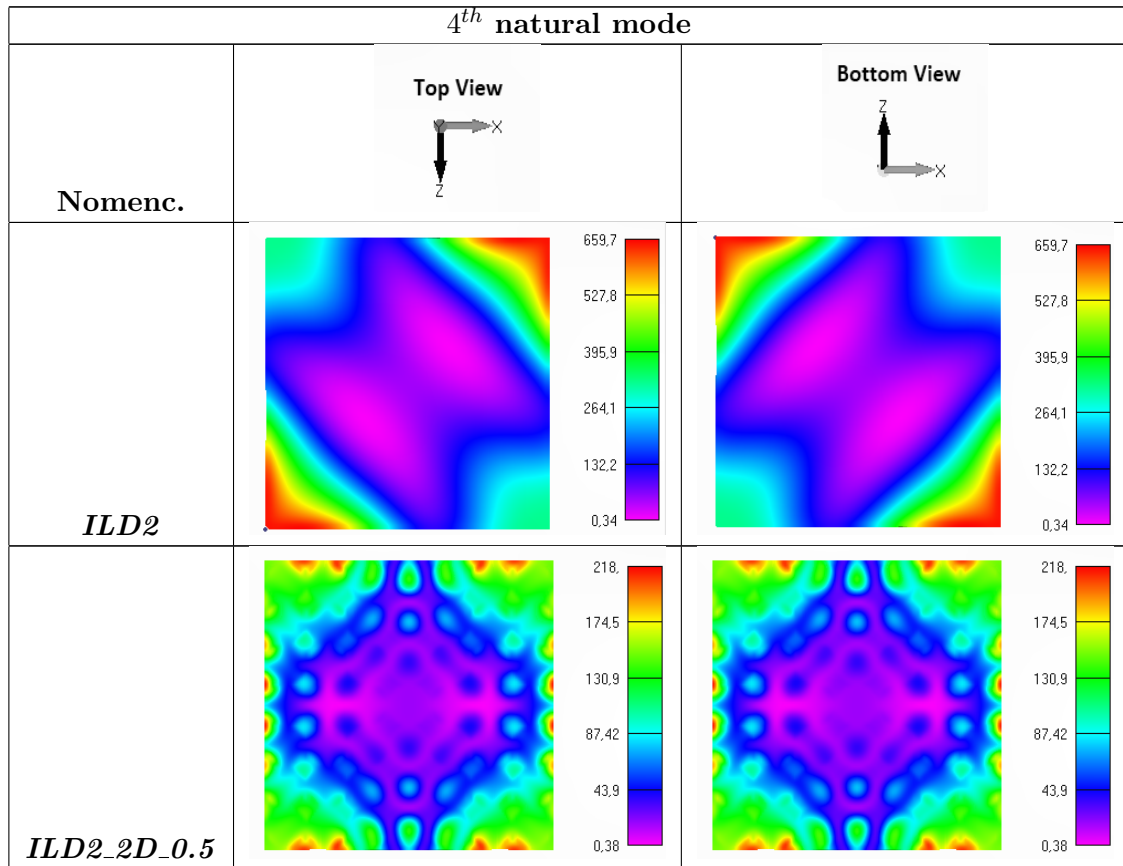


Table E.6: Distribution of the modal strain energy (4th mode) for the 2D wave models developed with free boundary conditions.



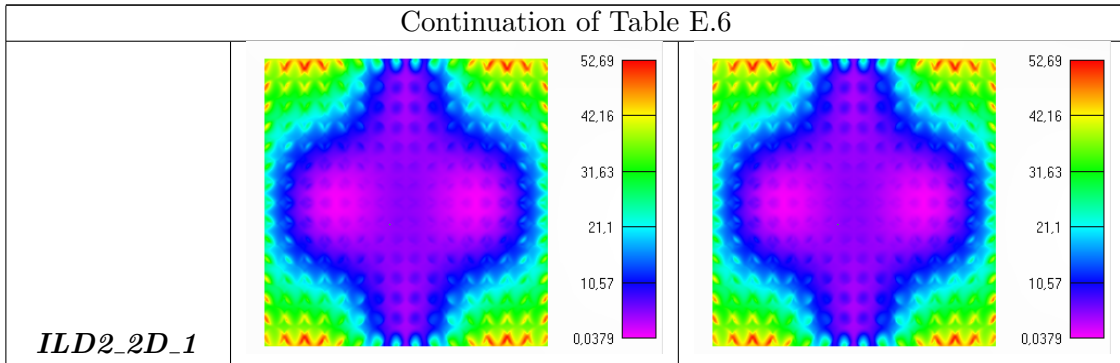
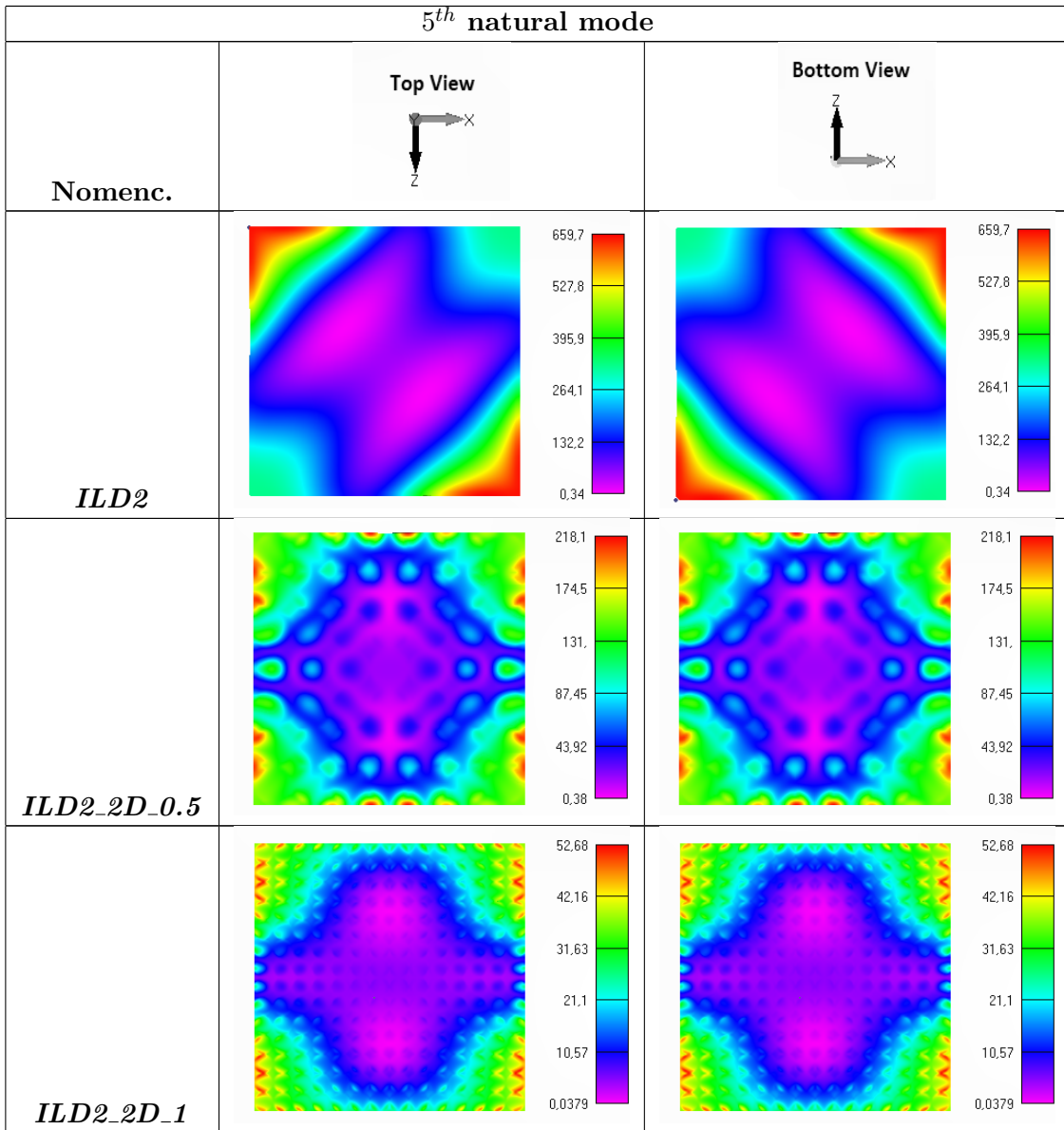


Table E.7: Distribution of the modal strain energy (5th mode) for the 2D wave models developed with free boundary conditions.



Interlaced models

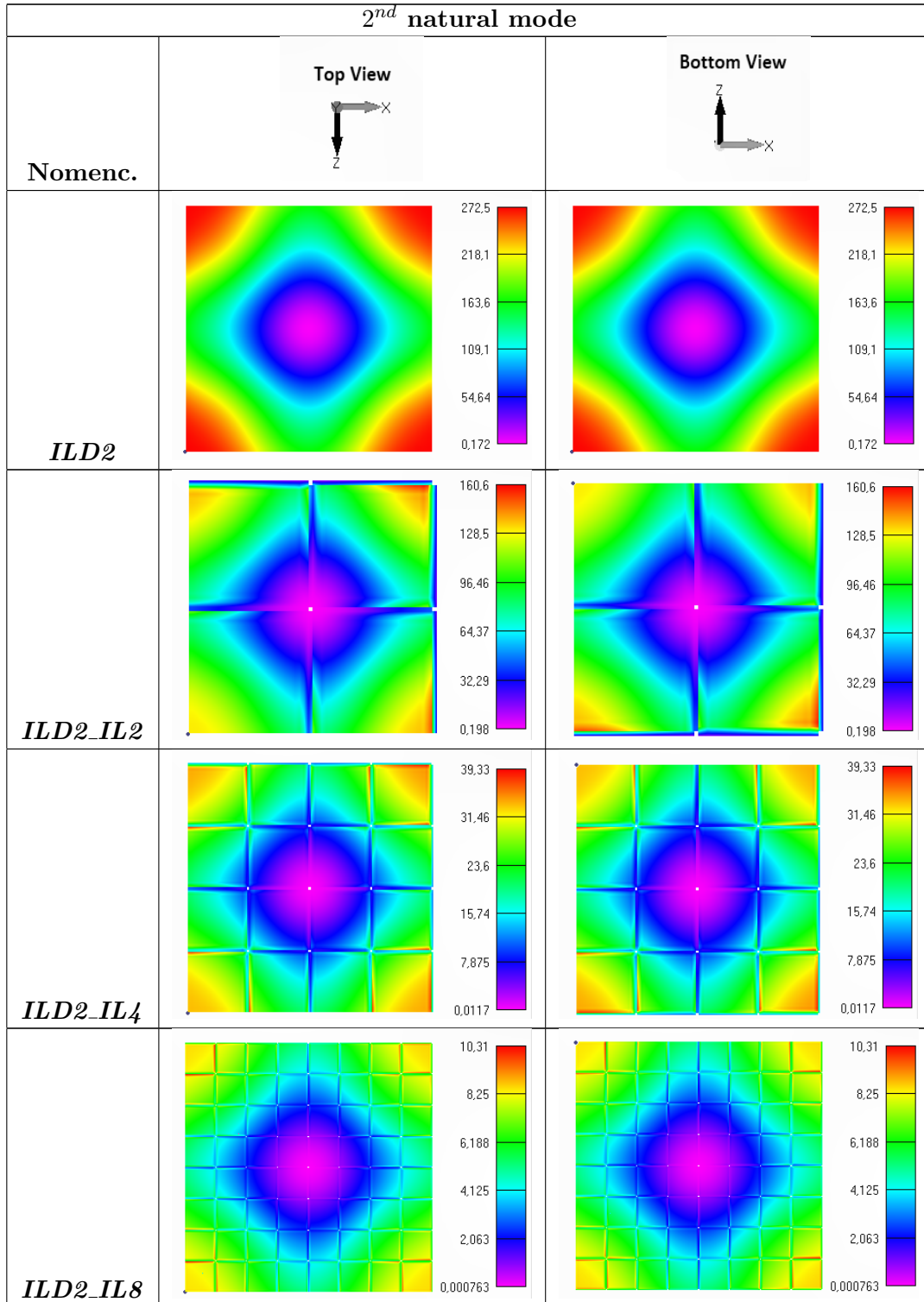
Table E.8: Distribution of the modal strain energy (2^{nd} mode) for the ILD square models developed with free boundary conditions.

Table E.9: Distribution of the modal strain energy (3^{rd} mode) for the ILD square models developed with free boundary conditions.

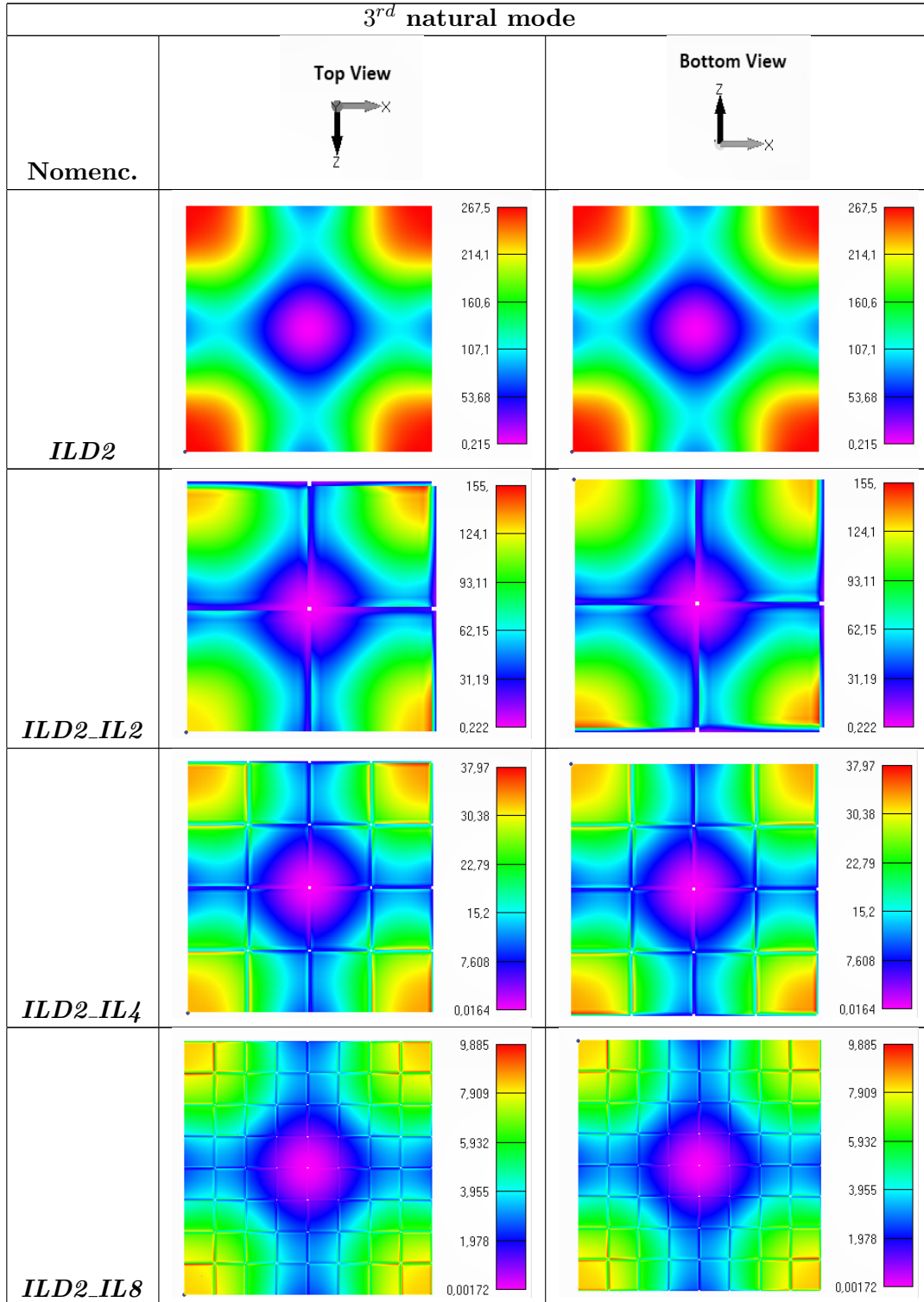


Table E.10: Distribution of the modal strain energy (4^{th} mode) for the ILD square models developed with free boundary conditions.

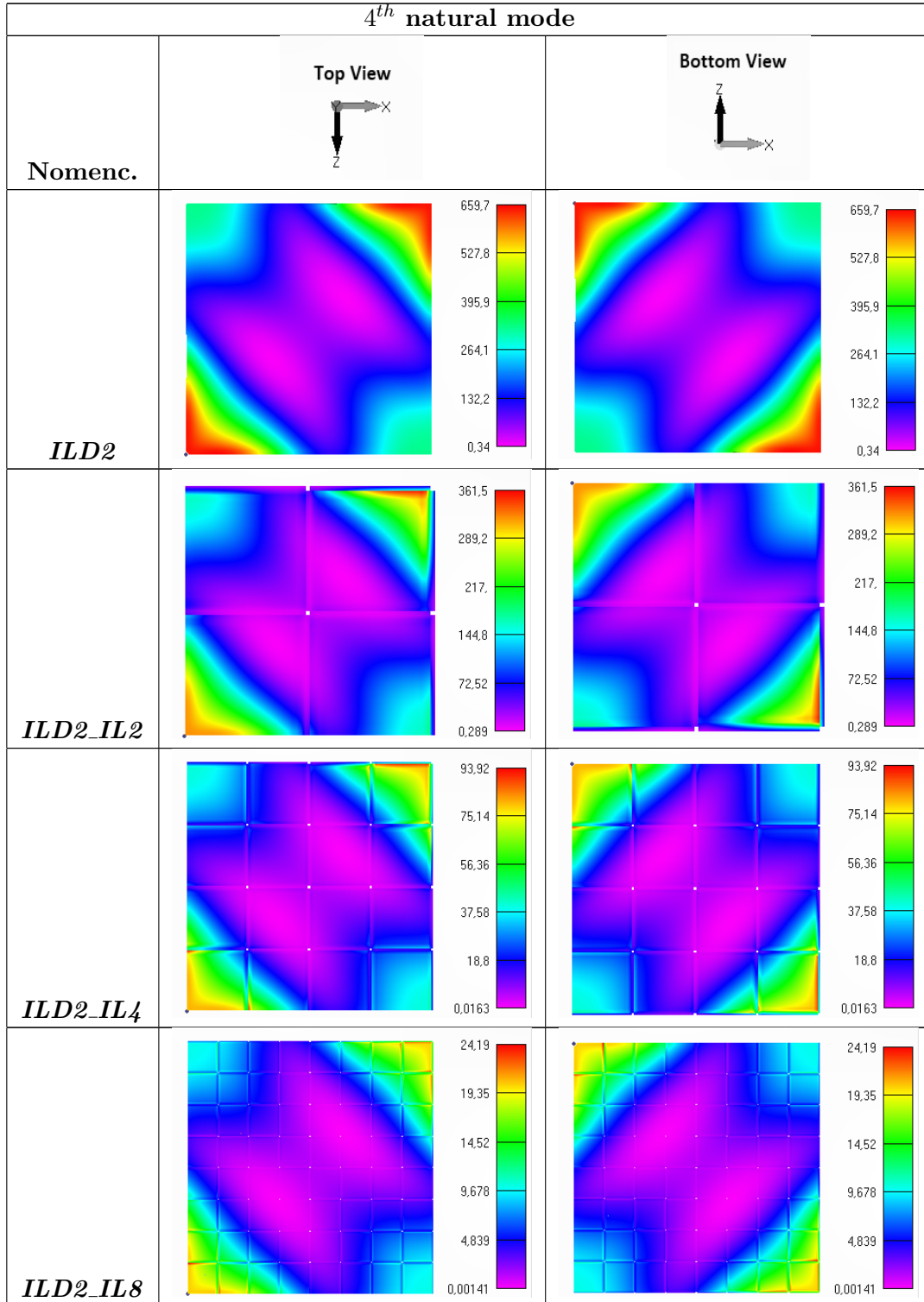


Table E.11: Distribution of the modal strain energy (5^{th} mode) for the ILD square models developed with free boundary conditions.


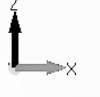
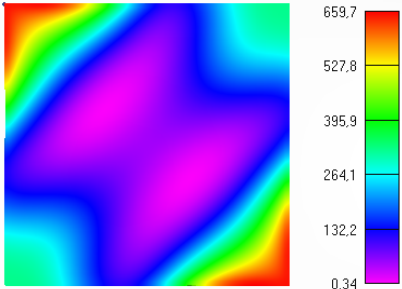
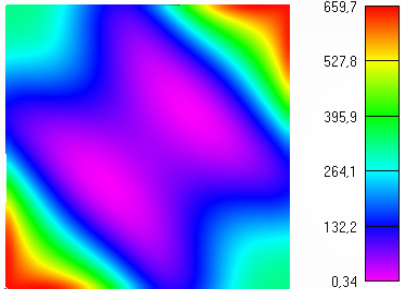
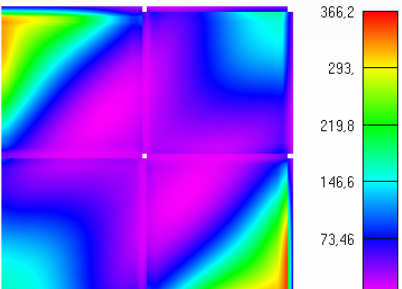
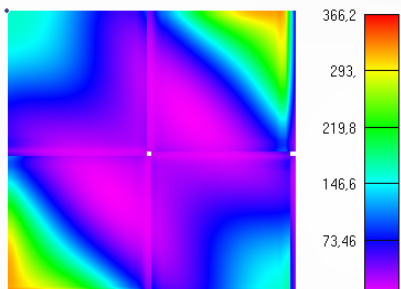
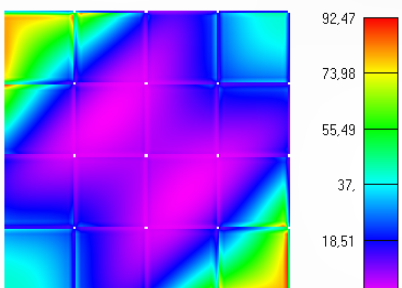
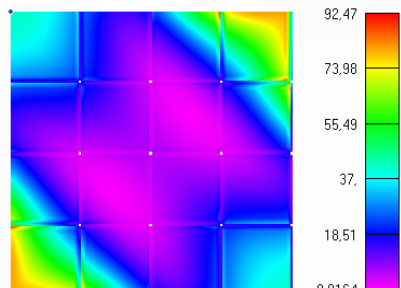
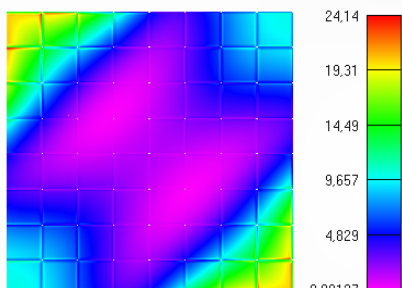
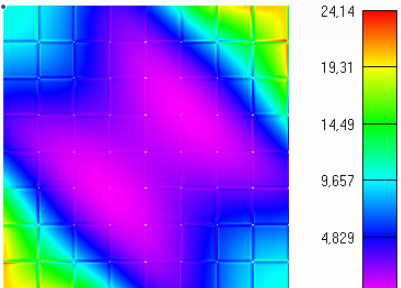
5^{th} natural mode			
Nomenc.	Top View 	Bottom View 	
<i>ILD2</i>			
<i>ILD2_IL2</i>			
<i>ILD2_IL4</i>			
<i>ILD2_IL8</i>			

Table E.12: Distribution of the modal strain energy (2^{nd} mode) for the CLD square models developed with free boundary conditions.


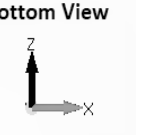
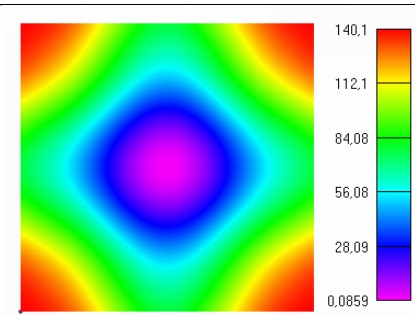
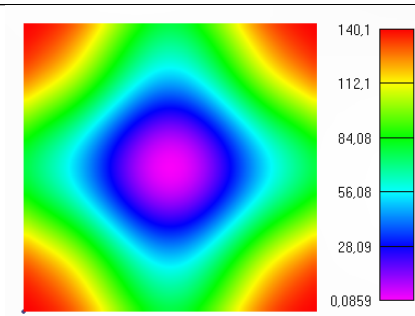
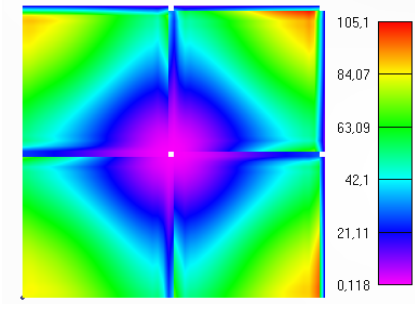
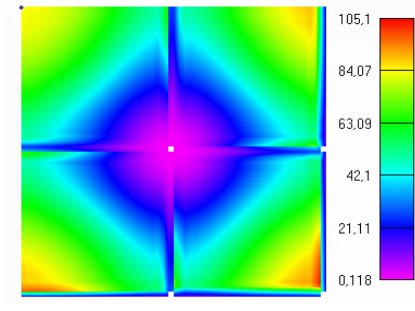
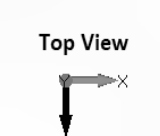
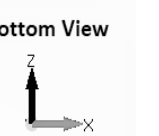
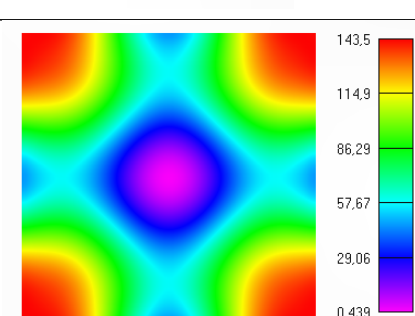
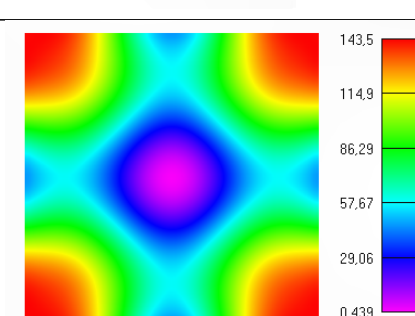
2^{nd} natural mode			
Nomenc.	Top View 	Bottom View 	
<i>CLD0.25</i>			
<i>CLD0.25_IL2</i>			

Table E.13: Distribution of the modal strain energy (3^{rd} mode) for the CLD square models developed with free boundary conditions.

3^{rd} natural mode			
Nomenc.	Top View 	Bottom View 	
<i>CLD0.25</i>			

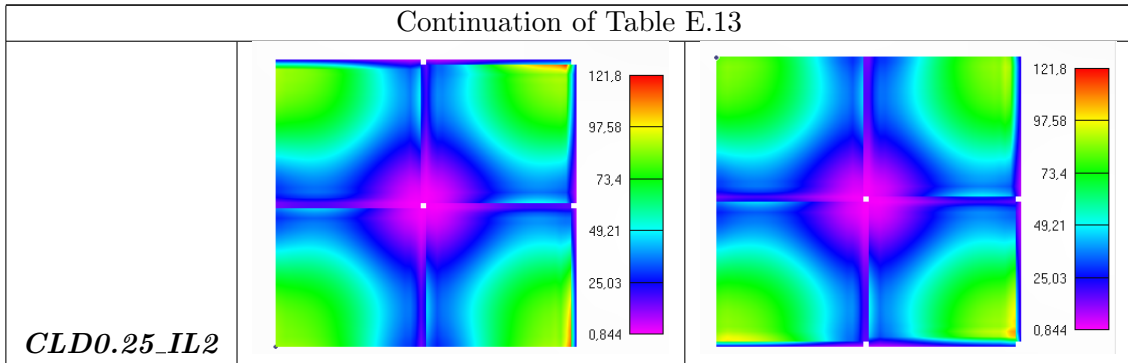


Table E.14: Distribution of the modal strain energy (4^{th} mode) for the CLD square models developed with free boundary conditions.

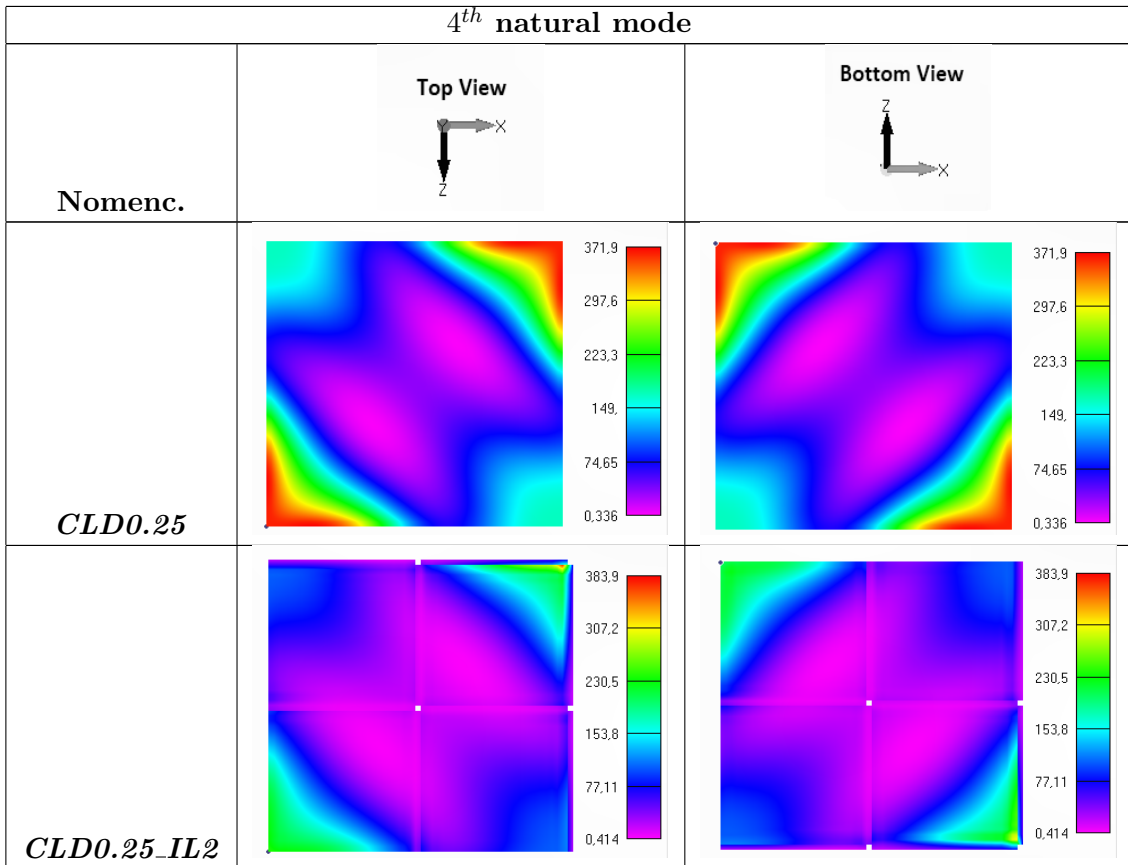


Table E.15: Distribution of the modal strain energy (5^{th} mode) for the CLD square models developed with free boundary conditions.

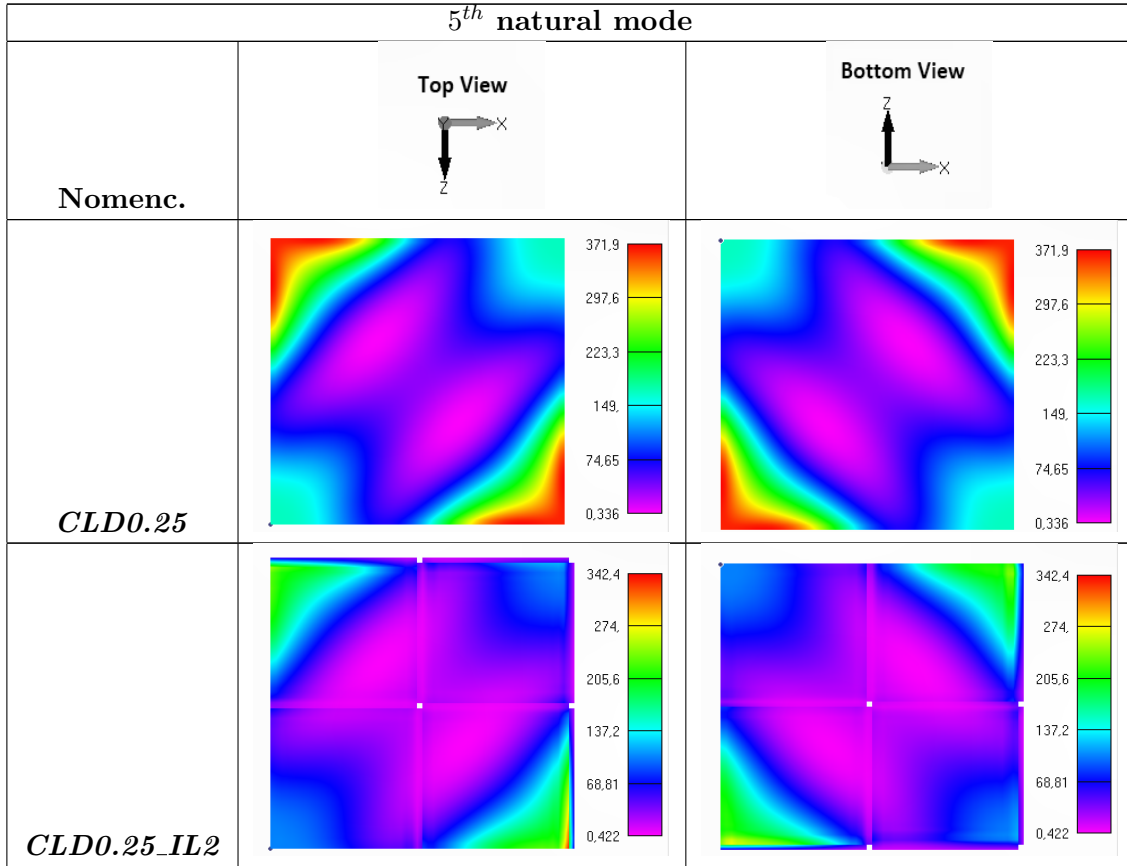
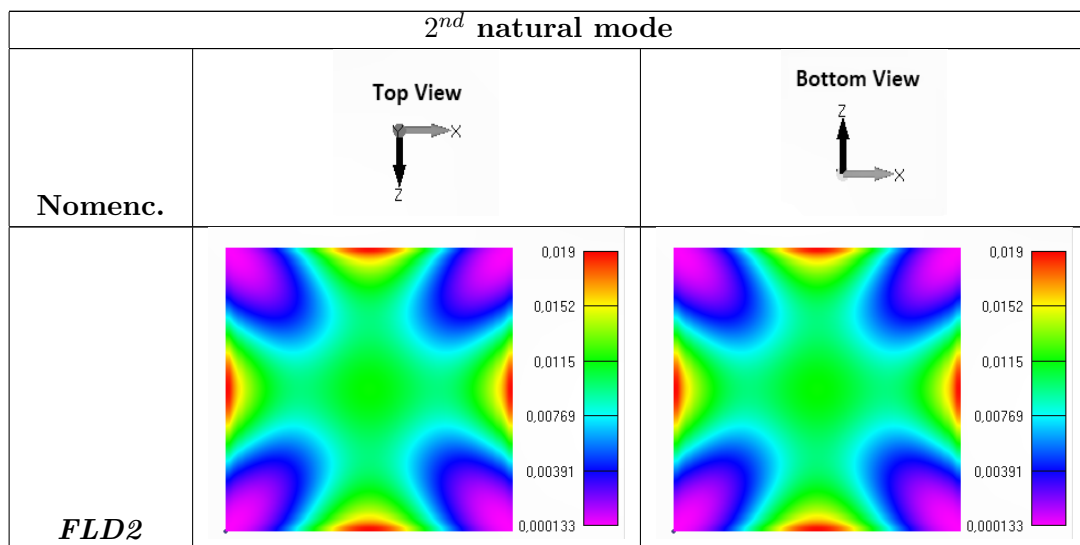


Table E.16: Distribution of the modal strain energy (2^{nd} mode) for the FLD square models without constraining stripes developed with free boundary conditions.



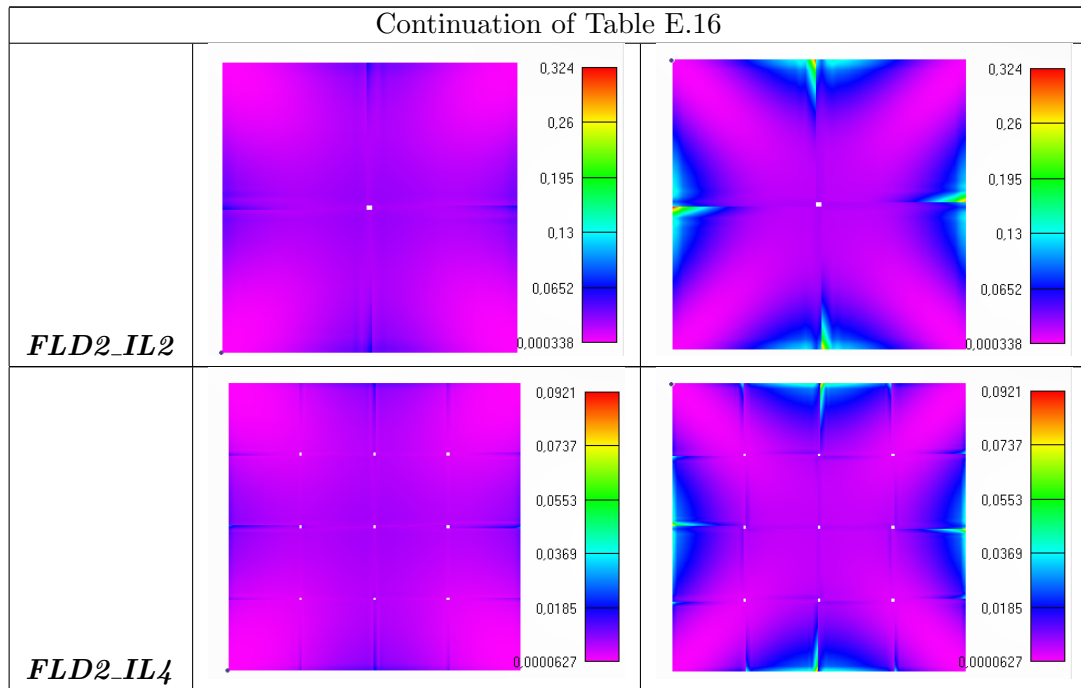
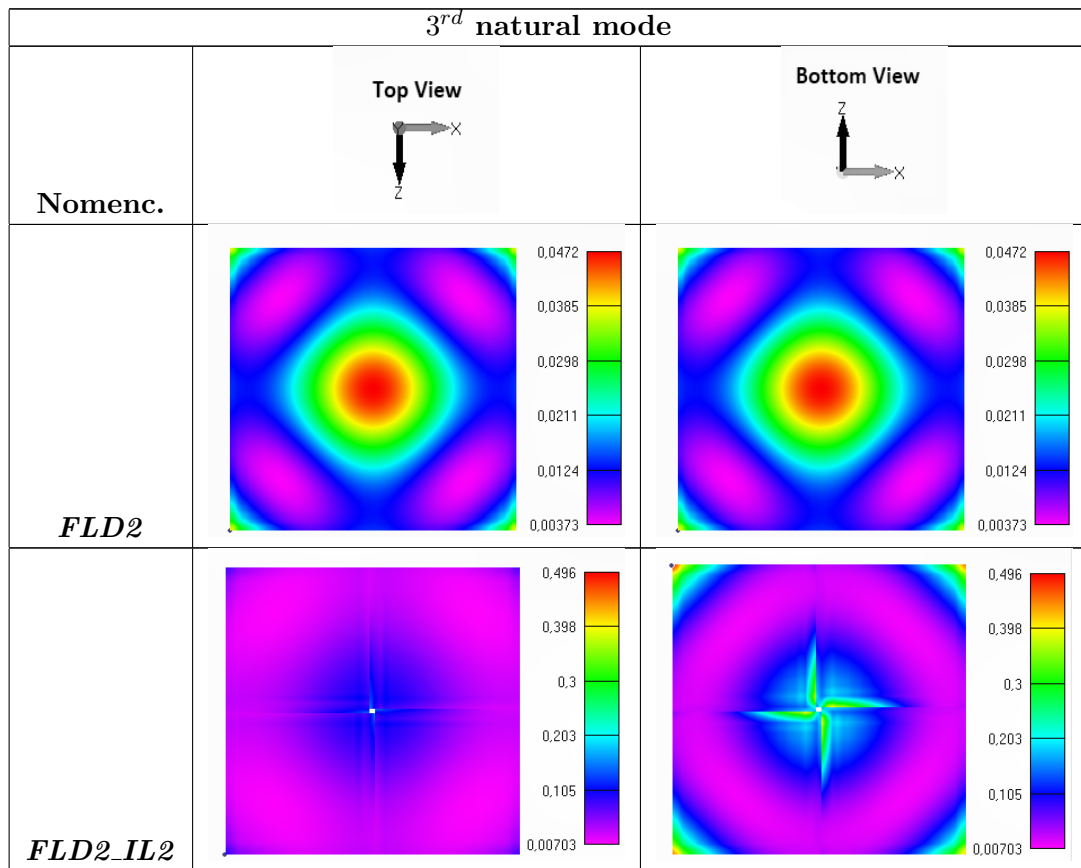


Table E.17: Distribution of the modal strain energy (3^{rd} mode) for the FLD square models without constraining stripes developed with free boundary conditions.



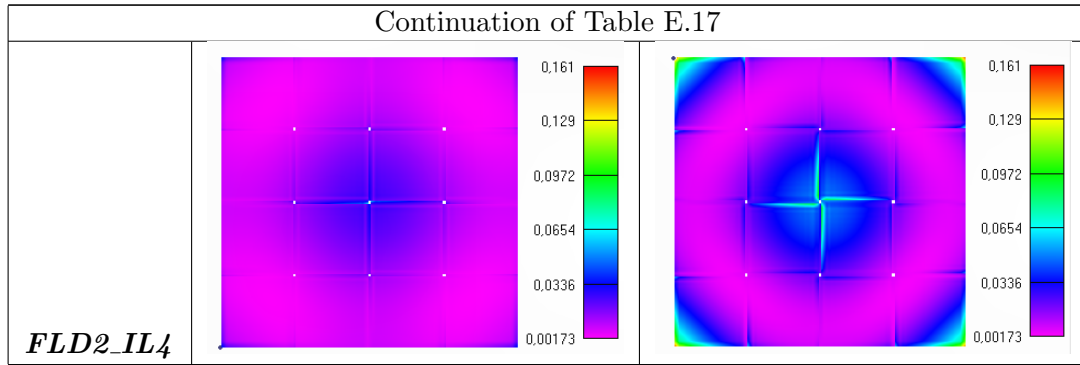


Table E.18: Distribution of the modal strain energy (4^{th} mode) for the FLD square models without constraining stripes developed with free boundary conditions.

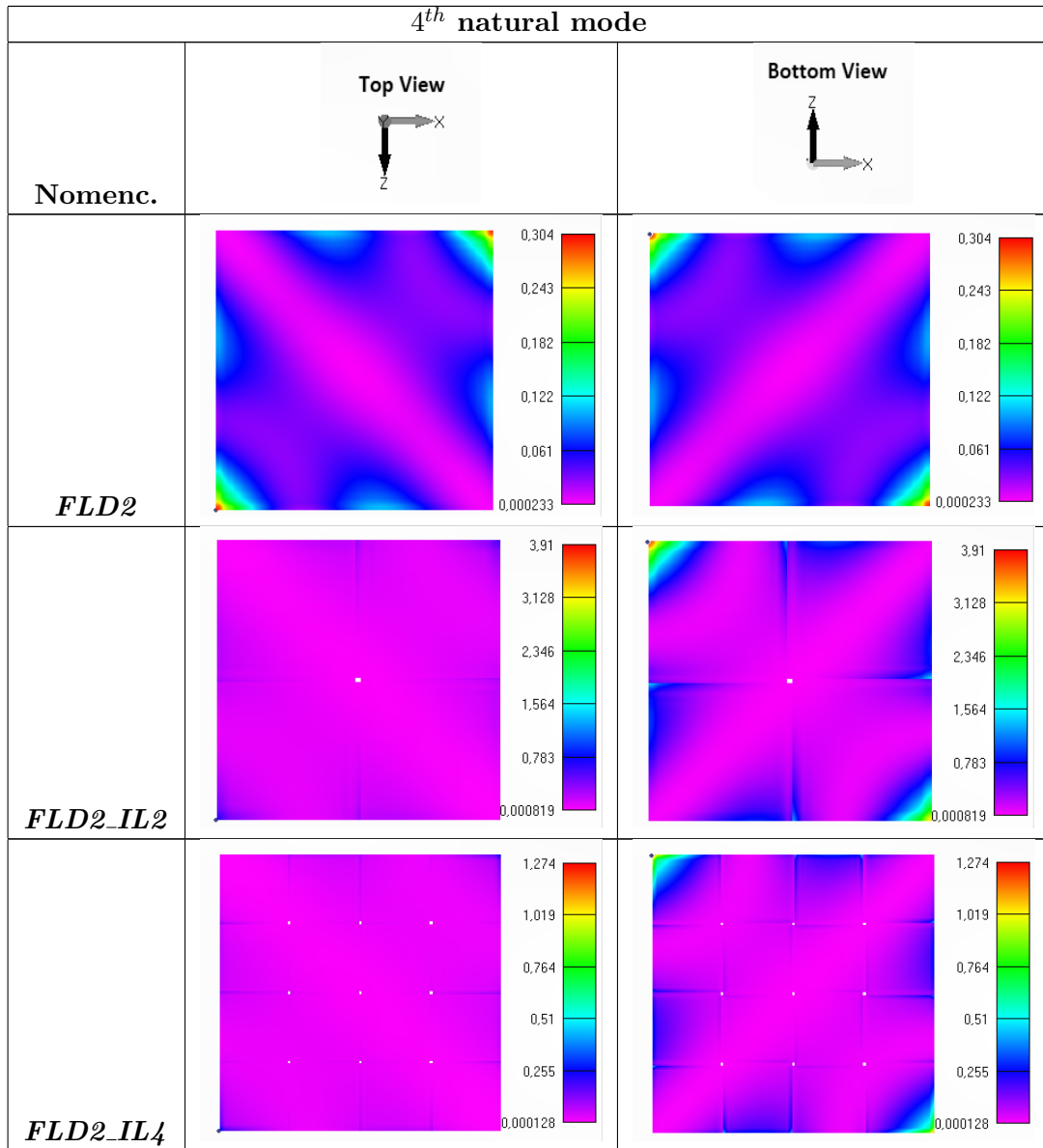


Table E.19: Distribution of the modal strain energy (5^{th} mode) for the FLD square models without constraining stripes developed with free boundary conditions.

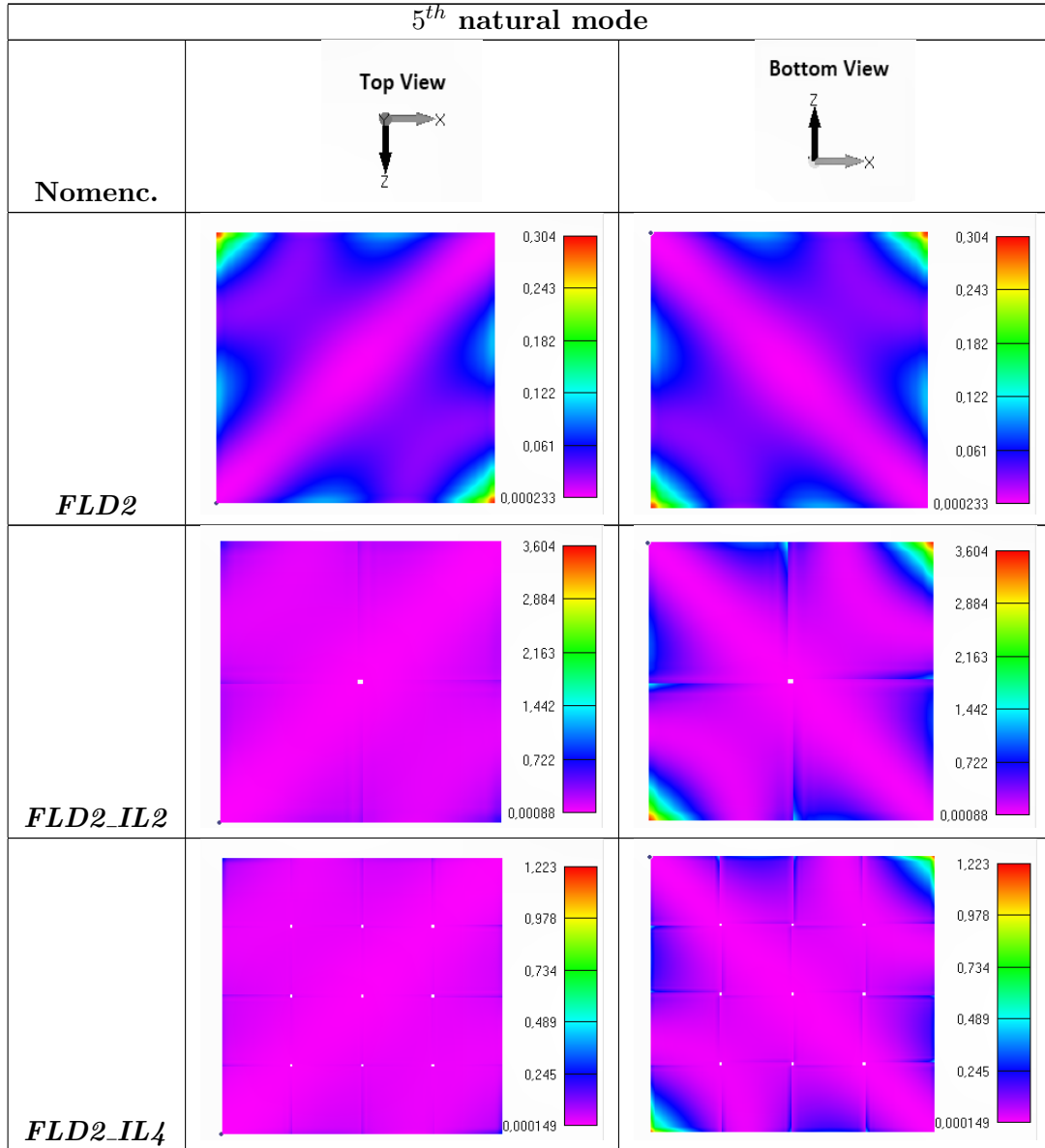


Table E.20: Distribution of the modal strain energy (2^{nd} mode) for the FLD square models with single layered constraining stripes developed with free boundary conditions.

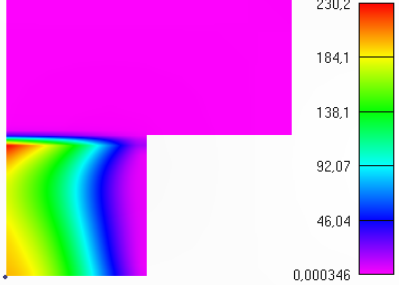
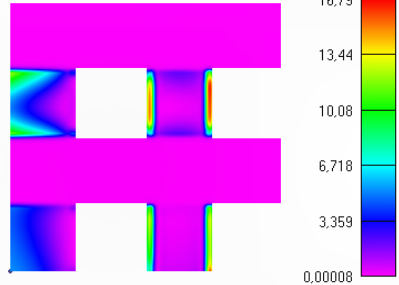
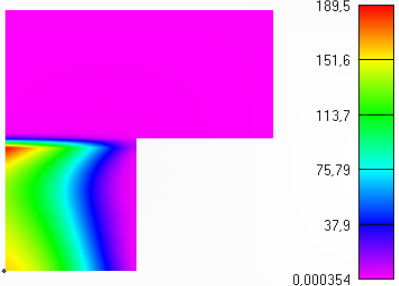
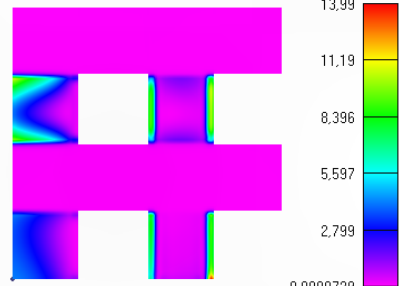
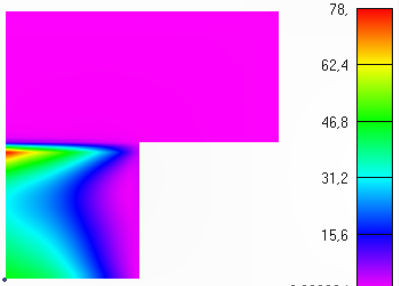
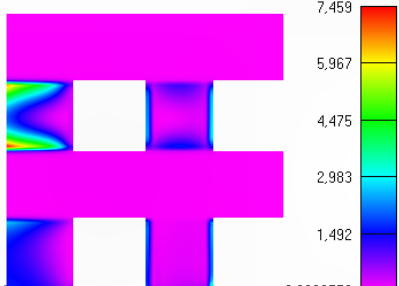
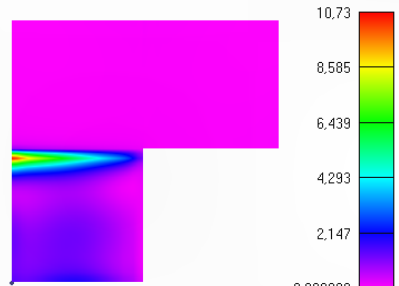

2^{nd} natural mode		
Nomenc.	2 stripes	4 stripes
<i>FLD2_IL_C70</i>		
<i>FLD2_IL_C50</i>		
<i>FLD2_IL_C10</i>		
<i>FLD2_IL_C1</i>		

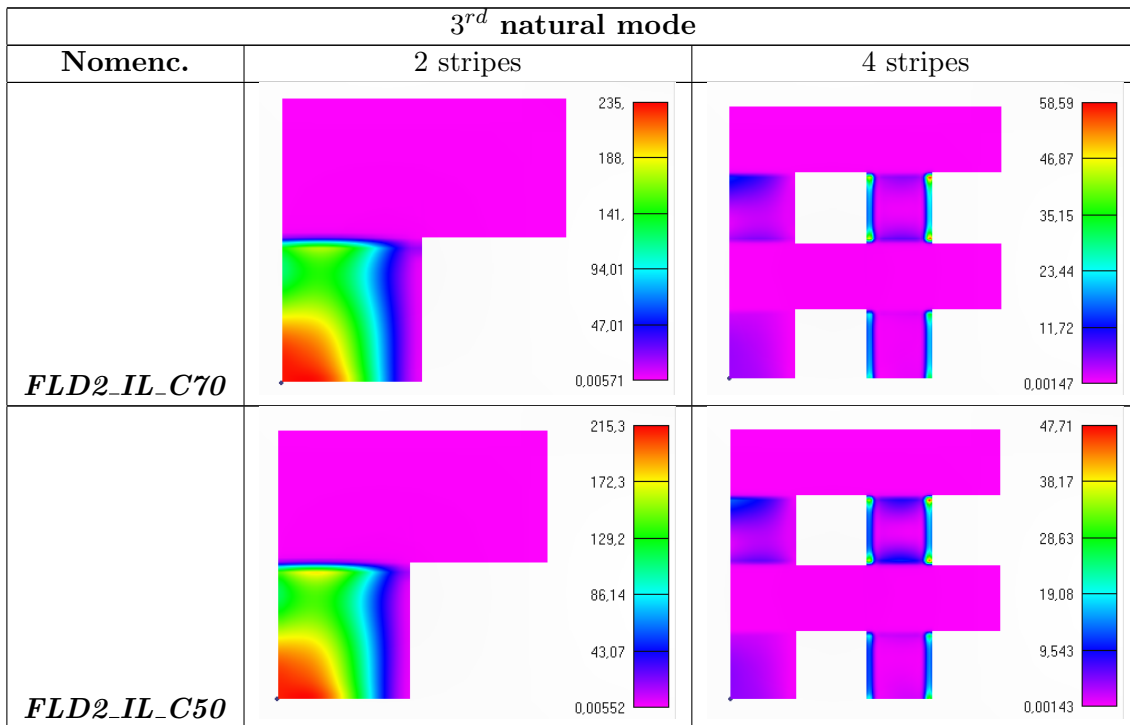
Table E.21: Natural frequency values (2^{nd} mode) for the FLD square models with single layered constraining stripes.

<i>mode 2</i>	Natural Frequencies [Hz]	
Nomenclature	2 stripes	4 stripes
<i>FLD2_IL_C70</i>	520.211	537.374
<i>FLD2_IL_C50</i>	504.437	515.037
<i>FLD2_IL_C10</i>	469.009	469.008
<i>FLD2_IL_C1</i>	456.873	455.877

Table E.22: Normalized loss factor values (2^{nd} mode) for the FLD square models with single layered constraining stripes.

<i>mode 2</i>	Normalized loss Factor [%]	
Nomenclature	2 stripes	4 stripes
<i>FLD2_IL_C70</i>	2.99	0.36
<i>FLD2_IL_C50</i>	2.46	0.29
<i>FLD2_IL_C10</i>	0.83	0.16
<i>FLD2_IL_C1</i>	0.05	0.04

Table E.23: Distribution of the modal strain energy (3^{rd} mode) for the FLD square models with single layered constraining stripes developed with free boundary conditions.



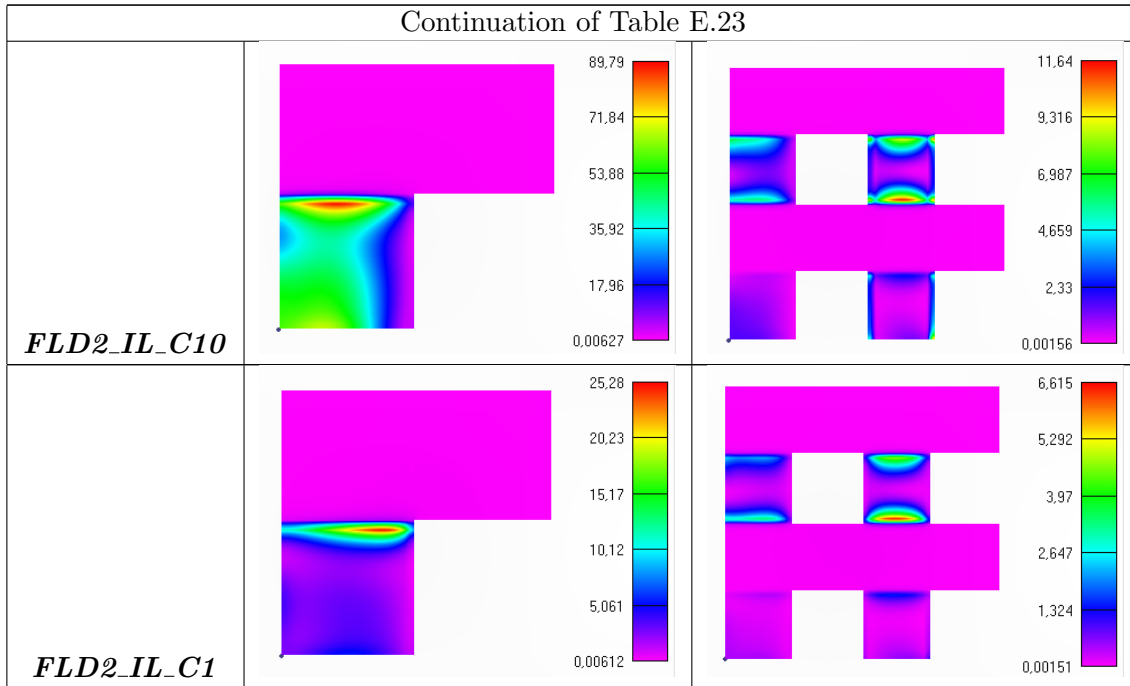


Table E.24: Natural frequency values (3^{rd} mode) for the FLD square models with single layered constraining stripes.

<i>mode 3</i>	Natural Frequencies [Hz]		
	Nomenclature	2 stripes	4 stripes
<i>FLD2_IL_C70</i>		636.144	658.015
<i>FLD2_IL_C50</i>		632.133	648.355
<i>FLD2_IL_C10</i>		584.902	584.868
<i>FLD2_IL_C1</i>		566.327	564.997

Table E.25: Normalized loss factor values (3^{rd} mode) for the FLD square models with single layered constraining stripes.

<i>mode 3</i>	Normalized loss Factor [%]		
	Nomenclature	2 stripes	4 stripes
<i>FLD2_IL_C70</i>		2.38	0.34
<i>FLD2_IL_C50</i>		2.27	0.32
<i>FLD2_IL_C10</i>		0.93	0.18
<i>FLD2_IL_C1</i>		0.11	0.08

Table E.26: Distribution of the modal strain energy (4^{th} mode) for the FLD square models with single layered constraining stripes developed with free boundary conditions.

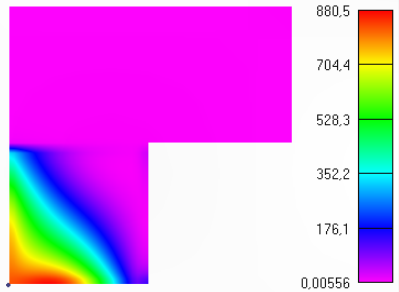
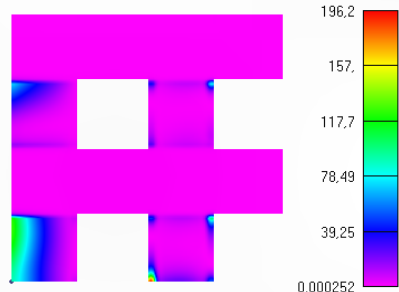
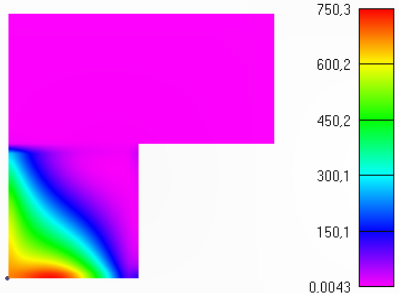
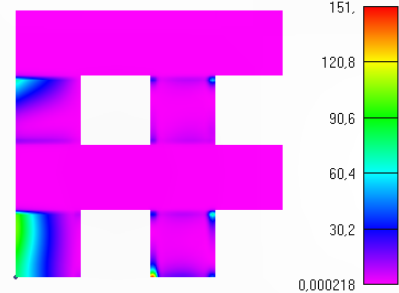
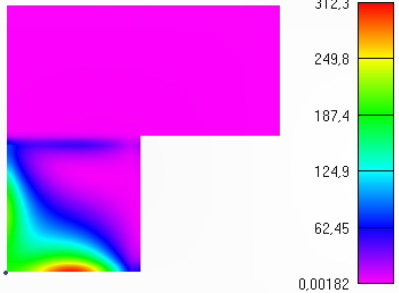
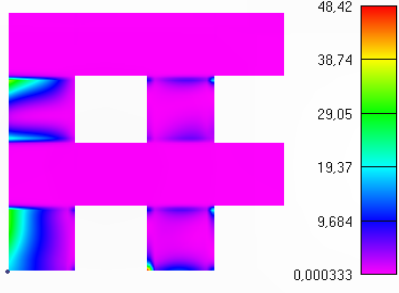
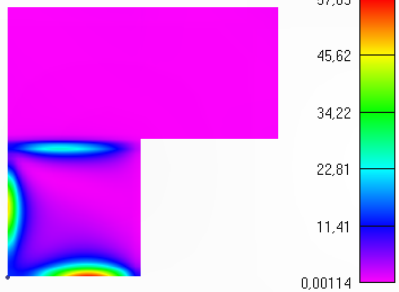
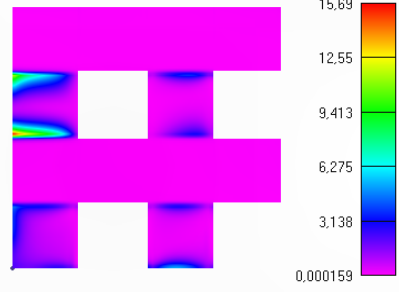
4^{th} natural mode		
Nomenc.	2 stripes	4 stripes
<i>FLD2_IL_C70</i>		
<i>FLD2_IL_C50</i>		
<i>FLD2_IL_C10</i>		
<i>FLD2_IL_C1</i>		

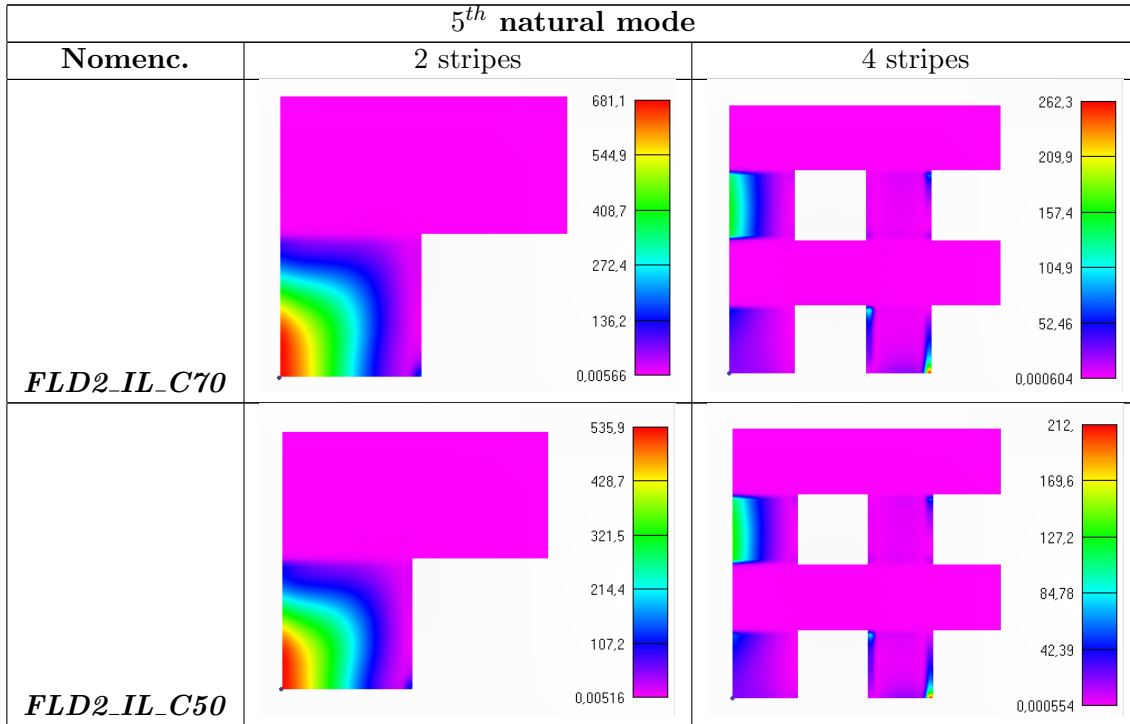
Table E.27: Natural frequency values (4^{th} mode) for the FLD square models with single layered constraining stripes.

<i>mode 4</i>	Natural Frequencies [Hz]	
Nomenclature	2 stripes	4 stripes
<i>FLD2_IL_C70</i>	907.239	931.651
<i>FLD2_IL_C50</i>	884.910	899.954
<i>FLD2_IL_C10</i>	828.668	827.265
<i>FLD2_IL_C1</i>	809.439	805.756

Table E.28: Normalized loss factor values (4^{th} mode) for the FLD square models with single layered constraining stripes.

<i>mode 4</i>	Normalized loss Factor [%]	
Nomenclature	2 stripes	4 stripes
<i>FLD2_IL_C70</i>	2.69	0.63
<i>FLD2_IL_C50</i>	2.31	0.57
<i>FLD2_IL_C10</i>	0.83	0.25
<i>FLD2_IL_C1</i>	0.10	0.08

Table E.29: Distribution of the modal strain energy (5^{th} mode) for the FLD square models with single layered constraining stripes developed with free boundary conditions.



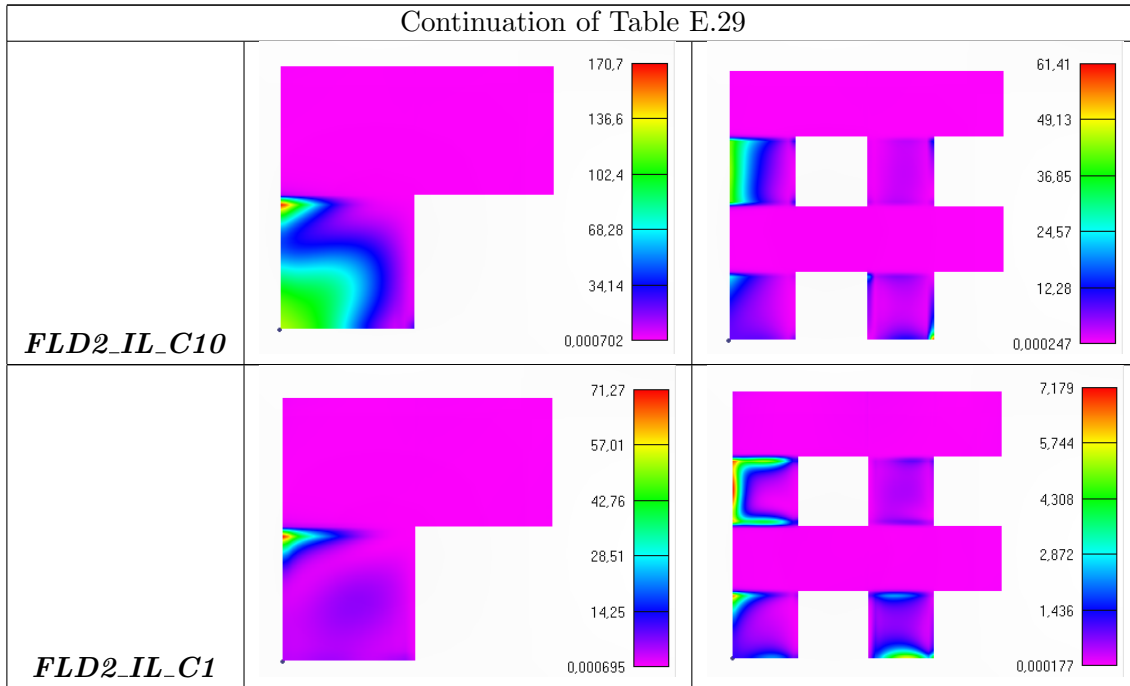


Table E.30: Natural frequency values (5^{th} mode) for the FLD square models with single layered constraining stripes.

<i>mode 5</i>	Natural Frequencies [Hz]	
	Nomenclature	
	2 stripes	4 stripes
<i>FLD2_IL_C70</i>	927.741	938.985
<i>FLD2_IL_C50</i>	900.487	906.400
<i>FLD2_IL_C10</i>	831.908	829.934
<i>FLD2_IL_C1</i>	809.965	806.933

Table E.31: Normalized loss factor values (5^{th} mode) for the FLD square models with single layered constraining stripes.

<i>mode 5</i>	Normalized loss Factor [%]	
	Nomenclature	
	2 stripes	4 stripes
<i>FLD2_IL_C70</i>	2.08	0.82
<i>FLD2_IL_C50</i>	1.72	0.74
<i>FLD2_IL_C10</i>	0.53	0.29
<i>FLD2_IL_C1</i>	0.06	0.05

Table E.32: Distribution of the modal strain energy (2^{nd} mode) for the FLD square models with single and double layered constraining stripes developed with free boundary conditions - top view.

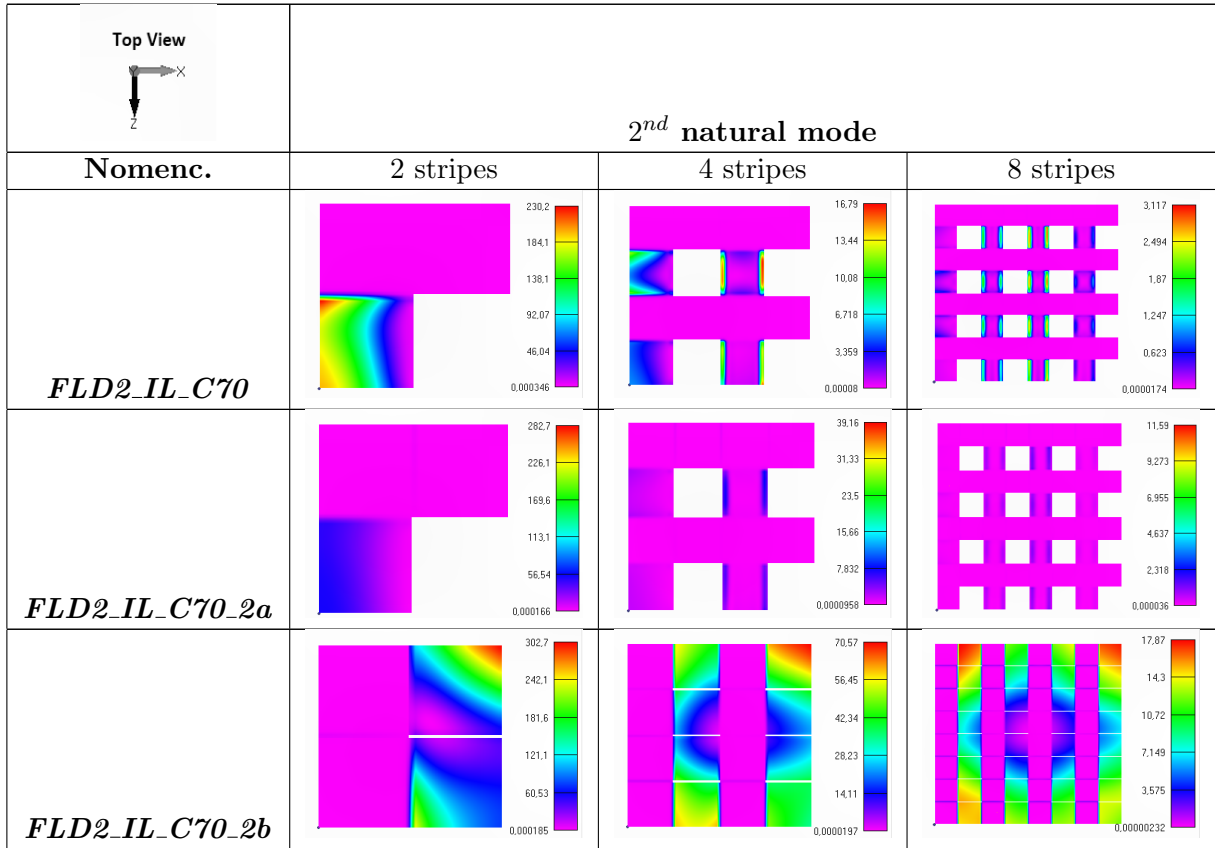
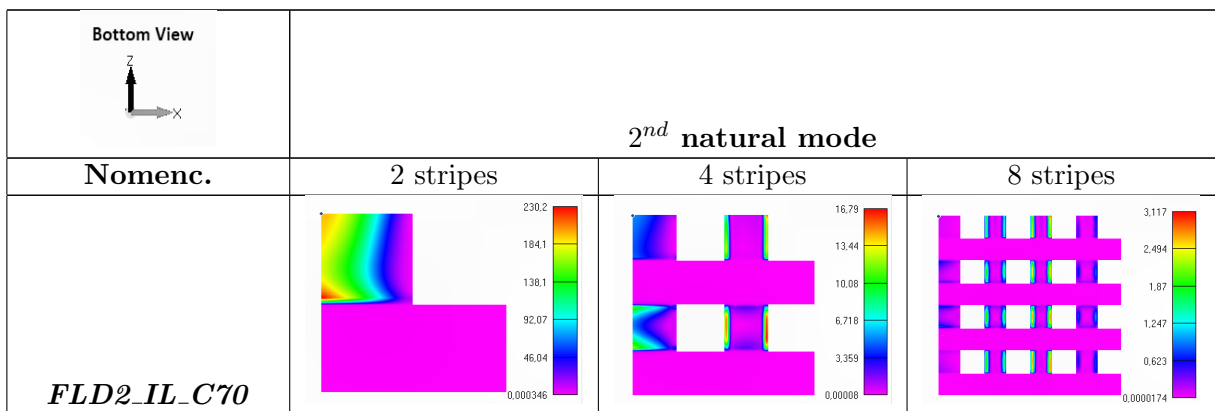


Table E.33: Distribution of the modal strain energy (2^{nd} mode) for the FLD square models with single and double layered constraining stripes developed with free boundary conditions - bottom view.



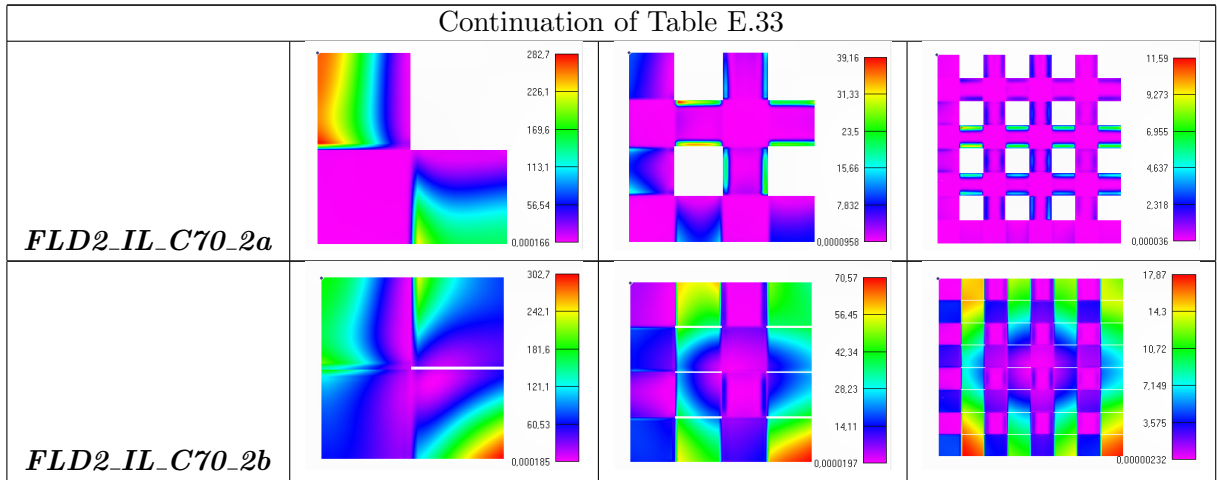



Table E.34: Natural frequency values (2^{nd} mode) for the FLD square models with single and double layered constraining stripes.

<i>mode 2</i>	Natural Frequencies [Hz]		
	Nomenclature	2 stripes	4 stripes
<i>FLD2_IL_C70</i>	520.211	537.374	540.574
<i>FLD2_IL_C70_2a</i>	523.995	589.833	604.769
<i>FLD2_IL_C70_2b</i>	502.355	520.159	523.248

Table E.35: Normalized loss factor values (2^{nd} mode) for the FLD square models with single and double layered constraining stripes.

<i>mode 2</i>	Normalized Loss Factor [1/kg]		
	Nomenclature	2 stripes	4 stripes
<i>FLD2_IL_C70</i>	2.99	0.36	0.19
<i>FLD2_IL_C70_2a</i>	3.64	0.54	0.36
<i>FLD2_IL_C70_2b</i>	6.06	5.36	5.56

Table E.36: Distribution of the modal strain energy (3^{rd} mode) for the FLD square models with single and double layered constraining stripes developed with free boundary conditions - top view.

<div style="text-align: center;"> Top View  </div>	3^{rd} natural mode			
	Nomenc.	2 stripes	4 stripes	8 stripes

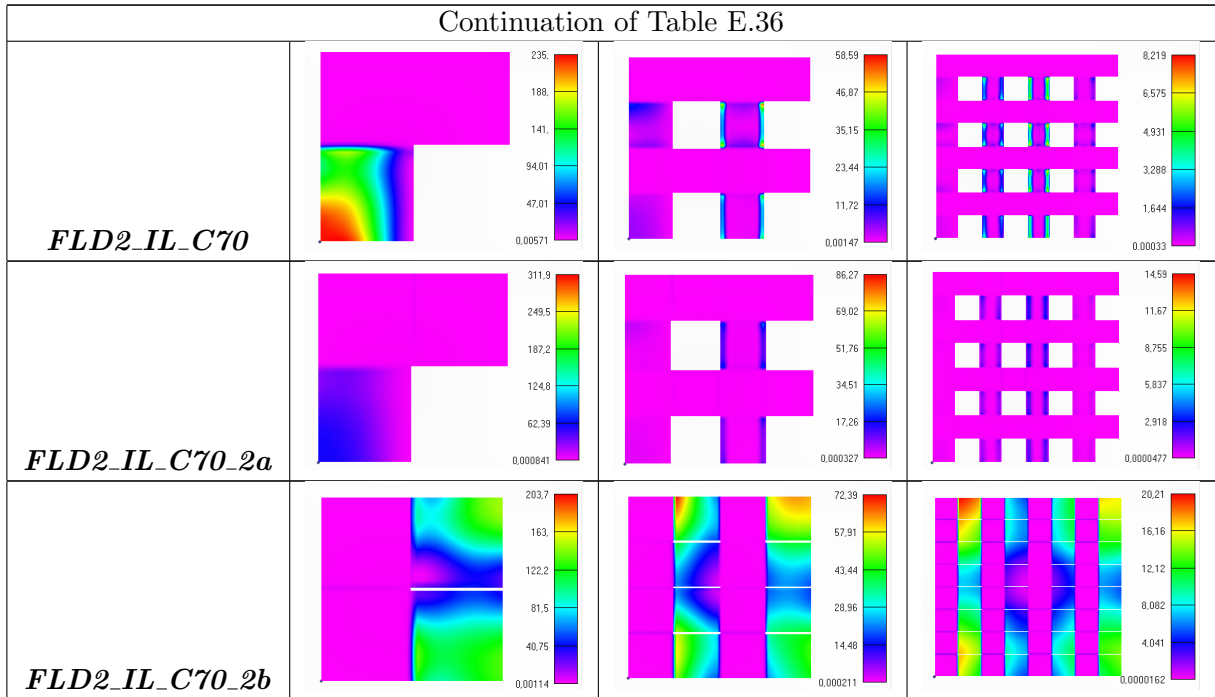
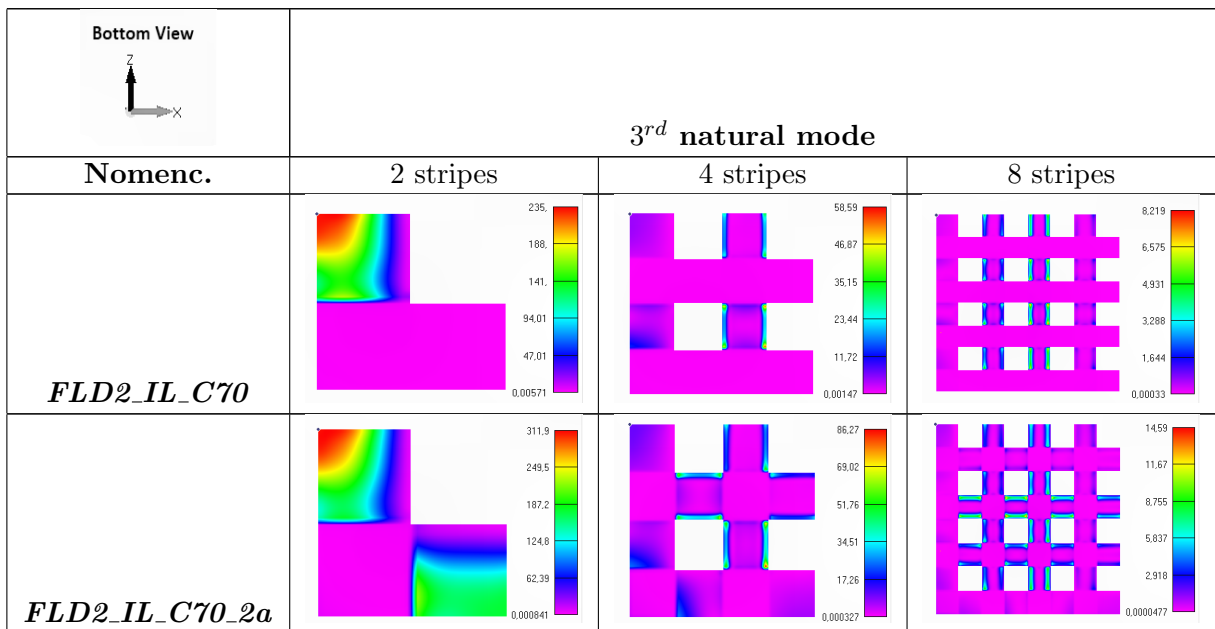


Table E.37: Distribution of the modal strain energy (3^{rd} mode) for the FLD square models with single and double layered constraining stripes developed with free boundary conditions - bottom view.



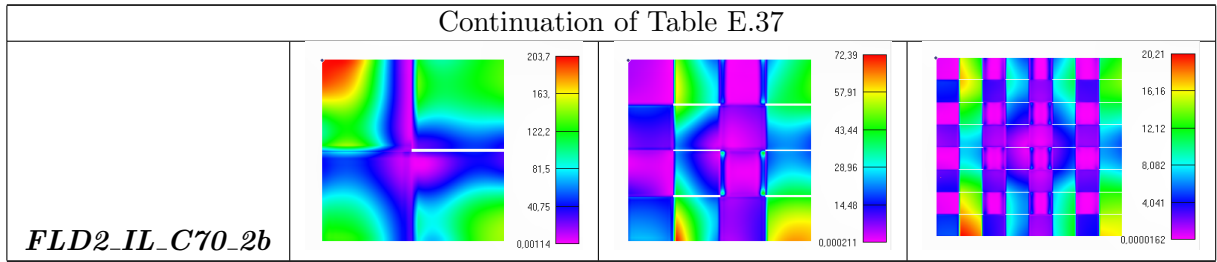


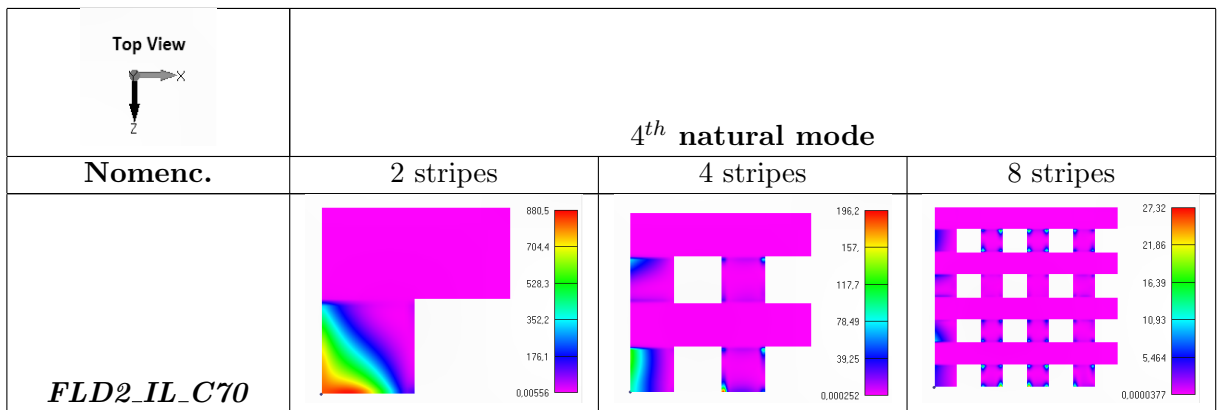
Table E.38: Natural frequency values (3^{rd} mode) for the FLD square models with single and double layered constraining stripes.

<i>mode 3</i>	Natural Frequencies [Hz]		
	Nomenclature	2 stripes	4 stripes
FLD2_IL_C70	636.144	658.015	660.605
FLD2_IL_C70_2a	628.705	705.941	720.70
FLD2_IL_C70_2b	609.277	629.842	631.944

Table E.39: Normalized loss factor values (3^{rd} mode) for the FLD square models with single and double layered constraining stripes.

<i>mode 3</i>	Normalized Loss Factor [1/kg]		
	Nomenclature	2 stripes	4 stripes
FLD2_IL_C70	2.38	0.34	0.23
FLD2_IL_C70_2a	2.90	0.51	0.38
FLD2_IL_C70_2b	4.22	3.68	3.81

Table E.40: Distribution of the modal strain energy (4^{th} mode) for the FLD square models with single and double layered constraining stripes developed with free boundary conditions - top view.



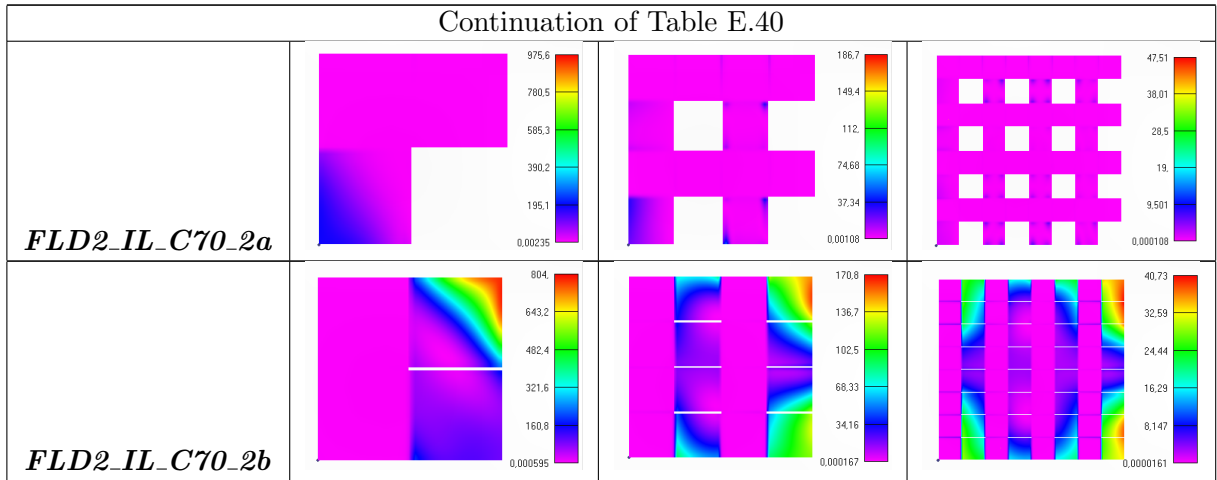


Table E.41: Distribution of the modal strain energy (4^{th} mode) for the FLD square models with single and double layered constraining stripes developed with free boundary conditions - bottom view.

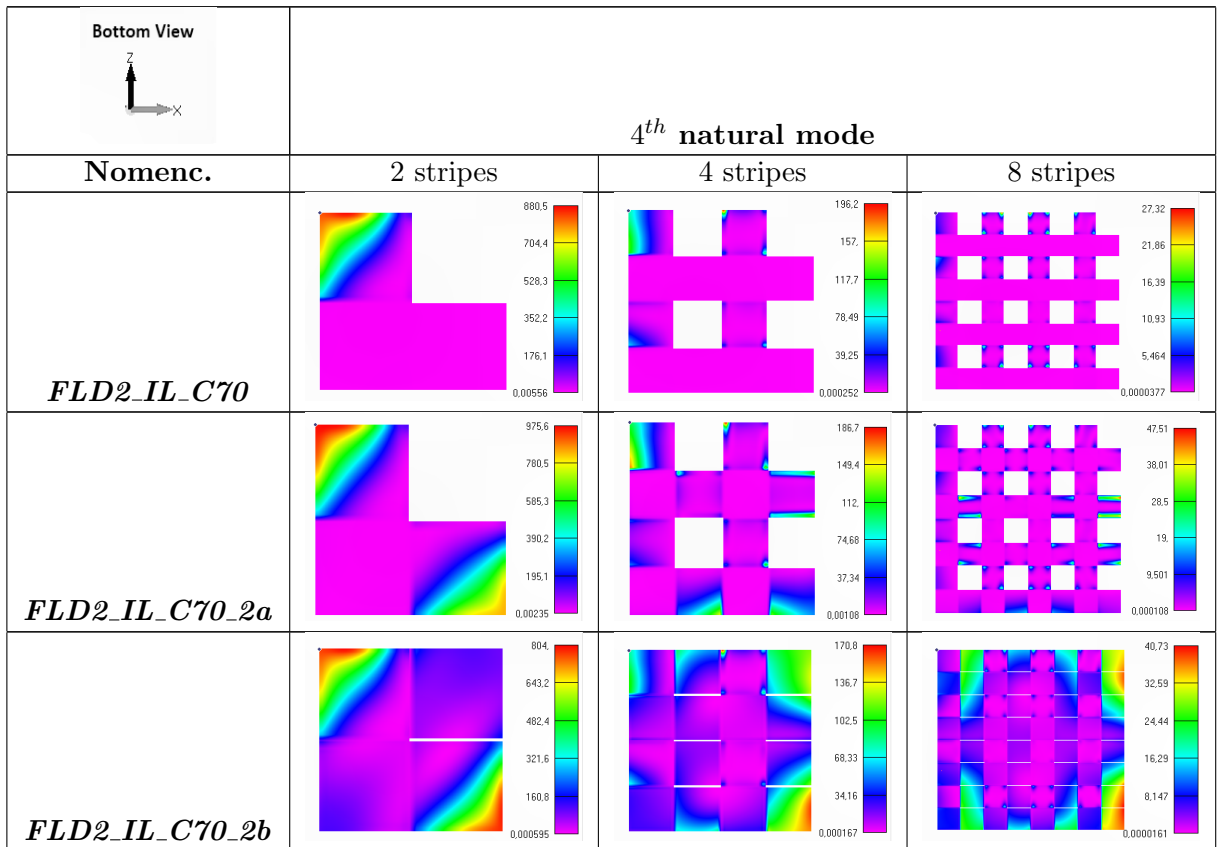


Table E.42: Natural frequency values (4^{th} mode) for the FLD square models with single and double layered constraining stripes.

<i>mode 4</i>	Natural Frequencies [Hz]		
Nomenclature	2 stripes	4 stripes	8 stripes
<i>FLD2_IL_C70</i>	907.239	931.651	939.173
<i>FLD2_IL_C70_2a</i>	892.816	979.178	1012.674
<i>FLD2_IL_C70_2b</i>	865.0234	886.664	892.447

Table E.43: Normalized loss factor values (4^{th} mode) for the FLD square models with single and double layered constraining stripes.

<i>mode 4</i>	Normalized Loss Factor [1/kg]		
Nomenclature	2 stripes	4 stripes	8 stripes
<i>FLD2_IL_C70</i>	2.69	0.63	0.20
<i>FLD2_IL_C70_2a</i>	3.32	0.82	0.40
<i>FLD2_IL_C70_2b</i>	3.61	2.72	2.61

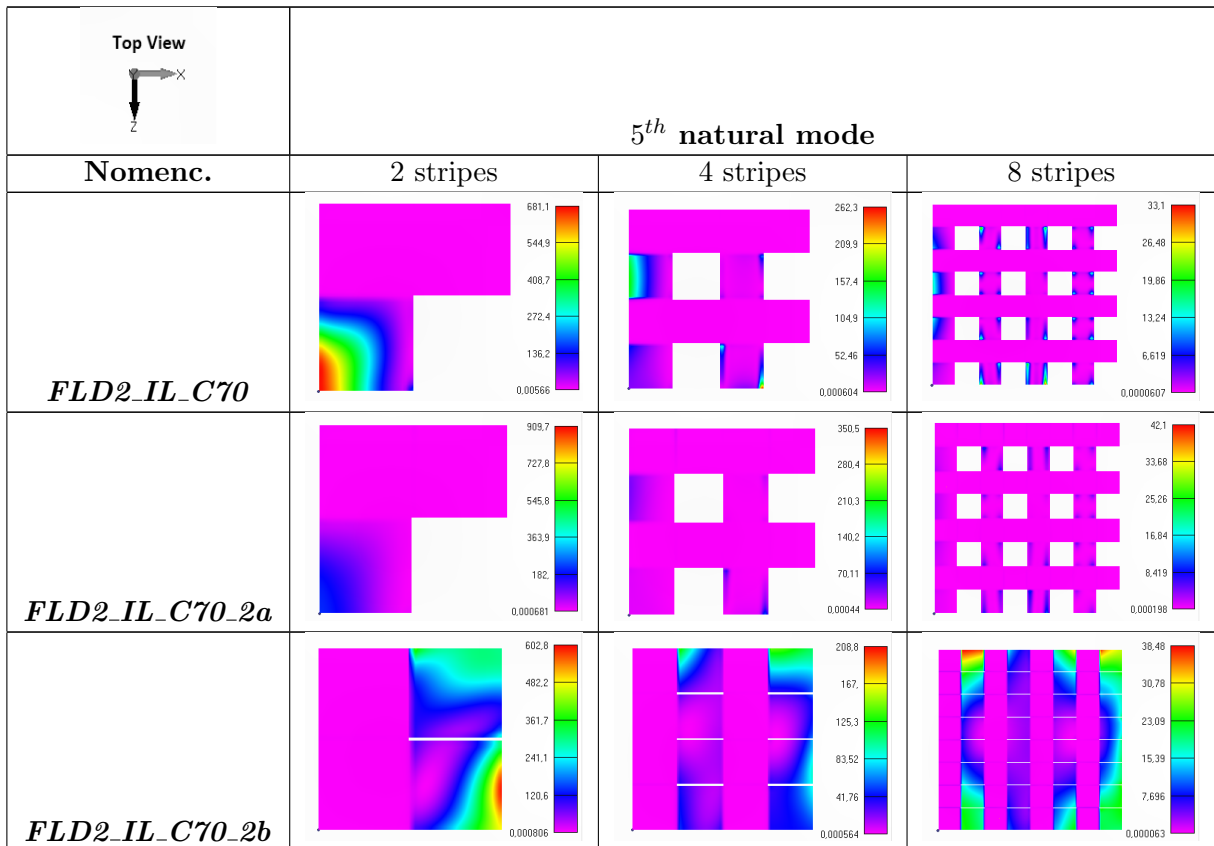
Table E.44: Distribution of the modal strain energy (5^{th} mode) for the FLD square models with single and double layered constraining stripes developed with free boundary conditions - top view.

Table E.45: Distribution of the modal strain energy (5^{th} mode) for the FLD square models with single and double layered constraining stripes developed with free boundary conditions - bottom view.

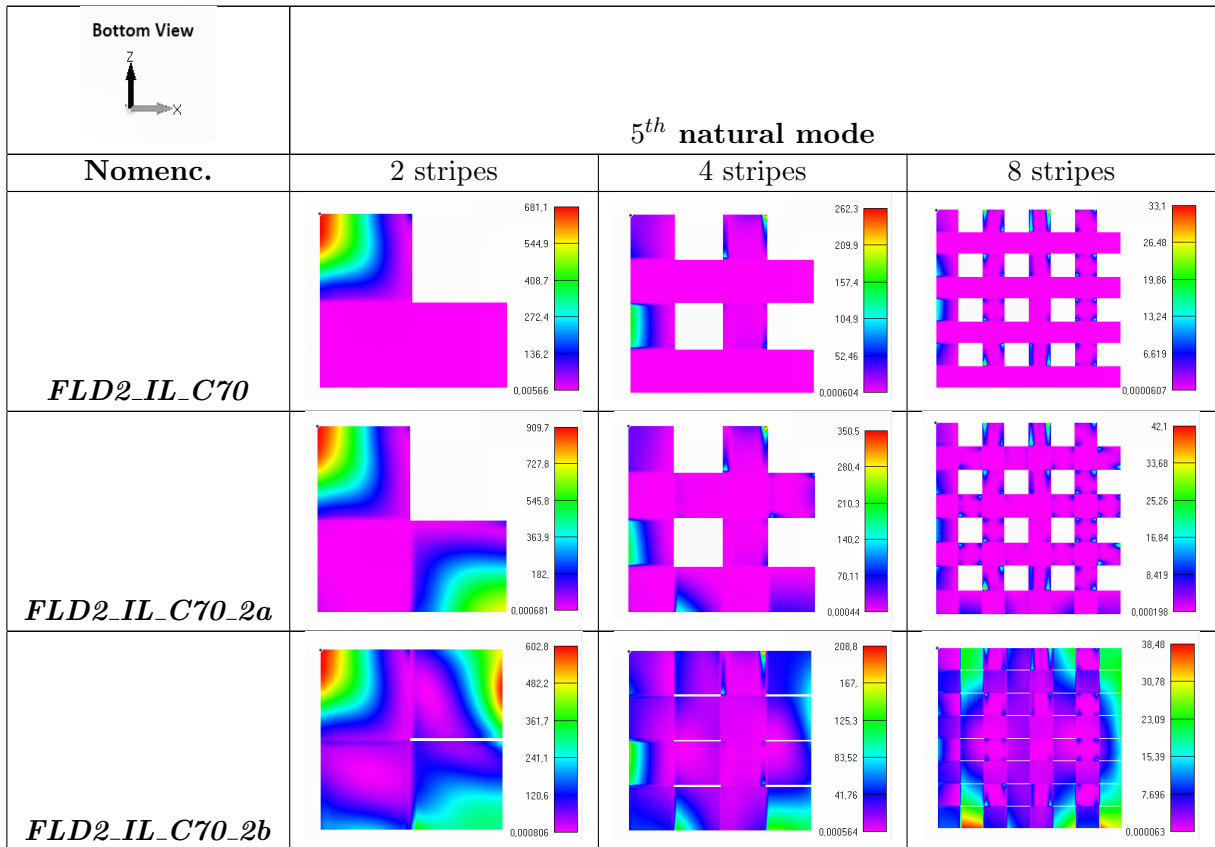


Table E.46: Natural frequency values (5^{th} mode) for the FLD square models with single and double layered constraining stripes.

<i>mode 5</i>	Natural Frequencies [Hz]		
Nomenclature	2 stripes	4 stripes	8 stripes
<i>FLD2_IL_C70</i>	927.741	938.985	947.569
<i>FLD2_IL_C70_2a</i>	947.427	987.466	1025.559
<i>FLD2_IL_C70_2b</i>	883.579	891.146	898.888

Table E.47: Normalized loss factor values (5^{th} mode) for the FLD square models with single and double layered constraining stripes.

<i>mode 5</i>	Normalized Loss Factor [1/kg]		
Nomenclature	2 stripes	4 stripes	8 stripes
<i>FLD2_IL_C70</i>	2.08	0.82	0.33
<i>FLD2_IL_C70_2a</i>	2.80	0.87	0.36
<i>FLD2_IL_C70_2b</i>	3.40	2.40	2.35

E.2.2 Rectangular plate models

Table E.48: Distribution of the modal strain energy (2^{nd} mode) for the CLD rectangular models developed with free boundary conditions.

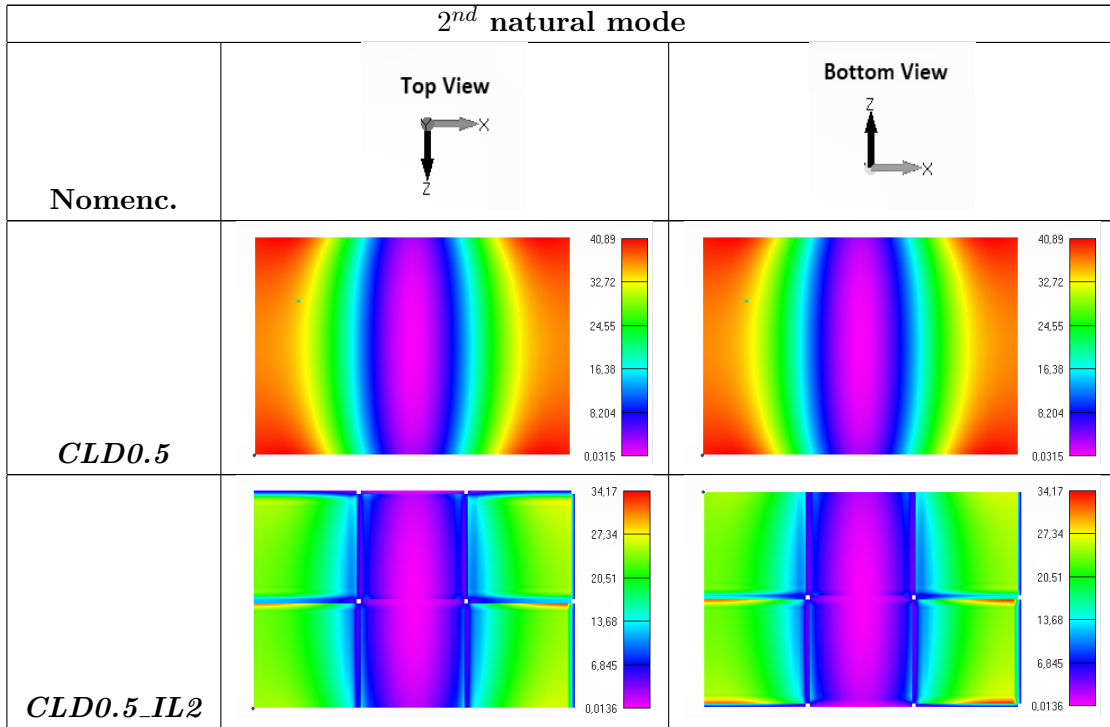
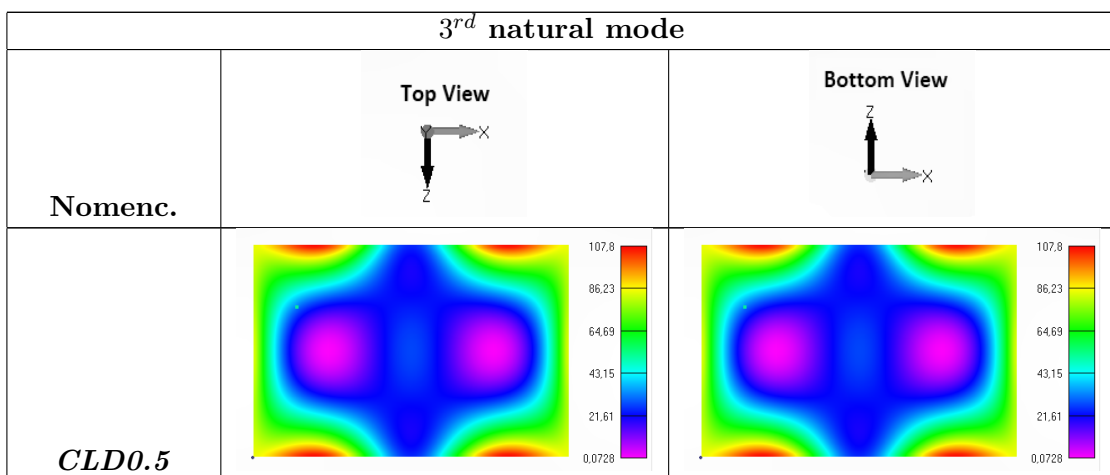


Table E.49: Distribution of the modal strain energy (3^{rd} mode) for the CLD rectangular models developed with free boundary conditions.



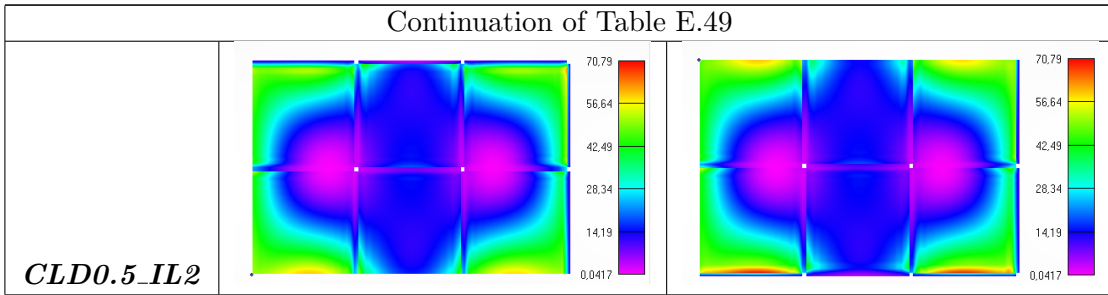


Table E.50: Distribution of the modal strain energy (4^{th} mode) for the CLD rectangular models developed with free boundary conditions.

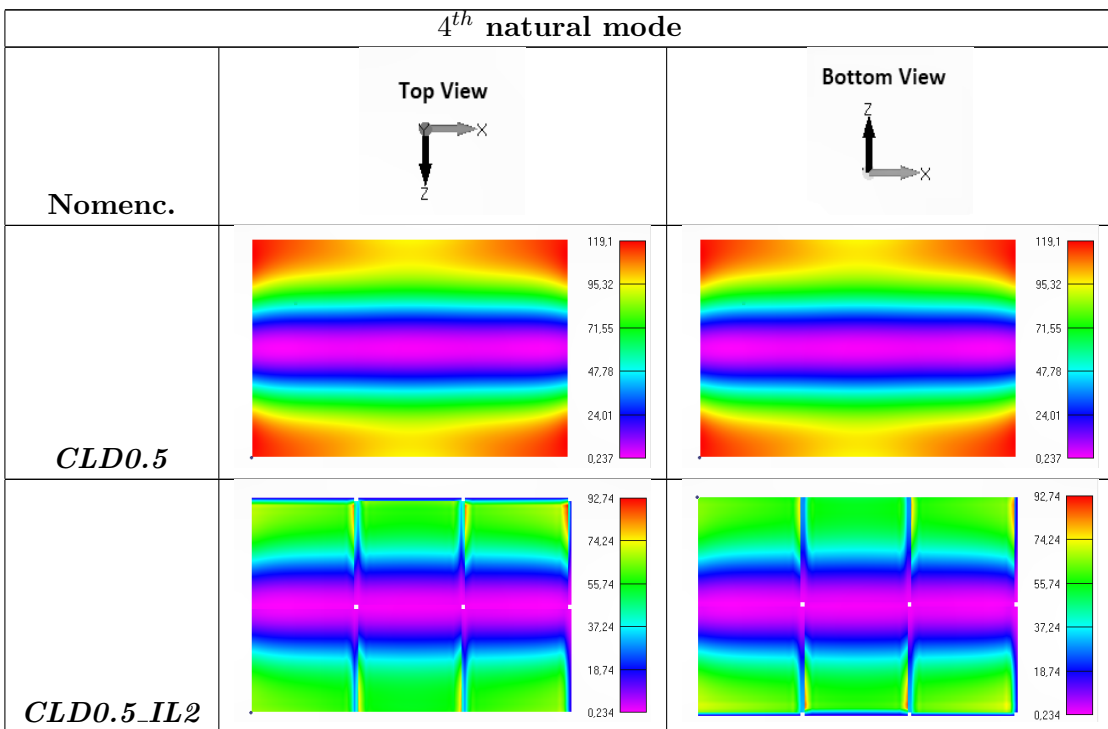
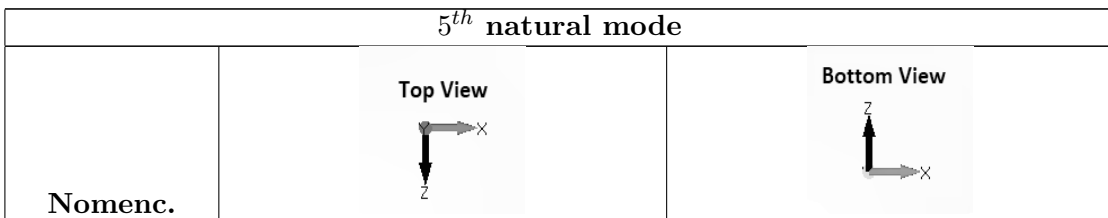


Table E.51: Distribution of the modal strain energy (5^{th} mode) for the CLD rectangular models developed with free boundary conditions.



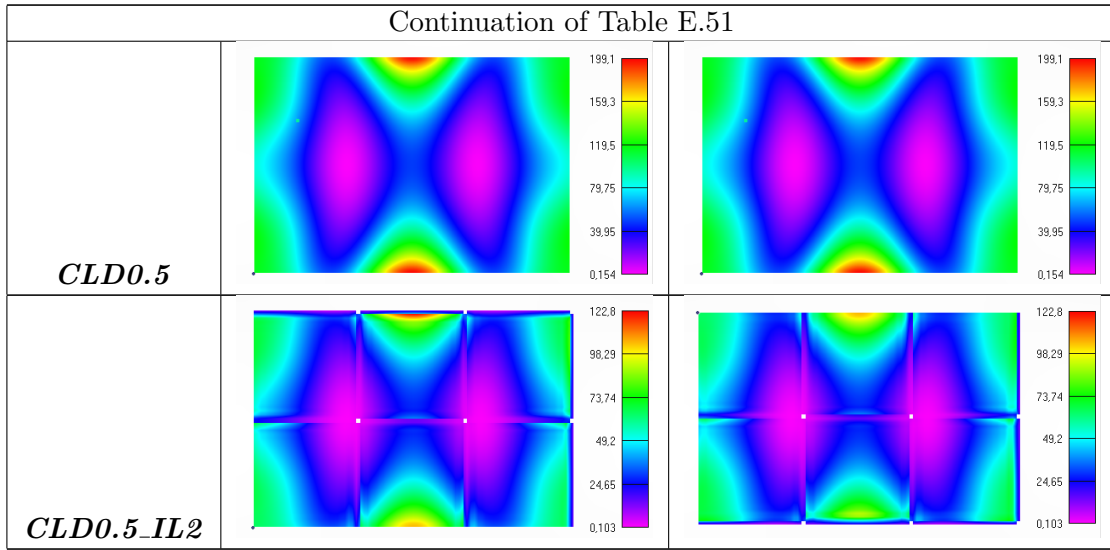


Table E.52: Distribution of the modal strain energy (2^{nd} mode) for the FLD rectangular models developed with free boundary conditions.

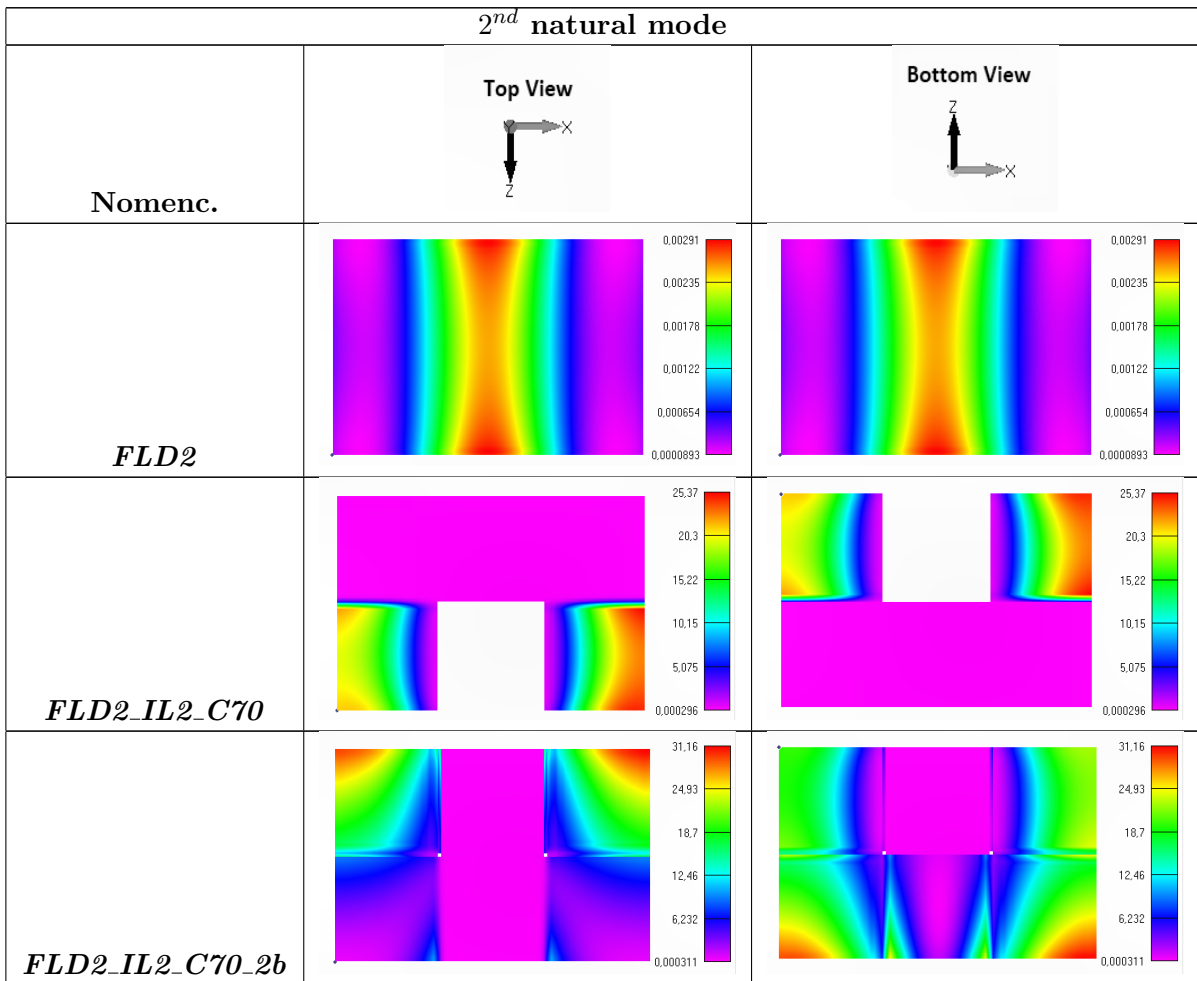


Table E.53: Distribution of the modal strain energy (3^{rd} mode) for the FLD rectangular models developed with free boundary conditions.

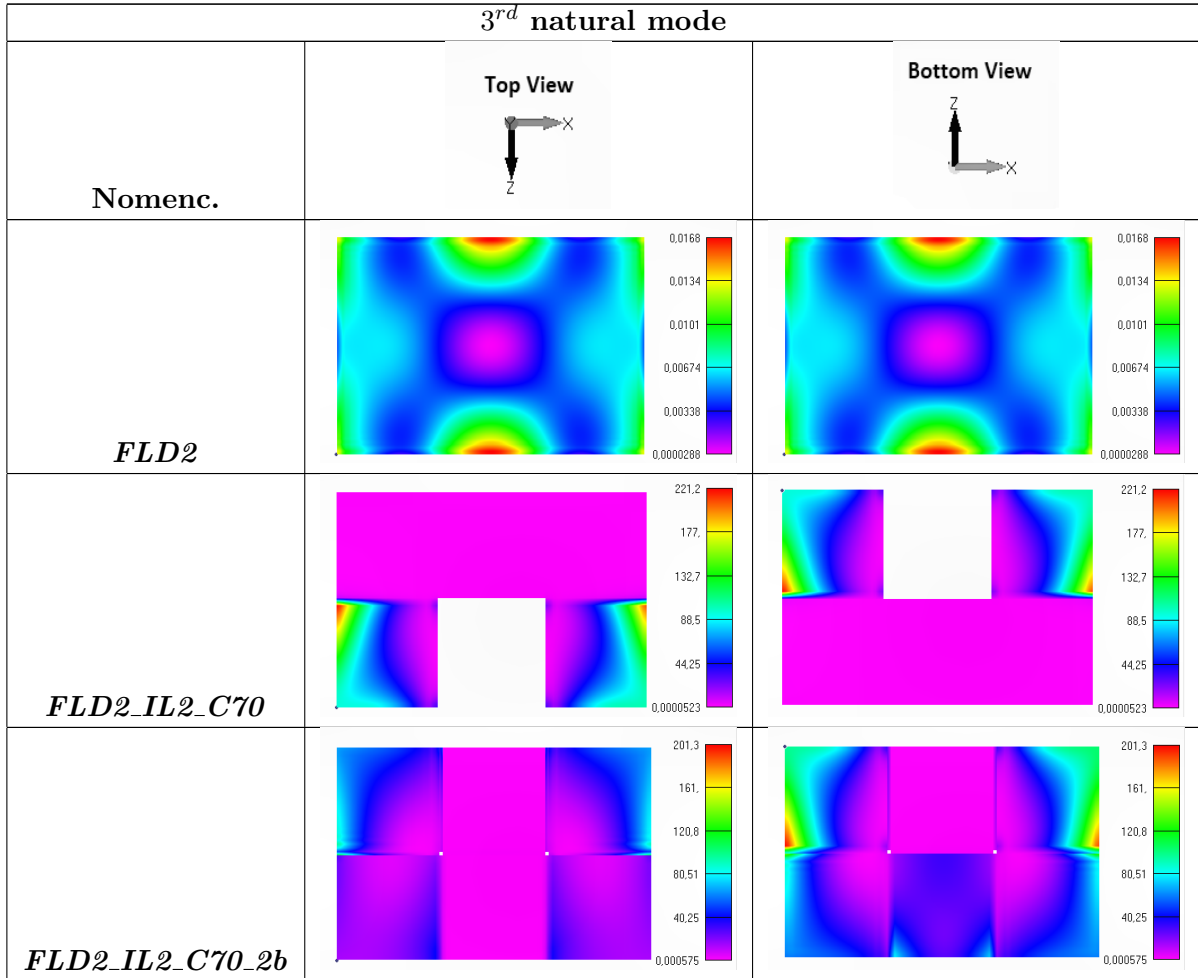
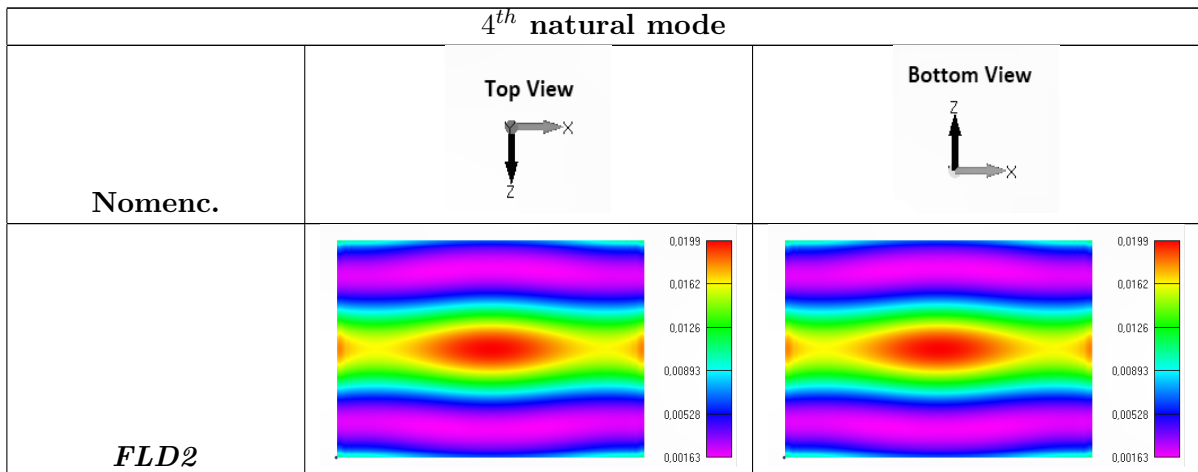


Table E.54: Distribution of the modal strain energy (4^{th} mode) for the FLD rectangular models developed with free boundary conditions.



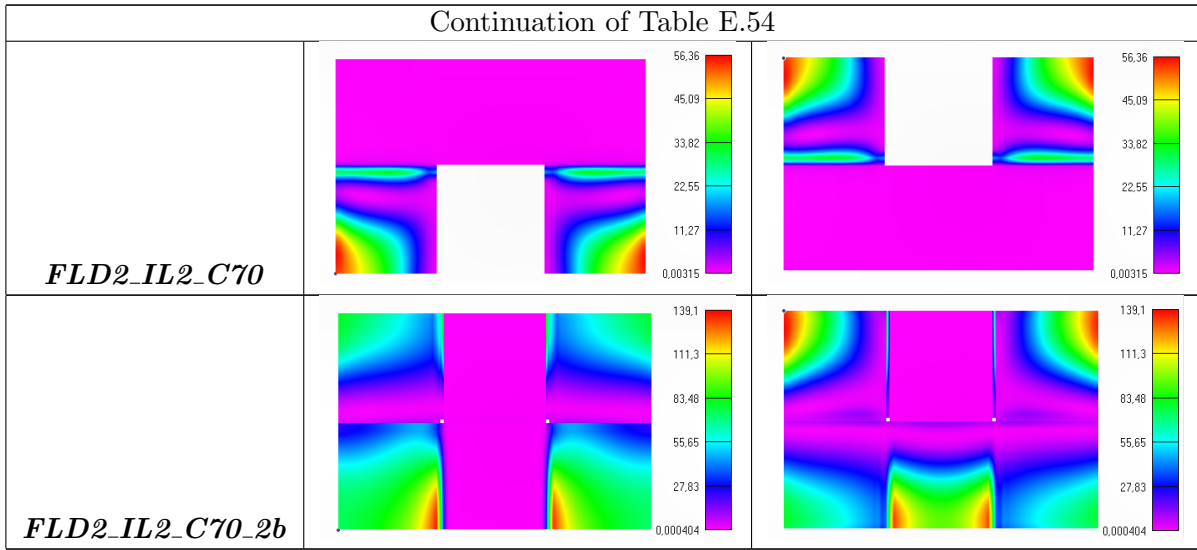


Table E.55: Distribution of the modal strain energy (5th mode) for the FLD rectangular models developed with free boundary conditions.

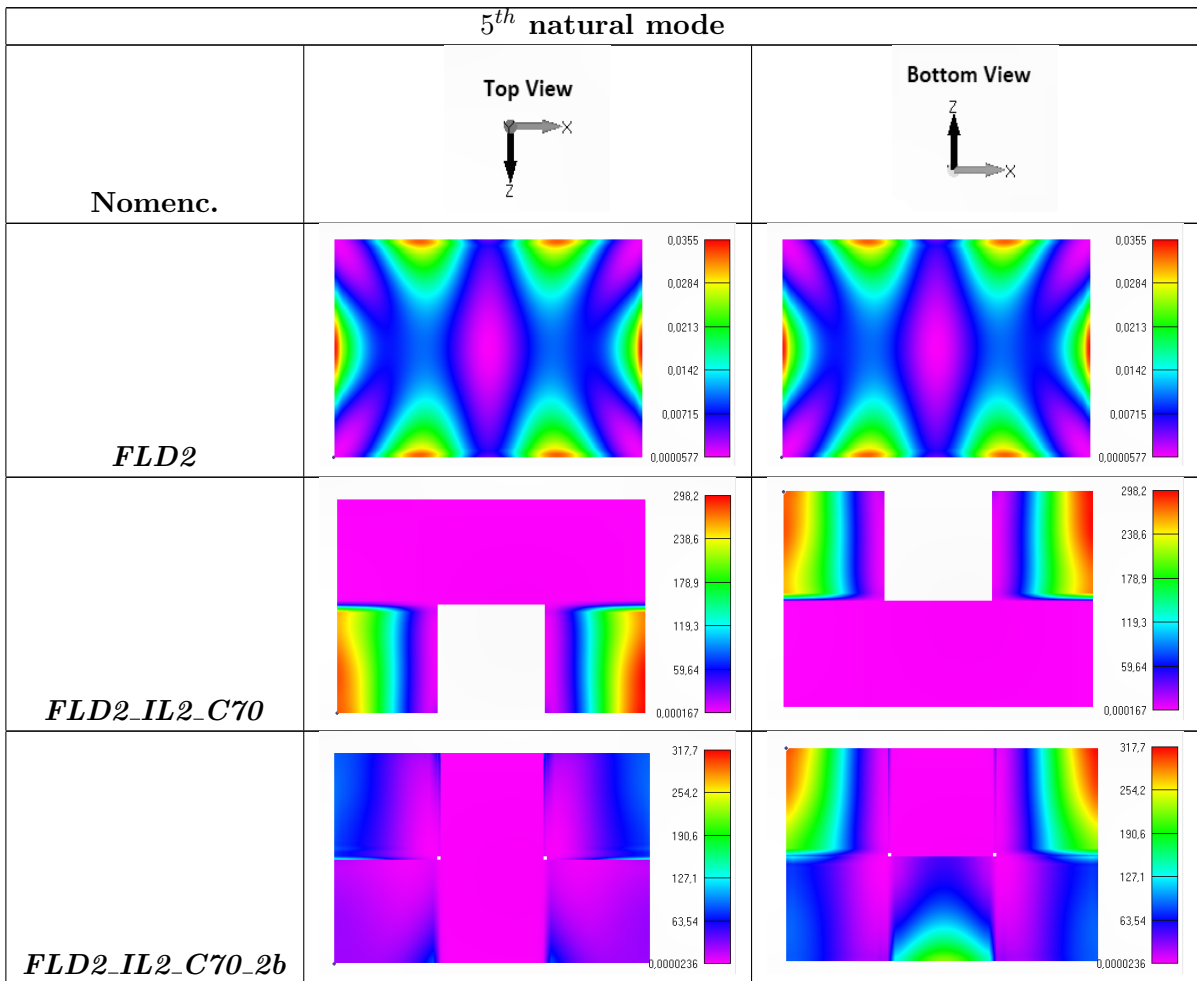


Table E.56: Distribution of the modal strain energy (2^{nd} mode) for the ILD rectangular model developed with free boundary conditions.

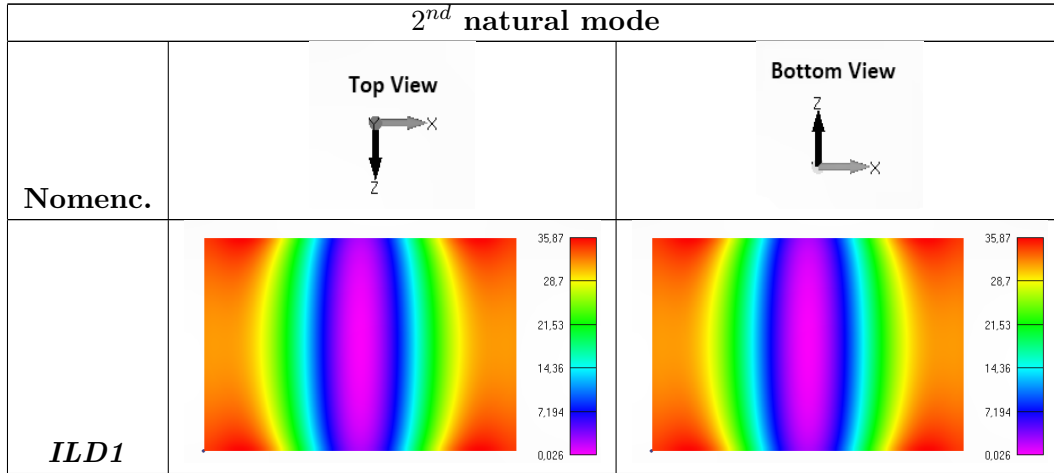


Table E.57: Distribution of the modal strain energy (3^{rd} mode) for the ILD rectangular model developed with free boundary conditions.

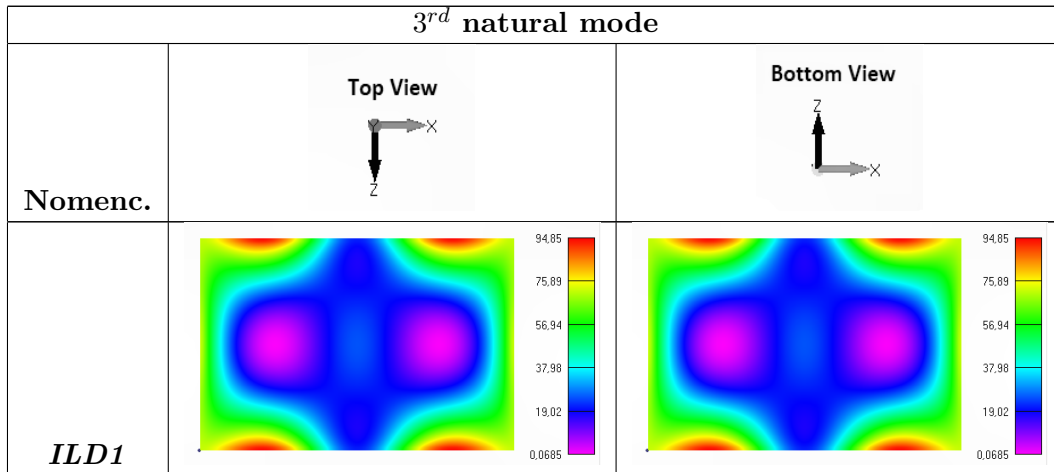
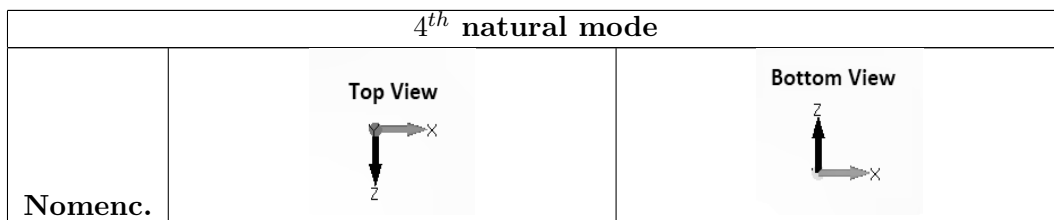


Table E.58: Distribution of the modal strain energy (4^{th} mode) for the ILD rectangular model developed with free boundary conditions.



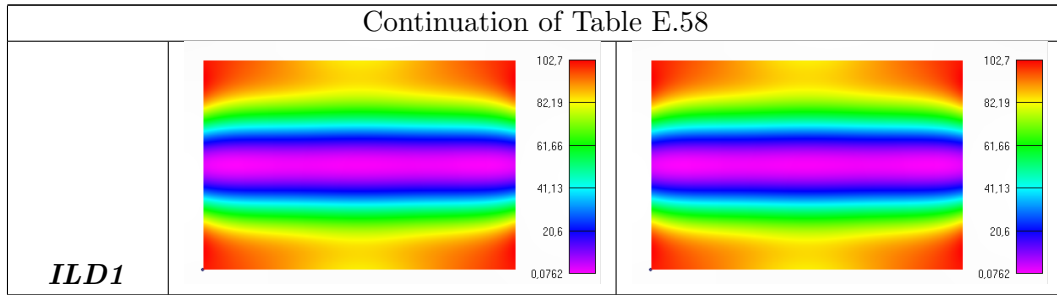


Table E.59: Distribution of the modal strain energy (5^{th} mode) for the ILD rectangular model developed with free boundary conditions.

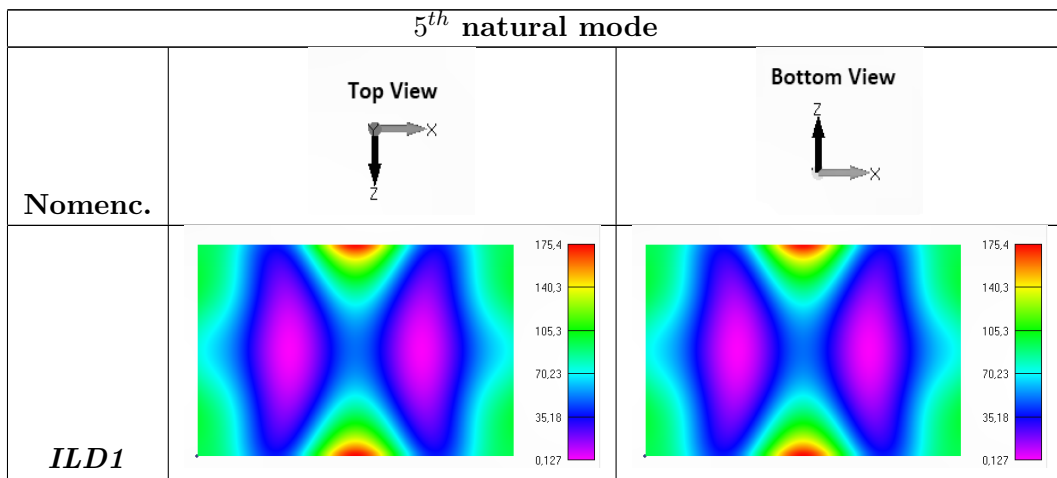


Table E.60: Distribution of the modal strain energy (2^{nd} mode) for the plate without treatment with free boundary conditions.

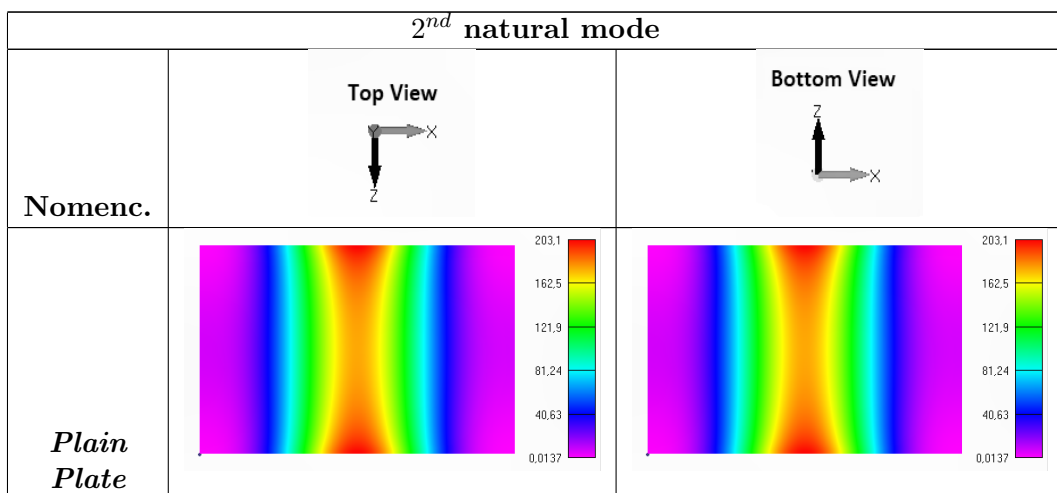


Table E.61: Distribution of the modal strain energy (3^{rd} mode) for the plate without treatment with free boundary conditions.

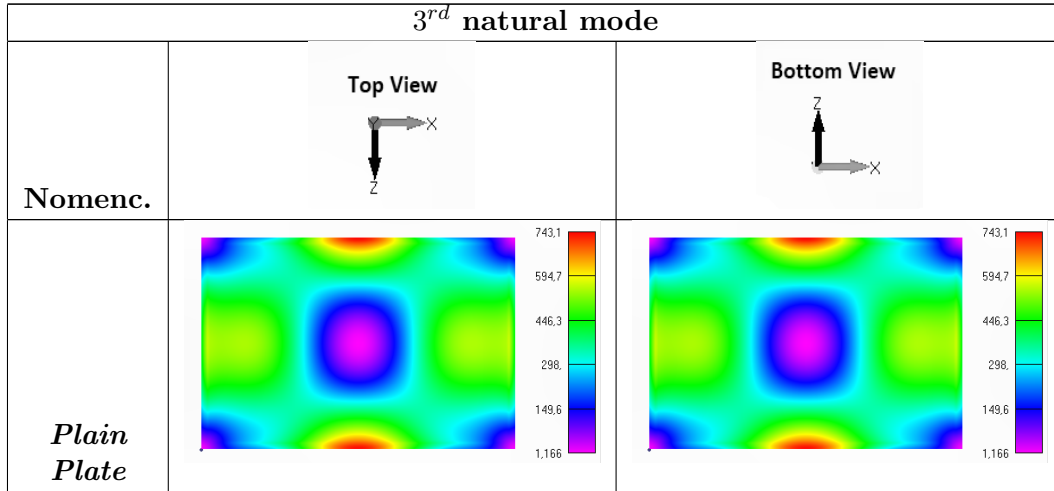


Table E.62: Distribution of the modal strain energy (4^{th} mode) for the plate without treatment with free boundary conditions.

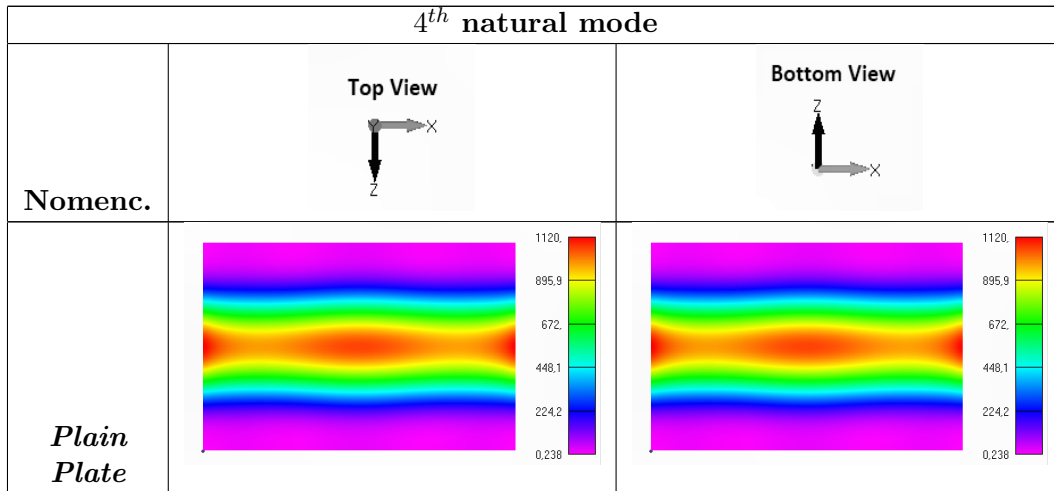
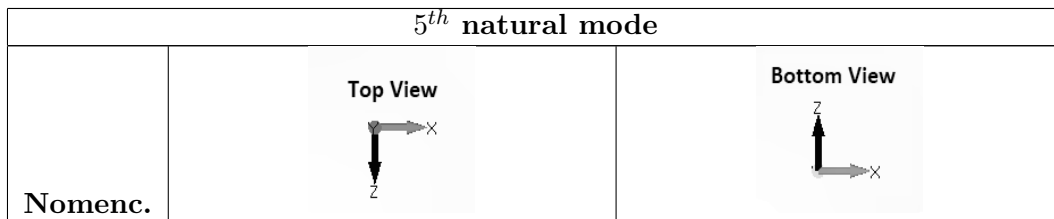
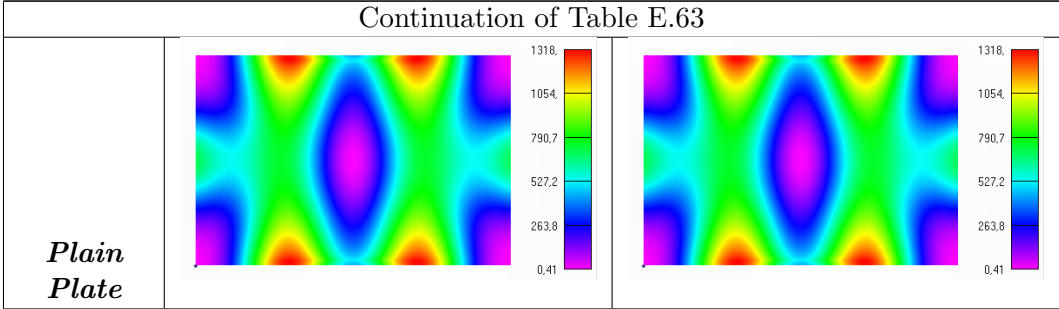


Table E.63: Distribution of the modal strain energy (5^{th} mode) for the plate without treatment with free boundary conditions.





Intentionally blank page.

References

- [1] R.A.S. Moreira, “Structural Dynamics and Viscoelastic Passive Damping Treatments,” in *Modern Mechanical Engineering*, ch. 5, pp. 325–365, 2014.
- [2] R.A.S. Moreira, *Modelação e análise de tratamentos viscoelásticos multi-camada para controlo passivo de vibrações*. PhD thesis, Nov. 2004.
- [3] R.A.S. Moreira, “Viscoelastic damping treatments,” in *Multifunctional Composites*, ch. 6, pp. 169 – 204, 2016.
- [4] D.J. Ewins, *Modal Testing: Theory and Practice*. Research Studies Press Ltd., 1984.
- [5] K.K. Denoyer and C.D. Johnson, “Recent achievements in vibration isolation systems for space launch and on-orbit applications,” in *Proceedings of 52nd International Astronautical Congress (AIAA)*, (Toulouse, France), October 2001.
- [6] R.A.S. Moreira and J. D. Rodrigues, “Partial constrained viscoelastic damping treatment of structures: A modal strain energy approach,” *International Journal of Structural Stability and Dynamics*, vol. 6, no. 3, pp. 397–411, 2006.
- [7] D. Z.A. Momin and S.H. Sung, “Evaluation of vibration damping treatments using a vehicle structural-acoustic analysis,” in *Proceedings of 5th International Modal Analysis Conference (IMAC V)*, (London, UK), pp. 330–335, 1987.
- [8] D. Battazzo and O. McDaniel, “Prediction of acoustical power using modal analysis: A case study on a plate treated with constrained layer damping,” in *Proceedings of 8th International Modal Analysis Conference (IMAC VIII)*, (Kissimmee, FL, USA), pp. 263–269, 1990.
- [9] L. L. Garibaldi and B. Piombo, “Acoustical emission control of metal plates using modal analysis to distribute visco-elastic materials,” in *Proceedings of 8th International Modal Analysis Conference (IMAC VIII)*, (Kissimmee, FL, USA), pp. 275–278, 1990.
- [10] D. D. Pei and H. X. Li, “Dynamic performance analysis and optimization of damping treatments on printed circuit board,” in *Proceedings of 4th International Modal Analysis Conference (IMAC 4)*, (Los Angeles, CA, USA), pp. 1494–1501, 1986.
- [11] B. Nakra, “Vibration control in machines and structures using viscoelastic damping,” *Journal of Sound and Vibration*, vol. 211, no. 3, pp. 449 – 466, 1998.

- [12] D. I. G. Jones, “Reflections on damping technology at the end of the twentieth century,” *Journal of Sound and Vibration*, vol. 190, no. 3, pp. 449 – 462, 1996.
- [13] D. I. G. Jones, A. D. Nashif, and J. P. Henderson, *Vibration Damping*. John Wiley & Sons, 1st ed., 1985.
- [14] D. I. G. Jones, *Handbook of viscoelastic vibration damping*. John Wiley & Sons, 1st ed., 2001.
- [15] R.A.S Moreira and J. D. Rodrigues, “Constrained Damping Layer Treatments: Finite Element Modeling,” *Journal of Vibration and Control*, vol. 10, pp. 575–595, 2004.
- [16] R.A.S. Moreira and J. D. Rodrigues, “Multilayer damping treatments: Modeling and experimental assessment,” *Journal of Sandwich Structures & Materials*, vol. 12, pp. 181–198, March 2010.
- [17] K. Stevens and S. Shostein, “Influence of partial viscoelastic damping treatments on the modal parameters of circular plates,” in *Proceedings of 7th International Modal Analysis Conference (IMAC VII)*, (Kissimmee, FL, USA), pp. 1616–1622, 1988.
- [18] A. Lumsdaine and R. Scott, “Shape optimization of unconstrained viscoelastic layers using continuum finite elements,” *Journal of Sound and Vibration*, vol. 216, no. 1, pp. 29 – 52, 1998.
- [19] A. Akanda, T. Onsay, and G. M. Goetchius, “Perforated damping treatment; a novel approach to reduction of weight,” *SAE transactions*, vol. 108, pp. 2551–2562, 1999.
- [20] Q. Chen and C. Levy, “Vibration analysis of a partially covered double sandwich cantilever beam with concentrated mass at the free end,” *International Journal of Solids and Structures*, vol. 31, no. 17, pp. 2377 – 2391, 1994.
- [21] X. Dechang and Y. Zuguang, “Forced vibration of sandwich beam with segmented elastic-viscoelastic layers,” in *Proceedings of 5th International Modal Analysis Conference (IMAC V)*, (London, UK), pp. 1033–1040, 1987.
- [22] W. Kelly and K. Stevens, “Application of perturbation techniques to the modal analysis of a shaft with added viscoelastic damping,” in *Proceedings of 7th International Modal Analysis Conference (IMAC VII)*, (Las Vegas, NV, USA), pp. 45–51, 1989.
- [23] B. Sher and R.A.S. Moreira, “Dimensionless analysis of constrained damping treatments,” *Composite Structures*, vol. 99, pp. 241 – 254, 2013.
- [24] K. Wang, “Computational intelligence in agile manufacturing engineering,” in *Agile Manufacturing: The 21st Century Competitive Strategy* (A. Gunasekaran, ed.), pp. 297 – 315, Oxford: Elsevier Science Ltd, 2001.
- [25] D. I. G. Jones, “Design of constrained layer treatments for broad temperature damping,” *Shock and Vibration*, vol. 5(44), pp. 1–12, 1974.

- [26] D. I. G. Jones, "Damping of stiffened plates by multiple layer treatments," *Journal of Sound and Vibration*, vol. 35, no. 3, pp. 417–427, 1974.
- [27] T. E. Alberts and H. Xia, "Design and Analysis of Fiber Enhanced Viscoelastic Damping Polymers," *Journal of Vibration and Acoustics*, vol. 117, pp. 398–404, 10 1995.
- [28] J. M. Biggerstaff and J. B. Kosmatka, "Shear measurements of viscoelastic damping materials embedded in composite plates," in *Smart Structures and Materials 1999: Passive Damping and Isolation* (T. T. Hyde, ed.), vol. 3672, pp. 82 – 92, International Society for Optics and Photonics, SPIE, 1999.
- [29] G. Lepoittevin and G. Kress, "Optimization of segmented constrained layer damping with mathematical programming using strain energy analysis and modal data," *Materials & Design*, vol. 31, no. 1, pp. 14 – 24, 2010.
- [30] M. Garrison, R. Miles, J. Sun, and W. Bao, "Random response of a plate partially covered by a constrained layer damper," *Journal of Sound and Vibration*, vol. 172, no. 2, pp. 231 – 245, 1994.
- [31] A. Van Vuure, I. Verpoest, and F. Ko, "Sandwich-fabric panels as spacers in a constrained layer structural damping application," *Composites Part B: Engineering*, vol. 32, no. 1, pp. 11 – 19, 2001.
- [32] E. Balmes, "Incorporating damping predictions in the vibroacoustic design process," *Proceedings of International Seminar on Modal Analysis, Leuven, Belgium*, 09 2004.
- [33] A. Baz and J. Ro, "Optimum Design and Control of Active Constrained Layer Damping," *Journal of Vibration and Acoustics*, vol. 117, pp. 135–144, 06 1995.
- [34] M. C. Ray, J. Oh, and A. Baz, "Active constrained layer damping of thin cylindrical shells," *Journal of Sound and Vibration*, vol. 240, pp. 921–935, 03 2001.
- [35] J. Oh, M. Ruzzene, and A. Baz, "Control of the dynamic characteristics of passive magnetic composites," *Composites Part B: Engineering*, vol. 30, no. 7, pp. 739 – 751, 1999.
- [36] C. Chantalakhana and R. Stanway, "Active constrained layer damping of clamped-clamped plate vibrations," *Journal of Sound and Vibration*, vol. 241, no. 5, pp. 755 – 777, 2001.
- [37] W. Liao and K. Wang, "On the analysis of viscoelastic materials for active constrained layer damping treatments," *Journal of Sound and Vibration*, vol. 207, no. 3, pp. 319 – 334, 1997.
- [38] T. Pritz, "Loss factor peak of viscoelastic materials: Magnitude to width relations," *Journal of Sound and Vibration*, vol. 246, pp. 265–280, 09 2001.
- [39] B. B. R. Allen, E. Ruhl and D. Sciulli, "Advanced isolation design for avionics on launch vehicles," in *Proceedings of 7th Smart Structures and Materials Conference (SPIE)*, (San Diego, CA), 2000.

- [40] J. M. Biggerstaff and J. B. Kosmatka, "Damping performance of cocured composite laminates with embedded viscoelastic layers," in *Smart Structures and Materials 1998: Passive Damping and Isolation* (L. P. Davis, ed.), vol. 3327, pp. 107 – 114, International Society for Optics and Photonics, SPIE, 1998.
- [41] J. M. Biggerstaff and J. B. Kosmatka, "Directional damping material for integrally damped composite plates," in *Smart Structures and Materials 1999: Passive Damping and Isolation* (T. T. Hyde, ed.), vol. 3672, pp. 368 – 374, International Society for Optics and Photonics, SPIE, 1999.
- [42] J. D. Ferry, E. R. Fitzgerald, L. D. Grand, and M. L. Williams, "Temperature dependence of dynamic mechanical properties of elastomers, relaxation distributions," *Industrial & Engineering Chemistry*, vol. 44, no. 4, pp. 703–706, 1952.
- [43] J. D. Ferry, J. Grandine, Lester D., and E. R. Fitzgerald, "The relaxation distribution function of polyisobutylene in the transition from rubber-like to glass-like behavior," *Journal of Applied Physics*, vol. 24, pp. 911–916, July 1953.
- [44] J. D. Ferry, *Viscoelastic properties of polymers*. Wiley, 1st ed., 1961.
- [45] B. Maxwell, "An investigation of the dynamic mechanical properties of polymethyl methacrylate," *Journal of Polymer Science*, vol. 20, no. 96, pp. 551–566, 1956.
- [46] H. Oberst, "Material of high inner damping," *Acustica : Journal international d'acoustique*, vol. 6, no. 1, pp. 144–153, 1956.
- [47] N.O. Myklestad, "The concept of complex damping," *Journal of Applied Mechanics*, vol. 19, no. 3, pp. 284–286, 1952.
- [48] R. BAGLEY and P. TORVIK, "Fractional calculus in the transient analysis of viscoelastically damped structures," 1983.
- [49] Y. Rossikhin and M. Shitikova, "Analysis of the Viscoelastic Rod Dynamics via Models Involving Fractional Derivatives or Operators of Two Different Orders," *The Shock and Vibration digest*, vol. 36, pp. 3–26, 2004.
- [50] A. Schmidt and L. Gaul, "FE Implementation of Viscoelastic Constitutive Stress-Strain Relations Involving Fractional Time Derivatives," *Proceedings of the 2nd European Conference on Constitutive Models for Rubber (ECCMR)*, pp. 79–89, 2001.
- [51] A. Schmidt and L. Gaul, "Application of fractional calculus to viscoelastically damped structures in the finite element method," in *Proceedings of the International Conference on Structural Dynamics Modelling (SDM)*, (Madeira, Portugal), pp. 297–306, 2002.
- [52] A. Schmidt and L. Gaul, "Parameter Identification and FE Implementation of a Viscoelastic Constitutive Equation Using Fractional Derivatives," *Pamm*, vol. 1, pp. 153–154, 2002.

- [53] M. Enelund, *Fractional calculus and linear viscoelasticity in structural dynamics*. PhD thesis, PhD Thesis, Chalmers University of Technology, Goteborg, Sweden, 1996.
- [54] A. C. Galucio, J.-F. Deü, and R. Ohayon, “Finite element formulation of viscoelastic sandwich beams using fractional derivative operators,” *Computational Mechanics*, vol. 33, no. 4, pp. 282–291, 2004.
- [55] K. Oldham and J. Spanier, *The fractional Calculus*. New York: Academic Press, 1974.
- [56] G. A. Lesiutre and E. Bianchini, “Time domain Modeling of linear viscoelasticity using anelastic displacement fields,” *Journal of Vibration and Acoustics, Transactions of the ASME*, vol. 117, no. 4, pp. 424–430, 1995.
- [57] G. A. Lesiutre and K. Govindswamy, “Finite element modeling of frequency-dependent and temperature-dependent dynamic behavior of viscoelastic materials in simple shear,” *International Journal of Solids and Structures*, vol. 33, no. 3, pp. 419–432, 1996.
- [58] D. J. McTavish and P. C. Hughes, “Modeling of Linear Viscoelastic Space Structures,” *Journal of Vibration and Acoustics*, vol. 115, pp. 103–110, jan 1993.
- [59] M. A. Trindade, *Contrôle hybride actif-passif des vibrations de structures par des matériaux piezoélectriques et viscoélastiques : poutres sandwich / multicouches intelligentes*. PhD thesis, These de Doctorat, Conservatoire National des Arts et Métiers, France, 2000.
- [60] M. J. Lam, *Hybrid active /passive models with frequency dependent damping*. PhD thesis, PhD Thesis, Faculty of the Virginia Polytechnic Institute and State University, USA, 1997.
- [61] Y. SHI, Z. LI, H. HUA, Z. FU, and T. LIU, “The modelling and vibration control of beams with active constrained layer damping,” *Journal of Sound and Vibration*, vol. 245, no. 5, pp. 785 – 800, 2001.
- [62] V. Balamurugan and S. Narayanan, “Finite element formulation and active vibration control study on beams using smart constrained layer damping (sclcd) treatment,” *Journal of Sound and Vibration*, vol. 249, pp. 227–250, 01 2002.
- [63] N. Wagner and S. Adhikari, “Symmetric state-space method for a class of nonviscously damped systems,” *AIAA Journal*, vol. 41, no. 5, pp. 951–956, 2003.
- [64] C. Johnson and D. A. Kienholz, “Finite element prediction of damping in structures with constrained viscoelastic layers,” *AIAA Journal*, vol. 20(9), pp. 1284–1290, 1982.
- [65] J. Killian and Y. Lu, “A finite element modeling approximation for damping material used in constrained damped structures,” *Journal of Sound and Vibration*, vol. 97(2), pp. 352–354, 1984.
- [66] J. Reddy, *Mechanics of laminated composite plates: theory and analysis*. 1997.

- [67] R.A.S. Moreira, F. J. Melo, and J. D. Rodrigues, “Static and dynamic characterization of cork compounds for sandwich beam cores,” *Journal for Materials Science*, vol. 45(12), pp. 3350–3366, 2010.
- [68] R.A.S. Moreira, J. D. Rodrigues, and A. Ferreira, “A generalized layerwise finite element for multi-layer damping treatments,” *Computational Mechanics*, vol. 37(5), pp. 426–444, 2006.
- [69] H. Oberst and K. Frankenfeld, “Ubie die dampfung biedgesch wingungen dunner blech durch fest haftende belage,” *Acustica*, vol. 4, pp. 181–194, 1952.
- [70] E. M. Kerwin Jr., “Damping of flexural waves by a constrained viscoelastic layer,” *Journal of Acoustical Society of America*, vol. 31, pp. 952–962, 1959.
- [71] D. Ross, E. E. Ungar, and E. M. Kerwin Jr., “Damping of plate flexural vibrations by means of viscoelastic laminae,” *Structural Damping – ASME publication*, pp. 49–88, 1959.
- [72] H. Yamaguchi and R. Adhikari, “Loss factors of damping treated structural cables,” *Journal of Sound and Vibration*, vol. 176, no. 4, pp. 487 – 495, 1994.
- [73] A. Bhimaraddi, “Sandwich beam theory and the analysis of constrained layer damping,” *Journal of Sound and Vibration*, vol. 179, no. 4, pp. 591 – 602, 1995.
- [74] T.-L. Teng and N.-K. Hu, “Analysis of damping characteristics for viscoelastic laminated beams,” *Computer Methods in Applied Mechanics and Engineering*, vol. 190, no. 29, pp. 3881 – 3892, 2001.
- [75] R. A. DiTaranto, “Theory of Vibratory Bending for Elastic and Viscoelastic Layered Finite-Length Beams,” *Journal of Applied Mechanics*, vol. 32, pp. 881–886, 12 1965.
- [76] D. Mead and S. Markus, “The forced vibration of a three-layer, damped sandwich beam with arbitrary boundary conditions,” *Journal of Sound and Vibration*, vol. 10, no. 2, pp. 163 – 175, 1969.
- [77] D. Mead and S. Markus, “Loss factors and resonant frequencies of encastré damped sandwich beams,” *Journal of Sound and Vibration*, vol. 12, no. 1, pp. 99 – 112, 1970.
- [78] D. K. Rao, “Frequency and loss factors of sandwich beams under various boundary conditions,” *Journal of Mechanical Engineering Science*, vol. 20, no. 5, pp. 271–282, 1978.
- [79] M.-J. Yan and E. H. Dowell, “Governing Equations for Vibrating Constrained-Layer Damping Sandwich Plates and Beams,” *Journal of Applied Mechanics*, vol. 39, pp. 1041–1046, 12 1972.
- [80] Y. Sadasiva Rao and B. Nakra, “Vibrations of unsymmetrical sandwich beams and plates with viscoelastic cores,” *Journal of Sound and Vibration*, vol. 34, no. 3, pp. 309 – 326, 1974.

- [81] E. E. Ungar and E. M. Kerwin, “Loss factors of viscoelastic systems in terms of energy concepts,” *The Journal of the Acoustical Society of America*, vol. 34, no. 7, pp. 954–957, 1962.
- [82] K.K. Stevens and H.Y. Hsu, “Modal damping and sound power reduction of plates with partial constrained layer damping treatments,” in *Proceedings of 3rd International Modal Analysis Conference (IMAC III)*, (Orlando, FL, USA), pp. 160–166, 1985.
- [83] M. K.K. Stevens and W.J. Kelly, “A comparison of exact and approximate methods of analysis for added viscoelastic damping treatments,” in *Proceedings of 6th International Modal Analysis Conference (IMAC VI)*, (Kissimmee, FL, USA), pp. 1602–1608, 1988.
- [84] B.-C. LEE and K.-J. KIM, “Shear and normal strain effects of core layers in vibration of square sandwich plates under clamped boundary conditions,” *Journal of Sound and Vibration*, vol. 228, no. 4, pp. 845 – 856, 1999.
- [85] Y. Shin and G. Maurer, “Vibration response of constrained viscoelastically damped plates: Analysis and experiments,” *Finite Elements in Analysis and Design*, vol. 7, no. 4, pp. 291 – 297, 1991.
- [86] E. Balmès, “Super-element representation of a model with frequency dependent properties,” in *Proceedings of International Seminar on Modal Analysis*, (Leuven, Belgium), pp. 1767–1778, 1996.
- [87] E. Balmès, “Model reduction for systems with frequency dependent damping properties,” in *Proceedings of 15th International Modal Analysis Conference (IMAC XV)*, (Orlando, FL, USA), pp. 223–229, 1997.
- [88] A. Plouin and E. Balmès, “Pseudo-modal representations of large models with viscoelastic behavior,” in *Proceedings of 16th International Modal Analysis Conference (IMAC XVI)*, (Santa Barbara, CA, USA), pp. 1440–1446, 1998.
- [89] A. Plouin and E. Balmès, “A test validated model of plates with constrained viscoelastic materials,” in *Proceedings of 17th International Modal Analysis Conference (IMAC XVII)*, (Kissimmee, FL, USA), pp. 194–200, 1999.
- [90] R.M.Lin and M.K.Lim, “Complex eigensensitivity-based characterization of structures with viscoelastic damping,” *Journal of Acoustical Society of America*, vol. 100(5), pp. 3182– 3191, 1996.
- [91] D. L. Safranski, “Chapter One - Introduction to Shape-Memory Polymers,” in *Shape-Memory Polymer Device Design* (D. L. Safranski and J. C. Griffis, eds.), *Plastics Design Library*, pp. 1–22, William Andrew Publishing, 2017.
- [92] ASTM, *E756-98 standard test method for measuring vibration-damping properties of materials. Annual Book of ASTM Standards*. New York: V.04.06. ASTM, 1998.
- [93] R.A.S. Moreira and R. De Carvalho, “Inverse method for dynamic characterisation of cork compounds,” *International Journal of Materials Engineering Innovation*, vol. 1(2), pp. 254–275, 2009.

- [94] K. K. Pradhan and S. Chakraverty, “Chapter Four - Finite Element Method,” in *Computational Structural Mechanics* (K. K. Pradhan and S. Chakraverty, eds.), pp. 25–28, Academic Press, 2019.
- [95] L. Gaul, “Structural damping in frequency and time domain,” in *7th international modal analysis conference (IMAC VII)*, (Las Vegas), pp. 177–185, 1989.
- [96] R.A.S. Moreira, J. Corte-Real, and J. D. Rodrigues, “A generalized frequency-temperature viscoelastic model,” *Shock and Vibration*, vol. 17(4-5), pp. 407–418, 2010.
- [97] G. A. Lesieutre and D. Mingori, “Finite element modelling of frequency-dependent material damping using augmenting thermodynamic fields,” *Journal of Guidance Control and Dynamics*, vol. 13(6), pp. 1040–1050, 1990.
- [98] G. A. Lesieutre, “Finite elements for dynamic modeling of uniaxial rods with frequency- dependent material properties,” *International Journal of Solids and Structures*, vol. 29(12), pp. 1567–1579, 1992.
- [99] K. Bathe, *Finite Element Procedures*. Prentice Hall, 2006.
- [100] A.T.H. Mitsuma and F. Sekimoto, “Experimental and theoretical study on damped joints in truss structure.,” in *Proceedings of the 8th International Modal Analysis Conference (IMAC VIII)*, (Kissimmee, FL, USA), pp. 8–14, 1990.
- [101] S.-W. Kung and R. Singh, “Complex eigensolutions of rectangular plates with damping patches,” *Journal of Sound and Vibration*, vol. 216, no. 1, pp. 1 – 28, 1998.
- [102] C.M.A Vasques, R.A.S. Moreira, and J. D. Rodrigues, “Viscoelastic damping technologies–part I: Modeling and finite element implementation,” *Journal of Advanced Research in Mechanical Engineering*, vol. 1, 01 2010.
- [103] B.-G. Hu, M. Dokainish, and W. Mansour, “A modified mse method for viscoelastic systems: A weighted stiffness matrix approach,” *Journal of Vibration and Acoustics*, vol. 117, 04 1995.
- [104] *MSC/Nastran for Windows Quick Start Guide*. MSC, February, 1995.
- [105] *MSC/Nastran for Windows Modelling Examples Manual*. MSC, October, 1998.
- [106] 3M™, “Viscoelastic Damping Polymer 112 Series,” p. 8, May 2017.
- [107] *MSC/Nastran for Windows Analysis Examples Manual*. MSC, November, 1998.
- [108] J. Salgado and J. Meireles, “Study of the experimental modal analysis techniques applied to structural dynamics,” in *Proceedings of 5th International Operational Modal Analysis Conference*, (Guimarães, Portugal), may 2013.
- [109] Siemens PLM, “Getting started with modal curvefitting.” <https://community.sw.siemens.com/s/article/getting-started-with-modal-curvefitting>.
- [110] Siemens PLM, “Modal assurance criterion.” <https://community.sw.siemens.com/s/article/modal-assurance-criterion-mac>.